

# Modelling of Neurodevelopmental Disorders Associated with 1q21.1 deletion and duplication using human iPSCs

By  
Gareth David Chapman

A thesis submitted to Cardiff University for the degree of Doctor of Philosophy  
December 2019

## Abstract

Copy number variation at the 1q21.1 locus (both deletion and duplication) has been associated with a wide variety of neurological phenotypes including changes in brain size and increased risk for developing psychiatric disorders. Deletion of the 1q21.1 locus is primarily associated with an increased risk of schizophrenia whereas duplication of the same locus is primarily associated with an increased risk of autism. These mutations present an untapped opportunity to understand the cellular deficits which underly both common and specific risk for psychiatric disorders. Patient derived iPSCs were made from individuals carrying either 1q21.1 deletion or duplication and were then used to model both neuronal and oligodendrocyte development. The presence of 1q21.1 CNVs was associated with significant changes in neuronal and oligodendroglial development. Deletion of the 1q21.1 locus was associated with increased neuronal activity and a reduced production of mature oligodendrocytes. On the other hand, duplication of the 1q21.1 locus was associated with deficits in the production of neurons and specification of oligodendrocytes. Key findings from the iPSC models were also validated using a 1q21.1 microdeletion mouse model and human brain imaging data from 1q21.1 carriers. These results constitute the first examination of human cellular dysfunction associated with copy number variation at the 1q21.1 locus. Furthermore, this work clearly demonstrates the importance of examining the effect of mutations on both glial and neuronal cells. To develop a system which could provide further insight into the interactions between these two cell types this study also examined the feasibility of bioprinting, as a technique for 3D cell culture. Using iPSC derived astrocytes and neurons a novel alginate based bioink was developed which could support the short-term maintenance of both cell types. Therefore, demonstrating that 3D bioprinting is a viable technique for generating 3D culture systems for iPSC derived neuronal cells.

## Acknowledgments

Firstly, I would like to thank my primary supervisor Dr. Yasir Syed and my secondary supervisor Prof. Adrian Harwood. Your support and encouragement have made me the scientist I am today. I would also like to thank my funders, The Waterloo Foundation (Changing Minds program) and the NMHRI for their support which has allowed me the freedom to do this work. My thanks also go to the technical staff of the NMHRI for their support and help along the way. I would also like to thank Prof. Adam Perriman and his lab at the university of Bristol for all their help and advice while I was developing my bioink.

The ups and downs of my PhD have also been made easier by the support of my friends and colleagues. I would like to thank all the members of Dr. Syed and Prof. Harwood's labs; you have all helped immensely. Specifically, I would like to thank Tanya Singh for your help and support in generating astrocytes for my bioprinting work. Also, my thanks to Sharna Lunn for her help in performing the trilineage differentiations. I would also like to thank Dr. Mouhamed Alsaqati because despite everything being your fault, the help and expertise you have provided with the MEAs has been invaluable. My thanks to Ana Silva for her help in analyzing the human DTI data and to Craig Joyce for your help in generating the induced pluripotent stem cells needed for this work. Finally, I would like to thank Bret Sanders for your support and encouragement, the value of having a friendly ear is often overlooked and I thank you for being that for me.

Lastly and most importantly I would like to thank my family. While he has no idea what I do for a living my grandfather has experienced every high and low of my PhD with me through our nightly conversations and without him I'm not sure I would have made it this far. I would also like to thank my father for his constant encouragement. Finally, I would like to thank my mother, despite the fact you are gone, I would not be the man I am today without you.

## Glossary of Abbreviations

aCSF	Artificial cerebral spinal fluid
AD	Axial diffusivity
ADM	Astrocyte differentiation media
ASD	Autism spectrum disorder
BD	Bipolar disorder
Chit	Chitosan
CNS	Central nervous system
CNV	Copy number variation
Col IV	Collagen IV
DMSO	Dimethyl sulfoxide
DTI	Diffusion tensor imaging
E8F	Essential 8™ flex media
ECM	Extra-cellular matrix
ESC	Embryonic stem cell
FA	Fractional anisotropy
FBS	Foetal bovine serum
GABA	Gamma aminobutyric acid
GAD	Generalised anxiety disorder
HA	Hyaluronic acid
ID	Intellectual disability
iPSC	Induced pluripotent stem cell
LDN	LDN193189
MA	Mode of anisotropy
MACS	Magnetically activated cell sorting
Mat	Matrigel
MDD	Major depression disorder
MEA	Multiple electrode array
miRNA	MicroRNA
MRI	Magnetic resonance imaging
NEAA	Non-essential amino acids
NES	NESTIN
NPC	Neuronal precursor cell
OCD	Obsessive compulsive disorder
OPC	Oligodendrocyte progenitor cell
PBS	Phosphate buffered saline
PBST	Phosphate buffered saline with triton-x-100
PCP	Phencyclidine
PCR	Polymerase chain reaction
PD	Personality disorder
PPI	Pre-pulse inhibition
qPCR	Quantitative polymerase chain reaction
RD	Radial diffusivity
RGD	Arginylglycylaspartic acid
SB	SB431542
SNP	Single nucleotide polymorphism
SYN	Synaptophysin
SZ	Schizophrenia
TAR	Thrombocytopenia with absent radius
TBS	Tris buffered saline
TBST	Tris buffered saline with tween-20
Ten R	Tenascin R

## List of Tables

<b>Table 1.1:</b> Previously identified rare copy number variants associated with an increased risk of neurodevelopmental and psychiatric disorders .....	4
<b>Table 1.2:</b> Genes within both the TAR and distal regions of the 1q21.1 locus .....	8
<b>Table 2.1:</b> List of consumables used in the study .....	40
<b>Table 2.2:</b> List of drugs and small molecules used in the study .....	41
<b>Table 2.3:</b> List of cell culture material used in the study .....	42
<b>Table 2.4:</b> List of molecular biology and staining reagents used in the study .....	44
<b>Table 2.5:</b> List of antibodies used in the study.....	45
<b>Table 2.6:</b> List of primers used in the study .....	46
<b>Table 3.1:</b> Patient information for all 1q21.1 patients used in the study .....	64
<b>Table 4.1:</b> The three main techniques currently employed for 3D bioprinting .....	137

## List of Figures

<b>Figure 1.1:</b> Diagrammatic representation of the classification of 1q21.1 deletion and duplication	6
<b>Figure 3.1:</b> Graphical representation of the structure of the cortex .....	50
<b>Figure 3.2:</b> Reprogramming of human fibroblasts into iPSCs .....	58
<b>Figure 3.3:</b> Characterization of iPSCs generated from 1q21.1 deletion patient 1 .....	59
<b>Figure 3.4:</b> Characterization of iPSCs generated from 1q21.1 deletion patient 2 .....	60
<b>Figure 3.5:</b> Characterization of iPSCs generated from 1q21.1 deletion patient 3 .....	61
<b>Figure 3.6:</b> Characterization of iPSCs generated from 1q21.1 duplication patient 1 .....	62
<b>Figure 3.7:</b> Characterization of iPSCs generated from 1q21.1 duplication patient 2 .....	63
<b>Figure 3.8:</b> Expression of NPC and Neuronal markers after 20 and 50 days of differentiation .....	65
<b>Figure 3.9:</b> Expression of 1q21.1 genes in day 50 cortical neurons .....	66
<b>Figure 3.10:</b> Gene expression of NPC markers in control and 1q21.1 day 20 differentiations .....	67
<b>Figure 3.11:</b> Gene expression of neuronal markers in control and 1q21.1 day 50 differentiations .....	69
<b>Figure 3.12:</b> Morphology of immature neurons produced by 1q21.1 mutant cells .....	72
<b>Figure 3.13:</b> Longitudinal expression of neuronal markers in control and 1q21.1 deletion or duplication neuronal differentiations .....	73
<b>Figure 3.14:</b> Expression of an excitatory and an inhibitory neuronal marker in day 40 differentiations .....	75
<b>Figure 3.15:</b> Lower layer cortical neuron patterning in control and 1q21.1 neuronal differentiations .....	77
<b>Figure 3.16:</b> Quantification of lower layer cortical markers in adult mouse brains modelling 1q21.1 microdeletion .....	78
<b>Figure 3.17:</b> The expression of synapse associated genes in control and 1q21.1 day 50 neuronal cultures .....	80
<b>Figure 3.18:</b> The quantification of presynaptic densities in day 50 neurons .....	81
<b>Figure 3.19:</b> Analysis of calcium kinetics in neurons carrying 1q21.1 mutations .....	82
<b>Figure 3.20:</b> The effect of inhibiting AMPA or NMDA signaling in day 50 neuronal cultures. Quantification .....	83
<b>Figure 3.21:</b> The activity and network behavior of neurons using MEAs .....	84
<b>Figure 3.22:</b> Inhibition of AMPA or NMDA signaling in 1q21.1 deletion neuronal cultures .....	85
<b>Figure 3.23:</b> The effect of 1q21.1 deletion on complex neuronal network behaviors .....	86
<b>Figure 3.24:</b> The effect of 1q21.1 deletion on complex neuronal network bursting behaviour .....	87
<b>Figure 3.25:</b> Pharmacological modulation of calcium kinetics in neurons with 1q21.1 mutations .....	89

<b>Figure 3.26:</b> Graphical explanations for the developmental phenotypes observed in 1q21.1 mutant cell lines .....	92
<b>Figure 4.1:</b> Key processes in the course of neurodevelopment .....	104
<b>Figure 4.2:</b> Schematic representation of fractional anisotropy .....	106
<b>Figure 4.3:</b> Graphical representation of differentiation paradigms currently used to generate glial cells from human iPSC .....	110
<b>Figure 4.4:</b> Intracranial volumes of individuals carrying 1q21.1 mutations .....	115
<b>Figure 4.5:</b> DTI metrics in the corpus callosum of individuals with CNV at the 1q21.1 locus .....	116
<b>Figure 4.6:</b> Changes in the number of oligodendrocytes in the corpus callosum of the 1q21.1 microdeletion mouse model .....	117
<b>Figure 4.7:</b> Early oligodendrocyte differentiation from iPSC .....	118
<b>Figure 4.8:</b> Modification to the non-adherent growth stages of oligodendrocyte generation .....	119
<b>Figure 4.9:</b> Oligodendrocyte differentiation and maturation .....	120
<b>Figure 4.10:</b> Gene expression changes in 1q21.1 cell lines after 12 days of oligodendrocyte differentiation .....	121
<b>Figure 4.11:</b> Changes in proliferation during early stages of oligodendrocyte development .....	122
<b>Figure 4.12:</b> Production of mature MBP+ oligodendrocytes in control and 1q.21.1 mutant oligodendrocyte differentiations .....	124
<b>Figure 4.13:</b> Gene expression and proliferation changes associated with 1q21.1 deletion during early oligodendrocyte development .....	125
<b>Figure 4.14:</b> The effect of 1q21.1 deletion on the production of OPCs .....	127
<b>Figure 4.15:</b> The production of mature oligodendrocytes from control and 1q21.1 deletion iPSCs .....	128
<b>Figure 5.1:</b> Generation and assessment of neurons generated from control iPSCs .....	154
<b>Figure 5.2:</b> Generation and assessment of astrocytes generated from control iPSCs .....	155
<b>Figure 5.3:</b> Testing the cytotoxicity of alginate based bioink and crosslinking salts .....	157
<b>Figure 5.4:</b> Testing the effect of bioprinting and procedural modifications on cell viability .....	159
<b>Figure 5.5:</b> The effect of adding neuronal ECM components into bioinks .....	161
<b>Figure 5.6:</b> Testing the effect of bioprinting using complex neuronal bioinks on astrocyte cell viability .....	162
<b>Figure 5.7:</b> The effect of neuron and astrocyte co-culture on cell viability and morphology .....	163

# Contents

Abstract .....	i
Acknowledgments .....	ii
Glossary of Abbreviations .....	iii
List of Tables .....	iv
List of Figures.....	v
1. Introduction .....	1
1.1 Clinical significance of pathogenic copy number variants in neurodevelopmental and psychiatric disorders .....	1
1.1.1 Contribution of rare CNVs for increasing the risk of neurodevelopmental and psychiatric disorders .....	1
1.1.2 Previously identified CNVs associated with increased risk for neurodevelopmental and psychiatric disorders .....	4
1.1.3 Clinical significance of copy number variation at the 1q21.1 locus.....	5
1.1.4 Genetic architecture of the 1q21.1 locus .....	7
1.1.5 Established evidence for the clinical effects of 1q21.1 mutations from animal models	9
1.1.6 Cellular mechanisms underlying the pathogenesis of ASD and schizophrenia .....	10
1.1.7 Modelling 1q21.1 phenotypes using human iPSCs .....	15
1.1.8 Aims and objectives.....	19
2. Material and Methods.....	20
2.1 iPSC culture .....	20
2.2 Neuronal differentiation.....	23
2.3 Oligodendrocyte differentiation .....	25
2.4 Calcium imaging .....	28
2.5 Multi electrode arrays .....	29
2.6 Immunocytochemistry .....	30
2.7 Western blotting .....	34
2.8 Quantitative PCR .....	35
2.9 Magnetically activated cell sorting .....	36
2.10 Human brain imaging .....	37
2.11 Statistical analysis.....	39
2.12 Materials .....	40
3. Deletion and Duplication of the Distal 1q21.1 Locus are Associated with Altered Neuronal Differentiation Resulting in Altered Functional Behavior.....	48
3.1 Introduction .....	48
3.1.1 Generating neurons from iPSCs using developmental patterning paradigms .....	48
3.1.2 The role of cortical neuronal dysfunction in neurodevelopmental and psychiatric disorders .....	49

3.1.3 Modelling CNVs and psychiatric disorders using iPSC derived neurons .....	52
3.1.4 Limitations and challenges of iPSC derived neurons for modelling phenotypes associated with psychiatric disorders .....	55
3.2 Chapter 1: Hypothesis and aims .....	57
3.3 Results.....	58
3.3.1 Characterization of iPSCs from patients carrying distal 1q21.1 mutations.....	58
3.3.3 Mutation at the 1q21.1 locus is associated with altered gene expression at both neuronal precursor and immature neuron stages of development.....	66
3.3.4 1q21.1 mutations are associated with alterations in the morphology and production of immature neurons .....	70
3.3.5 Deletions and duplications of the 1q21.1 region are associated with altered developmental trajectories .....	73
3.3.6 Mutations at the 1q21.1 locus are associated with altered early cortical development .....	75
3.3.7 A mouse model of 1q21.1 microdeletion shows altered cortical development .....	78
3.3.8 Neurons carrying 1q21.1 mutations have altered capacity to produce synapses.....	79
3.3.9 Deletion or duplication of the 1q21.1 locus changes the ability of neurons to function .....	81
3.3.10 The use of drugs targeting calcium related pathways can modulate the physiological phenotypes associated with 1q21.1 mutations.....	87
3.4 Discussion .....	90
3.4.1 Mutations at the 1q21.1 locus differentially regulate neuronal differentiation.....	90
3.4.2 Abnormal calcium homeostasis and decreased neuronal activity associated with 1q21.1 duplication are phenotypes relevant to psychiatric disorders .....	93
3.4.3 Increased neuronal activity and abnormalities in synchronicity associated with 1q21.1 deletion models the imbalance of excitation and inhibition common in psychiatric disorders .....	97
3.4.4 Study limitations and future perspectives.....	100
4. Mutations of the Distal 1q21.1 Locus are Associated with Decreased Oligodendrocyte Specification and Altered Oligodendrocyte Differentiation .....	104
4.1 Introduction .....	104
4.1.1 Evidence for white matter dysfunction associated with psychiatric disorders from human imaging studies .....	104
4.1.2 Evidence for the pathogenic role of oligodendrocyte dysfunction in psychiatric disorders .....	107
4.1.3 Generation of oligodendrocytes from human induced pluripotent stem cells.....	109
4.1.4 Limitation and challenges associated with <i>in vitro</i> generation of Oligodendrocytes.	111
4.2 Chapter 2: Hypothesis and aims .....	114
4.3 Results.....	115

4.3.1 Human brain imaging of 1q21.1 carriers show changes in DTI metrics in the corpus callosum.....	115
4.3.2 A mouse model of 1q21.1 microdeletion shows a loss of oligodendrocytes in the corpus callosum .....	117
4.3.3 Differentiation of iPSCs into oligodendrocytes.....	118
4.3.4 Deletion and duplication of the 1q21.1 locus are associated with aberrant oligodendrocyte differentiation and function.....	120
4.3.6 Deletion of the 1q21.1 locus is associated with decreased production of myelinating oligodendrocytes.....	125
4.4 Discussion .....	129
4.4.1 Duplication of the 1q21.1 locus is associated with changes in early oligodendrocyte differentiation .....	129
4.4.2 Loss of oligodendrocytes in 1q21.1 deletion is both physiologically relevant and indicative of psychiatric pathology .....	130
4.4.3 Study limitations and future perspective .....	132
5. Alginate Based Bio-inks modified with Key Extra-Cellular Matrix Proteins Provide a Substrate for Maintenance of Neuronal Cell Lineages in Defined 3D Cell Cultures .....	135
5.1 Introduction .....	135
5.1.1 The lessons learnt from 2D cell culture and the emerging world of 3D cell culture ..	135
5.1.2 Current technology and techniques available for bioprinting.....	136
5.1.3 The role and importance of bioink.....	140
5.1.4 Bioprinting as it relates to neuronal systems .....	142
5.1.5 Current paradigms for the use of bioprinted 3D neuronal constructs .....	144
5.2 Chapter 3: Hypothesis and aims .....	146
5.3 Methods.....	147
5.3.1 Neuronal differentiation.....	147
5.3.2 Astrocyte differentiation .....	147
5.3.3 Glutamate Assay.....	148
5.3.4 Viral generation.....	149
5.3.5 Plasmids .....	150
5.3.6 Bioprinting.....	151
5.3.7 Live/dead Imaging .....	152
5.3.8 Statistical analysis.....	153
5.4 Results.....	154
5.4.1 Functional neurons and astrocytes can be generated from iPSC.....	154
5.4.2 Key components of the bioprinting process show no inherent cytotoxicity.....	156
5.4.2 Bioprinting neurons using un-modified alginate based bioink results in low cell viability .....	157

5.4.3 Addition of neuronal extra cellular matrix compounds significantly increases neuronal viability .....	159
5.4.5 Astrocytes show higher initial cell viability after bioprinting which is maintained by complex neuronal specific bioink.....	161
5.4.6. Bioprinting co-cultures of neurons and astrocytes results in viable 3D constructs ..	162
5.5 Discussion .....	164
5.5.1 The inclusion of ECM compounds into 3D cell culture is critical for the survival of neuronal cells .....	164
5.5.2 Study limitations and future perspectives.....	166
6. General Discussion .....	169
6.1 Duplication of the 1q21.1 distal locus is associated with altered early neuronal development.....	169
6.2 Deletion of the 1q21.1 distal locus is associated with deficits in cellular function distinct from deficits in early differentiation.....	170
6.3 Mutations of the 1q21.1 locus model key aspects of cellular pathology associated with psychiatric disorders .....	172
6.4 Conclusions and future perspectives .....	174
7. Bibliography .....	176

# 1. Introduction

## 1.1 Clinical significance of pathogenic copy number variants in neurodevelopmental and psychiatric disorders

### 1.1.1 Contribution of rare CNVs for increasing the risk of neurodevelopmental and psychiatric disorders

It has been estimated that during our life times more than 1 in 5 people will be diagnosed with a common mental health disorder<sup>1</sup>. However, studies examining high risk populations such as children in foster care<sup>2</sup> or individuals living in conflict settings<sup>3</sup> suggests the prevalence to be alarmingly high. The prevalence of neurodevelopmental disorders has also been reported to be 3-4% in children from high income countries<sup>4</sup>. Neurodevelopmental and psychiatric disorders are complex neurological phenomena which cause significant distress and alter the ability of patients to function within society. Furthermore, these disorders are often highly distressing for care givers and result in a large burden on both patients and the larger community with the estimated lifetime health and social care costs of an individual with autism spectrum disorder (ASD) being as high as £2.4 million<sup>5</sup>.

Therefore, there is a significant focus on better understanding the causes of these disorders and developing novel treatments which target the underlying pathology rather than simply alleviating symptoms. Risk factors for neurodevelopmental and psychiatric disorders include environmental factors<sup>6</sup>, neurotoxins<sup>7</sup> and maternal immune activation<sup>8</sup> among many others. However, these disorders are also known to be highly heritable therefore indicating a genetic component to risk for these disorders<sup>9</sup>. This heritability is most clearly demonstrated in family and twin studies which show a higher risk for developing the same psychiatric disorder the more close the genetic relationship between individuals<sup>10</sup>.

Due to the advent of next generation sequencing platforms genetic risk for neurodevelopmental and psychiatric disorders has been widely studied. The genetic component of risk for neurodevelopmental and psychiatric disorders can take three forms: single nucleotide polymorphisms (SNPs), copy number variants (CNVs) and chromosomal abnormalities. These platforms allow fast large-scale evaluation of populations to determine novel SNPs, and to identify individuals with CNVs which are associated with risk for neurodevelopmental and psychiatric disorders. While large scale genetic studies have identified many SNPs which are involved in the heritable component of psychiatric

disorders<sup>11,12</sup> each individual SNP is unlikely to have a significant effect on an individual's likelihood of developing a psychiatric disorder. This technique has identified key pathways and more recent work has begun to link these large scale genetic studies to cellular subpopulation which are likely preferentially effected<sup>13</sup>. However, the results do not lend themselves to archetypal cellular models as recapitulating individual SNPs is likely to have little effect on cellular function. Furthermore, modelling many SNPs in a single cell population remains costly while introducing a large number of potentially confounding variables. On the other hand, due to their more highly penetrant nature, CNVs can act as an ideal model of psychiatric risk for investigating the link between genetic abnormalities and cellular phenotypes associated with psychiatric disorders.

Copy number variants are relatively large sections of DNA (generally >1kb<sup>14</sup>) that can be lost or duplicated. Copy number variation can occur due to homologous or non-homologous recombination. Homologous recombination requires sequence homology (~300bp in eukaryotes<sup>15</sup>) and when the incorrect partner strand is selected this can result in CNV. Therefore, areas of the genome with low copy number repeat sequences may be particularly susceptible to CNVs arising from this mechanism. Homologous recombination can result in CNVs due to unequal crossing, break induced repair or single strand annealing all of which involve the mis-selection of the repair template (as reviewed by Hastings *et al*<sup>16</sup>). However homologous recombination mainly occurs during replication whereas non-homologous recombination can occur during replication or quiescence. Non-homologous end joining; replication slippage; template switching and microhomology based repair are all non-homologous recombination-based mechanisms by which CNVs can arise (as reviewed by Hastings *et al*<sup>16</sup>).

This type of variation is relatively common in the general population with one study reporting 1,447 CNV regions in 270 individuals<sup>17</sup>. Dependent on the methodology used to identify CNVs, studies have reported between 1.5% to 12% of the human genome is encompassed by copy number variable regions<sup>17,18</sup>. The prevalence of these types of mutations attribute to a significant proportion of intraspecific genetic variation. This type of variation has been shown to be under positive selection<sup>19</sup> in certain cases; providing the basis for the expansion of many gene families<sup>20</sup> that are linked to an increase of genetic complexity observed through evolutionary time. However, these mutations have also been linked to various pathological phenotypes which can be due to: changes in the dose of a single gene within the mutated region<sup>21-24</sup>, the mutation of a contiguous gene set (Williams-

Beuren syndrome<sup>25</sup>, DiGeorge Syndrome<sup>26</sup> and Smith-Magenis syndrome<sup>27</sup>), or novel allele combinations. Many pathological CNVs have now been identified, however linking these mutations to the complex presentation seen in patients remains difficult. Investigations into the interaction between genes within these mutations and the biology of the systems underlying the pathology may provide critical insight into this relationship.

While neurodevelopmental and psychiatric disorders can be considered separate the link between these two families of disorders was suggested as early as 1987 when Murray and Lewis<sup>28</sup> suggested that schizophrenia (arguably one of the most studied psychiatric disorders) is in part a neurodevelopmental disorder. This concept now has a large body of evidence behind it including evidence from anatomical data, genetic studies and work on the environmental factors known to effect risk for developing schizophrenia (reviewed by Fatemi and Folsom<sup>29</sup>). There is also evidence from studies into ASD<sup>30,31</sup>, bipolar disorder<sup>32</sup>, major depression<sup>33</sup> and intellectual disability<sup>34</sup> that abnormal neurodevelopment plays a critical role in the aetiology of these disorders.

Therefore, modern research is focusing on elucidating periods where individuals are at particular risk for deviation from the normal course of neurodevelopment which may underly the establishment of risk for neurodevelopmental and psychiatric disorders. Recent publications<sup>35,36</sup> have identified mid-gestation as a key period for mutations associated with psychiatric disorders to have an effect on gene expression. This conclusion would suggest that dysregulation at very early stages of neurodevelopment may play a key role in developing psychiatric disorders. Furthermore, this work suggests a commonality between the time period (*in utero* development) and specific mutations when reviewing several psychiatric disorders, thereby cementing neurodevelopment as a critical factor for determining risk of developing a psychiatric disorder later in life.

While early neurodevelopment may be a critical time for mutations and environmental factors to exert their effect, there is still little consensus on the precise nature of the interaction between these factors and their involvement in the pathology of psychiatric disorders in terms of the pathways involved and the cell populations affected. While environmental factors which increase the risk for developing psychiatric disorders have been identified these remain largely difficult to study using currently available paradigms; with work focusing largely on the effect these risk factors have on animal models. Therefore, the focus of cellular work remains understanding the cellular consequences of genetic risk for neurodevelopmental and psychiatric disorders.

### 1.1.2 Previously identified CNVs associated with increased risk for neurodevelopmental and psychiatric disorders

The first CNV to be linked to a psychiatric disorder was velo-cardio-facial syndrome; first described in 1978<sup>37</sup>. The genetic cause of this syndrome was later discovered to be a deletion of the 22q11.2 loci<sup>38</sup>. Subsequent studies have shown this mutation to be linked to an increased risk of developing schizophrenia with around 25% of patients with 22q11.2 deletion being diagnosed with schizophrenia<sup>39</sup>, and it has also been estimated that this population accounts for around 1% of all recorded schizophrenics<sup>40</sup>. As with most mutations which have been linked to specific pathology, the penetrance of these types of mutations is highly variable with estimates ranging from as low as 2% in the case of 15q11.2 deletion carriers exhibiting schizophrenia, to as high as 88% of patients carrying 22q11.2 deletions having intellectual disabilities. While these mutations have an important role in the determination of psychiatric diagnosis, categorically they remain risk factors rather than determinants for diagnosis.

**Table 1.1: Previously identified rare copy number variants associated with an increased risk of neurodevelopmental and psychiatric disorders.** Each mutation is characterized as either a deletion or duplication and significant risk for development of intellectual disability/developmental delay (ID), autism spectrum disorder (ASD), schizophrenia (SZ) or bipolar disorder (BD) associated with each mutation is denoted (adapted from Malhortra and Sebat<sup>41</sup>).

CNV	Deletion or Duplication	ID	ASD	SZ	BD
<b>1q21.1</b>	Deletion	Yes	No	Yes	No
<b>1q21.1</b>	Duplication	Yes	Yes	Yes	Yes
<b>3q29</b>	Deletion	Yes	No	Yes	Yes
<b>7q11.2</b>	Duplication	Yes	Yes	Yes	No
<b>7q11.23</b>	Deletion	Yes	No	No	No
<b>7q36.3</b>	Duplication	No	No	Yes	No
<b>15q11.2</b>	Deletion	Yes	No	Yes	No
<b>15q11.2</b>	Duplication	Yes	Yes	No	No
<b>15q13.3</b>	Deletion	Yes	Yes	Yes	No
<b>16p11.2</b>	Duplication	Yes	Yes	Yes	Yes
<b>16p11.2</b>	Deletion	Yes	Yes	No	No
<b>16p13</b>	Duplication	Yes	No	Yes	No
<b>17q12</b>	Deletion	Yes	Yes	Yes	No
<b>22q11</b>	Deletion	Yes	Yes	Yes	Yes
<b>22q11</b>	Duplication	Yes	Yes	No	No

At least 11 CNV loci (Table 1.1) have been identified as having an association with an increased risk of developing a neurodevelopmental or psychiatric disorder including; ASD, bipolar disorder, intellectual disability or schizophrenia<sup>41,42</sup>. The increased risk of developing a psychiatric disorder can be associated with both or either deletion and

duplication of these loci. Of the aforementioned 11 loci (Table 1.1), 15 specific CNV mutations have been linked with an increased risk of developing psychiatric disorders. These mutations are also often associated with other pathologies, the most common of which is facial dysmorphism<sup>43</sup>, found in the majority of these CNV patients. Furthermore, many of the CNVs associated with an increased risk of psychiatric disorder are also associated with an increased risk of cardiac anomalies<sup>44</sup>. As such, these CNVs are often associated with complex multifactorial pathology and therefore can offer opportunities to examine the systems of patients with these mutations that have presented with non-psychiatric symptoms.

The most consistent association between these CNVs and neurological disorders is an increased risk of intellectual disability or developmental delay, which is a known phenotype of 14 of the 15 CNVs<sup>42,44-54</sup>. On the other hand, only 4 of the 15 CNVs have been significantly associated with an increased risk of developing bipolar disorder<sup>55-58</sup>. Furthermore, 4 CNV loci (1q21.1, 15q11.2, 16p11 and 22q11) have deletions and duplications spanning the same region, which are also associated with an increased risk of developing psychiatric disorders (Table 1.1). In 3 of the 4 reciprocal CNVs, one form of the CNVs (either the duplication or deletion) is significantly associated with an increased risk of developing all 4 psychiatric disorders (ASD, bipolar, intellectual disability and schizophrenia) whereas the other form is associated with only 2 of these disorders<sup>41</sup>. This suggests that there may be general mechanisms affected by any change in the expression of a gene underlying common risk for neurodevelopmental and psychiatric disorders. Although there are likely also genes within these CNVs and specific mechanisms which are only affected by an increase or decrease in the expression of specific genes which underly risk for specific neurodevelopmental and psychiatric disorders. Therefore, with the use of one of these differential CNV loci, it is possible to investigate common mechanisms which underly an increased risk of developing any psychiatric disorder whilst simultaneously researching mechanisms which may be more specific to an individual disorder.

### 1.1.3 Clinical significance of copy number variation at the 1q21.1 locus

The 1q21.1 region of the human genome carries at least four low copy number repeats, forming the substrate for the origin of CNVs, which explains the complex architecture of the CNVs in this area<sup>45</sup>. There are 5 types of CNVs which have been identified in this region<sup>59</sup> stratified by the deletion or duplication of this area and then

further delineated by the inclusion of two adjacent regions termed the thrombocytopenia with absent radius (TAR) and distal region (Figure 1.1). The TAR region is a complex gene rich region which is associated with the TAR syndrome. This syndrome is associated primarily with blood and skeletal issues<sup>60</sup> and has not been directly associated with an increased risk of developing psychiatric disorders. However, the TAR region has only been described as a microdeletion when examined separately from the distal region of 1q21.1 (Figure 1.1). The distal region of 1q21.1 can be found both deleted and duplicated and both with and without TAR region involvement; in some rare cases, a complex TAR deletion can be associated with a distal duplication (Figure 1.1).

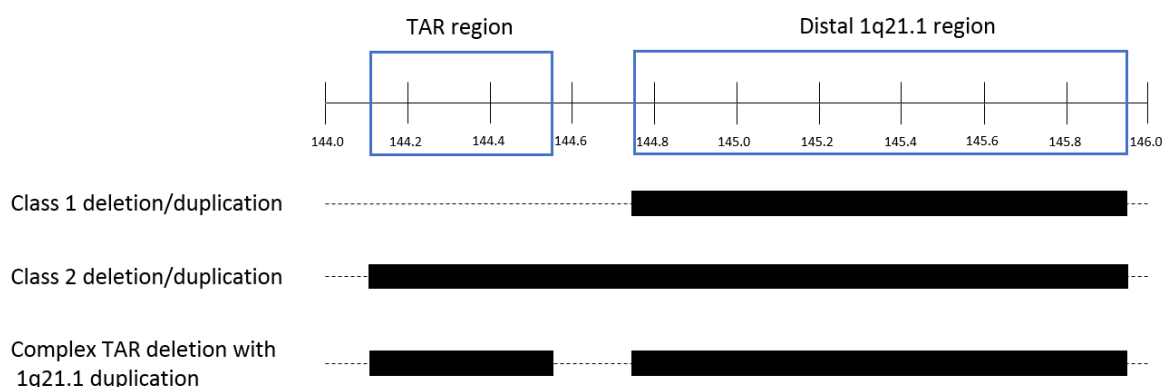


**Figure 1.1: Diagrammatic representation of the classification of 1q21.1 deletions and duplications.** Class 1 mutations involve the distal region whereas class 2 mutations involve both the TAR and distal regions. Finally, very rare cases have been identified with a TAR deletion and a duplication of the distal region (adapted from Brunetti-Pierri et al.<sup>45</sup>).

It is distal 1q21.1 CNVs which have been associated with an increased risk of developing psychiatric disorders<sup>45</sup>. However, similarly to other CNVs associated with psychiatric disorders, the 1q21.1 deletions and duplications also commonly present with other clinical features. The most common clinical features are facial dysmorphia<sup>42</sup>, cardiac abnormalities<sup>61,62</sup> and intellectual disability<sup>42</sup> which are all common to both deletions and duplications, although the prevalence between the two does differ. Deletion or duplication of the distal 1q21.1 region has also been linked to microcephaly and macrocephaly, respectively<sup>45</sup>. When specifically examining the relationship between the distal 1q21.1 CNV and psychiatric disorders, it has been reported that the deletion has a more significant association with an increased risk of developing schizophrenia, whereas the duplication is more significantly associated with an increased risk of developing ASD<sup>63</sup>. Therefore, while 1q21.1 deletions and duplications are associated with distinct clinical presentations the

shared associations with psychiatric disorders present an interesting paradigm to investigate the role of gene dosage on neurodevelopmentally relevant phenotypes.

#### 1.1.4 Genetic architecture of the 1q21.1 locus

While there are 28 genes within the combined TAR and distal regions of the 1q21.1 locus<sup>64</sup>, there are 12 genes which are contained within the class 1 deletions and duplications (Table 1.2). Studies have identified one of the gap junction proteins (Gap Junction Protein Alpha 5, *GJA5*) as being the most influential on prevalence of cardiac abnormalities associated with the distal 1q21.1 CNV<sup>61</sup>. Recent work has also identified the Notch 2 N-Terminal Like (*NOTCH2NL*) genes as playing a role in the correct development of the human cortex, providing a source of speculation as to the cause of the microcephaly/macrocephaly phenotypes commonly associated with distal 1q21.1 mutations<sup>65</sup>. There are several other genes found in this CNV which may also have key functions in neuronal systems including BCL9 Transcription Coactivator (*BCL9*), Hydrocephalus-Inducing Protein Homolog Like (*HYDIN1L*) and Chromodomain Helicase DNA Binding Protein 1 Like (*CHD1L*). *BCL9* functions as part of the WNT signaling pathway a key signaling pathway involved in the development of the central nervous system<sup>66</sup>. Furthermore, a GWAS meta-analysis identified SNPs in *BCL9* as associated with negative symptoms in schizophrenia<sup>67</sup> (defined using the assessment of negative symptoms described in phs000167.v1.p1). *HYDIN1L* is a paralog of the *HYDIN* gene; duplication of which causes hydrocephalus in mice<sup>68</sup>. Finally, *CHD1L* is a helicase DNA-binding protein involved in the modification of chromatin structure and by extension gene expression. The paralog of this gene, *CHD1*, is associated with a separate neurodevelopmental disorder (Pilarowski-Bjornsson syndrome) which is chiefly characterized by developmental delay and speech apraxia<sup>69</sup>. However, there is no direct evidence currently for how these mutations facilitate the increased risk for psychiatric disorders associated with 1q21.1 mutations and which specific genes are mediating this increased risk. While there are many genes in this CNV with known involvement in neurodevelopmental phenotypes, this CNV remains an untapped resource for gathering valuable insight into the pathogenesis and etiology of psychiatric disorders.

**Table 1.2: Genes within both the TAR and distal regions of the 1q21.1 locus.** Functions are listed only when clear evidence is present either based on previous work or structural analysis of the protein (information collated from GeneCards<sup>64</sup>)

Gene	TAR or Distal	Full Name	Function
ACP6	Distal	Acid Phosphatase 6, Lysophosphatidic	Histidine acid phosphatase
ANKRD35	TAR	Ankyrin Repeat Domain 35	Unknown
BCL9	Distal	B-Cell CLL/Lymphoma 9	Unknown
CD160	TAR	CD160 Molecule	Natural Killer Cell Receptor BY55
CHD1L	Distal	Chromodomain Helicase DNA Binding Protein 1 Like	DNA helicase protein involved in DNA repair
FM05	Distal	Flavin Containing Monooxygenase 5	Metabolic N-oxidation of the diet-derived amino-trimethylamine (TMA)
GJA5	Distal	Gap Junction Protein Alpha 5	Component of gap junctions
GJA8	Distal	Gap Junction Protein Alpha 8	Transmembrane connexin necessary for lens growth
GPR89A	TAR	G Protein-Coupled Receptor 89A	Voltage dependent anion channel
GPR89B	Distal	G Protein-Coupled Receptor 89B	Unknown
GPR89C	TAR	G Protein-Coupled Receptor 89C	Unknown
HFE2	TAR	Hemochromatosis Type 2	Iron metabolism
HYDIN2	TAR	Hydrocephalus Inducing Homolog 2	Pseudogene
ITGA10	TAR	Integrin Subunit Alpha 10	Collagen binding
LINC00624	Distal	Long Intergenic Non-Protein Coding RNA 624	Long non-coding RNA
LIX1L	TAR	Limb and CNS Expressed 1 Like	Unknown
NBPF24	Distal	Neuroblastoma Breakpoint Family, Member 24	Unknown
NUDT17	TAR	Nudix Hydrolase 17	Unknown
NOTCH2NL	Distal	Notch 2 N-Terminal Like	Notch Signalling
PDZK1	TAR	PDZ Domain Containing 1	Scaffold protein involved in cholesterol metabolism
PEX11B	TAR	Peroxisomal Biogenesis Factor 11 Beta	Peroxisomal proliferation
PIAS3	TAR	Protein Inhibitor of Activated STAT 3	Small ubiquitin-like modifier (SUMO)-E3 ligase
POLR3C	TAR	RNA Polymerase III Subunit C	Component of the RNA polymerase III complex
POLR3GL	TAR	RNA Polymerase III Subunit G Like	Unknown
PRKAB2	Distal	Protein Kinase AMP-Activated Non-Catalytic Subunit Beta 2	Non-catalytic subunit of AMP-activated protein kinase (AMPK)
RBM8A	TAR	RNA Binding Motif Protein 8A	Component of the exon junction complex
RNF115	TAR	Ring Finger Protein 115	E3 ubiquitin-protein ligase
TXNIP	TAR	Thioredoxin Interacting Protein	Cellular redox signalling

### 1.1.5 Established evidence for the clinical effects of 1q21.1 mutations from animal models

Given the clinical relevance of 1q21.1 mutations, previous work has used genes within this region and the contiguous deletion to model increased psychiatric risk in both fly and mouse models. The Protein Kinase AMP-Activated Non-Catalytic Subunit Beta (PRKAB2) mouse model, phenotypically characterized by the International Mouse Phenotyping Consortium, indicated that PRKAB2 is expressed in the adult mouse brain, specifically in the cerebellum and cerebral cortex<sup>70</sup>. Furthermore, this model showed that homozygous deletion of PRKAB2 was lethal at the preweaning stage and that heterozygous deletion significantly decreased mean platelet volume as measured postnatally. Finally, using the pre-pulse inhibition test on this model showed that females with heterozygous PRKAB2 deletions had a significantly decrease pre-pulse inhibition. Pre-pulse inhibition involves examining the change in startle response when a weak stimulus precedes the startling stimulus. Abnormalities in pre-pulse inhibition have been associated with alterations in dopaminergic and glutamatergic neurotransmission and have been robustly associated with schizophrenia<sup>71-73</sup>. This description of PRKAB2 indicates that loss of expression has effects on a phenotype commonly associated with models of psychiatric disorders.

PRKAB2 has also been used as the basis for generating a fly (*D. melanogaster*) model using deletion of the PRKAB2 ortholog AMPK $\beta$  in the nervous system<sup>74</sup>. This work showed that these flies were more sensitive to starvation and were unable to sleep properly. Specifically, AMPK $\beta$  was shown to be required for initiation and maintenance of sleep following sleep deprivation. Deletion of AMPK $\beta$  also reduced the dendritic branching in class-IV sensory neurons indicating a specific role in neuronal morphology and maintenance. Furthermore, this model shows learning deficits as measured by courtship conditioning. While using this model system limits assessment of more complex behavioral phenotypes seen in humans, this evidence suggests that deletion of PRKAB2 has demonstrable effects on neuronal morphology and more complex behaviors.

The International Mouse Phenotyping Consortium have also phenotyped a CHD1 (paralog of the 1q21.1 gene CHD1L) gene knockout resulting in many developmentally relevant phenotypes<sup>70</sup>. Firstly, homozygous knockout of CHD1 is lethal, definitively proving its necessity during development. The heterozygous knockout of CHD1 has a significant effect on cranial morphology including the maxilla and tooth morphology, and eye morphology resulting in anophthalmia and abnormal eye morphology. Finally, reduced

dosage of CHD1 has a negative effect on embryonic growth resulting in a decreased postnatal body mass. These results show that CHD1 has a significant effect on early development, indicating that CHD1L is an interesting candidate when evaluating causes of the craniofacial abnormalities and micro/macrocephaly associated with the 1q21.1 mutation.

Finally Nielsen *et al*<sup>75</sup> generated a mouse model of the 1q21.1 microdeletion which encompasses the mouse paralogs of the genes found to be lost in the human 1q21.1 deletion carriers. These mice were shown to be significantly shorter than wild-type littermates and were also slightly lighter. However, there were no significant differences in general behavior, appearance, or gross brain morphology (including myelination and numbers of parvalbumin positive interneurons) reported. The 1q21.1 microdeletion mouse was shown to be more sensitive to psychostimulants than wild-type littermates including an increase in activity associated with a low dose of amphetamine and an increased PCP-induced disruption of pre-pulse inhibition. These phenotypes were reported to be due to alterations in the direct dopamine pathway, specifically alterations in the activity of neurons in the ventral tegmental area. Dysfunction in dopamine production and signaling forms a core hypothesis for the origin of certain symptoms associated with schizophrenia (mainly positive and psychotic symptoms) based on the effects of dopamine receptor antagonists<sup>76</sup> and amphetamine<sup>77</sup>. Therefore, this rodent model suggests that 1q21.1 deletion has significant effects on schizophrenia-related neuronal pathways, providing further evidence that this CNV is particularly relevant to study this paradigm.

Overall, animal models focus on the loss of genes within the 1q21.1 region. These models identify a myriad of phenotypes some of which are associated with schizophrenia related pathways. Therefore, furthering the evidence from human studies which show deletion of the 1q21.1 region is associated with an increased risk of developing schizophrenia.

#### 1.1.6 Cellular mechanisms underlying the pathogenesis of ASD and schizophrenia

Deletion of the 1q21.1 region has been most highly associated with an increased risk of developing schizophrenia whereas duplication of the same locus is most highly associated with developing ASD<sup>41</sup>. While the precise pathogenesis of either disorder, remains unclear previous work has led to the formation of several hypotheses which provide a rationale for the development of these disorders. Historically, schizophrenia has

been the focus of a large body of research which has led to two primary hypotheses for the cellular deficits which cause this disorder. The dopamine hypothesis and the glutamate hypothesis have both been proposed to underly the pathogenesis of schizophrenia. While neither hypothesis provides a perfect explanation for all the symptoms of schizophrenia both hypotheses have merit in describing the pathogenesis of specific symptoms.

The dopamine (DA) hypothesis of schizophrenia states that schizophrenia may be related to a relative increase in DA-dependant neuronal activity. The primary evidence for this hypothesis is the reaction of schizophrenic patients to drugs that agonise and antagonise DA dependant neuronal activity<sup>78</sup>. It is now well established that drugs that decrease DA activity have anti-psychotic effects<sup>79</sup> whereas drugs that promote DA activity may exacerbate psychotic symptoms of schizophrenia and induce similar symptoms in otherwise healthy individuals<sup>80</sup>. While work on this hypothesis has mostly focussed on the modulation of DA signalling for therapeutic purposes some work has also suggested that these deficits may originate due to deficits in postnatal neurogenesis<sup>81</sup>. Studies have additionally shown that neurodevelopmental insults (specifically prenatal/maternal immune activation) can result in DA dysfunction in adult animals<sup>82-84</sup>. Furthermore, studies<sup>85,86</sup> have suggested that dysfunction in the ventral hippocampus at early developmental stages can cause DA dysfunction and trigger behavioural changes later in development. Therefore, suggesting that DA dysfunction associated with schizophrenia may have a developmental origin pointing towards neurodevelopmental dysfunction as a source of this dysfunction.

However, as previously stated this paradigm has been heavily investigated for pharmacological targeting and first-generation antipsychotics largely focussed on antagonism of the D<sub>2</sub> dopamine receptor<sup>79</sup>. Second generation (or atypical antipsychotics) also antagonise the D<sub>2</sub> dopamine receptor however they also target the serotonin 5-HT<sub>2A</sub> receptor<sup>79</sup>. These treatments are effective in some patients however they largely target the psychotic and negative symptoms of schizophrenia failing to effectively modulate the cognitive symptoms. As discussed extensively by Kesby *et al.*<sup>87</sup> the lack of novel drugs targeting the DA dysfunction associated with schizophrenia suggests that the current paradigms for investigating the DA hypothesis of schizophrenia are insufficient for the advancement of this hypothesis. Overall, the DA hypothesis of schizophrenia provides a clear explanation for the origin of some of the symptoms associated with this disorder (primarily the negative and psychotic symptoms).

In a similar fashion to the DA hypothesis the glutamate hypothesis of schizophrenia finds evidence from the action of N-methyl-D-aspartate receptor (NMDAR) antagonists which can induce schizophrenia-like symptoms<sup>88,89</sup>. Unlike the DA hypothesis the glutamate hypothesis of schizophrenia has been suggested to underly the cognitive symptoms of schizophrenia<sup>90</sup>. The administration of phencyclidine (PCP) or ketamine (both NMDAR antagonists<sup>89</sup>) has been shown to induce both the negative symptoms and the cognitive dysfunction associated with schizophrenia<sup>91,92</sup>. Furthermore, the effects of these drugs remain in the absence of dopamine activity<sup>93-95</sup> suggesting a separate mechanism driving this pathogenic mechanism.

More recent work has demonstrated gene expression changes in NMDAR related genes associated with schizophrenia<sup>96-98</sup>. There is also evidence that NMDA dysfunction associated with schizophrenia can be driven by both neuronal<sup>99</sup> and glial<sup>100-102</sup> dysfunction. Evidence from human brain tissue shows morphological changes of dendrites in glutamatergic neurons of the cerebral cortex in schizophrenia patients along with reduced levels of synapse markers<sup>103</sup>. However, NMDAR dysfunction in inhibitory neurons has also been suggested to be of particular relevance as this may result in widespread disinhibition of glutamatergic neurons<sup>99</sup>.

The link between disinhibition of excitatory glutamatergic neurons and dysfunction of GABAergic interneurons (explored by Gordon<sup>104</sup>) clearly links this pathogenic mechanism with the concept of excitatory/inhibitory dysfunction which is a mechanism thought to underly the pathogenesis of other psychiatric disorder including ASD. Indeed, while the pathogenic mechanisms of ASD are less widely explored than schizophrenia perhaps due to the lack of historic literature on this topic one of the familiar themes is alterations in the balance of excitation and inhibition<sup>105</sup>. Similarly, to schizophrenia this dysfunction has been suggested to be a result of dysfunction in glutamate signalling. However, the precise cellular mechanisms are considerably less well understood in this case.

The concept of ASD as a disorder of excitatory/inhibitory imbalance was popularized by Rubenstein and Merzenich<sup>106</sup> who suggested ASD was caused by reduced GABAergic signalling resulting in cortical hyper-activity. More recent evidence from monogenic and syndromic forms of ASD has suggested that dysfunction in both excitatory and inhibitory neurons (see review by Nelson and Valakh<sup>105</sup>) can be associated with the pathogenesis of this disorder. Therefore, while the precise cellular mechanism may be less

well understood in ASD compared to schizophrenia the balance between excitation and inhibition forms a key mechanism which may underly the pathogenesis of both disorders.

Another broader pathogenic mechanism suggested to underly the development of both ASD and schizophrenia is dysfunction in connectivity. In ASD the primary finding in terms of connectivity has been reduced long range connectivity with increased local connectivity in specific brain regions (reviewed by Amaral *et al.*<sup>107</sup> and Judson *et al.*<sup>108</sup>). The dysfunction in connectivity has also been indicated in diffusion tensor imaging studies which have indicated abnormalities in multiple white matter tracts<sup>109,110</sup> pointing towards oligodendrocyte or myelin dysfunction. The phenotype of aberrant connectivity has been suggested to influence the balance of excitation and inhibition on a more global scale adding to the disturbances seen in this phenotype<sup>106</sup>. Similarly in schizophrenia dysfunction in connectivity across brain regions has been associated with the cognitive symptoms of this disorder<sup>111</sup>. Furthermore, a study<sup>112</sup> differentiating patients based on a clinical staging model separating prodromal, first episode and chronic patients showed increasingly widespread functional dysconnectivity over the course of the disorder from prodromal to chronic patients. Finally, white matter abnormalities have been more consistently reported in schizophrenic patients<sup>113-115</sup> further indicating a link between long range connectivity and schizophrenia pathogenesis. Taken together these studies provide clear evidence for dysfunction in long range connectivity in both ASD and schizophrenia which may be mediated by dysfunction in both neurons and glia.

Disruption of neuronal connectivity and imbalances between excitation and inhibition are both large scale explanations for the pathogenesis of both ASD and schizophrenia. However, underlying these overarching phenotypes is synaptic dysfunction which has also been evidenced in both disorders and may underpin the dysfunction driving other hypotheses for the pathogenesis of ASD and schizophrenia. A recent meta-analysis of synaptic protein and mRNA levels<sup>116</sup> found evidence for a decreased expression of the pre-synaptic marker synaptophysin in the hippocampus and cingulate cortices. A similar meta-analysis also showed evidence for a decrease in the density of postsynaptic elements in schizophrenia<sup>117</sup>. These results support earlier hypotheses that grey matter loss (without neuronal degeneration) and the temporal onset of schizophrenia point towards a loss of synapses as a critical feature of schizophrenia<sup>118</sup>. Furthermore, analysis based on schizophrenia GWAS data<sup>119</sup> showed synapse related genes including post synaptic density genes and genes involved in synaptic plasticity account for significantly enriched heritability

for schizophrenia. Therefore, suggesting that the genetic risk for schizophrenia converges on synaptic dysfunction. Finally using a brain imaging paradigm Onwordi *et al.*<sup>120</sup> inferred a decrease in synapse density in schizophrenic patients (specifically in the anterior cingulate cortices) and further showed in a rat model that this measure was not changed by the administration of an antipsychotic.

Similarly to schizophrenia the genetic risk for ASD coalesces on genes related to synapses including cell adhesion molecules, scaffold proteins and protein involved in synaptic signalling<sup>121</sup>. Furthermore, multiple syndromic forms of ASD have been associated with synaptic dysfunction resulting in altered neuronal function<sup>122,123</sup>. There have also been reports that genes which are associated with syndromic forms of ASD may play roles in the correct elimination of synapses<sup>124</sup>. Additionally, mouse models of ASD (15q11–13 duplication and neuroligin-3 R451C point mutation) show similar deficits in synapse maintenance and stability<sup>125</sup>. However unlike in schizophrenia direct imaging of post-mortem tissue establishing the precise nature of synaptic dysfunction or loss in this disorder is lacking. Overall, there is clear evidence that synaptic dysfunction plays a role in the pathogenesis of schizophrenia and ASD.

The synaptic dysfunction associated with both ASD and schizophrenia has also been suggested to be a result of aberrations in the function of microglia and the immune system. Microglia are the resident immune cells of the brain and are involved in the process of synaptic pruning during postnatal development. Therefore, overactivation of microglia caused by a combination of genetic and environmental factors would cause a loss of synapses and other synaptic dysfunctions. There is evidence that ASD patients have increased microglial activation<sup>126-128</sup> accompanied by an increased level of inflammatory cytokines and chemokines<sup>129</sup>. Beyond activated microglia inducing increased synaptic pruning the increased level of cytokines has also been shown to affect neuronal synaptic function<sup>129</sup>. Furthermore, maternal immune activation has been shown to be an important risk factor for ASD<sup>130,131</sup>. This is also mirrored by schizophrenia with multiple murine schizophrenia models based on maternal immune activation able to induce the symptomology and cellular deficits commonly associated with schizophrenia murine models<sup>130</sup>. Work by Sellegren *et al.*<sup>132</sup> also showed an increased synapse elimination using schizophrenic patient derived microglia. Overall, there is evidence that synaptic dysfunction associated with both ASD and schizophrenia may be a result of aberrant

microglia function caused by overactivation of the immune system further indicating the importance of glial cells to the pathogenesis of ASD and schizophrenia.

Ultimately all the pathogenic mechanisms detailed above can be linked directly or indirectly with dysfunction during neurodevelopment<sup>133</sup>. Small scale changes like the loss or perturbation of synapses (caused by genetic or environmental factors) are likely to be most pronounced during neurodevelopment when a large proportion of synapses are established. These changes can propagate and along with other neurodevelopmental deficits caused by genetic or environmental factors can lead to deficits in DA and NMDA signalling. Furthermore, developmental deficits in myelination and oligodendrocyte development (which have been reported in schizophrenia<sup>113,134</sup>) can compound issues of neuronal connectivity generated by dysfunction in other systems. Finally, these phenotypes can lead to the aberrant development of excitatory and inhibitory systems both at a local and global scale which can lead to chronic imbalances in these systems. The deficits in the balance of excitation and inhibition are also likely to effect signalling through DA and NMDA dependant pathways. Therefore, while there are many individual pathogenic mechanisms that have been proposed for both ASD and schizophrenia it is critical not to examine any one mechanism to the exclusion of all others as there is likely interconnectivity between pathogenic mechanisms. Furthermore, deficits which appear on the surface simple (i.e. reduction in synapse production or myelination potential) can have profound effects when propagated through complex multicellular tissues which rely on tightly controlled system for optimum functionality. Thus, reductionist models (like iPSC derived neurons and glia) are important to understand the fundamental cellular deficits which may underly the complex pathogenesis of these disorders. However, increasing the complexity of these models and using them to investigate paradigms that are directly relevant to the mechanisms discussed in this section remains critical to the further development of this field.

#### 1.1.7 Modelling 1q21.1 phenotypes using human iPSCs

There is clear evidence that CNV at the 1q21.1 locus is associated with increased risk for developing neurodevelopmental and psychiatric disorders, and genes within this region are likely to play roles in the development of the human CNS. However, as yet there has been no investigation of the precise cellular phenotypes resulting from deletion or duplication of the 1q21.1 region using human models. Induced pluripotent stem cells

(iPSCs) provide a critical model to investigate the effect of 1q21.1 mutations on neuronal and glial development. The advent of induced pluripotent stem cells<sup>135</sup> generated from adult somatic cells (like fibroblasts) by expression of key transcription factors has allowed the development of protocols to generate human derived neurons and glia that resemble their *in vivo* counterparts.

iPSCs can be used to model neuronal development by differentiating iPSCs into neurons and glia, which can be done using multiple paradigms each with key advantages and limitations. Broadly there are two approaches to differentiating iPSCs into neuronal cells, direct differentiation involves the overexpression of key transcription factors and developmental patterning involves recapitulating the signalling which drives *in vivo* development. Both approaches have been shown to produce functional neurons<sup>136-138</sup> and glia<sup>139-142</sup> which can be used as a basis to understand the effect of 1q21.1 mutations. Assessing the phenotypes associated with mutations in iPSC derived neuronal cells is largely dependent on the mutation under investigation and the specific sub-type of cell being generated.

One of the common mechanisms proposed to underly the development of both ASD and schizophrenia is alterations in the balance between excitation and inhibition<sup>143</sup>. While examining the balance between excitation and inhibition is difficult using neurons generated from iPSCs; technologies such as multiple electrode arrays (MEAs) have allowed more complex analysis of neuronal function. MEAs are microscopic arrays of electrodes which can measure the extracellular action potentials (or field potentials) of neurons. This activity can then be related to spatial and temporal information resulting in a more complex view of neuronal activity. This technology can therefore be used to begin to understand the formation of neuronal networks which may in turn be disrupted causing an imbalance of excitation and inhibition<sup>144</sup>. As this technique relies upon predominantly excitatory neurons excitatory glutamatergic neurons are a particularly interesting cell type to examine. Protocols to generate glutamatergic neurons are robust<sup>145,146</sup> and the cells produce have been shown to form functional neuronal networks on MEAs<sup>144</sup>. Furthermore, this population of cells allows the investigation of cortical development and synapse formation, both key aspects of development which have been shown to be dysregulated in psychiatric disorders. Therefore, glutamatergic neurons provide a platform to assess the developmental and function consequences of 1q21.1 mutations in paradigms relevant to the pathogenesis of psychiatric disorders.

Another suggested link between psychiatric disorder is the concept of dysconnectivity which has been suggested to underly multiple disorders<sup>147,148</sup>. This concept integrates not only neuronal dysfunction but also suggest one possible mechanism by which the glial dysfunction now commonly being associated with psychiatric disorders<sup>132,149,150</sup> may manifest. There has been a large body of work which has identified changes in white matter<sup>151</sup>, myelination<sup>152</sup> and oligodendrocytes<sup>153,154</sup> as associated with the pathogenesis of psychiatric disorders. There are strong associations between schizophrenia and oligodendrocyte pathology. The apparent loss of myelination associated with schizophrenia is likely to have profound effects on the connectivity of neuronal circuits and therefore may compound phenotypes observed directly in neurons.

Recent advances in the generation of oligodendrocytes from iPSCs have resulted in protocols which can now robustly generate mature myelinating cells<sup>155,156</sup>. Importantly these protocols result in oligodendrocyte development comparable to that seen in humans<sup>156</sup> and therefore offer a critical system to investigate the deficits in oligodendrocyte development and function associated with schizophrenia. While the assessment of neuronal dysfunction associated with psychiatric disorders is still a critical facet of understanding the pathogenesis of these disorders the glial component of psychiatric risk remains poorly understood. Deletion of the 1q21.1 locus present an opportunity to investigate oligodendrocyte dysfunction associated schizophrenia using iPSC derived oligodendrocytes.

Monoculture 2D iPSC-based models remain a critical tool in identifying cellular dysfunction associated with psychiatric disorders and present the best opportunity to dissect the complex phenotypes observed in individual cell types. However, these types of models fail to recapitulate much of the complexity found in human CNVs. Therefore, exploring methods which can be used to better model the complexity of neuronal systems is becoming increasingly important in understanding the complex multicellular deficits associated with increased risk for psychiatric disorders. With the goal of identifying both individual cellular dysfunction and the contribution of that dysfunction to abnormalities seen at the systems level. Organoids and bioprinting currently present the best approaches for modelling multicellular neuronal interactions. However, while cerebral organoids<sup>157</sup> generated from iPSCs are becoming a popular choice for 3D neuronal models there remains

a lack of literature on the feasibility of using bioprinting as an alternative for generating 3D neuronal models using iPSC derived neuronal cell types.

Overall, 1q21.1 deletions and duplications present a novel basis for investigating increased risk for developing psychiatric disorders. Using patient derived iPSCs allows for the dissection of specific cellular deficits associated with these mutations. Finally, investigating alternative approaches which can be used to generate more complex cellular models may provide the future basis of understanding how the dysfunction in disparate cell types results in the complex clinical presentation seen in patients.

### 1.1.8 Aims and objectives

The studies presented in this thesis focus on developmental patterning approaches to generate neuronal cells from human iPSCs as these approaches allow dissection of developmental phenotypes associated with 1q21.1 mutations. This is of interest given the link between 1q21.1 mutations and neurodevelopmental disorders and phenotypes. Therefore, the first two results chapters of this work will focus on phenotypes associated with neuronal and oligodendrocyte development respectively.

While 1q21.1 deletions and duplications share some clinical associations there are also clear clinical distinctions between these two mutations. Deletion of the 1q21.1 locus is associated primarily with microcephaly and an increased risk of developing schizophrenia. On the other hand, duplication of the 1q21.1 locus is associated with macrocephaly and an increased risk of developing ASD. Therefore, the objectives of the first two results chapters are to elucidate cellular deficits which may underly the specific clinical features of 1q21.1 deletions and duplications.

Reductionist approaches using iPSC derived monocultures provide critical systems to understand the cellular dysfunction associated with genetic risk factors for psychiatric disorders. However, they fail to capture the combined effect of more complex cellular systems. Therefore, the third results chapter focuses on the use of bioprinting to develop a model which may be able to capture more of the complexity seen in the human CNS. The objective of this chapter is to assess the feasibility of using bioprinting in this endeavour and the effect this technique has on iPSC derived astrocytes and neurons.

## 2. Material and Methods

Methods presented in this chapter were used in the generation and assessment of 1q21.1 deletion/duplication neurons and oligodendrocytes.

### 2.1 iPSC culture

#### 2.1.1 Ethics Statement

Generation and use of human iPSC were approved by the Cardiff University and HSE (GMO130/19.3). All methods were performed in accordance with the approved guidelines. Clinical and psychometric testing of participants and skin biopsies were approved by the Regional Ethics Committee of the National Health Service (study 14/WA/0035). Formal informed consent was obtained from all subjects.

#### 2.1.2 Generation

Fibroblasts were collected and maintained by Dr. Craig Joyce. Fibroblasts were reprogrammed into induced pluripotent stem cells (iPSCs) using the CytoTune™-IPS 2.0 Sendai reprogramming kit (ThermoFisher Scientific) according to the manufactures recommended protocol. Specifically, fibroblasts were grown in fibroblast media (DMEM, 10% FBS, 1x Non-essential amino acids (NEAA) and 55  $\mu$ M  $\beta$ -mercaptoethanol all from Gibco™) until 50-60% confluent (Day 0). The cells were then transduced with the 3 viral mixes and were incubated overnight before the media was replaced. The media was then replaced daily for the subsequent 7 days; for the first 3 days using fibroblast media then with Essential 8™ Flex media (E8F, Gibco™) for the subsequent 4 days. Cells were then passaged onto Geltrex™ (Gibco™) and media was replaced every 48 hours for 2 weeks. Passaging was performed using versene solution (Gibco™) incubating for 5-7 minutes or until cells were detached. Versene solution was inactivated by diluting 1:10 using E8F and cells were collected by centrifugation (200 r.c.f. for 5 minutes) before being re-suspended in the required volume of E8F supplemented with RevitaCell™ supplement (Gibco™). Geltrex™ culture ware was prepared by incubating a 1:100 dilution of Geltrex™ (stored as undiluted aliquots at -80°C) in DMEM/F12 (Gibco™) on culture ware in a 37°C incubator. Clear iPSC like morphology was observed as early as day 10.

After 2 weeks colonies were isolated by manual picking, and each colony was individually expanded (at least 8 colonies per fibroblast line). Individual colonies were picked into a well on a 96 well plate then when the colony covered more than 1/3 of the

well surface it was passaged. Colonies were incubated with RevitaCell™ supplement for 1 hour then passed into a single well on a 48 well plate using versene solution and scratching. Again, cells were expanded until they covered at least 1/3 of the well surface and then they were passaged in a similar fashion as previously into a well on a 24 well plate. This process was repeated increasing the size of wells used until cells were covering 1/3 of a well on a 6-well plate at which point they were again passaged in a similar manner and re-plated at a 1:6 ratio. Once each cell line was growing in a complete 6 well plate each line was considered an iPSC line at passage 0.

During the first 2 passages after the expansion phase, cells were incubated with RevitaCell™ supplement for 1 hour before passaging. Passaging was done using versene solution to dissociate cells before manually scratching cells off the cell culture surface. After the first 2 passages cells were passaged without the use of RevitaCell™ supplement unless indicated by a low cell number or an estimated >70% loss of cells during passaging. Cell were re-plated at a ratio between 1:3 and 1:6 for all passages. Once these colonies had been expanded sufficiently (a minimum of 3 passages) a single clonal line was selected which showed the best morphology and survival through passaging without the addition of RevitaCell™ supplement. While all other lines were frozen for storage in liquid nitrogen (see section 2.1.3) the selected cell lines (one from each of the original patient lines) were sub cloned 3 times. Sub-cloning was carried out by plating cells at low density (<10,000 cells/cm<sup>2</sup>), feeding and maintaining cells until colonies were ~100 cells in size and then individual colonies which showed ideal morphology were manually picked and expanded. Once lines were established DNA was isolated using a DNeasy Blood & Tissue Kit (Qiagen) according to the manufacturer's recommended protocol. The DNA was then sent for sequencing to confirm the original CNV diagnosis. Sequencing and CNV calling was performed by Dr. Elliot Rees. Cell lines were also differentiated using the STEMdiff™ Trilineage Differentiation Kit (Stemcell Technologies) as per the manufacturer's protocols. Trilineage differentiations and subsequent staining were performed by Sharna Lunn.

### 2.1.3 Maintenance

Induced pluripotent stem cells were grown on Geltrex™ coated plates in E8F media with media changed every 48 hours and were maintained between 30 and 80% confluency at 37°C and 5% CO<sub>2</sub> unless otherwise stated. When iPSCs were between 70 and 80% confluent they were passaged using versene solution and manual dissociation. Briefly,

iPSCs were washed with DPBS (Gibco™) and incubated with versene solution for 2-3 minutes at 37°C. Versene solution was then removed and fresh E8F media was added to the cells. Cells were then detached by scratching the surface with a 2- or 5-mL serological pipet and cells were then resuspended and re-plated at a ratio of between 1:3 and 1:6.

#### 2.1.4 Freezing

For cryostorage, cells were incubated with RevitaCell™ supplement for a minimum of 1 hour before the media was collected and cells were dissociated using versene in a similar manner to that described for passaging (see section 2.1.2) preserving a large colony size. Once detached cells were centrifuged (at 120 r.c.f. for 3 minutes), the supernatant was removed, and cells were lightly resuspended in 500 µL conditioned media for every well of a 6-well plate (or equivalent) that the cells originated from. Cryopreservation media was prepared using the conditioned media by adding 20% Dimethyl Sulfoxide (DMSO, Sigma-Aldrich). Cryovials were prepared with 500 µL of cell suspension and then an equal volume of cryopreservation media was added dropwise while mixing. Cryovials were then frozen to -80°C at -1°C per minute before being stored in liquid nitrogen.

#### 2.1.5 Defrosting

To recover cells from cryostorage vials were partially defrosted in a 37°C water bath until approximately half of the solution was still frozen. Warm E8F media was then added to finish defrosting the cells and the cells were resuspended in a total volume of 10 mL using E8F media, all manipulation involving defrosted cells were carried out using 5mL serological pipettes. The suspension was then centrifuged (at 120 r.c.f. for 5 minutes), the supernatant was removed and 2 mL E8F media containing RevitaCell™ supplement was added before cells were plated on Geltrex™ coated plates. Cells were incubated for 48 hours before the media was changed and were maintained for a maximum of 7 days before passaging. Once successfully defrosted cells were passaged at least once before use in further experiments.

## 2.2 Neuronal differentiation

The protocol for generating cortical excitatory neurons is based on the dual SMAD inhibition protocol published by Chambers *et al.*<sup>145</sup> with modifications based on work published by Telezhkin *et al.*<sup>146</sup> and Qi *et al.*<sup>158</sup>.

### 2.2.1 Neuronal media formations

**N2B27 media:** was comprised of 2/3 DMEM/F12 (Gibco™) and 1/3 Neurobasal (Gibco™) supplemented with N2 supplement (1:150, Gibco™) and B27 supplement (1:150, Gibco™) either with or without vitamin A depending on the stage of differentiation. The use of B27 with vitamin A is denoted by + and the use of B27 without vitamin A is denoted by -. This media was further supplemented with  $\beta$ -mercaptoethanol (55  $\mu$ M, Gibco™) and a cocktail of antibiotics and antimycotics (1:100, Sigma-Aldrich).

**BrainPhys:** media was comprised of BrainPhys™ Neuronal Medium (Stemcell Technologies) supplemented with ascorbic acid (200  $\mu$ M, Sigma-Aldrich), B27 supplement (1:50), BDNF (10 ng/mL, Peprotech) and a cocktail of antibiotics and antimycotics (1:100).

### 2.2.2 Generation of neuronal precursors

Induced pluripotent stem cells were maintained in E8F media on Geltrex™ until 90-100% confluent at which point the media was changed to N2B27- supplemented with LDN-193189 (LDN, Cambridge Bioscience) at 250 nM and SB431542 (SB, Stratech) at 10  $\mu$ M. For the subsequent 10 days half the media was changed every other day using fresh N2B27- supplemented with LDN and SB.

The cells were then incubated with Y-27632 (Stratech) at 10  $\mu$ M in un-supplemented N2B27- for 1 hour and the media was collected. Cells were then passaged using versene solution (see section 2.1.2) onto fibronectin (15  $\mu$ g/mL, Millipore) coated plates at a 2:3 ration in 1:1 conditioned to fresh media. Half the media was then replaced every other day for the following 10 days using un-supplemented N2B27-. At which point cells were considered neuronal precursor cells (NPCs) and were used in downstream experiments; frozen for long term storage or were terminally differentiated into cortical excitatory neurons.

### 2.2.3 Freezing and defrosting neuronal precursors

For cryostorage, cells were incubated with Y-27632 for a minimum of 1 hour and then dissociated by incubating with Accutase™ (Sigma-Aldrich) for 7-10 minutes at 37°C. Accutase™ was subsequently inactivated by a minimum of 1:5 dilution in DMEM/F12. Cells were then collected by centrifugation (at 200 r.c.f. for 5 minutes). The supernatant was removed, and cryopreservation media was added containing 20% DMSO. Cryovials were then frozen to -80°C at -1°C per minute before being stored in liquid nitrogen.

To recover cells from cryostorage vials were partially defrosted in a 37°C water bath. Warm N2B27- media was then added to finish defrosting the cells. The suspension was then centrifuged (at 200 r.c.f. for 5 minutes), the supernatant was removed and fresh N2B27- media was added before cells were plated onto poly-D-lysine (10 µg/mL, Sigma-Aldrich) and laminin (20 µg/mL, Roche or Sigma-Aldrich). Defrosted NPCs after 24 hours recovery were considered identical to passed NPC at day 20 of differentiation.

### 2.2.4 Terminal differentiation of cortical excitatory neurons

Day 20 neuronal differentiations were passaged using Accutase™ as previously described (see section 2.2.3) at a ratio of (1:4) onto poly-D-lysine (10 µg/mL) and laminin (20 µg/mL) coated cultureware (chamber slides, coverslips or multi-well plates) at a density of  $2.5-3.5 \times 10^5$  per  $\text{cm}^2$ . The media was changed to N2B27+ and cells were left to adhere and recover for 48 hours. After 48 hours the media was changed and CultureOne™ supplement (Gibco™) was added to the media.

After two days half the media was replaced with fresh N2B27+ with CultureOne™ supplement. After a further day the media was replaced with fresh N2B27+ supplemented with DAPT (5 µM, Stratech) and PD0332991 (5 µM, Stratech) and again half the media was replaced every 2 days with fresh media. After 7 days the media was changed to fresh N2B27+ without any further supplements. Cells were then maintained at 37°C and 5% CO<sub>2</sub>; collections for RNA, protein and immunofluorescence were taken periodically, after 40 days of differentiation cells were passaged and used for calcium imaging and after 50 days of differentiation cells were used for MEAs.

### 2.3 Oligodendrocyte differentiation

The protocol for the generation of oligodendrocytes is based on previous work by Douvaras and Fossati<sup>159</sup> with minor modifications.

#### 2.3.1 Oligodendroglial media Formations

**Basal media:** was comprised of DMEM/F12 supplemented with NEAA (1x), alanyl-glutamine (2 mM, Sigma-Aldrich), 2-mercaptoethanol (55  $\mu$ M) and antibiotics and antimycotics (1x)

**Neural induction media:** was comprised of basal media supplemented with SB (10  $\mu$ M), LDN (250 nM), retinoic acid (100 nM, Sigma-Aldrich) and insulin (25  $\mu$ g/ml, Sigma-Aldrich)

**N2 media:** was comprised of basal media supplemented with N2 supplement (1:100), SAG (1  $\mu$ M, Stratech) and retinoic acid (100 nM)

**OPC media:** was comprised of basal media supplemented with N2 supplement (1:100), B27 supplement without vitamin A (1:50), SAG (1  $\mu$ M), retinoic acid (100 nM) and insulin (25  $\mu$ g/ml)

**PDGF media:** was comprised of basal media supplemented with N2 supplement (1:100), B27 supplement without vitamin A (1:50), PDGF $\alpha\alpha$  (10 ng/mL, Cambridge Bioscience), IGF-1 (10 ng/mL, R&D systems), HGF (5 ng/mL, Gibco™), NT3 (10 ng/mL, Insight), T3 (60 ng/mL, Sigma-Aldrich), cAMP (1  $\mu$ M, Sigma-Aldrich) and insulin (25  $\mu$ g/mL).

**PDGF light media:** was comprised of basal media supplemented with N2 supplement (1:100), B27 supplement without vitamin A (1:50), PDGF $\alpha\alpha$  (5 ng/mL), IGF-1 (5 ng/mL), HGF (5 ng/mL), NT3 (10 ng/mL), T3 (100 ng/mL), cAMP (10  $\mu$ M) and insulin (25  $\mu$ g/mL).

**Maturation media:** was comprised of basal media supplemented with N2 supplement (1:100), B27 supplement without vitamin A (1:50), HEPES (10 mM,

Sigma-Aldrich), T3 (60 ng/mL), Biotin (100 ng/mL), cAMP (10  $\mu$ M), insulin (25  $\mu$ g/mL) and ascorbic acid (20  $\mu$ g/mL).

### 2.3.2 Generation of ventralized neuronal precursors

Cells were dissociated using Accutase™ as previously described (see section 2.1.3), after centrifugation cells were counted and resuspended in E8F supplemented with RevitaCell™ supplement (1:100) at a density of  $5 \times 10^4$  to  $1 \times 10^5$  cells/mL and then plated into either 6 well plates or cover-slips both coated with Geltrex™. After 48 hours media was changed to neural induction media and media was changed daily for 8 days. Media was then replaced with N2 media for 4 days with media changed daily.

### 2.3.3 Generation of oligodendrocyte precursors

After 12 days of differentiation cells were passaged into ultra-low attachment plates using Accutase™ as previously described (see section 2.2.3) with a 12-minute incubation. Cells were resuspended in OPC media and were passed through a 40 $\mu$ m cell strainer (Stemcell Technologies) before being counted and plated into low attachment plates at a density of  $5 \times 10^5$  cells/mL.

Cells were checked daily for sphere formation or sphere aggregation and cultures were fed by 2/3 media changes every other day. After 48 hours (and assuming clear production of cell aggregates) plates were placed onto a gyratory shaker and were again checked daily for undue sphere aggregation. For media changes cultures were collected in 50mL centrifuge tubes and centrifuged (at 100 r.c.f. for 2 minutes), 2/3 of the media was removed and spheres were resuspended by titration 10 times using a 1 mL pipet. Fresh media was then added, and cells were re-plated into the same ultra-low attachment plates evenly distributing cell aggregates or spheres.

After 20 days of differentiation the media was changed to PDGF media by collecting spheres in 50 mL conical tubes and allowing them to sediment for 5-10 minutes. Most of the media was removed ( $\geq 95\%$ ) taking care not to disturb the sedimented spheres. Fresh PDGF media was added and the spheres were resuspended by titration using a 1mL pipet. Cells were redistributed into the same ultra-low attachment plates. Cells were maintained in PDGF media for the subsequent 10 days with 2/3 media changes performed every other day, cultures were also checked for sphere aggregation and if observed cultures were again titrated 10 times using a 1 mL pipet. To perform media changes spheres were allowed to

sediment for 5-10 minutes in 50 mL centrifuge tubes before 2/3 media was removed and replaced with fresh media.

#### 2.3.4 Terminal differentiation of mature oligodendrocytes by dissociated spheres

After 18 days in non-adherent culture ideal spheres were collected, dissociated and sorted for A2B5+ cells using magnetically activated cell sorting (MACS, see section 2.9) and plated onto poly-ornithine (50 µg/mL, Sigma-Aldrich) and laminin (20 µg/mL) coated plasticware at a density of 20,000 cells/cm<sup>2</sup>. Spheres were manually selected based on density, shape and size with ideal spheres being between 400 and 1200 µm in diameter with smooth spherical shape and a dense core indicated by a dark brown appearance under a standard light microscope. After 2 days cells were fed by replacing 2/3 of the media with fresh PDGF light media with media replacements performed every 3 days afterwards. Cells were grown in the presence of cytarabine (1 µM, Sigma-Aldrich) and were collected for downstream analysis after 25 days (Day 55) or media was changed to maturation media supplemented with cytarabine (1 µM) and cells were maintained for a further 20 days (day 75) before collection and downstream analysis.

#### 2.3.5 Terminal differentiation of mature oligodendrocytes by adherent culture

After 18 days of differentiation in non-adherent cultures ideal spheres were collected and plated onto poly-ornithine (50 µg/mL, Sigma-Aldrich) and laminin (20 µg/mL) coated plasticware. Spheres were manually selected based on density, shape and size with ideal spheres being between 400 and 1200 µm in diameter with smooth spherical shape and a dense core indicated by a dark brown appearance under a standard light microscope. Spheres were incubated for 3 days to allow adherence to the basement membrane and then were fed with PDGF light media every 3 days for 20 days by replacing ½ the media while avoiding any unnecessary movement of the spheres. Spheres were monitored for the production of astrocytes and any sphere producing large numbers of astrocytes (4-8% of spheres from control iPSC) was discarded immediately. Cells were then passaged and sorted using Accutase™ as previously described (see section 2.2.3) using a 20-minute incubation. Cells were plated onto poly-ornithine and laminin coated culture-ware at a density of 15,000 cells/cm<sup>2</sup>. Cells were grown in the presence of cytarabine (1 µM, Sigma-Aldrich) and were collected for downstream analysis after 5 days (Day 55) or media was

changed to maturation media supplemented with cytarabine (1  $\mu$ M) and cells were maintained for a further 20 days (day 75) before collection and downstream analysis.

## 2.4 Calcium imaging

### 2.4.1 Preparation of cells for calcium imaging

Day 40 neuronal differentiations were dissociated using Accutase™ as previously described (see section 2.2.3) and strained through a 40  $\mu$ m nylon mesh before being passaged onto poly-D-lysine (10  $\mu$ g/mL) and laminin (20  $\mu$ g/mL) coated coverslips at a density of 50,000 cells/cm<sup>2</sup>. Cells were then maintained in a 50:50 combination of conditioned and fresh N2B27+ media for 2 days before being switched to BrainPhys media. When media was switched, drugs to modulate calcium homeostasis were added (Calcitriol: 10 nM (EC<sub>50</sub>=0.23nM), Clozapine: 500 nM (EC<sub>50</sub>=11nM), Roscovitine: 15  $\mu$ M (EC<sub>50</sub>=12 $\mu$ M) and Verapamil: 50 nM (EC<sub>50</sub>=17.3nM)) and were maintained through all media changes.

### 2.4.2 Dye loading

After 10 days neurons were loaded with 1 $\mu$ M Calbryte-520™ (AAT Bioquest) for 1 hour in BrainPhys media containing 0.02% Pluronic F127 at 37°C. The media was then replaced with fresh BrainPhys media and cells were incubated for a further hour at 37°C. Coverslips were then transferred into artificial cerebrospinal fluid (aCSF) containing: 125 mM NaCl, 26 mM NaHCO<sub>3</sub>, 1.25 mM KH<sub>2</sub>PO<sub>4</sub>, 2.5 mM KCl, 1 mM MgCl<sub>2</sub>, 2 mM CaCl<sub>2</sub> and 25 mM Glucose (all from Sigma-Aldrich) with or without either DL-AP5 or NQBX (at a final concentration of 10  $\mu$ M, from R&D systems). Coverslips were perfused using aCSF throughout the experiment and were maintained at 37°C.

### 2.4.3 Image acquisition

For each coverslip and condition a minimum of 3 fields were selected based on the presence of clear neuronal morphology and minimal cell density as seen using standard light microscopy. Cells were pre-exposed to fluorescent light for 3 minutes before images were collected. Images were taken using an epifluorescence microscope at intervals of 100ms for 5 minutes.

#### 2.4.4 Data analysis

Masks for the images were created using NeuroCa<sup>160</sup> software this data was then transferred to FluoroSNNAP<sup>161</sup> software (using custom matlab scripts supplied by Dr. Will Plumbly) which identified the calcium transients. The data was then manually curated for events with both a fast rise (<1 second) and fall time (<2 seconds). Regions of interest with 0 calcium events identified were maintained in the data set when calculating percentage of active cells, however they were removed when analyzing for number of calcium events. All data is comprised of a minimum of 3 coverslips differentiated independently. Each coverslip was imaged across a minimum of 3 separate fields each with a minimum of 10 neurons and results from each coverslip were averaged before statistical analysis.

#### 2.5 Multi electrode arrays

##### 2.5.1 Plating cells onto MEAs

Plating and maintenance of MEAs was carried out by Dr. Mouhamed Alsaqati. All experiments were performed using Cytoview MEA 24 well plates (Axion) composed of 24 wells each embedded with 16 electrodes. Multiple electrode arrays were incubated with 0.1% Polyethyleneimine (Sigma-Aldrich) for a minimum of 1 hour. The multiple electrode arrays (MEAs) were then washed with distilled water and left to dry completely (approximately 30 minutes). Cultures to be used for MEA were switched to Brainphys media at least 4 days prior to dissociation. Conditioned media was collected from day 50 neuronal cultures and cells were then dissociated using Accutase™ as described previously (see section 2.2.3) until most of the culture was a single cell suspension (10-12 minutes). The suspension was then centrifuged (at 120r.c.f. for 5 minutes), the supernatant removed, and the pellet resuspended in fresh Brainphys media.

Cells were then counted using a hemocytometer and the cells were again centrifuged and a 1:1 mix of fresh and conditioned media was added achieving a  $5 \times 10^6$  cells/mL suspension. Laminin (20  $\mu$ g/mL) was then added to the cell suspension and 10  $\mu$ l of this suspension was added directly to the MEA electrodes. The MEAs were then placed in a 37°C incubator for 1 hour before further fresh media was added to the MEAs.

## 2.5.2 Data collection and analysis

Readings from MEA plates were recorded by Dr. Mouhamed Alsaqati. Analysis of MEA data was carried out with help from Dr. Mouhamed Alsaqati and MATLAB scripts written by Dr. William Plumbly. The hardware consisted of the Maestro Pro complete with Maestro 768-channel amplifier. Data acquisition was managed by Axion's integrated studio (AxIS 1.5.2). Channels were sampled simultaneously with a gain of 1000× and a sampling rate of 12.5 kHz/channel. During the recording, the temperature was maintained constant at 37°C. A Butterworth band-pass filter (with a high-pass cut-off of 200 Hz and low-pass cut-off of 3000 Hz) was applied along with a variable threshold spike detector set at 5.5× standard deviation on each channel. Offline analysis was achieved with custom scripts written in MATLAB. Briefly, spikes were detected from filtered data using an automatic threshold-based method set at  $-5.5 \times \sigma$ , where  $\sigma$  is an estimate of the noise of each electrode based upon the median absolute deviation <sup>1</sup>. Bursting was detected based on three parameters; inter-burst period longer than 200 ms, more than 3 spikes in each burst and a maximum inter-spike (intra-burst) interval of 300 ms. Network activity was illustrated by creating array-wide spike detection rate (ASDR) plots with a bin width of 200 ms. Further analysis for network bursting was performed using AxIS software (Axion biosystems) specifically the Axion built-in neural metric analysis tool employing the envelope algorithm. The algorithm defines a network burst as an occurrence when the histogram exceeds a threshold of 1 standard deviation above or below the mean with a minimum of 200 ms between SBs and at least 10% of electrodes included. All data is acquired from a minimum of 3 MEA wells each differentiated independently.

## 2.6 Immunocytochemistry

### 2.6.1 Cell preparation and staining

Cells were washed once with sterile DPBS and then incubated with 4% paraformaldehyde (Sigma-Aldrich) for 10 minutes at room temperature. Paraformaldehyde was removed, and cells were washed twice with sterile DPBS. Cells were then stored at 4°C covered with sterile phosphate buffered saline (PBS) for a maximum of 3 months before staining proceeded.

Cells were blocked and permeabilized for a minimum of 1 hour using a solution of 5% donkey or goat serum in sterile PBS with triton-X-100 (PBST, all supplied by Sigma-Aldrich) ranging in concentration from 0.01% to 0.1% based on the antigen being targeted. Primary antibodies (see Table 2.5) were then made up in the blocking solution and incubated overnight at 4°C. Primary antibody solution was removed, and cells were washed 3 times with sterile PBS. Secondary antibodies (see Table 2.5) were diluted 1:1000 in PBST and applied for 1 hour at room temperature or were diluted 1:2000 and applied overnight at 4°C. The secondary antibody solution was then removed, cells were washed twice with PBS before counterstaining with DAPI (1 µg/mL, Sigma-Aldrich) and mounting using Fluoromount™ Aqueous Mounting Medium (Sigma-Aldrich) or ProLong™ Glass Antifade Mountant (Invitrogen™). Imaging was done on a Zeiss LSM710 confocal microscope and a Leica DMI600B inverted time-lapse microscope.

#### 2.6.2 Cryosectioning mouse brains

Mouse brains from animals modelling 1q21.1 microdeletion was purchased from Taconic and received in PBS. Brains were from male and female animals (3 of each per group) and all animals were sacrificed at one month of age. Brains were incubated in 30% w/v sucrose (Sigma-Aldrich) at pH 7 for a minimum of 24 hours and before continuing brains had to have sunk to the bottom of the receptacle. Brains were then removed from sucrose and quickly washed in PBS before drying using a paper towel. To freeze the brains, they were dropped into 3-Methyl-1-butene (Sigma-Aldrich) which was precooled in a -80°C freezer and left to freeze for a minimum of 30 seconds. Brains were removed from the 3-Methyl-1-butene using tweezers which were precooled to -20°C and were immediately placed into a Cryostar™ NX50 cryostat (Thermofisher).

Brains were mounted into square molds using OCT (Thermofisher) and the cryobar in the Cryostar™ NX50 cryostat at -20°C. Firstly, the mold was prechilled and a layer of O.C.T was placed in the bottom of the mold and allowed to partially freeze. Before the OCT was completely solidified the mouse brain was placed on top using precooled tweezers and lightly pressed into the OCT. Small pellets of dry ice were arranged around the mold in contact with the four sides and further OCT was added around the brain slowly with each layer being allowed to partially solidify before the next was added. Once the brain was completely covered with OCT the mounted brains were placed into a -80°C freezer for between 1 and 3 hours.

Mounted brains were removed from the -80°C freezer and molds were removed before the block was placed in the Cryostar™ NX50 cryostat at -20°C for 30 minutes to 1 hour. The mounted brain was then attached to the chuck using OCT. Excess OCT and unwanted brain tissue was then removed by sectioning at 100µm. Brains were sectioned at 10µm after the appearance of the primary somatosensory cortex with sections mounted sequentially on sets of 10 slides with 3 sections mounted per slide. A total of 100 slides were cut from each brain and slides were anatomically compared with similar coronal sections selected for staining. After cryosectioning sections were stored at -80°C.

### 2.6.3 Slide preparation and staining

Slides were removed from storage in the -80°C freezer and were placed on a heat block at 60°C for 20 seconds to dry the slides. Antigen retrieval was performed using citrate buffer (Sigma-Aldrich) and high heat generated by either a water-bath or a pressure cooker. For antigen retrieval using the water bath, citrate buffer was heated to 90°C in a coplin jar in a water bath. Slides were then placed in the coplin jar for 10 minutes before being placed into a second coplin jar with room temperature PBS.

For antigen retrieval using a pressure cooker citrate buffer was heated in a pressure cooker in a microwave until boiling but not under high pressure (around 10 minutes at full power). Slides were then placed in the pressure cooker in plastic heatproof slide rack and heat was again applied until the pressure cooker was under pressure (3-5 minutes at full power). The microwave power was then reduced to 70% and the pressure cooker was heated for a further 7 minutes. Slides were removed into a coplin jar containing room temperature PBS.

Tissue sections were circled using a hydrophobic pen before blocking for 1 hour using 5% donkey serum and 0.5% triton-x-100 in PBS. Primary antibodies (see Table 2.5) were added at the required concentration in blocking solution overnight at 4°C. Slides were washed in PBS, 3 times for 5 minutes each before secondary antibodies (see Table 2.5) were applied at a 1:1000 dilution in blocking solution. Secondary antibodies were incubated on slides for 1-2 hours at room temperature in the dark before slides were again washed in PBS, 3 times for 5 minutes each. Sections were counterstained using DAPI (1µg/mL) and mounting was done using Fluoromount™ Aqueous Mounting Medium or ProLong™ Glass Antifade Mountant. Imaging was done on a Zeiss LSM710 confocal microscope and a Leica DMI600B inverted time-lapse microscope.

#### 2.6.4 Image processing and analysis

When appropriate quantification was performed using a minimum of 3 random fields selected from each coverslip or well (each field containing a minimum of 20 cells as quantified by DAPI staining). Quantification of mouse brain staining was performed using a minimum of 3 brain sections per animal with the required area imaged from both hemispheres.

Quantification of nuclear staining was done using CellProfiler<sup>162</sup> using a Cell/particle counting pipeline which counted the number of objects in each channel and then related one or more channels to DAPI allowing the enumeration of the percentage positive cells. All objects which were identified in non-DAPI channels which did not overlap with DAPI were eliminated. In each case the pipeline was tailored to the specific density and resolution of the images with ImageJ<sup>163</sup> used to estimate the diameter of nuclei in pixels for each image set and then the CellProfiler settings were set with a minimum (20% below the measurement from ImageJ) and a maximum (20% above the measurement from ImageJ). The images generated by CellProfiler were periodically checked for accuracy and compared to object counts performed manually using ImageJ.

As some staining used in this work are cytoplasmic (GFAP, MAP2) the quantification of these staining was performed differently. Instead of using DAPI staining (nuclei) as the standard the staining was used as the standard with objects identified under the same procedure described above based on measurements taken in ImageJ. These objects were then filled in as in the case of GFAP especially the area where the nuclei were, was often unstained or lightly stained. These primary objects were then only counted if there was a nucleus within the area covered by the staining. This was then compared to the total number of nuclei in each field measured by a separate analysis module. The parameters used to identify the primary objects (positive stained cells) were refined by examining the output images and were tailored to the density and size of each image set. The counts generated by this analysis were periodically checked for accuracy by manual analysis using ImageJ.

Analysis of neuronal morphology was performed using a combination of ImageJ and CellProfiler. The soma area was measured using CellProfiler by measuring the area of objects identified for the quantification of MAP2 staining. Both the number of primary processes and the length of primary processes was determined in ImageJ by manually counting the number of processes and measuring the length of each process from the

junction with the soma to the furthest point from the soma. The length of each process was measured by matching short linear segments along the process approximating the curves of the process as close as possible.

Finally, the quantification of synapse density was performed using Intellicount: a machine learning system which relates the number of synaptic puncta to the area covered by filamentous staining i.e. MAP2. Full explanation of the software can be found in the paper by Fantuzzo *et al.*<sup>164</sup> the object area (size of synaptic puncta) was estimated using measurements from ImageJ and all other settings were maintained as recommended by the software. Quantification is presented as the number of puncta per  $1\mu\text{m}^2$  of MAP2 staining.

## 2.7 Western blotting

### 2.7.1 Protein isolation and quantification

Cells were collected by Accutase™ dissociation as previously described (see section 2.2.3) and were pelleted by centrifugation (at 900 r.c.f. for 5 minutes). The resulting pellet was re-suspended in RIPA buffer (Millipore) with protease and phosphatase inhibitors (Sigma-Aldrich) and then incubated on ice for 30 minutes with vortexing every 5 minutes. The samples were then centrifuged (at 18,500 r.c.f. for 5 minutes at 4°C) and the supernatant split, a small sample was retained in this state for quantification. The remainder of the supernatant was combined with Bolt™ LDS sample buffer (Invitrogen™) and Bolt™ sample reducing buffer (Invitrogen™) then incubated at 70°C for 10 minutes before being stored at -80°C. The small sample was used to quantify the protein concentration in the large sample using the DC™ protein assay (Biorad) according to the manufacturer's protocol, the standards used ranged from 2 mg/ml to 100  $\mu\text{g}/\text{ml}$  of BSA (Invitrogen™) and absorbance was read at 750nm. The total protein level in the isolate was estimated and if the estimated protein concentration was above 2 mg/ml then the sample was diluted, and the assay was re-run.

### 2.7.2 Western blotting and imaging

Samples were thawed and prepared on ice; (unless otherwise stated) 20 $\mu\text{g}$  of protein per lane was loaded onto Bis-Tris 4-12% gradient gels along with the PageRuler™

plus prestained protein ladder (Thermo Fisher™). The gel was run using Bolt™ MES SDS Running Buffer (Invitrogen™) and then the proteins were transferred to a nitrocellulose membrane (GE Healthcare). The transfer was done using Bolt™ Transfer Buffer (Invitrogen™) at 4°C. Where necessary the protein transfer was visualized using Ponceau S dye (Sigma-Aldrich) which was subsequently washed out with water. The membrane was blocked in blocking solution comprised of 5% Amersham ECL Prime Blocking Reagent (GE Healthcare) in tris-buffered saline (TBS, Fisher) with 0.1% Tween-20 (TBST, Sigma-aldrich) for 1 hour at room temperature. Primary antibodies (see Table 2.5) were diluted in blocking solution and then applied to the membranes over night at 4°C on an orbital shaker. The membranes were washed in TBST and the secondary antibodies (see Table 2.5) were applied at a 1:15000 dilution in blocking solution for 1-1.5 hours at room temperature on an orbital shaker. The membranes were then washed again twice in TBST and then once in TBS before being visualized using the Odyssey CLx (LiCor). Quantification of band intensity was done using the Image Studio™ software (LiCor). All results were normalized to GAPDH as an endogenous control before further analysis was carried out. All data is presented as an average of 3 independent differentiations.

## 2.8 Quantitative PCR

### 2.8.1 RNA isolation and cDNA production

Cells were collected by Accutase™ dissociation as previously described (see section 2.2.3) and were pelleted by centrifugation. The supernatant was discarded, and RNA was isolated using a GeneElute™ mammalian total RNA miniprep kit (Sigma-Aldrich) according to the manufacturers protocol. RNA was eluted in 30 µl of elution buffer and the concentration of RNA was measure using a nanodrop machine (BioSpectrometer, Eppendorf). A minimum of 500 ng of RNA was then used to create cDNA using a high-capacity cDNA reverse transcription kit (Applied Biosystems) based on the manufacturers protocol.

### 2.8.2 Quantitative PCR

For quantitative real-time polymerase chain reaction (qPCR) 100 ng of cDNA was used per reaction, primer sequences are available in Table 2.6 and were taken from

previously published papers, primerbank<sup>165</sup> or independently designed. Primers were diluted in TE buffer (Sigma-Aldrich) and were used at a concentration of 400 nM. Reactions were run on a StepOnePlus™ real-time PCR system (Applied Biosystems) with qPCR BIO SyGreen Blue Mix Hi-ROX (PCR Biosystems) under the following conditions: initial denaturation at 95°C for 2 min; denaturation at 95°C for 5 seconds and annealing at 60°C for 30 seconds for 40 cycles. PCR products were detected by incorporation of SYBR-green. Primers were validated by melt curve analysis and by gel electrophoresis to prove the production of a single PCR product, of the correct length. Threshold cycle (CT) numbers during the log phase of amplification were normalized to the expression of GAPDH. The relative expression in each sample was calculated by the  $2^{-\Delta\Delta CT}$  method<sup>166</sup>. Each reaction was run in triplicate and outliers were eliminated based on  $C_T$  values and averaged before further analysis. All data is presented as an average of 3 independent differentiations.

## 2.9 Magnetically activated cell sorting

### 2.9.1 Cell preparation

Cells grown adherently were dissociated with Accutase™ as previously described (see section 2.2.3) incubating for a minimum of 15 minutes, then collected by centrifugation (200 r.c.f. for 5 minutes). Cells were resuspended in 80  $\mu$ L (per  $10^5$ ) cells of buffer solution comprised of PBS supplemented with 0.5% BSA (Gibco™) pre-cooled to 4°C. Cells grown as non-adherent spheres were dissociated using the GentleMACS™ Octo dissociator with heaters (Miltenyi Biotec). Aggregates were collected in  $\leq 1$  mL of media and combined with 9 mL PBS, after allowing aggregates to sediment the supernatant was removed leaving  $\leq 100$   $\mu$ L liquid. Aggregates were then transferred to a C tube (Miltenyi Biotec) and 2 mL dissociation solution was added (10 mg/mL papain, 1 mM L-Cysteine, 10U/mL DNase I and 0.5 mM EDTA in DMEM/F12 all from Sigma-Aldrich). Dissociation was carried out using the GentleMACS™ Octo dissociator with heaters, spheres were digested using protocols based on the digestion of murine brain tissue. Cells were then collected by centrifugation (200 r.c.f. for 5 minutes) and resuspended in 80  $\mu$ L per  $10^5$  cells of buffer solution pre-cooled to 4°C.

## 2.9.2 Cell sorting

The required microbeads were added to the cell suspensions using 20  $\mu\text{L}$  of microbeads per  $10^5$  cells. Cells were incubated on ice for 10 minutes before adding 1 mL of buffer solution, cells were then collected by centrifugation (200 r.c.f. for 5 minutes) and resuspended in 500  $\mu\text{L}$  of buffer solution per  $10^5$  cells. Positive selection was carried out using MS columns and an OctoMACS™ separator (both from Miltenyi Biotec). The column was prepared by washing with 500  $\mu\text{L}$  of buffer solution before the cell suspension was added. The flow through was collected and then the column was washed with a further 500  $\mu\text{L}$  of buffer solution with the flow through again collected and combined with the original. The column was removed from the magnet and 1 mL of buffer solution was added and flushed through the column using the plunger. Both the flow through and desired cells were collected by centrifugation (200 r.c.f. for 5 minutes). All cells were then resuspended in the desired media and the number of cells in each population was quantified. Cells were plated and maintained as described in section 2.3.4.

## 2.10 Human brain imaging

### 2.10.1 Human brain imaging data collection and processing

The human brain data used in this study is a subsample of participants in the UK Biobank project ([www.ukbiobank.ac.uk](http://www.ukbiobank.ac.uk)). All subjects provided informed consent to participate in UK Biobank, and ethical approval was granted by the North West Multi-Centre Ethics committee. Data was released to Cardiff University after application to the UK Biobank (project ref. 17044). For full details on sample processing see UK Biobank documentation at: <https://biobank.ctsu.ox.ac.uk/crystal/refer.cgi?id=155581>. CNV calling was based on procedures published by Kendall *et al*<sup>167</sup>.

Complete details of the image acquisition and processing are freely-available on the UK Biobank website in the form of: a protocol (<http://biobank.ctsu.ox.ac.uk/crystal/refer.cgi?id=2367>), brain imaging documentation (<http://biobank.ctsu.ox.ac.uk/crystal/refer.cgi?id=1977>) and in a publication from Miller *et al*<sup>168</sup>. Only intracranial volume and DTI measurements are presented in this study; for detailed descriptions of metrics used see Alfaro-Almagro<sup>169</sup>.

### 2.10.2 Statistical analysis

Statistical analysis was performed by Ana Silva using RStudio version 3.5.1 (RStudio: Integrated development environment for R; Boston, MA, USA. Available from [www.rstudio.org](http://www.rstudio.org)). Prior to analysis extreme values (defined as values  $\pm 2.5$  standard deviations from each group mean) were removed from the data based on protocols published by Warland *et al*<sup>170</sup>. In order to mitigate any effects from known diseases either neurological or psychological, participants with any history of neuropsychiatric disorders (i.e. schizophrenia, psychosis, ASD, dementia or intellectual disability) or neurological condition (i.e. alcohol or other substance dependency, Parkinson's, Alzheimer, multiple sclerosis or other neurodegenerative conditions) were excluded from analysis. Exclusion was based on self-reported diagnosis based on medical assessments or from hospital records. After exclusions there was a total of 15177 individuals with 8 1q21.1 deletion carriers and 10 1q21.1 duplication carriers used for this study. The individuals used in this study had an average age of 63 and the cohort was 47% male.

Linear regression analysis was performed for each DTI measure with age, sex and intracranial volume specified as covariates of no interest. Post hoc pairwise comparisons were performed to assess differences between groups and to account for multiple testing P values were corrected using the FDR methodology<sup>171</sup>. Where appropriate uncorrected P values (clearly marked) are presented due to the low number of individuals with 1q21.1 mutations. To assess the magnitude of the changes in DTI metrics Cohen's d effect sizes were calculated comparing 1q21.1 deletion vs No CNV and 1q21.1 duplication vs No CNV and plotted using diverging bars. The adjusted means were the residuals from the linear regression model:  $\text{lm}(\text{genotype} \sim \text{age} + \text{sex} + \text{ICV})$ . Cohen classified effect sizes as negligible ( $d < 0.2$ ), small ( $d > 0.2$ ), medium ( $d > 0.5$ ), and large ( $d > 0.8$ )<sup>172</sup>. For full methodology on the DTI metrics used in this study refer to Silva *et al*<sup>173</sup>.

## 2.11 Statistical analysis

Statistical analysis was carried out using a combination of GraphPad prism version 7.00 and 8.00 (GraphPad Software; La Jolla, CA, USA, Available from [www.graphpad.com](http://www.graphpad.com)) and RStudio version 3.5.1 (RStudio: Integrated development environment for R; Boston, MA, USA. Available from [www.rstudio.org](http://www.rstudio.org)). All technical replicates were averaged before statistical analysis and specific statistical tests used for each data analysis are detailed in figure legends. The number of cell lines used for each analysis are listed in the figure legends as N numbers for control, deletion and duplication separately. The number of separate differentiations used in each analysis is also listed in figure legends as n. Unless specifically stated the same number of separate differentiations was used for each cell lines therefore the total number of samples per data point can be calculated simply by  $N \times n$ . When different numbers of differentiations were used for groups (control, deletion and duplication) the specific n is listed for each group.

## 2.12 Materials

**Table 2.1: List of consumables used in the study**

<b>Item</b>	<b>Supplier</b>	<b>Code</b>
<b>6 well plates</b>	Starlab	CC7682-7506
<b>12 well plates</b>	Starlab	CC7682-7512
<b>24 well plates</b>	Starlab	CC7682-7524
<b>48 well plates</b>	Starlab	CC7682-7548
<b>96 well plates</b>	Starlab	CC7682-7596
<b>1 mL Tips</b>	Starlab	S1112-1720
<b>200 µL Tips</b>	Starlab	S1111-1700
<b>10 µL Tips</b>	Starlab	S1111-3700
<b>50 mL Tubes</b>	Greiner	227261
<b>25 mL Universals</b>	Fisher Scientific	11319153
<b>15 mL Tubes</b>	Fisher Scientific	11765075
<b>50 mL Serological pipettes</b>	Fisher Scientific	10702541
<b>25 mL Serological pipettes</b>	Fisher Scientific	10606151
<b>10 mL Serological pipettes</b>	Fisher Scientific	10084450
<b>5 mL Serological pipettes</b>	Fisher Scientific	10420201
<b>1 mL RPT Tips</b>	Starlab	S1161-1720
<b>200 µL RPT Tips</b>	Starlab	S1163-1700
<b>10 µL RPT Tips</b>	Starlab	S1161-3700
<b>1 mL Filter Tips</b>	Starlab	S1122-1730
<b>200 µL Filter Tips</b>	Starlab	S1120-8710
<b>20 µL Filter Tips</b>	Starlab	S1123-1710
<b>1.5 mL Tubes</b>	Fisher Scientific	11569914
<b>2 mL Tubes</b>	Fisher Scientific	11579914
<b>Cryovials</b>	Starlab	E3110-6122
<b>PCR tubes (Singles)</b>	Starlab	I1402-8108
<b>PCR tubes (Rows)</b>	Starlab	I1402-3700
<b>PCR plates</b>	Starlab	E1403-7700-C
<b>Coverslips (24 well)</b>	Fisher Scientific	15737602
<b>Coverslips (12 well)</b>	Fisher Scientific	11588482
<b>Chamber Slides</b>	Millipore	PEZGS0816
<b>FACS tubes with cell strainers</b>	Fisher Scientific	10585801
<b>MEA plates</b>	Axion	M384-tMEA-24W
<b>C Tubes</b>	Miltenyi Biotec	130-096-334
<b>MS columns</b>	Miltenyi Biotec	130-042-201
<b>qPCR plates</b>	Starlab	E1403-7700
<b>qPCR films</b>	Starlab	E2796-9795
<b>Lenti-X™ GoStix™ Plus</b>	Takara	631280
<b>0.22 µm PES membrane filters</b>	Starlab	E4780-1226
<b>1.5 mL Syringes</b>	VWR	10080264
<b>20 mL Syringes</b>	Fisher Scientific	11866071
<b>16 Gauge Needles</b>	Fisher Scientific	10518554

Table 2.2: List of drugs and small molecules used in the study

Compound	Supplier	Code
Y27632	Stratech	S1049
Retinoic Acid	Sigma-Aldrich	R2625
SB431542	Stratech	S1067
LDN193189	Cambridge Bioscience	SM23-1
SAG	Stratech	S7779
PDGF-AA	Cambridge Bioscience	GFH16-10
IGF-1	R and D	291-G1
HGF	Gibco	PHG0254
NT3	Insight	TP750019
Biotin	Sigma-Aldrich	B4639
cAMP	Sigma-Aldrich	D0260
T3	Sigma-Aldrich	T2877
Ascorbic acid	Sigma-Aldrich	A4403
SU-5402	Sigma-Aldrich	SML0443
PD0332991	Stratech	S1579
DAPT	Stratech	S2215
BDNF	Cambridge Biosi	GFH1AF
NBQX	R and D	1044
Doxycycline	Sigma-Aldrich	D9891
Cytarabine	Sigma-Aldrich	BP383
DL-AP5	R and D	0105

Table 2.3: List of cell culture material used in the study

Item	Supplier	Code
CytoTune™-IPS 2.0 Sendai reprogramming kit	Invitrogen	A16518
DMEM	Gibco	41965062
FBS	Gibco	16000044
NEAA	Gibco	11140035
β-mercaptoethanol	Gibco	31350010
Essential 8™ Flex media	Gibco	A2858501
DMEM/F12	Gibco	11320033
RevitaCell™ supplement	Gibco	A2644501
Versene solution	Gibco	15040033
DPBS	Gibco	14190169
DMSO	Sigma-Aldrich	D2650
Antibiotic and antimycotic solution	Sigma-Aldrich	A5955
BrainPhys™ Neuronal Medium	Stemcell Technologies	05790
Neurobasal	Gibco	21103049
N2 supplement	Gibco	17502001
B27 supplement	Gibco	17504001
B27 supplement without vitamin A	Gibco	12587001
Geltrex™	Gibco	A1413302
STEMdiff™ Trilineage Differentiation Kit	Stemcell Technologies	05230
Fibronectin	Millipore	ECM001
Accutase™	Sigma-Aldrich	A6964
Poly-D-lysine	Sigma-Aldrich	P7280
Laminin	Roche	11243217001
Laminin	Sigma-Aldrich	L2020
CultureOne™ supplement	Gibco	A3320201
Alanyl-glutamine	Sigma-Aldrich	A8185
Insulin	Sigma-Aldrich	I9278
HEPES	Sigma-Aldrich	H3537
Poly-ornithine	Sigma-Aldrich	P3655
Calbryte-520™	AAT bioquest	20653
NaCl	Sigma-Aldrich	S7653
NaHCO <sub>3</sub>	Sigma-Aldrich	S5761
KH <sub>2</sub> PO <sub>4</sub>	Sigma-Aldrich	P5655
KCl	Sigma-Aldrich	P9333
MgCl <sub>2</sub>	Sigma-Aldrich	M8266
CaCl <sub>2</sub>	Sigma-Aldrich	C1016
Glucose	Sigma-Aldrich	G7528
Polyethyleneimine	Sigma-Aldrich	765090
HCl	Sigma-Aldrich	H9892
NaOH	Sigma-Aldrich	S2770
Papain	Sigma-Aldrich	P4762
L-Cysteine	Sigma-Aldrich	30089
EDTA	Sigma-Aldrich	E6758

<b>DNase</b>	Sigma-Aldrich	AMPD1
<b>Lenti-X-concentrator</b>	Takara	631232
<b>TrypLE™ Express</b>	Gibco	12605010
<b>Advanced DMEM/F12</b>	Gibco	12634028
<b>TransIT Virusgen</b>	Mirus	MIR 6700
<b>Pluronic® F-127</b>	Sigma-Aldrich	P2443
<b>Sodium alginate</b>	Sigma-Aldrich	W201502
<b>Matrigel</b>	Fisher Scientific	11573620
<b>RGD-alginate</b>	Dupont	4270129
<b>Tenascin R</b>	R&D systems	3865-TR-050
<b>Chitosan</b>	Sigma-Aldrich	448877
<b>Collagen IV</b>	Sigma-Aldrich	C7521
<b>Hyaluronic acid</b>	Sigma-Aldrich	94137
<b>Calcein-AM</b>	Sigma-Aldrich	17783
<b>Propidium iodide</b>	Sigma-Aldrich	P4864
<b>Astrocyte Growth Supplement</b>	Caltag Medsystems	SC-1852
<b>Glutamate Assay Kit</b>	Abcam	ab83389

Table 2.4: List of molecular biology and staining reagents used in the study

<b>Item</b>	<b>Supplier</b>	<b>Code</b>
<b>DNeasy Blood &amp; Tissue Kit</b>	Qiagen	69504
<b>Paraformaldehyde</b>	Sigma-Aldrich	P6148
<b>PBS tablets</b>	Sigma-Aldrich	P4417
<b>Triton-x-100</b>	Sigma-Aldrich	T9284
<b>Donkey Serum</b>	Sigma-Aldrich	S30-M
<b>Goat Serum</b>	Sigma-Aldrich	S26-M
<b>Fluoromount™ Aqueous Mounting Medium</b>	Sigma-Aldrich	F4680
<b>ProLong™ Glass Antifade Mountant</b>	Invitrogen	P36984
<b>Sucrose</b>	Sigma-Aldrich	S7903
<b>Ethanol</b>	Sigma-Aldrich	51976
<b>3-Methyl-1-butene</b>	Sigma-Aldrich	257931
<b>O.C.T</b>	Thermofisher	23-730-571
<b>Citrate Buffer</b>	Sigma-Aldrich	C9999
<b>Superfrost plus glass slides</b>	Fisher Scientific	12-550-15
<b>Bolt™ LDS sample buffer</b>	Invitrogen	B0007
<b>Bolt™ Sample reducing buffer</b>	Invitrogen	B0009
<b>Bolt™ 4-12% Bis-Tris Plus Gels</b>	Invitrogen	NW04125BOX
<b>DC™ protein assay</b>	Biorad	5000112
<b>BSA protein standards</b>	Invitrogen	23209
<b>Amersham Protran 0.45 NC nitrocellulose Western blotting membrane</b>	GE Healthcare	10600002
<b>PageRuler™ Plus Prestained Protein Ladder</b>	Invitrogen	26619
<b>Bolt™ Transfer Buffer</b>	Invitrogen	BT00061
<b>Methanol</b>	Sigma-Aldrich	34860
<b>Amersham ECL Prime Blocking Reagent</b>	GE Healthcare	RPN418
<b>TBS solution</b>	Thermo Scientific	28358
<b>Tween-20</b>	Sigma-Aldrich	P7949
<b>GeneElute™ mammalian total RNA miniprep kit</b>	Sigma-Aldrich	RTN70
<b>High-capacity cDNA reverse transcription kit</b>	Applied Biosystems	4368814
<b>qPCRBIO SyGreen Blue Mix Hi-ROX</b>	PCR Biosystems	PB20.12-51
<b>TE buffer</b>	Sigma-Aldrich	T9285
<b>RIPA buffer</b>	Millipore	R0278
<b>Phosphatase and protease inhibitors</b>	Sigma-Aldrich	MS-SAFE

Table 2.5: List of antibodies used in the study

Antibody	Code	Company	Species
488-Donkey	A21202	Thermo	Mouse
488-Donkey	A21208	Thermo	Rat
488-Donkey	A11039	Thermo	Chicken
488-Donkey	A21206	Thermo	Rabbit
555-Donkey	A31572	Thermo	Rabbit
555-Donkey	A31570	Thermo	Mouse
555-Goat	A32727	Thermo	Mouse
594-Donkey	A21209	Thermo	Rat
647-Donkey	A31571	Thermo	Mouse
647-Goat	A32733	Thermo	Rabbit
680-Goat	92668070	Licor	Mouse
800-Goat	92632211	Licor	Rabbit
A2B5 microbeads	130-093-392	Miltenyi Biotec	-
APC	AB16794	Abcam	Mouse
APC	AB15270	Abcam	Rabbit
BRACHYURY	SC374321	Santa Cruz	Mouse
CTIP2	AB70453	Abcam	Rabbit
CTIP2	AB18465	Abcam	Rat
GAPDH	AB8245	Abcam	Mouse
GAPDH	AB181602	Abcam	Rabbit
GFAP	Z0334	Dako	Rabbit
Map2	AB32454	Abcam	Rabbit
Map2	M9942	Sigma-Aldrich	Mouse
Map2	MAB8304	RND	Mouse
MAP2	M1406	Sigma-Aldrich	Mouse
MBP	MAB386	Sigma-Aldrich	Rat
NANOG	D73G4	CellSignalling	Rabbit
OCT4	C30A3	CellSignalling	Rabbit
O4	O7139	Sigma	Mouse
O4	MAB345	Sigma-Aldrich	Mouse
Olig2	MABN50	Sigma-Aldrich	Mouse
Olig2	AB109186	Abcam	Rabbit
PAX6	AB5790	Abcam	Rabbit
PAX6	AB195045	Abcam	Rabbit
PSD95	AB2723	Abcam	Mouse
SOX10	AB212843	Abcam	Mouse
SOX17	AB84990	Abcam	Mouse
SYN	AB32127	Abcam	Rabbit
Tbr1	AB31940	Abcam	Rabbit

Table 2.6: List of primers used in the study

Gene	Forward Primer (5'-3')	Reverse Primer (5'-3')	Primer Origin
<b>ACP6</b>	AGATGGCAGTAGGCCATTC	ACAGCTTCTGATCTTGTCGG	Primerbank <sup>165</sup>
<b>ASCL1</b>	TCTTCGCCCGAACTGATGC	CAAAGCCAGGTTGACCAACT	Primerbank <sup>70</sup>
<b>BCL9</b>	GGCCATACCCTAAAGCACTC	CGGAAATACTTCGCTCCCTTTT	Primerbank <sup>70</sup>
<b>BRACHYURY</b>	TATGAGCCTCGAATCCACATAGT	CCTCGTTCTGATAAGCAGTCAC	Yuan <i>et al.</i> <sup>174</sup>
<b>CACNA1B</b>	GACAACGTCGTCGCAAATAC	CCCGATGAAATAGGGCTCCG	Primerbank <sup>70</sup>
<b>CACNA1C</b>	GAAGCGGCAGCAATATGGGA	TTGGTGGCGTTGGAATCATCT	Primerbank <sup>70</sup>
<b>CACNA1G</b>	ACACTTGAACCGGCTTGAC	AGCACACGGACTGTCCTGA	Primerbank <sup>70</sup>
<b>CD160</b>	GCTGAGGGGTTTGTAGTGT	GTGTGACTTGGCTTATGGTGA	Primerbank <sup>70</sup>
<b>CHD1L</b>	GCTATGAGCGTGTGGATGGTT	TGCTGTTAAGTTCATGCCAACTC	Primerbank <sup>70</sup>
<b>CMYC</b>	TCAAGAGGCGAACACACAAC	GGCCTTTTCATTGTTTTCCA	Sese <i>et al.</i> <sup>175</sup>
<b>CTIP2</b>	CTCCGAGCTCAGGAAAGTGTC	TCATCTTACCTGCAATGTTCTCC	Primerbank <sup>70</sup>
<b>CUX1</b>	GCTCTCATCGGCCAATCACT	TCTATGGCCTGCTCCACGT	Pasca <i>et al.</i> <sup>136</sup>
<b>DCX</b>	CCTTGGCTAGCAGCAACAGT	CCACTGCGGATGATGGTAA	Pasca <i>et al.</i> <sup>136</sup>
<b>DDC</b>	ACTGGCTCGGGAAGATGCT	CCGATGGATCACTTTGGTCC	Primerbank <sup>70</sup>
<b>DLX1</b>	CCATGCCAGAAAAGTCTCAACA	GGCCCAAACCTCATAAACACC	Primerbank <sup>70</sup>
<b>EN1</b>	GAGCGCAGGCGACCAAATA	AATAACGTGTGCAGTACACCC	Primerbank <sup>70</sup>
<b>ETV1</b>	CTGGATGACCCGGCAAATCT	CCTCTTCAGGCTCAATCAGTTT	Primerbank <sup>70</sup>
<b>FMO5</b>	TGTCCTCCTCAAGACACCTCT	GATTTTCTGGAACCTCCAGAGC	Primerbank <sup>70</sup>
<b>FOXP1</b>	AGACAAAAAGTAACGGTTCAGCC	CGCACTCTAGTAAGTGGTTGC	Primerbank <sup>70</sup>
<b>GAD67</b>	GCCAGACAAGCAGTATGATGT	CCAGTTCAGGCATTGTTGAT	Primerbank <sup>70</sup>
<b>GAPDH</b>	CTGGTAAAGTGATATTGTTGCCAT	TGGAATCATATTGGAACATGTAACCC	Own design
<b>GCH1</b>	ACAAGTTCAGGAGCGCCTTAC	AGTAGAGGGCTCAACCCTTTATT	Primerbank <sup>70</sup>
<b>GJA5</b>	GCTGCCAGAATGTCTGTCTAC	GGTACTCGTAAGAGCCAGA	Primerbank <sup>70</sup>
<b>GJA8</b>	GACCCTGCTGAGGACCTACAT	CCCAACTCCATCACGTTGAG	Primerbank <sup>70</sup>
<b>GLUA1</b>	CGAGCTTCCCGTTGATACAT	TCTGCCACTTGAATGGTCAATG	Primerbank <sup>70</sup>
<b>GPR89B</b>	GGAGTGACTCTCATGGCTCTT	TCACACCTAGTGCCACTTGT	Own design
<b>GRIN1</b>	CTACCGCATACCCGTGCTG	GCATCATCTCAAACCACACGC	Primerbank <sup>70</sup>
<b>GSX2</b>	ATGTCGCGCTCCTTCTATGTC	ATGCCAAGCGGGATGAAGAAA	Primerbank <sup>70</sup>
<b>KI67</b>	TCCTTTGGTGGGCACCTAAGACCTG	TGATGGTTGAGGTCGTTCTTGATG	Prihantono <i>et al.</i> <sup>176</sup>
<b>KLF4</b>	CCACCCACACTTGTGATTACG	GCGGGCGAATTTCCATC	Own design
<b>MAP2</b>	CTGCTTTACAGGGTAGCACAA	TTGAGTATGGCAAACGGTCTG	Primerbank <sup>70</sup>
<b>MBP</b>	GTCCTGAGCAGATTTAGCTG	GAATCCCTTGTGAGCCGATTT	Primerbank <sup>70</sup>
<b>MSX2</b>	CACCCTGAGGAAACACAAGAC	AACTCTGCACGCTCTGCAAT	Primerbank <sup>70</sup>
<b>NCAM</b>	ACATCACCTGCTACTTCTGA	CTTGGACTCATCTTCGAGAAGG	Primerbank <sup>70</sup>
<b>NESTIN</b>	TCCAGAACTCAAGCACCA	AAATTCTCCAGGTTCCATGC	Primerbank <sup>70</sup>
<b>NKX2.1</b>	CGCATCCAATCTCAAGGAAT	TGTGCCCAGAGTGAAGTTTG	Primerbank <sup>70</sup>
<b>NKX2.2</b>	GACAACTGGTGGCAGATTCGCTT	AGCCACAAAGAAAGGAGTTGGACC	Hu <i>et al.</i> <sup>177</sup>
<b>NURR1</b>	ACCACTCTTCGGGAGAATACA	GGCATTGGTACAAGCAAGGT	Primerbank <sup>70</sup>
<b>OCT4</b>	GCTTGGAGACCTCTCAGCCT	TTGATGCTCTGGGACTCCTC	Ren <i>et al.</i> <sup>178</sup>
<b>OLIG2</b>	CAGAAGCGCTGATGGTCAT	CGGCAGTTTTGGGTTATTC	Own design
<b>PAX6</b>	CAACTCCATCAGTTCCAACG	TGGATAATGGGTTCTCTCAAACCTC	Primerbank <sup>70</sup>
<b>PLP1</b>	TGCTGATGCCAGAATGTATGG	GCAGATGGACAGAAGGTTGGA	Primerbank <sup>70</sup>
<b>PLZF</b>	GGGACTTTGTGCGATGTGGT	ATTGCGGTGGGAAGAGGATCTC	Primerbank <sup>70</sup>
<b>PRKAB2</b>	ATGCGTTTCGATCTGAGGAAAG	GGTTCAGCATAACATGTTGGG	Primerbank <sup>70</sup>

<b>PSD-95</b>	AGCCCCAGGATATGAGTTGC	GATGTGTGGGTTGTCAGTGC	Jiang <i>et al.</i> <sup>179</sup>
<b>REELIN</b>	TCCGGGACAAGAATACCATGT	CCAAATCCGAAAGCACTGGAA	Primerbank <sup>70</sup>
<b>S100B</b>	TGGCCCTCATCGACGTTTTTC	ATGTTCAAAGAACTCGTGGCA	Zhang <i>et al.</i> <sup>180</sup>
<b>SATB2</b>	CCGCACACAGGGATTATTGTC	TCCACTTCAGGCAGGTTGAG	Primerbank <sup>70</sup>
<b>SOX10</b>	ATGTCAGATGGGAACCCCGA	TGGACATTACCTCGTGGCTG	Varghese <i>et al.</i> <sup>181</sup>
<b>SOX17</b>	GTGGACCGCACGGAATTTG	GGAGATTCACACCGGAGTCA	Own design
<b>SOX2</b>	GAGTGGAAACTTTTGTCCGAGA	GAAGCGTGTACTTATCCTTCTTCAT	Ehm <i>et al.</i> <sup>182</sup>
<b>SYN</b>	TGGTGTTCGGCTTCCTGAA	GCGGCCACGCTGTCT	Own design
<b>TBR1</b>	GGGCTCACTGGATGCGCCAAG	TCCGTGCCGTCTCGTTCACT	Primerbank <sup>70</sup>
<b>TBR2</b>	CCGGGCACCTATCAGTACAG	GGTTGCACAGGTAGACGTG	Primerbank <sup>70</sup>
<b>TH</b>	CCGCGGTTTCATTGGGCG	CACCAGCTCACCTCAAACAC	Primerbank <sup>70</sup>
<b>VGLUT1</b>	CGACGACAGCCTTTTGTGGT	GCCGTAGACGTAGAAAACAGAG	Primerbank <sup>70</sup>
<b>VGLUT2</b>	GGGAGACAATCGAGCTGACG	CAGCGGATACCGAAGGAGATG	Primerbank <sup>70</sup>
<b>VGLUT3</b>	AAACCGGAAATTCAGACAGCA	CCAAAGACCCTGTTAGCAGCA	Primerbank <sup>70</sup>
<b>VIM</b>	GGACCAGCTAACCAACGACA	AAGGTCAAGACGTGCCAGAG	Boros <i>et al.</i> <sup>183</sup>
<b>ZO1</b>	AGTCCCTTACCTTCGCCTGA	TCTCTTAGCATTATGTGAGCTGC	Primerbank <sup>70</sup>

### 3. Deletion and Duplication of the Distal 1q21.1 Locus are Associated with Altered Neuronal Differentiation Resulting in Altered Functional Behavior

#### 3.1 Introduction

##### 3.1.1 Generating neurons from iPSCs using developmental patterning paradigms

Early protocols for generating neurons from iPSCs exploited the principle that pluripotent cells have a tendency to default to neuroepithelia when drivers of pluripotency are removed and these cells can be driven towards neuronal precursors with minimal interference<sup>184</sup>. However, while this protocol can be used to generate neurons and glia there was little control over the specific types of cells produced. Therefore, results using these very simple protocols were highly variable. More advanced protocols were developed specifying a specific subtype of neuronal precursor which could then be driven towards a specific subtype of neuron<sup>185</sup>. The publication of the use of dual SMAD inhibition for the conversion of iPSCs into neuronal stem cells<sup>145</sup> provided a critical stepping stone in the development of more robust protocols for the generation of neuronal cells. The combination of two SMAD inhibitors drives the loss of pluripotency and the induction of neuroepithelia by the repression of endogenous BMP signalling. This protocol allows the production of cortical neurons primarily producing lower layer excitatory glutamatergic neurons with the possibility of producing both upper layer glutamatergic neurons and GABAergic interneurons. Importantly these protocols also reproduce the course of early human cortical development producing persistent progenitors and then immature neurons which mature into functional cells.

Further protocols have been developed with a focus on decreasing the time taken to generate neurons, as dual SMAD inhibition-based protocols can take 40-50 days to generate neurons and a further 40-50 days for the development of fully functional neuronal networks. Therefore, efforts have been focussed on the use of mitotic inhibitors to synchronise the differentiation of neuronal differentiations while simultaneously preventing the continued proliferation of neuronal precursors<sup>186,187</sup>. While this approach does move away from the original aim of recapitulating neuronal development it does produce a more homogeneous product which allows for the discrimination of the more subtle phenotypes which are likely to be relevant to neurodevelopmental and psychiatric disorders. Recent work has expanded on these concepts to develop very short protocols for the generation of cortical neurons using developmental patterning approaches<sup>158</sup>.

However, this approach moves even further away from recapitulating *in vivo* neuronal development and therefore has limited utility as a model for neurodevelopmental disorders

While these neurons are not identical to those found in the adult patients from whom the cells are derived it is believed that they share developmental trajectories and recapitulate key features of early human neuronal development. At a simplistic level these cells have the key components that mature neurons have and can be used to form functional synapses and neuronal networks. While the functionality may not be as complex as that found in adult human brains these cells provide a critical reductionist model to assess the effects of mutations, drugs and other insults on the development and function of human neurons<sup>188</sup>. Numerous publications have used these models to delve into the cellular pathology associated with disorder such as ASD<sup>189</sup> and schizophrenia<sup>190</sup> allowing a greater understanding of the cellular pathology which underlies the phenotypes known to be relevant in the pathogenesis of neurodevelopmental and psychiatric disorders.

### 3.1.2 The role of cortical neuronal dysfunction in neurodevelopmental and psychiatric disorders

The cerebral cortex is the outermost layer of the brain comprising of tightly compacted neurons, which form a highly organised structure with a high level of neuronal diversity. The cortex is made of two broad classes of neurons. Excitatory cortical neurons are generated from the ventricular zone of the dorsal telencephalon<sup>191</sup> migrating tangentially to generate the layered structure of the cortex. Inhibitory interneurons are generated in the caudal and medial ganglionic eminences<sup>192</sup> and migrate laterally to infiltrate the developing cortex. This results in a highly complex and diverse structure which is formed from the base starting with layer VI neurons and finishing with layer I neurons with most progenitors continuing to reside in the ventricular and subventricular zone below layer VI (Figure 3.1). This structure is also highly evolutionarily conserved with largely similar structures present in most higher animals including mice<sup>193</sup>. Given the complex structure of the cortex and the critical role it plays in cognition and information processing it has long been suggested that small abnormalities in this system could underly some of the pathologies associated with neurodevelopmental and psychiatric disorders.

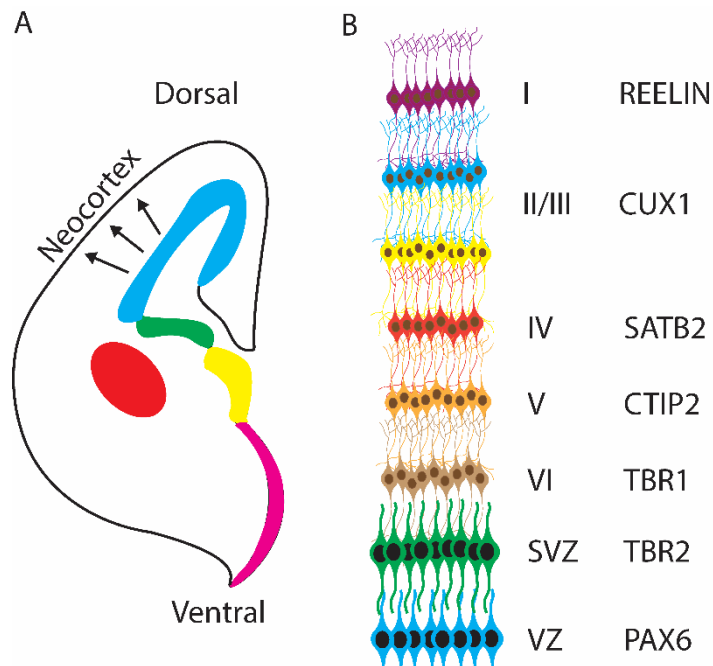


**Figure 3.1: Graphical representation of the structure of the cortex.** **A** The structure of the developing brain, the neocortex is formed from the ventricular zone (blue). Also marked are the lateral ganglionic eminence (green), medial ganglionic eminence (yellow), preoptic area (purple) and striatum (red). **B** The layered structure of the cortex is formed by the division of progenitors in the ventricular zone (VZ) and the subventricular zone (SVZ). The layers are organized from layer VI to layer I with layer I being the surface of the brain. Each layer including both VZ and SVZ can be marked by the expression of certain genes indicated to the right of each layer. Image adapted from Mukhtar and Taylor<sup>98</sup>.

Imaging studies have been carried out to examine gross structural changes in the cortex associated with psychiatric disorders. These studies have indicated a thinning of the cortex associated with schizophrenia<sup>194</sup> and bipolar (specifically type 1<sup>195</sup>). A further study examining the longitudinal development of the cortex found a delayed development associated with ADHD diagnosis<sup>196</sup>. Studies examining cortical development in ASD patients have shown overgrowth at very early stages<sup>197</sup> with some evidence for cortical thinning at later stages of development<sup>198</sup>. Furthermore, links have been provided between genetic risk factors for psychiatric disorders and cortical abnormalities. A rare mutation associated with bipolar disorder and schizophrenia<sup>199</sup> (Disrupted in schizophrenia 1, *DISC1*) has been shown to effect cortical development affecting both the differentiation of cortical neurons and the final structure of the cortex<sup>200</sup>. Finally, in a rodent model of 22q11.2 deletion it has been shown that the intrinsic properties of cortical neurons are altered<sup>201</sup>. This evidence combines to suggest that widespread cortical abnormalities may indeed underly the phenotypes associated with neurodevelopmental and psychiatric disorders.

One theory which may explain how these cellular changes associated with cortex development result in the phenotypes related to neurodevelopmental disorders is altered excitatory-inhibitory balance which ultimately results in aberrant neuronal activity. The balance between excitation and inhibition is critical to the proper functioning of neuronal

networks<sup>202</sup> and the connections between these system is particularly critical to cortical function. Therefore, while the imbalance between excitation and inhibition may not be a purely cortical phenomenon; the critical function of the cortex and the presence of both excitatory and inhibitory neurons, in this complex highly regulated structure, have made it a particularly interesting target for investigating this phenotype. In practical terms the major excitatory neurotransmitter is glutamate and the major inhibitory neurotransmitter is gamma aminobutyric acid (GABA) therefore changes in the balance between excitation and inhibition are likely to involve changes in the production, distribution and removal of these molecules. These imbalances may be due to changes in the proportion of excitatory neurons, inhibitory neurons or a combination of both systems. Indeed, post-mortem studies have indicated structural abnormalities in both excitatory and inhibitory circuits in patients with either ASD or schizophrenia<sup>203-206</sup>.

This imbalance can also result from changes in the expression or function of genes encoding relevant receptors or other synaptic proteins. Many of these genes have now been identified as risk factors for developing psychiatric disorders. In terms of glutamatergic neurons, many genes have been identified which are correlated with an increased risk of developing psychiatric disorders. These genes include post synaptic density proteins (such as the SH3 And Multiple Ankyrin Repeat Domains, SHANK proteins<sup>207,208</sup>), subunits of NMDA receptors (such as Glutamate Ionotropic Receptor NMDA Type Subunit 2, *GRINR2A/B/C*<sup>209,210</sup>) and other proteins involved in synapse formation (such as Neuregulin 1, *NRG1*<sup>211</sup> and Erb-B2 Receptor Tyrosine Kinase 4, *ERBB4*<sup>212</sup>). In terms of GABAergic neurons, the majority of studies have focused on the reduction of GAD67 (the principle enzyme for synthesising GABA) which was reduced in patients with psychiatric disorders<sup>213-215</sup>. More recent work on Cytoplasmic FMR1 Interacting Protein 1 (*CYFIP1*) and Cytoplasmic FMR1 Interacting Protein 2 (*CYFIP2*) has shown that changes in the expression of these protein can have effects on both excitatory and inhibitory synapses<sup>216</sup>. Animal models have indicated that loss of genes such as neurexin-1 $\alpha$  (a protein involved in synapse organization) is associated with social behaviours which can be connected with both ASD and schizophrenia<sup>217</sup>. This evidence indicates that an imbalance of excitation and inhibition is a significant factor in the pathogenesis of psychiatric disorders this may be caused by gross changes in the proportion of cell types or by fine changes in the composition and function of the synapses formed by these cells. Therefore, to understand the increased risk for developing psychiatric disorders

associated with specific mutations it is critical to consider both a neurodevelopmental paradigm to investigate the production of neuronal populations and a more focused investigation of the role the mutation may play in the function of these neurons.

### 3.1.3 Modelling CNVs and psychiatric disorders using iPSC derived neurons

The use of iPSCs carrying previously recognised CNVs associated with an increased risk of developing psychiatric disorders is becoming a popular paradigm for studying the genetics associated with psychiatric disorders. However, to date only neuronal modelling of 15q11.2, 22q11.2 and 22q13.3 deletions and 16p11.2 deletions and duplications, all of which are associated with an increased risk of developing multiple neurodevelopmental and psychiatric disorders, have been reported. Mutations at the 15q11.2 locus have been the focus of a large volume of work largely related to the loss of *CYFIP1* expression. While this is not the only gene within this region the two functions of this gene (actin polymerization and protein translation<sup>218</sup>) suggest it to be the cause of the phenotypes associated with 15q11.2 deletions. These mutations have been modelled in rodents identifying several behavioural and cellular phenotypes<sup>219</sup>. Modelling using 15q11.2 deletion iPSC has also found reductions in the expression of key genes within this locus and altered dendritic morphology like that seen previously in rodent models indicating that iPSCs can be used to model phenotypes previously identified in rodent models<sup>220</sup>.

Toyoshima *et al*<sup>221</sup> showed that cells carrying 22q11.2 deletions have a reduced ability to form neurons and the function of these neurons is impaired. Further studies<sup>190</sup> have also shown widespread gene expression changes associated with 22q11.2 deletion in pathways relevant to neuronal development and function. However, the gene within this locus which has been focussed on as the driver of these phenotypes is *DGCR8* Microprocessor Complex Subunit (*DGCR8*)<sup>222</sup>, which is involved in the processing of microRNAs (miRNAs) and was shown to alter the expression of many miRNAs which could underly complex alterations in gene expression. These changes in miRNA expression are believed to drive the upregulation of p38 $\alpha$  which in turn drove the altered neurogenic-to-gliogenic competence ratio found by Toyoshima *et al*.

Deletion of the 22q13.3 locus (also known as Phelan-McDermid syndrome) has been studied for effects on iPSC derived neuronal function. This mutation has been associated with increased input resistance and decreases in the frequency of excitatory post synaptic currents mediated by AMPA and NMDAR<sup>223</sup>. These functional changes have

been associated with loss of SH3 And Multiple Ankyrin Repeat Domains 3 (*SHANK3*) expression (a postsynaptic density protein in the 22q13 region) and overexpression of *SHANK3* or treatment with IGF1 have been shown to rescue the loss of pre and post synaptic puncta associated with 22q13.3 deletion<sup>223</sup>. These results highlight the power of using iPSC derived neurons to identify genes within complex mutations which may drive the phenotypes associated with these mutations.

The only CNV with both deletion and duplication forms associated with an increased risk of developing psychiatric disorders which has been studied using human iPSCs is 16p11.2. The study by Deshpande *et al*<sup>224</sup> showed reciprocal changes in neuronal morphology with deletion neurons having increased soma size and dendritic length and duplication neurons having smaller soma and shorter dendrites. However, the functional deficits were similar irrespective of whether the mutation was a deletion or duplication of the 16p11.2 locus. Both types of mutation resulted in a decrease in the density of synapses and an increase in the amplitude of mini excitatory postsynaptic currents. This study demonstrates the fact that opposing mutations can show both reciprocal and convergent phenotypes.

Beyond CNVs iPSC derived neurons have also been used to examine other genetic risk factors for developing psychiatric disorders. Work by Hoffman *et al*<sup>225</sup> has shown that gene expression changes in iPSC derived NPCs and neurons from schizophrenic patients show concordance with gene-expression found in post-mortem adult brains. Many studies have been carried out to examine differences between iPSC NPCs and neurons derived from psychiatric patients and controls. The majority of studies comparing NPCs have shown there is no specific change in the quantity of NPCs produced from psychiatric patient derived cells<sup>226-228</sup>. Yet studies have shown morphological deficits<sup>229</sup> and organizational abnormalities associated with patient derived cells<sup>230</sup>.

Examining the production of neurons; studies have also largely reported no differences between the production of neurons in patient samples compared to controls<sup>228,231,232</sup>. However, there has been some evidence presented of deficits in the generation of dopaminergic neurons<sup>229,233</sup> and the subsequent secretion of catecholamine in association with schizophrenia. In terms of functional deficits early work by Brennand *et al*<sup>231</sup> demonstrated that iPSC derived neurons from schizophrenic patients had decreased connectivity which could be modulated using a specific antipsychotic (loxapine). Further work has demonstrated defects in glutamatergic synapse maturation association with

mutations in the *DISC1* gene, resulting in altered connectivity<sup>226</sup>. Finally, studies have shown that neuronal activity regulated expression of genes including lncRNAs and this gene expression is altered by the functional deficits associated with iPSC neurons derived from schizophrenic patients<sup>234</sup>. The lncRNAs can in turn effect the alternative splicing of genes such as *DISC1* and *ERBB4*<sup>235</sup> reaffirming the fundamental link between gene expression and function.

Studies modelling ASD have largely focussed on syndromic forms of the disorders with studies carried out using patients with Rett syndrome, fragile X syndrome and Timothy syndrome. Studies from Rett syndrome patients showed morphological changes in neurons associated with these mutations and decreases in both the number of synapses and the connectivity of the system produced<sup>236</sup>. Furthermore, these deficits could be partially rescued using insulin-like growth factor 1 which is known to partially rescue Rett phenotypes observed in mouse models<sup>237</sup>. Studies in fragile X syndrome have shown fewer and shorter spines<sup>238</sup> with impaired synaptic outgrowth<sup>239</sup> while this is similar to findings in other syndromic forms of ASD this is in contrast to data from post-mortem studies showing an increased spine density<sup>240</sup>. Work by Tian *et al*<sup>189</sup> has shown that iPSC neurons generated from patients with Timothy syndrome have gene expression changes enriched for ASD susceptibility gene sets and are similar to genes known to be altered in ASD post-mortem brains. While limited studies have been carried out examining the phenotypes associated with non-syndromic ASD with studies focussing on Contactin 5 (CNTN5), Euchromatic Histone Lysine Methyltransferase 2 (EHMT2), Transient Receptor Potential Cation Channel Subfamily C Member 6 (TRPC6) or SHANK2 hypofunction showing aberrant neuronal differentiation resulting in hyper-connective and/or hyperactive neuronal networks<sup>241-243</sup>.

Collectively the studies into ASD, schizophrenia and CNVs associated with psychiatric disorders using iPSC derived neurons have identified a myriad of phenotypes which may be underlying these conditions. However, the reappearance of synaptic phenotypes in many of the studies points towards this as a particularly critical underlying mechanisms and it remains critical that these phenotypes are related to higher order functionality to demonstrate their relevance to real world pathology.

### 3.1.4 Limitations and challenges of iPSC derived neurons for modelling phenotypes associated with psychiatric disorders

The advent of induced pluripotent stem cells and the use of these cells to generate human cell types of pathological interest has opened new avenues in the understanding of diseases especially those with complex multifactorial pathologies. However, these techniques also introduce novel limitations into these studies. The two approaches used to generate the cell types of interest present an interesting interplay between advantages and limitations. As detailed previously developmental patterning approaches present perhaps the cell types with the most similarity to those cells seen *in vivo* in terms of developmental stages and cellular intermediates. Cells derived from direct differentiation may be unable to recapitulate key developmental stages and cellular intermediates. Therefore, studying the interactions between genotype and neurodevelopment must be carried out using a developmental pattern approach or risk missing phenotypes which occur at specific time points in development. This limitation of direct differentiation approaches was elegantly illustrated by the recent work of Schafer *et al*<sup>244</sup>, which showed that the use of neurons generated using the established Neurogenin 2 (NGN2) direct differentiation system obscured key developmental phenotypes which could be seen using a developmental patterning approach.

Another limitation to using iPSCs is heterogeneity introducing confounding variables from unwanted cell types. This is especially relevant in developmental patterning approaches where there is less control being exerted over the system which can result in higher levels of heterogeneity. There are however strategies to address this limitation, the most common being some form of selection for the specific cell type of interest which is a popular method employed in more complex developmental patterning approaches. This usually takes the form of FACS using markers specific to the cell type of interest<sup>245</sup> however again this is not a perfect solution and often there will be some inclusion of undesired cells. Furthermore, while the population of cells collected after FACS is very pure these cells are often not the final mature cell type which is desired as post mitotic functional iPSC derived cells often do not survive this process. Therefore, these cells are often some form of intermediate progenitor cell which therefore may retain some element of multipotency and therefore still introduce some form of heterogeneity.

A final limitation to be considered is that imposed by the use of iPSC themselves as while they have provided critical insight into human development and pathology; as with

all model systems they are not without their limitations. There are two critical limitations when using iPSC, the first is the identification of suitable populations for study and the second partially linked limitations is the background genotype of these individuals. Firstly, it is important to consider the selection of a population for the generation of iPSCs and subsequent study. To study the genetic component of neurodevelopmental and psychiatric disorders one must select a population with similar and significant genetic risk for these disorders. This is achievable using high penetrance low prevalence mutations like CNVs however these are often only identified in patients who also have a psychiatric diagnosis, or some other malady related to the CNV. Therefore, this population may be a subpopulation within the larger population of CNV carriers. Thus, studies using these cohorts may not describe directly the phenotype found in all CNV carriers but may be describing a phenotype found in a subpopulation caused by both the CNV and other environmental and genetic factors. This consideration then links to the second key limitation of using iPSCs and that is the background genotype of these individuals. Patients are likely to have other mutations which may also increase or decrease the risk for developing developmental and neuropsychiatric disorders and these may mask or increase the phenotypes which are directly caused by the mutations of interest. This limitation may be addressed by increasing the number of individuals studied and by correcting the mutations in the cell lines produced therefore creating isogenic controls. However, increasing the number of individuals studied is often not possible due to the low prevalence of these types of mutations. Furthermore, production of isogenic control lines is costly, complex and is only viable when a single gene or small area is mutated which is often not the case in CNVs. Therefore, while iPSCs provide a critical material to study neurodevelopmental and psychiatric disorders it is important to consider the limitations of both the original cell type and the cell type produced to study these disorders.

### 3.2 Chapter 1: Hypothesis and aims

My hypothesis is that iPSC derived neurons with 1q21.1 deletions or duplications will have developmental and functional deficits. Therefore, the aims of this chapter are to investigate the role of 1q21.1 deletion and duplication on the course of early human neuronal development with a specific focus on the development of glutamatergic cortical neurons. Specifically, cortical neurons will be produced based on a developmental paradigm and examined for the production of key neuronal markers. Further investigation will delve into the functionality of these neurons to determine if mutations at the 1q21.1 locus have any effect on neuronal function at both the individual and network level. Finally, by analyzing changes in gene expression caused by mutations at the 1q21.1 locus the previously identified phenotypes will be targeted for pharmacological rescues.

### 3.3 Results

#### 3.3.1 Characterization of iPSCs from patients carrying distal 1q21.1 mutations

Fibroblasts from patients carrying 1q21.1 mutation (Table 3.1) were reprogrammed using non integrating sendai vectors. Cells began with clear fibroblast morphology (flat large cells), 4 days after viral transduction hallmarks of iPSC morphology could be seen with cells shrinking and the nuclear to cytoplasm ratio increasing (Figure 3.2). After 12 days iPSC colonies could be clearly differentiated from the surrounding cells (Figure 3.2). Ultimately successfully reprogrammed iPSCs were isolated and cultured before testing for the expression of key markers of pluripotency at both the gene expression and protein level. These assessments indicated that all cell lines expressed similar levels of the pluripotency markers to an already established and validated iPSC cell line (Figure 3.3 - 3.8). Furthermore, all cell lines stained positive for key markers of pluripotency (Figure 3.4 - 3.8). Finally, each cell line was assessed for 1q21.1 status by exome sequencing to confirm no alteration of this mutation and to assess if any other mutations were present which could confound results. No common mutations other than those at the 1q21.1 locus was identified and therefore all 5 iPSC lines were used for this study (Table 3.1).

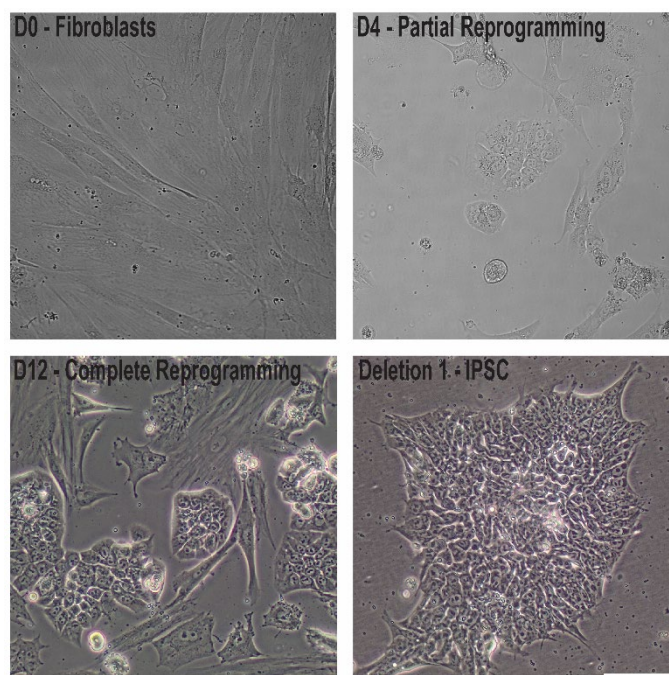


**Figure 3.1: Reprogramming of human fibroblasts into iPSCs.** Example images from the production of iPSC from human fibroblasts highlighting the emergence of iPSC like morphology 4 days post transduction and the clear emergence of iPSCs 12 days after transduction. Scale bars = 100  $\mu$ m

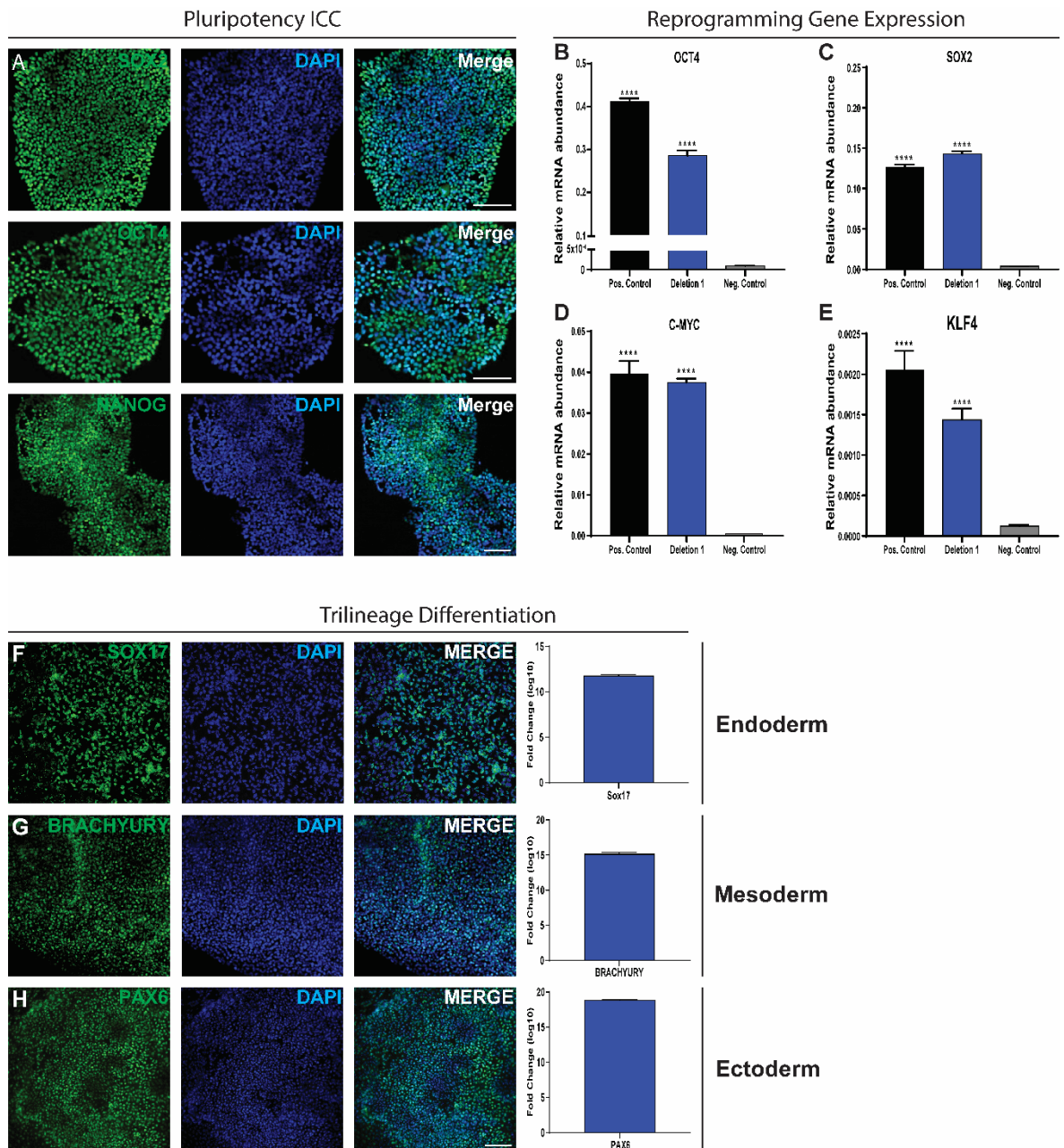


**Figure 3.2: Characterization of iPSCs generated from 1q21.1 deletion patient 1.** **A** Representative image of iPSCs stained for 3 markers of pluripotency (SOX2, OCT4 and NANOG). **B** Expression of *OCT4* in iPSCs generated from 1q21.1 deletion patient 1 as compared to a positive control (hESCs) and a negative control (control iPSC derived neurons). **C** Expression of *SOX2* in iPSCs generated from 1q21.1 deletion patient 1 as compared to a positive control (hESCs) and a negative control (control iPSC derived neurons). **D** Expression of *C-MYC* in iPSCs generated from 1q21.1 deletion patient 1 as compared to a positive control (hESCs) and a negative control (control iPSC derived neurons). **E** Expression of *KLF4* in iPSCs generated from 1q21.1 deletion patient 1 as compared to a positive control (hESCs) and a negative control (control iPSC derived neurons). **F** Representative images and gene expression of *SOX17* in iPSCs pushed to an endoderm fate. **G** Representative images and gene expression of *BRACHYURY* in iPSCs pushed to a mesoderm fate. **H** Representative images and gene expression of *PAX6* in iPSCs pushed to an ectoderm fate. Relative mRNA abundance was calculated compared to *GAPDH* expression. All data is presented as mean  $\pm$  SEM, (n $\geq$ 3) and where appropriate data was analyzed by students T-Test: \*\*\*\*P<0.0001 vs negative control. Scale bar = 100  $\mu$ m.

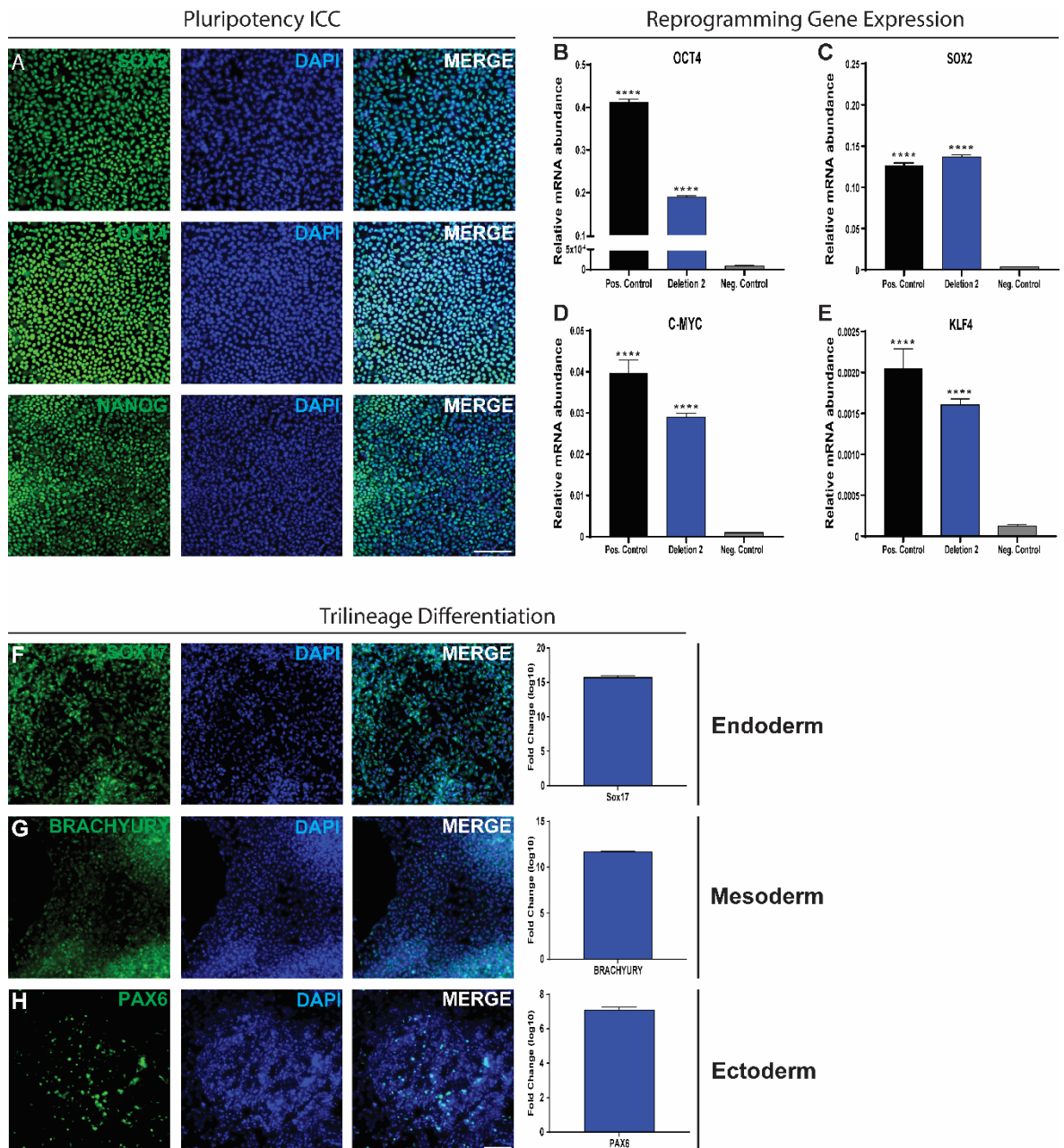


**Figure 3.3: Characterization of iPSCs generated from 1q21.1 deletion patient 2.** **A** Representative image of iPSCs stained for 3 markers of pluripotency (SOX2, OCT4 and NANOG). **B** Expression of *OCT4* in iPSCs generated from 1q21.1 deletion patient 2 as compared to a positive control (hESCs) and a negative control (control iPSC derived neurons). **C** Expression of *SOX2* in iPSCs generated from 1q21.1 deletion patient 2 as compared to a positive control (hESCs) and a negative control (control iPSC derived neurons). **D** Expression of *C-MYC* in iPSCs generated from 1q21.1 deletion patient 2 as compared to a positive control (hESCs) and a negative control (control iPSC derived neurons). **E** Expression of *KLF4* in iPSCs generated from 1q21.1 deletion patient 2 as compared to a positive control (hESCs) and a negative control (control iPSC derived neurons). **F** Representative images and gene expression of *SOX17* in iPSCs pushed to an endoderm fate. **G** Representative images and gene expression of *BRACHYURY* in iPSCs pushed to a mesoderm fate. **H** Representative images and gene expression of *PAX6* in iPSCs pushed to an ectoderm fate. Relative mRNA abundance was calculated compared to *GAPDH* expression. All data is presented as mean  $\pm$  SEM, (n $\geq$ 3) and where appropriate data was analyzed by students T-Test. \*\*\*\*P<0.0001 vs negative control. Scale bar = 100  $\mu$ m.

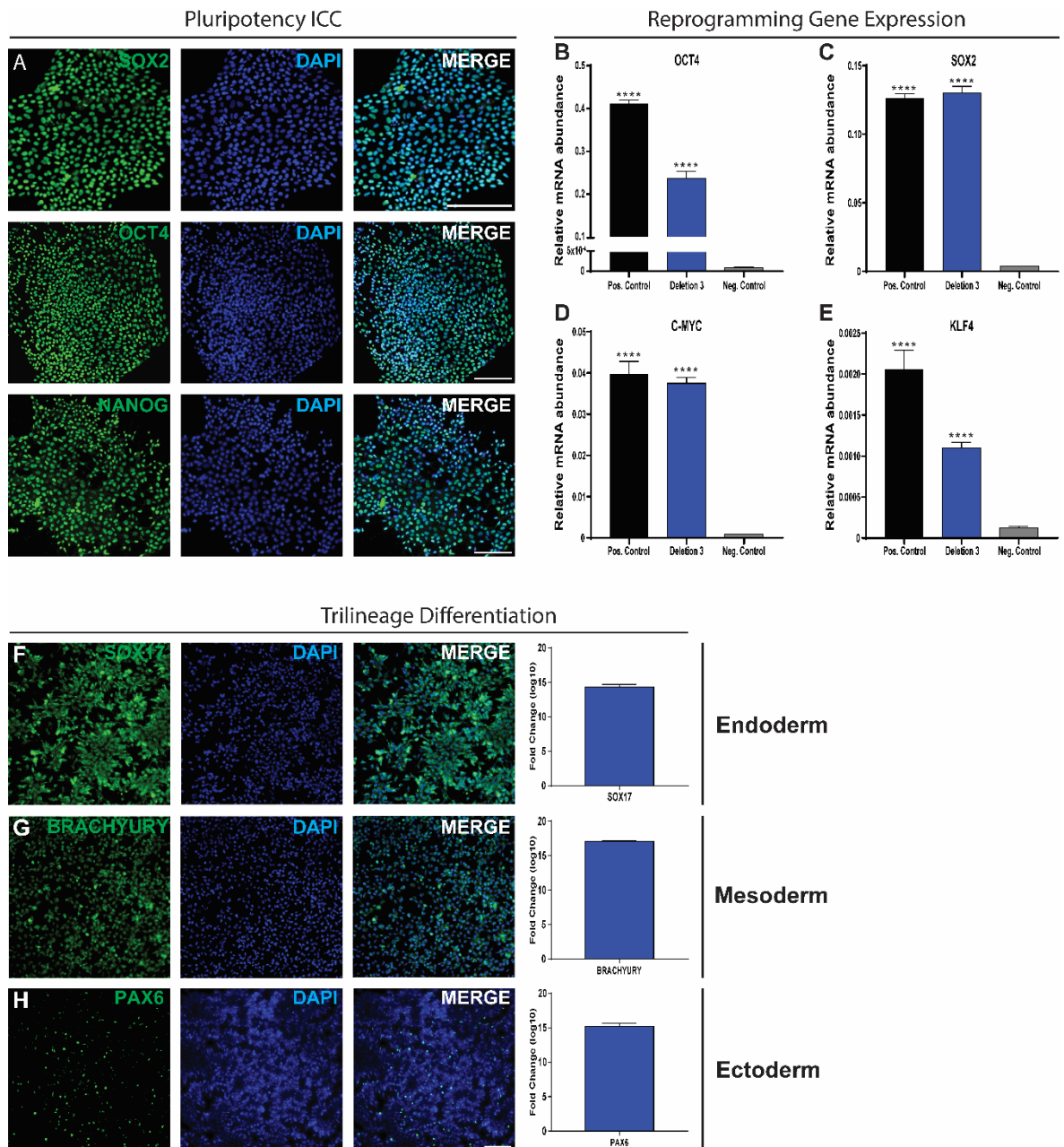


**Figure 3.4: Characterization of iPSCs generated from 1q21.1 deletion patient 3.** **A** Representative image of iPSCs stained for 3 markers of pluripotency (SOX2, OCT4 and NANOG). **B** Expression of *OCT4* in iPSCs generated from 1q21.1 deletion patient 3 as compared to a positive control (hESCs) and a negative control (control iPSC derived neurons). **C** Expression of *SOX2* in iPSCs generated from 1q21.1 deletion patient 3 as compared to a positive control (hESCs) and a negative control (control iPSC derived neurons). **D** Expression of *C-MYC* in iPSCs generated from 1q21.1 deletion patient 3 as compared to a positive control (hESCs) and a negative control (control iPSC derived neurons). **E** Expression of *KLF4* in iPSCs generated from 1q21.1 deletion patient 3 as compared to a positive control (hESCs) and a negative control (control iPSC derived neurons). **F** Representative images and gene expression of *SOX17* in iPSCs pushed to an endoderm fate. **G** Representative images and gene expression of *BRACHYURY* in iPSCs pushed to a mesoderm fate. **H** Representative images and gene expression of *PAX6* in iPSCs pushed to an ectoderm fate. Relative mRNA abundance was calculated compared to *GAPDH* expression. All data is presented as mean  $\pm$  SEM, (n $\geq$ 3) and where appropriate data was analyzed by students T-Test: \*\*\*\*P<0.0001 vs negative control. Scale bar = 100  $\mu$ m.

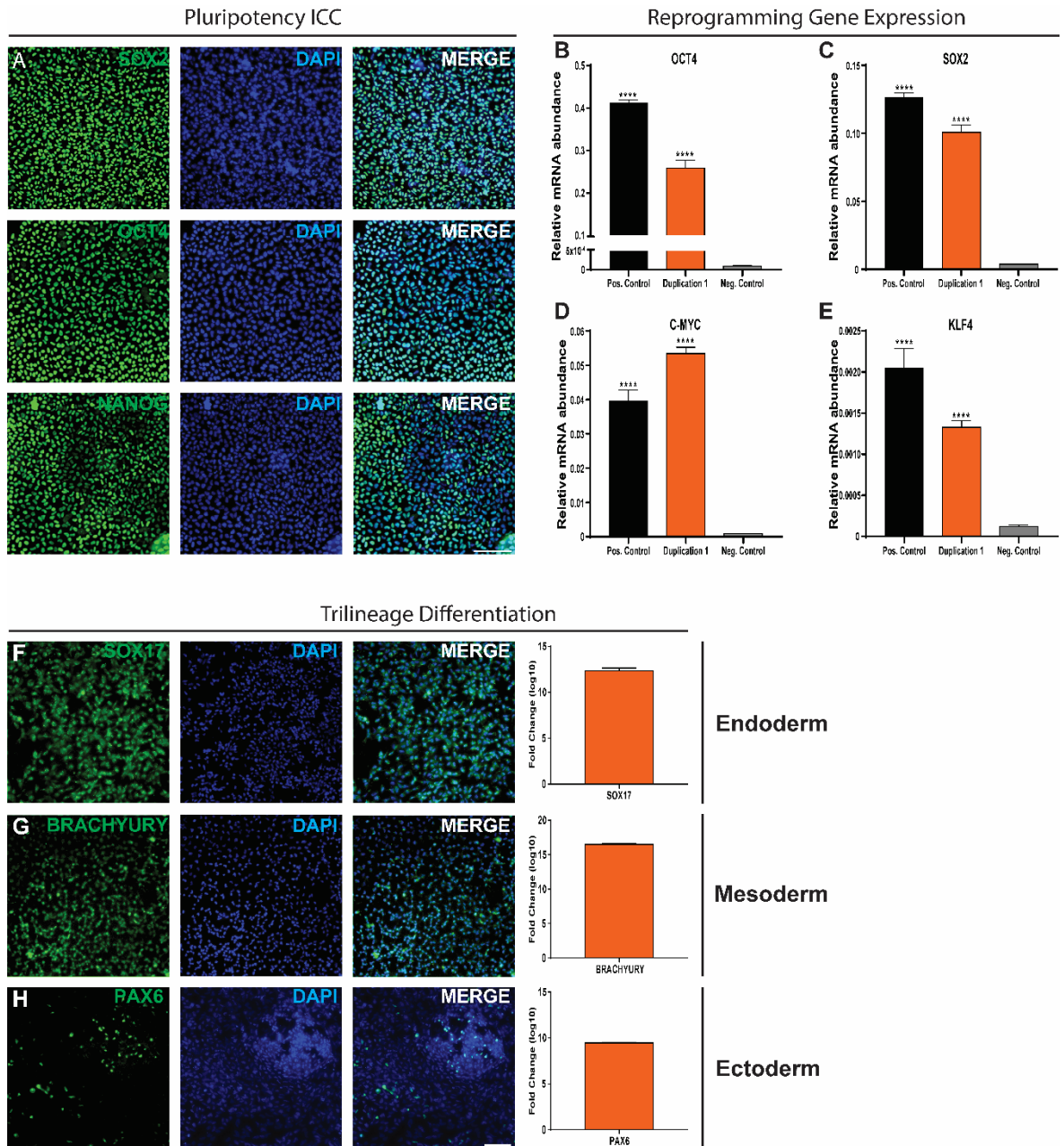


**Figure 3.5: Characterization of iPSCs generated from 1q21.1 duplication patient 1.** **A** Representative image of iPSCs stained for 3 markers of pluripotency (SOX2, OCT4 and NANOG). **B** Expression of *OCT4* in iPSCs generated from 1q21.1 duplication patient 1 as compared to a positive control (hESCs) and a negative control (control iPSC derived neurons). **C** Expression of *SOX2* in iPSCs generated from 1q21.1 duplication patient 1 as compared to a positive control (hESCs) and a negative control (control iPSC derived neurons). **D** Expression of *C-MYC* in iPSCs generated from 1q21.1 duplication patient 1 as compared to a positive control (hESCs) and a negative control (control iPSC derived neurons). **E** Expression of *KLF4* in iPSCs generated from 1q21.1 duplication patient 1 as compared to a positive control (hESCs) and a negative control (control iPSC derived neurons). **F** Representative images and gene expression of *SOX17* in iPSCs pushed to an endoderm fate. **G** Representative images and gene expression of *BRACHYURY* in iPSCs pushed to a mesoderm fate. **H** Representative images and gene expression of *PAX6* in iPSCs pushed to an ectoderm fate. Relative mRNA abundance was calculated compared to *GAPDH* expression. All data is presented as mean  $\pm$  SEM, (n $\geq$ 3) and where appropriate data was analyzed by students T-Test: \*\*\*\*P<0.0001 vs negative control. Scale bar = 100  $\mu$ m.

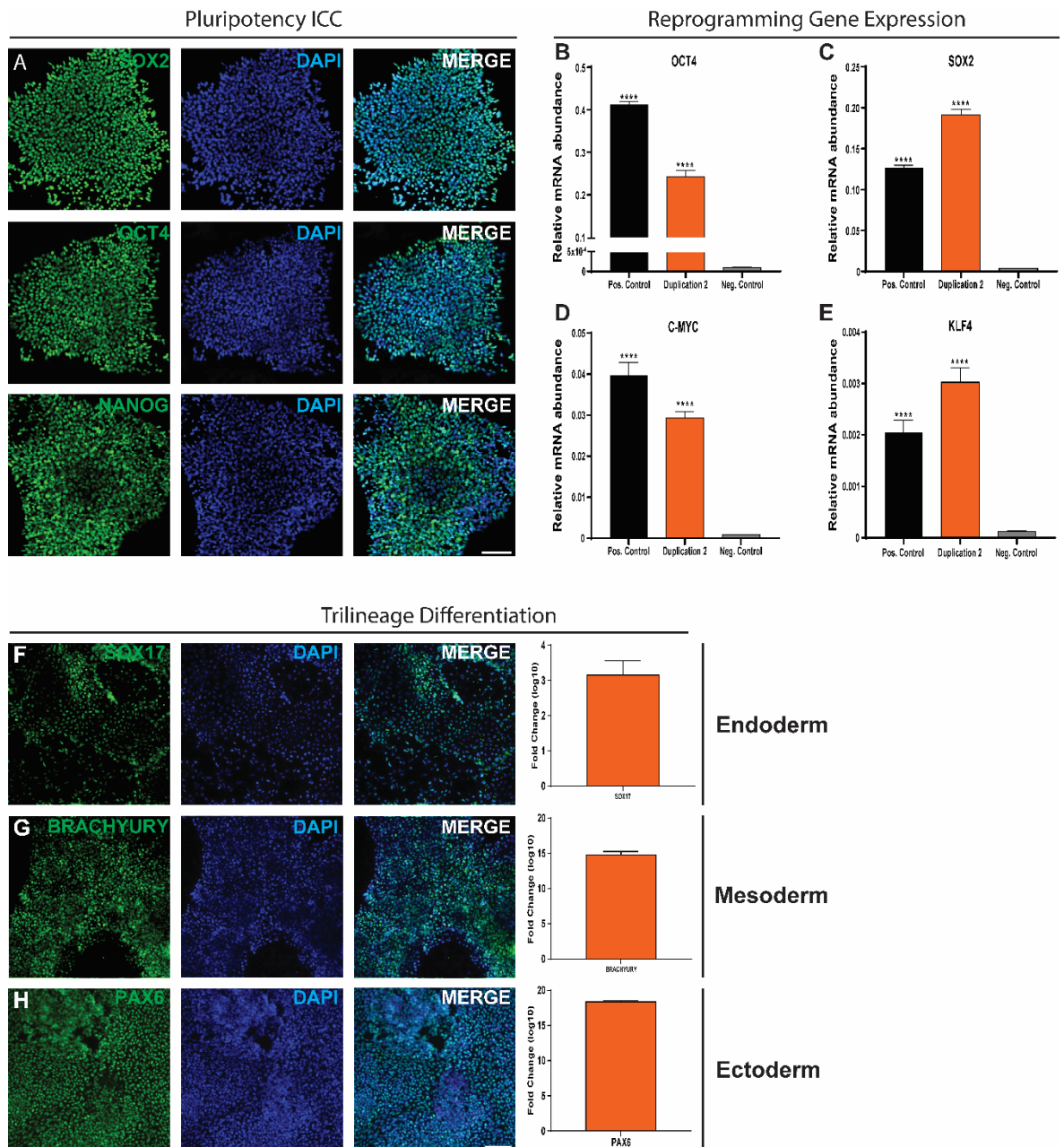


**Figure 3.6: Characterization of iPSCs generated from 1q21.1 duplication patient 2.** **A** Representative image of iPSCs stained for 3 markers of pluripotency (SOX2, OCT4 and NANOG). **B** Expression of *OCT4* in iPSCs generated from 1q21.1 duplication patient 2 as compared to a positive control (hESCs) and a negative control (control iPSC derived neurons). **C** Expression of *SOX2* in iPSCs generated from 1q21.1 duplication patient 2 as compared to a positive control (hESCs) and a negative control (control iPSC derived neurons). **D** Expression of *C-MYC* in iPSCs generated from 1q21.1 duplication patient 2 as compared to a positive control (hESCs) and a negative control (control iPSC derived neurons). **E** Expression of *KLF4* in iPSCs generated from 1q21.1 duplication patient 2 as compared to a positive control (hESCs) and a negative control (control iPSC derived neurons). **F** Representative images and gene expression of *SOX17* in iPSCs pushed to an endoderm fate. **G** Representative images and gene expression of *BRACHYURY* in iPSCs pushed to a mesoderm fate. **H** Representative images and gene expression of *PAX6* in iPSCs pushed to an ectoderm fate. Relative mRNA abundance was calculated compared to *GAPDH* expression. All data is presented as mean  $\pm$  SEM, (n $\geq$ 3) and where appropriate data was analyzed by students T-Test: \*\*\*\*P<0.0001 vs negative control. Scale bar = 100  $\mu$ m.

**Table 3.1: Patient information for all 1q21.1 patients used in the study.** GAD: generalized anxiety disorder; MDD: major depressive; OCD: obsessive compulsive disorder; PD: personality disorder.

Cell Line	Sex	Full Scale IQ	Clinical Symptoms	Medication	1q21.1 Mutation Coordinates	Other CNVs
Deletion 1	Male	77	agoraphobia, avoidant PD, obsessivecompulsive PD, depressive PD, other substance-related disorder, conduct disorder	N/A	chr1:146496661-147375981	chr12:2027625-2550818_dup
Deletion 2	Female	78	Adjustment Disorder, cardiac: deformed valve, narrowing of aorta, thyroid problems, hearing difficulties, sleep apnoea	Citalopram	chr1:146330584-147825662	chr1:63918079-64038174_dup, chr5:19503096-19985234_del
Deletion 3	Male	109	social phobia, OCD, MDD, avoidant PD; interstitial cystitis (daily catheterisation), short stature, recurrent infections; tremor	Propranolol	chr1:146496661-147391614	
Duplication 1	Female	89	social phobia, GAD, MDD, avoidant PD, conduct disorder, hearing difficulties	N/A	chr1:146330584-146982763	
Duplication 2	Female	109	social phobia, panic disorder, agoraphobia, OCD, MDD, psychotic symptoms, schizotypal PD, Borderline PD; osteoarthritis, visual difficulties	Propranolol	chr1:146330584-147825662	

### 3.3.2 Differentiation of iPSCs into cortical excitatory neurons

Generation of cortical excitatory neurons was carried out using a protocol based on dual SMAD inhibition<sup>145</sup> resulting in a neuronal population resembling that of the developing forebrain. This protocol has previously been demonstrated to generate a high proportion of glutamatergic excitatory neurons and recapitulates the development of the lower layers of the human cortex<sup>246</sup>. To demonstrate the predominate cell populations present at two critical points during the neuronal differentiation. The expression of 3 characteristic markers of NPCs and 3 characteristic markers of neurons was assessed after 20 and 50 days of differentiation in 2 control cell lines. Two established iPSC lines were used as controls (IBJ4 see Plumbly *et al*<sup>247</sup> and HPSI1013i-wuye\_2 purchased from HipSci) both cell lines have no known pathogenic CNVs and are from healthy individuals. After 20 days of differentiation the expression of the three NPC markers (Nestin: NES, Zinc Finger And BTB Domain Containing 16: PLZF and Tight Junction Protein 1: ZO1) was high with a significant decrease in the expression of two of these markers after a further 30 days of differentiation (Figure 3.8). In contrast to this the expression of 3 characteristic markers of maturing neurons (Doublecortin: DCX, Neural Cell Adhesion Molecule 1: NCAM and Microtubule Associated Protein 2: MAP2) shows low expression at day 20 with a significant increase in expression after a further 30 days of differentiation (Figure 3.8). Therefore, these results confirm that at day 20 of differentiation cultures are predominantly NPCs and after 50 days of differentiation there is efficient conversion of NPCs into neurons.

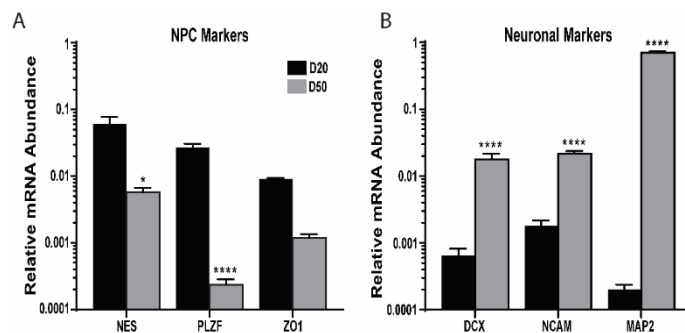


**Figure 3.7: Expression of NPC and Neuronal markers after 20 and 50 days of differentiation.** **A** The expression of NESTIN (*NES*), *PLZF* and *ZO1* mRNA at day 20 and 50 of neuronal differentiation. The time point samples were taken had a significant effect on expression of the three markers ( $F_{1,30}=23.2$ ;  $P<0.0001$ ; Control  $N=2$  and  $n=3$ ). **B** The expression of *DCX*, *NCAM* and *MAP2* mRNA at day 20 and 50 of neuronal differentiation. The time point samples were taken had a significant effect on expression of the three markers ( $F_{1,30}=98.4$ ;  $P<0.0001$ ; Control  $N=2$  and  $n=3$ ). Relative mRNA abundance was calculated compared to *GAPDH* expression. Data sets were analyzed by two-way ANOVA with post hoc comparisons comparing to day 20 samples. Stars above points represent Sidak-corrected post hoc tests. All data presented as means  $\pm$  SEM \* $P<0.05$ ; \*\* $P<0.01$ ; \*\*\*\* $P<0.0001$  vs. Day 20.

### 3.3.3 Mutation at the 1q21.1 locus is associated with altered gene expression at both neuronal precursor and immature neuron stages of development

To demonstrate the validity of this approach for assessing any effect of 1q21.1 mutation on the formation and function of neurons the expression of genes known to be within the 1q21.1 region was assessed first for any expression after 50 days of neuronal differentiation and then for any changes in expression associated with 1q21.1 mutations. Four genes known to be in the distal 1q21.1 region (*BCL9*, *CHD1L*, *GPR89B* and *PRKAB2*) showed relatively high expression in neurons after 50 days of differentiation (Figure 3.9). Examining the expression of these four genes in 1q21.1 neurons showed that two of the four had reciprocal expression associated with deletion and duplication of the 1q21.1 region with *BCL9* and *CHD1L* having significantly lower expression than controls in 1q21.1 deletion neurons and both genes showing increased expression in 1q21.1 duplication neurons. These results indicate that genes within the 1q21.1 locus are expressed in maturing neurons and mutations of the 1q21.1 region are associated with corresponding gene dosage effects in maturing neurons.

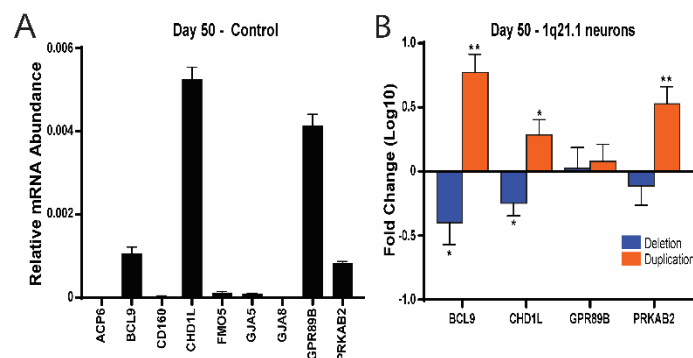


**Figure 3.8: Expression of 1q21.1 genes in day 50 cortical neurons.** **A** The expression of 9 genes localized to the 1q21.1 locus and known to be part of all distal 1q21.1 mutations used for this work (Control N=2 and n=3). **B** Relative gene expression of the 4 most highly expressed genes in the 1q21.1 locus comparing 1q21.1 deletion and duplication neurons to controls (Control N=2, Deletion N=3, Duplication N=2 and n=3). Relative mRNA abundance was calculated compared to *GAPDH* expression. Data was analyzed by Students T-test. All data presented as means  $\pm$  SEM \*P<0.05; \*\*P<0.01; vs. control neurons.

To probe the effect of 1q21.1 mutation on the differentiation of neurons the expression of key genes was assessed at both the neuronal precursor stage (Figure 3.10) and after cells had been allowed to mature into immature neurons (Figure 3.11). At day 20 of differentiation (Figure 3.10) the expression the general neuronal progenitor marker *NES* was upregulated in both 1q21.1 deletion and duplication differentiations compared to control. Furthermore *PLZF* (another general marker of neuronal precursors) was also upregulated in 1q21.1 duplication cultures when compared to controls, while the

expression of *ZO1* remains similar across all cell lines. Examining markers of early dorsal forebrain patterning (Paired Box 6: *PAX6* and T-Box Brain Protein 2: *TBR2*) showed an upregulation of *TBR2* in both 1q21.1 deletion and duplication compared to controls. However, the expression of *PAX6* was up regulated in 1q21.1 deletion and down regulated in 1q21.1 duplication compared to controls. There were also no changes in the expression of midbrain and hindbrain markers (Achaete-Scute Family BHLH Transcription Factor 1: *ASCL1*, Distal-Less Homeobox 1: *DLX1*, NK2 Homeobox 1: *NKX2.1*, GS Homeobox 2: *GSX2*, Engrailed Homeobox 1: *EN1*, Msh Homeobox 2: *MSX2* and Nuclear Receptor Subfamily 4 Group A Member 2: *NURR1*). Furthermore, the expression of these genes was very low (~0.01% of *GAPDH* expression) compared to the expression of the general neuronal precursor markers (~5% of Glyceraldehyde-3-Phosphate Dehydrogenase: *GAPDH* expression) and *PAX6* (Figure 3.10). Overall 1q21.1 mutations are associated with changes in the expression of key NPC gene which are highly expressed at early stages of differentiation (*NESTIN*, *PLZF* and *PAX6*), with no significant changes in the expression of low abundance mRNAs.

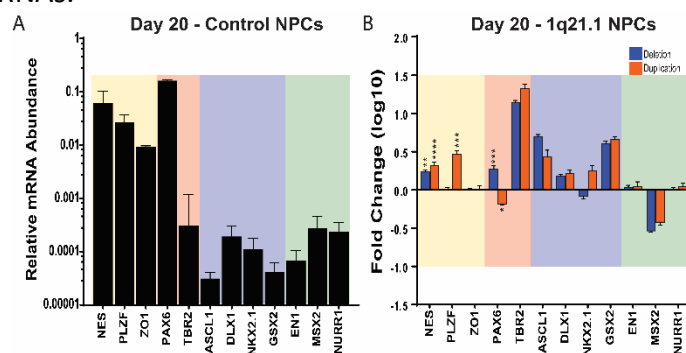


**Figure 3.9: Gene expression of NPC markers in control and 1q21.1 day 20 differentiations.** **A** Expression of general NPC markers (yellow) and markers of forebrain (red), midbrain (blue) and hindbrain (green) development in control day 20 cultures (Control N=2 and n=3). **B** Expression of general NPC markers (yellow) and markers of forebrain (red), midbrain (blue) and hindbrain (green) development in 1q21.1 day 20 differentiations (Control N=2, Deletion N=3, Duplication N=2 and n=3). Relative mRNA abundance was calculated compared to *GAPDH* expression. Fold change is normalized to control day 20 differentiations and all data is presented as mean  $\pm$  SEM. Data was analyzed using multiple T-Tests. Stars represent Holm-Sidak corrected p-values: \*\*P<0.01; \*\*\*P<0.001; \*\*\*\*P<0.0001 vs. control.

Similarly, after 50 days of differentiation genes which are characteristically expressed by immature neurons show high expression (Figure 3.11) in control cultures. The expression of three pan neuronal markers (*DCX*, *NCAM* and *MAP2*) was high with *MAP2* mRNA being particularly abundant. Expression of 3 voltage gated calcium channel subunits was high with Calcium Voltage-Gated Channel Subunit Alpha 1 G (*CACNA1G*) having the highest expression. The expression of *GLUA1* (Glutamate Ionotropic Receptor AMPA Type Subunit 1, a subunit of the AMPA receptor) and *GRIN1* (Glutamate Ionotropic Receptor

NMDA Type Subunit 1, a subunit of the NMDA receptor) was also high, however the expression of *GRIN1* was around 10-fold higher than *GLUA1* therefore suggesting neurons generated in this manner from control iPSCs have a greater amount of NMDA receptors than AMPA receptors. The expression of all 3 glutamate transporters (Vesicular Glutamate Transporter 1/2/3, *VGLUT1/2/3*) was relatively high with *VGLUT1* having the highest expression and while there is some expression of genes related to dopamine synthesis this expression is low compared to all other genes assayed. These results confirm the production of a largely glutamatergic excitatory neuron population in control neuronal differentiations.

The expression of all 3 pan neuronal markers is affected by mutations of the 1q21.1 locus (Figure 3.11) with both deletions and duplication being associated with an increase in *DCX* expression compared to controls. However, there are reciprocal changes in both *NCAM* and *MAP2* expression with 1q21.1 deletions being associated with an increase in expression compared to controls and 1q21.1 duplications being associated with a decrease in expression compared to controls. This indicates the production or maturation of neurons is improved in 1q21.1 deletions and impaired in 1q21.1 duplications.

Three calcium channels were also selected to assess any changes in the expression of three key families of calcium channels. The three genes selected were Calcium Voltage-Gated Channel Subunit Alpha 1B (*CACNA1B*), Calcium Voltage-Gated Channel Subunit Alpha 1C (*CACNA1C*) and Calcium Voltage-Gated Channel Subunit Alpha 1G (*CACNA1G*). Each subunit comprises a critical component of N-type, L-type and T-type calcium channels all found to some degree in neurons of the CNS. The change in expression of voltage gated calcium channels shows a largely similar pattern to that seen with *MAP2* as in the case of both *CACNA1B* and *CACNA1G* there is an increase in expression in 1q21.1 deletion and a decreased expression in 1q21.1 duplication cultures (Figure 3.11). However, in the case of *CACNA1C* both 1q21.1 deletion and duplication are associated with a decrease in expression. The pattern of expression seen in *MAP2* and both *CACNA1B* and *CACNA1G* is again mirrored by *GLUA1* and *GRIN1* expression with a small increase of expression in 1q21.1 deletion cultures and a larger decrease of expression in 1q21.1 duplication cultures. There are also changes in the expression of glutamate transporters resulting from 1q21.1 mutations with a general upregulation of all three transporters with the exception of *VGLUT3* in 1q21.1 deletions which shows a down regulation compared to controls (Figure 3.11). However, *VGLUT1* and *VGLUT2* are the predominant glutamate transporters

expressed in neurons and therefore the upregulation of these two genes is likely more prescient than the changes in vGlut3 expression. There is also a general upregulation of dopamine related genes associated with 1q21.1 deletion and a downregulation associated with duplication. Due to the low overall expression of these genes the changes in expression are likely to have minimal effect.

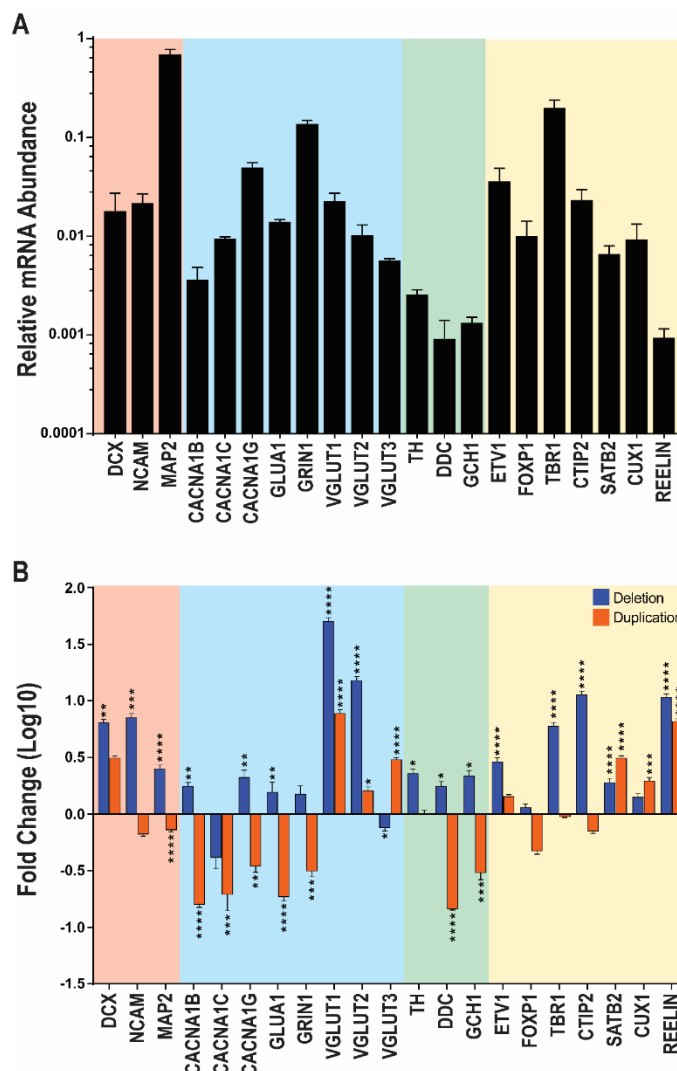


**Figure 3.10: Gene expression of neuronal markers in control and 1q21.1 day 50 differentiations.** **A** Expression of general neuronal markers (red), channels and receptors (blue), dopamine related genes (green) and cortical layer markers (yellow) in control day 50 cultures (Control N=2 and n=3). **B** Expression of general neuronal markers (red), channels and receptors (blue), dopamine related genes (green) and cortical layer markers (yellow) in 1q21.1 deletion and duplication day 50 cultures (Control N=2, Deletion N=3, Duplication N=2 and n=3). Relative mRNA abundance was calculated compared to *GAPDH* expression. Fold change is normalized to control day 50 differentiations and all data is presented as mean  $\pm$  SEM. Data was analyzed using multiple T-Tests. Stars represent Holm-Sidak corrected p-values: \*P<0.05; \*\*P<0.01; \*\*\*P<0.001; \*\*\*\*P<0.001 vs. control.

As this protocol is used to model early human cortical development the expression of cortical layer markers was also assessed. As expected, the levels of lower cortical layer markers (ETS Variant Transcription Factor 1: *ETV1*, Forkhead Box P1: *FOXP1*, T-Box Brain Transcription Factor 1: *TBR1* and BAF Chromatin Remodeling Complex Subunit: *CTIP2*) was high with particularly high expression of *TBR1* (Figure 3.11). Using protocols based on dual

SMAD inhibition it has been previously demonstrated that there is large scale production of lower layer cortical neurons<sup>246</sup>. Therefore, high expression of *TBR1* in particular is expected as this marks the lowest layer of cortical neurons. Both *ETV1* and *FOXP1* are promiscuous markers of the lower layer of the cortex and the expression of these genes is also correspondingly high. Moving up through the cortex the expression of the corresponding markers decreases from that of *TBR1*. The expression of *CTIP2* and *SATB* Homeobox 2 (*SATB2*) are both still relatively high as both mark lower layer cortical neurons and the expression of Cut Like Homeobox 1 (*CUX1*) is also relatively high suggesting there is some production of upper layer cortical neurons. However, the expression of Reelin is very low confirming there is likely little to no production of true upper layer cortical neurons.

In terms of the effect of 1q21.1 mutations on cortical development deletion of the 1q21.1 region is associated with a general increase in the expression of cortical layer markers with a particularly large increase of both *TBR1* and *CTIP2* expression. On the other hand, 1q21.1 duplication was associated with no significant changes in the expression of lower layer cortical neuron markers and an upregulation of genes associated with upper layer cortical neurons. These results confirm that this protocol is a valid model of early human cortical development producing largely lower layer glutamatergic cortical neurons with some small-scale production of upper layer neurons. Furthermore, 1q21.1 mutations have a significant effect on the expression of general neuronal makers and markers specific to both cortical fate and neuronal function.

#### 3.3.4 1q21.1 mutations are associated with alterations in the morphology and production of immature neurons

To investigate the effect of 1q21.1 on the production of immature neurons, the morphology and quantity of neurons was assessed after 30 days of differentiation. At this time point cells are transitioning from NPCs to neurons and begin to express MAP2, however while the morphology of these cells is changing complex neuronal morphology is not yet observable. Measuring the soma size of MAP2 positive immature neurons showed a decrease in 1q21.1 deletions and a corresponding increase in 1q21.1 duplications (Figure 3.12), however the effect sizes of these changes were small with an increase or decrease of around 10  $\mu\text{m}^2$ . Unlike soma size the changes in primary process length and number of primary processes did not show reciprocal changes with 1q21.1 mutation, both deletion

and duplication of the 1q21.1 locus was associated with an increase in primary process length and number of primary processes (Figure 3.12). However, again the effect size of these changes is relatively small particularly when considering the number of primary processes. All immature neurons have either 2 or 3 primary processes and therefore the increase in primary processes in neurons with 1q21.1 mutation is due to a small increase in the proportion of neurons with 3 primary processes. The changes in primary process length are of particular interest as the largest change is in 1q21.1 duplication cells with an almost 20  $\mu\text{m}$  increase in average process length, with 1q21.1 deletion associated with a smaller and more variable increase in process length. Therefore, both 1q21.1 deletion and duplication are associated with changes in immature neuronal morphology.

However, assessing the expression of *DCX* at day 30 of differentiation showed that while 1q21.1 deletion cultures are able to produce immature neurons with similar basic morphology to controls, there is a decrease in the expression of *DCX* (Figure 3.12). As this result and previous data on MAP2 expression at day 50 suggest duplication cultures have a decrease propensity to form neurons, the percentage of MAP2+ cells was evaluated in day 30 cultures. In control cultures most cells are MAP2+ with around 25% of nuclei remaining MAP2-, representing the small population of NPCs (or MAP2- neurons) which remain at this time point. In 1q21.1 deletion cultures there is a small but significant increase in the proportion of MAP2+ cells. On the other hand in 1q21.1 duplication cultures there is a large (almost 50%) loss of MAP2+ cells (Figure 3.12). These results confirm that the gene expression changes are caused by changes in the production of immature neurons with 1q21.1 deletion cultures producing similar amounts of neurons to controls and 1q21.1 duplication cultures producing significantly fewer neurons.

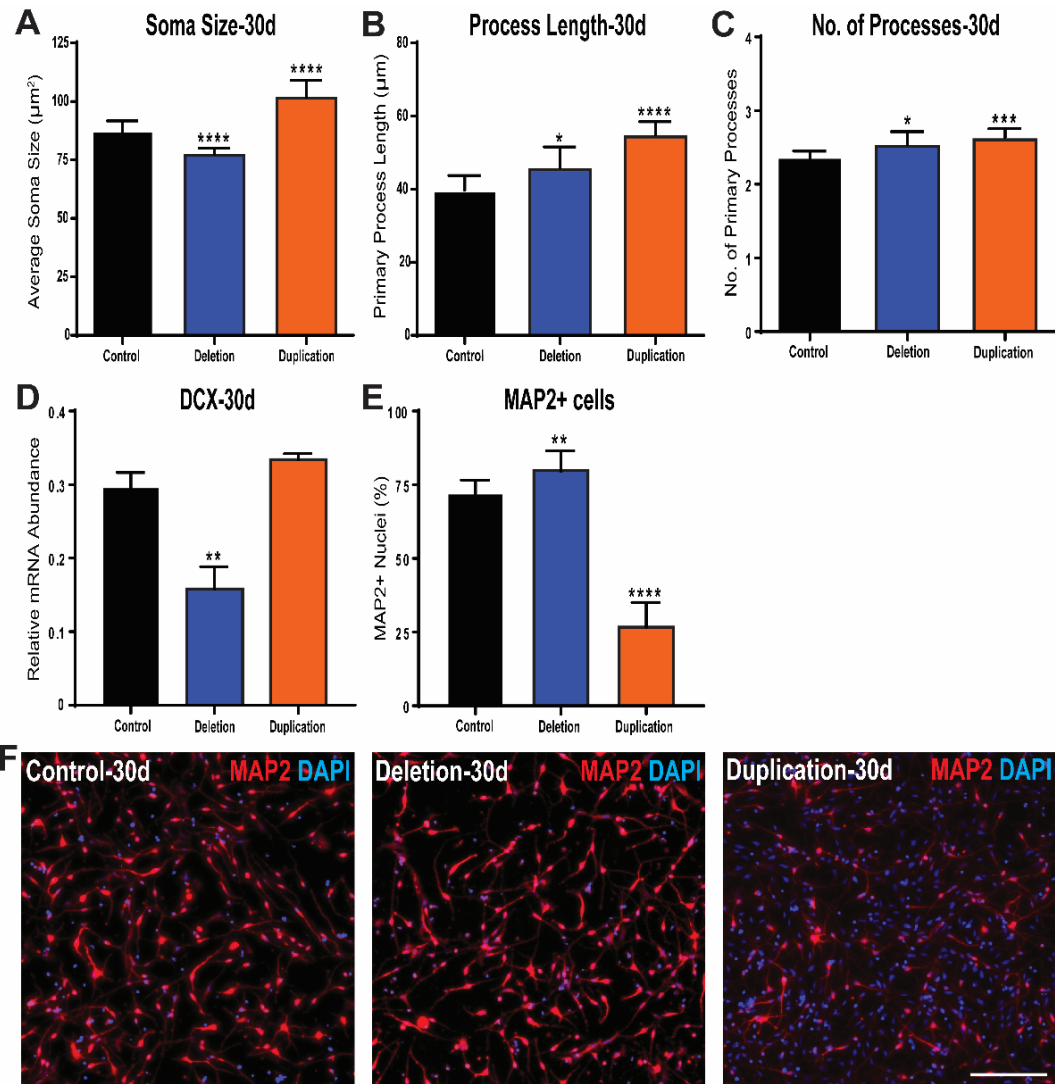


**Figure 3.11: Morphology of immature neurons produced by 1q21.1 mutant cells.** **A** Quantification of average soma size of neurons after 30 days of differentiation (Control N=2, Deletion N=3, Duplication N=2 and n=3). **B** Quantification of MAP2+ process length of neurons after 30 days of differentiation (Control N=2, Deletion N=3, Duplication N=2 and n=3). **C** Quantification of the number of primary MAP2+ branches of neurons after 30 days of differentiation (Control N=2, Deletion N=3, Duplication N=2 and n=3). **D** The expression of *DCX* mRNA at day 30 of neuronal differentiation (Control N=2, Deletion N=3, Duplication N=2 and n=3). Relative mRNA abundance was calculated compared to *GAPDH* expression. **E** Quantification of the percentage of DAPI+ nuclei with were colocalized with Map2 positivity in immature neuronal cultures after 30 days of differentiation (Control N=2, Deletion N=3, Duplication N=2 and n=3). Data was analyzed using Students T-Tests and all data is presented as means  $\pm$  SEM \*P<0.05, \*\*P<0.01; \*\*\*P<0.001; \*\*\*\*P<0.001 vs. control. **F** Representative images of MAP2 positive immature neurons after 30 days of differentiation from a control, deletion and duplication cell line. Scale bar = 50  $\mu\text{m}$ .

### 3.3.5 Deletions and duplications of the 1q21.1 region are associated with altered developmental trajectories

With evidence of changes in the production of neurons after 30 days of differentiation and similar indications from gene expression changes after 50 days of differentiation the longitudinal expression of 3 genes was examined (*PAX6*, *NES* and *MAP2*); each marking a separate stage of early neuronal differentiation (Figure 3.13). As a marker of neuroectodermal specification the expression of *PAX6* was highest at day 20 of differentiation and all cultures followed a similar trajectory with a large decrease in *PAX6* expression. However, after 30 days of differentiation 1q21.1 duplication cultures had a decrease level of *PAX6* expression compared to both controls and 1q21.1 deletions and after 40 days of differentiation 1q21.1 deletion cultures had an increase in the expression of *PAX6* compared to both control and 1q21.1 duplication cultures. The expression of *NES* (a marker of NPCs) showed a largely similar pattern to *PAX6* with a general decrease in expression across all cultures with 1q21.1 duplication cultures starting with a higher expression than either control or deletion cultures.

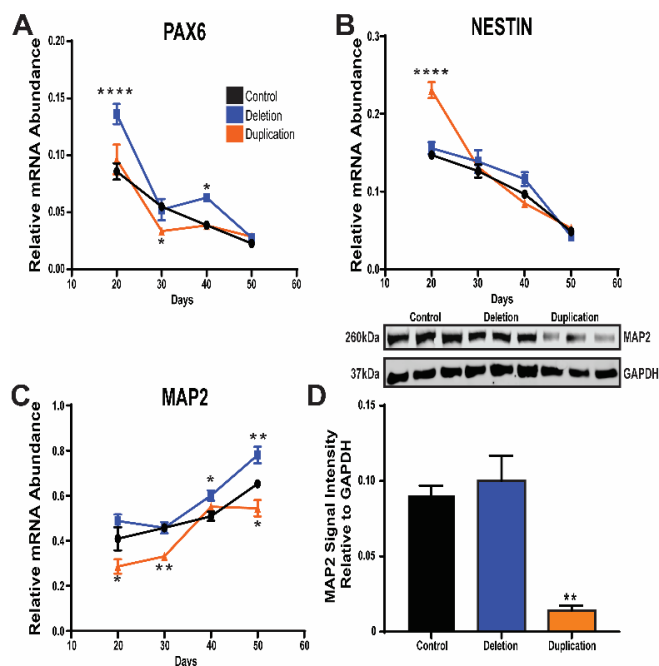


**Figure 3.12: Longitudinal expression of neuronal markers in control and 1q21.1 deletion or duplication neuronal differentiations.** **A** The expression of *PAX6* through the course of the neuronal differentiations (from day 20 to day 50). Both genotype ( $F_{2,65}=15.06$ ;  $P<0.0001$ ; Control N=2, Deletion N=3, Duplication N=2 and n=3) and time ( $F_{3,65}=99.75$ ;  $P<0.0001$ ; Control N=2, Deletion N=3, Duplication N=2 and n=3) had significant effects on *PAX6* expression. **B** The expression of *NES* through the course of the neuronal differentiations (from day 20 to day 50). Both genotype ( $F_{2,65}=7.94$ ;  $P<0.001$ ; Control N=2, Deletion N=3, Duplication N=2 and n=3) and time ( $F_{3,65}=193$ ;  $P<0.0001$ ; Control N=3, Duplication N=2 and n=3) had significant effects on *NES* expression. **C** The expression of *MAP2* through the course of the neuronal differentiations (from day 20 to day 50). Both genotype ( $F_{2,65}=28.17$ ;  $P<0.0001$ ; Control N=2, Deletion N=3, Duplication N=2 and n=3) and time ( $F_{3,65}=53.13$ ;  $P<0.0001$ ; Control N=2, Deletion N=3, Duplication N=2 and n=3) had significant effects on *MAP2* expression. Relative mRNA abundance was calculated compared to *GAPDH* expression. Data sets were analyzed by two-way ANOVA with post hoc comparisons using Dunnett's multiple comparisons test comparing to control samples. Stars above points represent Dunnett-corrected post hoc tests. **D** Representative western blot protein bands and histograms for Map2 expression normalized to GAPDH. Data was analyzed using Students T-Test ( $n\geq 3$ ). All data presented as means  $\pm$  SEM \* $P<0.05$ ; \*\* $P<0.01$ ; \*\*\*\* $P<0.0001$  vs. control.

Finally, *MAP2* (a general marker of immature neurons and neuronal complexity) showed an opposing pattern with a significant increase in *MAP2* expression from early time points to later time points (Figure 3.13). For all time points except day 40 1q21.1 duplication cultures were associated with a decreased expression of *MAP2* compared to control or deletion cultures. On the other hand, 1q21.1 deletion cultures show no change in *MAP2* expression between day 20 and day 30 of differentiation followed by a sharp and sustained increase in *MAP2* expression for the remainder of the time course. At both day 40 and day 50 of differentiation 1q21.1 deletion cultures have an increase expression of *MAP2* compared to controls. Similarly, previous results (Figure 3.13) have illustrated a small but significant increase in *MAP2* positive cells at day 30 of differentiation. Taken together these results suggest that 1q21.1 deletion cultures produce more *MAP2* and therefore likely produce more neurons from early time points through to later time points.

To confirm the differences in *MAP2* expression at day 50 the protein levels of *MAP2* were quantified by western blot (Figure 3.13) which showed a largely similar level of *MAP2* in control and 1q21.1 deletion cultures indicating that the changes in *MAP2* mRNA expression may not be fully translated in protein. However, there was a large decrease in the levels of *MAP2* protein in 1q21.1 duplication cultures reconfirming that there were significantly fewer immature neurons in these cultures. Overall these results suggest that cells carrying 1q21.1 deletions are capable of producing neurons in similar if not larger quantities than controls but cell with 1q21.1 duplications have a deficit in neuronal production.

As *MAP2* is a general marker of neuronal maturity and therefore only an indication of an increased production of neurons it was important to consider if the production of particular subgroups of neurons was affected. The simplest way of subgrouping neurons is into excitatory and inhibitory neurons and given dual SMAD inhibition based protocols are known to produced largely excitatory neurons with a small proportion of inhibitory neurons it was critical to assess if this proportionality was altered by the increase in neuronal production associated with 1q21.1 deletion. Using a marker of inhibitory neurons (Glutamate Decarboxylase 1, *GAD67*) and a marker of excitatory neurons (*VGLUT1*) it was clear that the increase in neurons in 1q21.1 deletion cultures is likely a specific increase in excitatory (*VGLUT1*+) neurons rather than a general increase in all neurons (Figure 3.14). While there is also a small increase in *GAD67* and *VGLUT1* in 1q21.1 duplication cultures this is orders of magnitude smaller than the increase in *VGLUT1* seen in 1q21.1 deletion

cultures suggesting that there may be small changes in the production of these markers but consistent with a similar or lower production of neurons in these cultures. These results suggest that 1q21.1 deletion and not duplication influences the proportionality of excitatory and inhibitory neurons produced under this protocol.

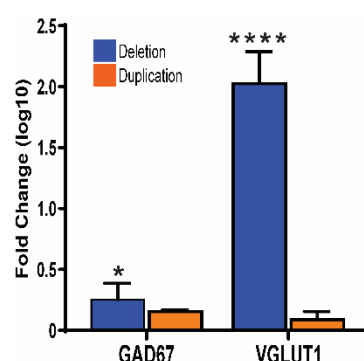


**Figure 3.13: Expression of an excitatory and an inhibitory neuronal marker in day 40 differentiations.** Expression of *GAD67* and *VGLUT1* in day 40 neuronal cultures. Relative mRNA abundance was calculated compared to *GAPDH* expression. Fold change was normalized to the expression in control cultures. Data was analyzed using Students T-Test (Control N=2, Deletion N=3, Duplication N=2 and n=3). All data presented as means  $\pm$  SEM \* $P$ <0.05; \*\*\*\* $P$ <0.0001 vs. control.

### 3.3.6 Mutations at the 1q21.1 locus are associated with altered early cortical development

To further examine the impact of 1q21.1 mutations on the ability of lower cortical neuron production the expression of two lower cortical layer markers was examined (*TBR1* and *CTIP2*). As previously stated, the primary neurons produced at early stages of this protocol are *TBR1*<sup>+</sup> neurons and thus the expression of *TBR1* mRNA increases rapidly in all cultures (Figure 3.15). However, by far the largest increase in *TBR1* expression is in 1q21.1 deletion cultures which diverge from duplication and control cultures at day 40 and continue to increase in expression at day 50. The increase in *TBR1* in 1q21.1 deletion cultures is also seen at the protein level (measured at day 50) but while there is a trend for an increase in the number of *TBR1*<sup>+</sup> cells this is not significant at day 50. While 1q21.1 duplication cultures also have a small but significant increase of *TBR1* mRNA expression at day 30 and 40 the slow rate of increase compared to controls means that by day 50 there is no significant difference between 1q21.1 duplication cultures and controls. The similarities in *TBR1* expression between control and 1q21.1 duplication cultures are also seen at protein level and there is no significant difference between the percentage of *MAP2*<sup>+</sup> cells which are also *TBR1*<sup>+</sup> in 1q21.1 duplication cultures compared to controls.

The expression of *CTIP2* shows a much more reciprocal relationship with 1q21.1 deletion and duplication cultures diverging from control after day 20 (Figure 3.15). In 1q21.1 deletion cultures there is a sharp increase in expression of *CTIP2* mRNA after day

30 of differentiation resulting in higher expression than control cultures at both day 40 and day 50. The increase of CTIP2 mRNA is also seen at protein level, observed by western blotting and at a cellular level with more MAP2+ cells which also stain positive for CTIP2; suggesting the increased production of CTIP2+ cells in 1q21.1 deletion cultures is a particularly robust phenotype. The expression of *CTIP2* mRNA in 1q21.1 duplication cultures shows a reciprocal phenotype with a decreased expression from day 40 compared to controls. However similarly to *TBR1* there is no significant difference between control and 1q21.1 duplication cultures when examining CTIP2 protein levels or the number of MAP2+ cells co-expressing CTIP2. Given previous results on the decrease MAP2 expression in 1q21.1 duplication cultures it is critical that both cell counts are normalised to MAP2 positivity therefore bypassing any changes in the number of neurons. These results show that 1q21.1 deletion cultures produce more CTIP2+ neurons and indicate there may be an increase production of TBR1 neurons or an overexpression of *TBR1* in TBR1+ neurons. However, 1q21.1 duplication cultures show similar expression of TBR1 and CTIP2 therefore indicating that while there may be deficits in the production of neurons the neurons produced (as identified by MAP2 expression) express markers of lower layer cortical neurons at similar proportions to control cultures.

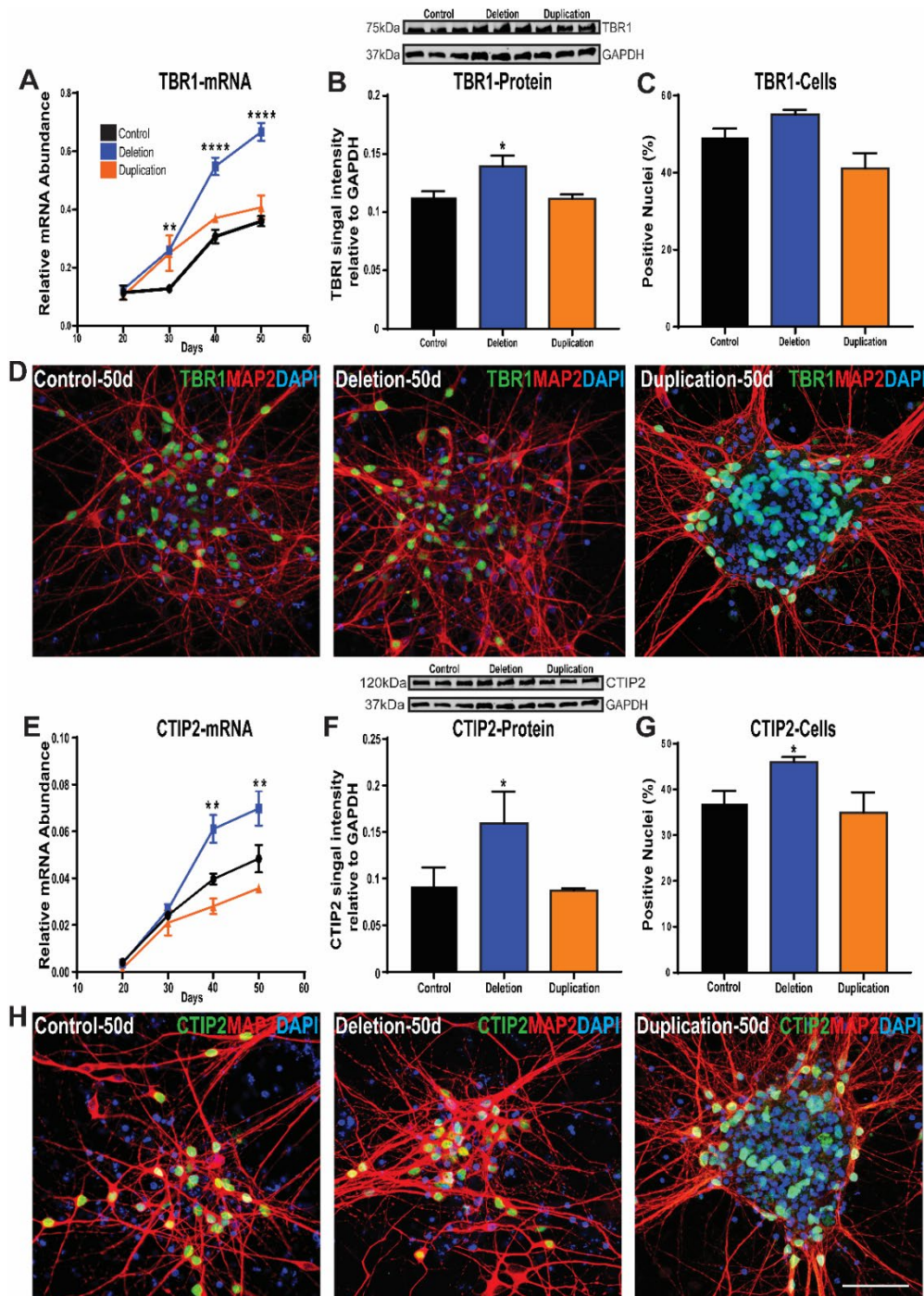


**Figure 3.14: Lower layer cortical neuron patterning in control and 1q21.1 neuronal differentiations.** **A** The expression of TBR1 through the course of the neuronal differentiations (from day 20 to day 50). Both genotype ( $F_{2,84}=57.55$ ;  $P<0.0001$ ; Control  $N=2$ , Deletion  $N=3$ , Duplication  $N=2$  and  $n=3$ ) and time ( $F_{3,84}=365.8$ ;  $P<0.0001$ ; Control  $N=2$ , Deletion  $N=3$ , Duplication  $N=2$  and  $n=3$ ) had significant effects on TBR1 expression. Relative mRNA abundance was calculated compared to *GAPDH* expression. **B** Representative western blot protein bands and histograms for TBR1 expression normalized to *GAPDH* (Control  $N=2$ , Deletion  $N=3$ , Duplication  $N=2$  and  $n=3$ ). **C** Quantification of the percentage of MAP2 positive cells which co-express TBR1 (Control  $N=2$ , Deletion  $N=3$ , Duplication  $N=2$  and  $n=3$ ). **D** Representative images of MAP2 and TBR1 colocalization from a control, deletion and duplication cell line. **E** The expression of CTIP2 through the course of the neuronal differentiations (from day 20 to day 50). Both genotype ( $F_{2,84}=199.7$ ;  $P<0.0001$ ; Control  $N=2$ , Deletion  $N=3$ , Duplication  $N=2$  and  $n=3$ ) and time ( $F_{3,84}=133.2$ ;  $P<0.0001$ ; Control  $N=2$ , Deletion  $N=3$ , Duplication  $N=2$  and  $n=3$ ) had significant effects on CTIP2 expression. Relative mRNA abundance was calculated compared to *GAPDH* expression. **F** Representative western blot protein bands and histograms for CTIP2 expression normalized to *GAPDH* (Control  $N=2$ , Deletion  $N=3$ , Duplication  $N=2$  and  $n=3$ ). **G** Quantification of the percentage of MAP2 positive cells which co-express CTIP2 (Control  $N=2$ , Deletion  $N=3$ , Duplication  $N=2$  and  $n=3$ ). **H** Representative images of MAP2 and CTIP2 colocalization from a control, deletion and duplication cell line. Scale bar = 50  $\mu\text{m}$ . Data sets were analyzed by Students T-Test or two-way ANOVA with post hoc comparisons using Dunnett's multiple comparisons test comparing to control samples. Where appropriate (A and E) stars above points represent Dunnett-corrected post hoc tests otherwise stars represent results from T-Tests. All data presented as means  $\pm$  SEM \* $P<0.05$ ; \*\* $P<0.01$ ; \*\*\* $P<0.001$  \*\*\*\* $P<0.0001$  vs. control.

### 3.3.7 A mouse model of 1q21.1 microdeletion shows altered cortical development

With human 1q21.1 neuronal differentiations showing deficits in the production of lower cortical layer neurons a mouse model of 1q21.1 microdeletion was assessed for the production of lower layer cortical neurons using the same two markers (Tbr1 and Ctip2). This assessment showed that the 1q21.1 microdeletion mouse model had an increase in Tbr1+ cells compared to litter mate controls (Figure 3.16). However, there was no difference in the number of Ctip2+ cells when comparing the 1q21.1 mouse model to litter mate controls. While these results are limited to these two markers, they do indicate a cortical layer phenotype in the mouse model suggesting that the underlying genotype driving this phenotype may be common between both mice and human.

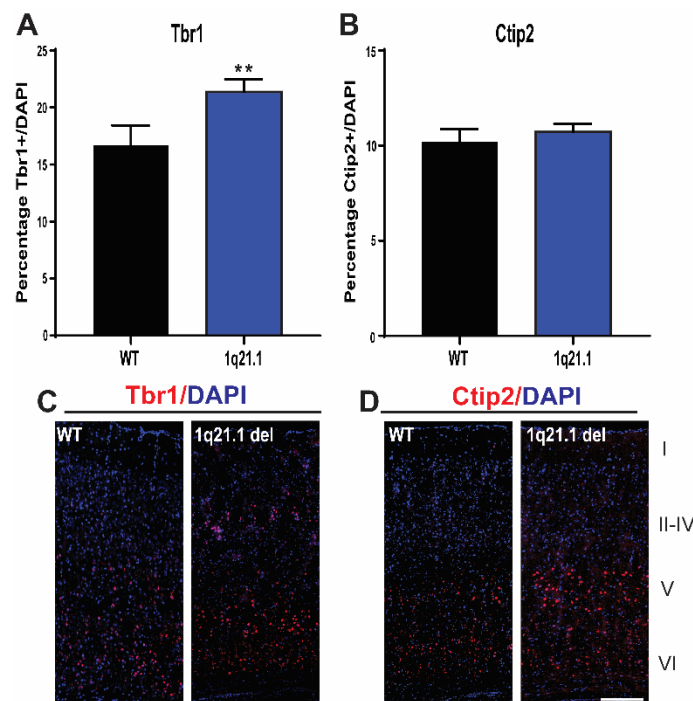


**Figure 3.15: Quantification of lower layer cortical markers in adult mouse brains modelling 1q21.1 microdeletion.** **A** Quantification of Tbr1+ nuclei in the somatosensory cortex of adult mice modelling 1q21.1 microdeletion and litter matched controls given as a percentage of nuclei in a 300  $\mu$ m section of cortex. **B** Quantification of Ctip2+ nuclei in the somatosensory cortex of adult mice modelling 1q21.1 microdeletion and litter matched controls given as a percentage of nuclei in a 300  $\mu$ m section of cortex. All data presented as mean  $\pm$  SEM; \*\*P<0.01. Data was analyzed using Student's T-tests with 6 animals per group and n=3 for each animal. **C** Example images of Tbr1+ cells in the somatosensory cortex of adult mice both wild type (WT) and from the 1q21.1 microdeletion model (1q21.1). **D** Example images of Ctip2+ cells in the somatosensory cortex of adult mice both wild type (WT) and from the 1q21.1 microdeletion model (1q21.1). Markers correspond to cortical layers. Scale Bar = 100  $\mu$ m.

### 3.3.8 Neurons carrying 1q21.1 mutations have altered capacity to produce synapses

To investigate the effect the changes in differentiation may have on the functionality of the resultant cells the production of synapses was assessed. To understand the effect of 1q21.1 mutation on the production of synapses the expression of a pre-synaptic protein, Synaptophysin (*SYN*), and a post-synaptic protein, Discs Large MAGUK Scaffold Protein 4 (*PSD-95*), was examined. The expression of *SYN* mRNA showed an increased expression in 1q21.1 deletion neurons compared to controls whereas 1q21.1 duplication neurons showed a similar expression to controls (Figure 3.17). However, the expression of *PSD-95* mRNA showed a reciprocal pattern with an increased expression in 1q21.1 deletion neurons and a decreased expression in 1q21.1 duplication neurons compared to control.

However, given the previously identified changes in the production and complexity of neurons in these cultures it was critical to identify if these changes were simply due to changes in the amount or complexity of neurons. To achieve this the expression of both markers was assessed at protein level and normalised to an endogenous control (*GAPDH*) and then further normalised to the expression of *MAP2* protein. This quantification therefore begins to examine the expression of these markers without the confound of differential neuronal production or morphology. Unlike at mRNA level *SYN* protein expression normalised to *MAP2* showed that both 1q21.1 deletion neurons and control neurons had similar expression of *SYN* protein, but 1q21.1 duplication neurons showed a significant loss of *SYN* protein compared to control (Figure 3.17). On the other hand, *PSD-95* protein expression showed a similar pattern to mRNA expression with increased expression in 1q21.1 deletion neurons and a decreased expression in 1q21.1 duplication neurons.

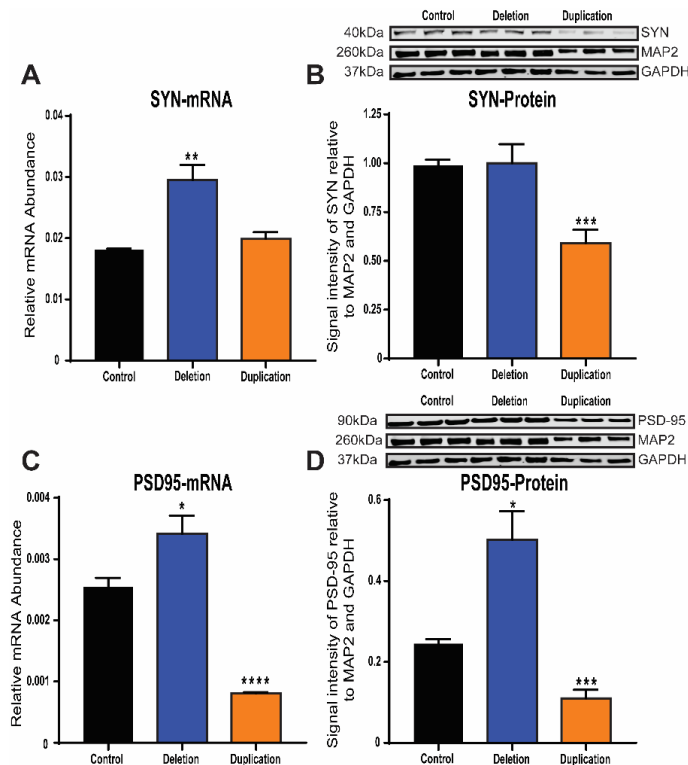


**Figure 3.16: The expression of synapse associated genes in control and 1q21.1 day 50 neuronal cultures.** **A** The expression of SYN mRNA at day 50 of neuronal differentiation (Control N=2, Deletion N=3, Duplication N=2 and n=3). Relative mRNA abundance was calculated compared to *GAPDH* expression. **B** Representative western blot protein bands and histograms for SYN expression normalized to both GAPDH and MAP2 (Control N=2, Deletion N=3, Duplication N=2 and n=3). **C** The expression of PSD-95 mRNA at day 50 of neuronal differentiation (Control N=2, Deletion N=3, Duplication N=2 and n=3). Relative mRNA abundance was calculated compared to *GAPDH* expression. **D** Representative western blot protein bands and histograms for PSD-95 expression normalized to both GAPDH and MAP2 (Control N=2, Deletion N=3, Duplication N=2 and n=3). Data was analyzed using Students T-Tests and all data is presented as means  $\pm$  SEM; \* $P < 0.05$ ; \*\* $P < 0.01$ ; \*\*\* $P < 0.001$ ; \*\*\*\* $P < 0.0001$  vs. control.

Finally, to confirm the changes in SYN expression the number of SYN+ puncta was quantified and normalised to the total area of MAP2+ staining thereby again assessing the number of SYN+ pre-synaptic termini account for some of the changes in number and complexity of neurons. This quantification showed a similar pattern to that seen in PSD-95 expression with an increased number of SYN+ puncta in 1q21.1 deletion neurons and a decrease in puncta in 1q21.1 duplication neurons (Figure 3.18). These results confirm that 1q21.1 mutations have an effect on the production of synapses and critically while this effect may be linked to the previously identified differentiation phenotypes the changes in synapse production may not simply be due to an increase in the number of neurons or an increase in the complexity of the neurons produced as indicated by increased expression of MAP2 in previous data.

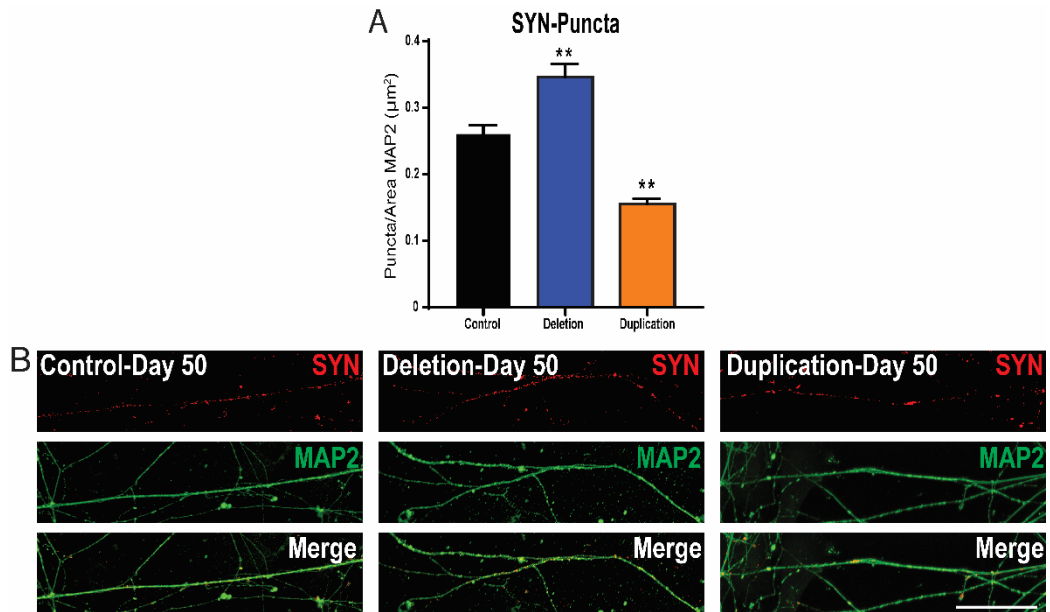


**Figure 3.17: The quantification of presynaptic densities in day 50 neurons.** **A** Quantification of the number of SYN positive puncta normalized to the area which stained positive for MAP2 (Control N=2, Deletion N=3, Duplication N=2 and n=3). **B** Representative images of SYN positive puncta in a control, deletion and duplication cell line. Scale bar = 50 µm. Data was analyzed using Students T-Tests and all data is presented as means ± SEM \*\*P<0.01 vs. control.

### 3.3.9 Deletion or duplication of the 1q21.1 locus changes the ability of neurons to function

Calcium measurements in iPSC-neurons provide information about neuronal activity providing a convenient method to begin to assess the effect of 1q21.1 mutations on neuronal function. Cells were preloaded with a fluorescent calcium indicator, and changes in intracellular calcium levels were recorded as a proxy to monitor neuronal activity. Using this paradigm, it is possible to ascertain if differences in neuronal differentiation, morphology and synapse production are likely to have an effect on neuronal function. Given previous data on the differential ability of 1q21.1 mutant cells to produce neurons; firstly the percentage of cells identified (using commercially available software) which showed at least one characteristically neuronal calcium event (defined as a rise time <1 second, fall time <2 seconds) was quantified. This analysis showed that in both control and 1q21.1 deletion cultures around 80% of the cells identified using the automated analysis showed at least one characteristically neuronal calcium event in a 5 minute recording (Figure 3.19). In 1q21.1 duplication cultures the percentage of active cells was significantly lower with only around 35% of cells showing at least one neuronal calcium event across the 5-minute recording.

Examining the number of neuronal calcium events per minute the difference between 1q21.1 deletion neurons and controls became clear, with 1q21.1 deletion neurons being around 30% more active than control neurons (Figure 3.14). However, in this case the duplication and control neurons were similar in their activity. These results show that while 1q21.1 duplication cultures produce fewer active cells (as measured by calcium activity) the neurons which are produced function in a similar fashion to the controls. Whereas the deletion of the 1q21.1 region has no significant effect on the number of active cells (as measured by calcium activity) but significantly increases the activity of these cells. Finally, examining the traces of these calcium events it is clear that deletion of the 1q21.1 region is more commonly associated with trains of spikes (Figure 3.19) with clear definition between spikes but troughs between these peaks failing to return to base line.

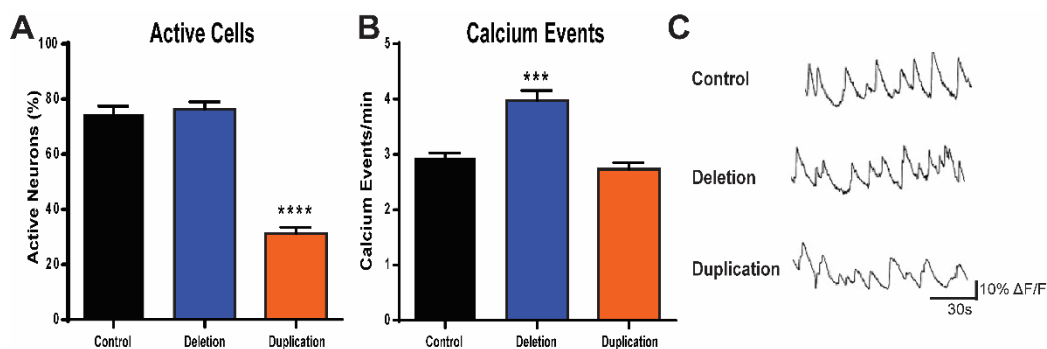


**Figure 3.18: Analysis of calcium kinetics in neurons carrying 1q21.1 mutations.** **A** Quantification of soma which show at least 1 characteristically neuronal calcium event (Control N=2, Deletion N=3, Duplication N=2 and n=3). **B** Number of characteristically neuronal calcium events recorded per minute (Control N=2, Deletion N=3, Duplication N=2 and n=3). **C** Representative traces of calcium events as measured by changes in fluorescence from a control, deletion and duplication cell line (Control N=2, Deletion N=3, Duplication N=2 and n=3). Data was analysed using Students T-Tests and all data is presented as means  $\pm$  SEM \*\*\*P<0.001; \*\*\*\*P<0.0001 vs. control.

To examine the contribution of AMPA and NMDA signalling on the activity of neurons within these cultures the NMDA receptor antagonist AP5 (D-2-amino-5-phosphonopentanoate) and the AMPA receptor antagonist CNQX (6-Cyano-7-nitroquinoxaline-2,3-dione) were added to cultures for 10 minutes. After incubation with either AP5 or CNQX the percentage of active cells was again quantified. This analysis showed that inhibition of either AMPA or NMDA signalling in control or 1q21.1 deletion cultures reduced the percentage of active cells by around 1/3 (Figure 3.20). In the case of 1q21.1 deletion cultures this reduction put the levels of active cells into a similar range, to that found in 1q21.1 duplication cultures suggesting that the reduced level of activity in these cultures may be due to a lack of neuronal signalling through either AMPA or NMDA pathways. In 1q21.1 duplication cultures only the inhibition of AMPA signalling by CNQX

significantly reduced the percentage of active cells. This result suggests that in 1q21.1 duplication cultures AMPA signalling is more prevalent than NMDA signalling. However, while the loss of active cells was significant due to inhibition of AMPA signalling this loss was very small. Taken together these results further suggest a lack of neuronal signalling in 1q21.1 duplication cultures.

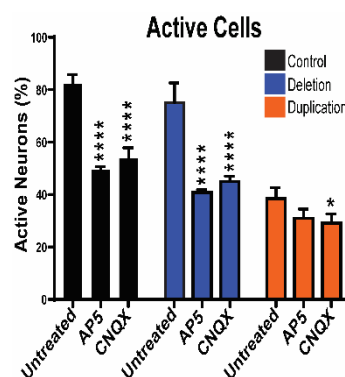


**Figure 3.19: The effect of inhibiting AMPA or NMDA signaling in day 50 neuronal cultures.** Quantification of soma which show at least 1 characteristically neuronal calcium event. Both genotype ( $F_{2,19}=97.44$ ;  $P<0.0001$ ; Control N=2, Deletion N=3, Duplication N=2 and n=3) and drug ( $F_{2,19}=100.5$ ;  $P<0.05$ ; Control N=2, Deletion N=3, Duplication N=2 and n=3) had significant effects on the percentage of active cells. There was also a significant interaction between the effect of genotype and drug ( $F_{4,19}=10.16$ ;  $P=0.0001$ ; Control N=2, Deletion N=3, Duplication N=2 and n=3) on the percentage of active cells. Data sets were analyzed by two-way ANOVA with post hoc comparisons using Dunnett's multiple comparisons test comparing to control samples. Stars represent Dunnett-corrected post hoc tests. All data presented as means  $\pm$  SEM \* $P<0.05$ ; \*\*\*\* $P<0.0001$  vs. untreated.

Examining calcium kinetics is a powerful technique to analyse the function of neurons however this analysis is a proxy measure of the function of these cells. Therefore, to directly measure the functionality of these cells and to understand how mutations at the 1q21.1 locus effect neuronal network behaviour MEAs were used. The use of MEAs allows an examination of both simple metrics such as activity and more complex metric such as bursting and network bursting. Once cells are plated onto MEAs there is a recovery period of 10 days to allow the reformation of complex neuronal morphology and synapses and from this point forward the activity of these cells increases over the course of the subsequent 50 days. Therefore, as expected control cultures show a slow and steady increase of activity. However, 1q21.1 duplication cultures show a decrease in activity across the 50-day period of MEA recording (Figure 3.21). In contrast 1q21.1 deletion cultures also show a steady increase in activity over this period with a similar rate of increase to controls up to day 80 and then a larger increase in activity over the subsequent 20 days.

The simplest metric beyond total activity is bursting, which is a dynamic state in which neurons repeatedly fire discrete spikes. This behaviour is critical to neuronal function and drives the communication and synchronisation of neuronal networks. This type of

activity is not seen in at early time points (around day 60 or 70) but begins to present later (after day 80). In control cultures again as expected there is an increase in the number of bursts per minute from day 60 to day 100 with a sharp increase from day 70 to 80 followed by a plateau in the number of bursts per minute (Figure 3.21) speaking to the transition from an active unorganised network to an active and organised network. In 1q21.1 deletion cultures there was a similar increase in the number of bursts per minute as in control cultures between days 60 and 80. However, rather than the number of bursts plateauing after day 80 the bursts per minute continued to increase at a higher rate resulting in a 2 fold increase in the number of bursts per minute in 1q21.1 deletion cultures as compared to controls. In a similar pattern to that seen with activity there is a small increase in bursting in 1q21.1 duplication cultures at day 70; however, this is not sustained and by day 100 there is no observable bursting in 1q21.1 duplication cultures. These results suggest that the increase activity seen in 1q21.1 deletion cultures does not preclude the formation of organised neuronal activity and rather results in more active neuronal firing patterns. Whereas the lack of activity in 1q21.1 duplication cultures results in a lack of neuronal network behaviour.

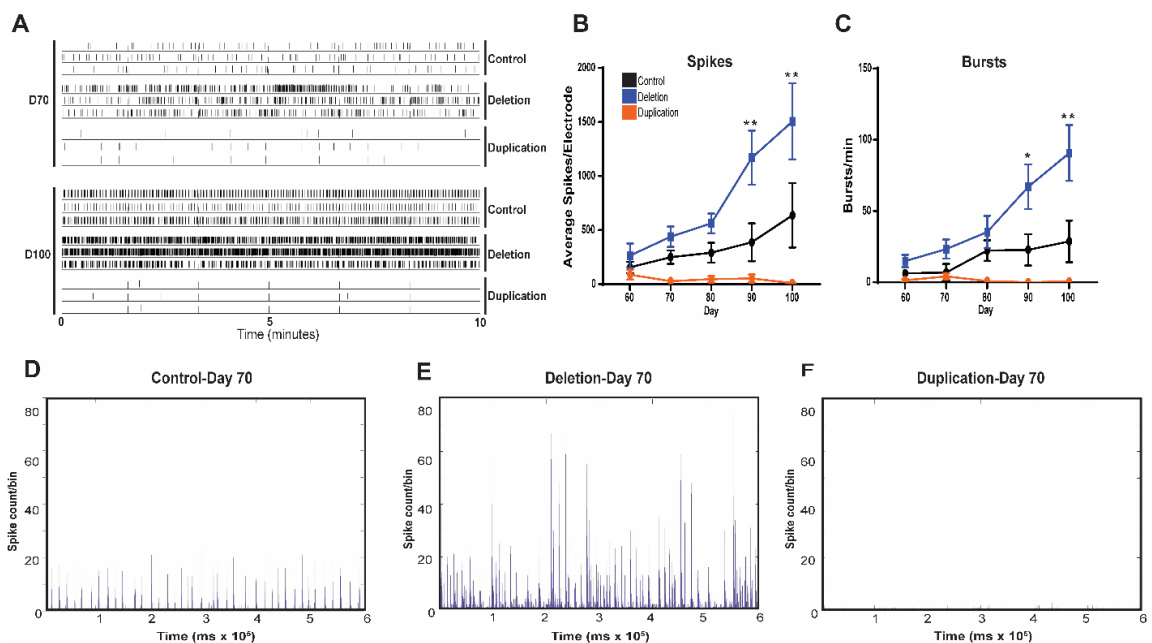


**Figure 3.20: The activity and network behavior of neurons using MEAs. A** Representative trace of electrical activity as measured by MEAs (at day 70 and day 100 of differentiation) with each row representing a single electrode. **B** The average number of spikes recorded per electrode across the 50-day MEA period. Both genotype ( $F_{2,76}=18.06$ ;  $P<0.0001$ ; Control  $N=2$ , Deletion  $N=3$ , Duplication  $N=2$  and  $n=3$ ) and time ( $F_{4,76}=3.536$ ;  $P<0.05$ ; Control  $N=2$ , Deletion  $N=3$ , Duplication  $N=2$  and  $n=3$ ) had significant effects on the average number of spikes per electrode. **C** The average number bursts (defined as when more than 3 electrodes were active in the same 200ms time frame) per culture across the 50 days cells were maintained on MEAs. Only genotype ( $F_{2,61}=8.637$ ;  $P<0.001$ ; Control  $N=2$ , Deletion  $N=3$ , Duplication  $N=2$  and  $n=3$ ) had a statically significant effects on the number of bursts per culture per recording. **D,E,F** Array-wide spike detection rate plots from control, 1q21.1 deletion and 1q21.1 duplication MEAs. Data sets were analyzed by two-way ANOVA with post hoc comparisons using Dunnett's multiple comparisons test comparing to control samples. Stars above points represent Dunnett-corrected post hoc tests. All data presented as means  $\pm$  SEM \* $P<0.05$ ; \*\* $P<0.01$ ; \*\*\* $P<0.001$  \*\*\*\* $P<0.0001$  vs. control.

Previous work using similar MEA systems has shown that neuronal bursting is dependent on both AMPA and NMDA signalling<sup>247</sup>. To assess the effect of inhibiting AMPA and NMDA signalling AP5 or CNQX were added for 10 minutes before MEA recordings were taken. Mirroring the results from calcium imaging experiments addition of either AMPA or NMDA signalling prevented the emergence of neuronal bursting resulting in a decrease in the spike counts/bin on the ASDR plots (Figure 3.22). While this pharmacological intervention did not prevent all neuronal activity, the remaining activity was similar to that seen as background activity in untreated cultures. This therefore indicates that neuronal network activity in 1q21.1 deletion cultures is dependent on both AMPA and NMDA signalling however not all activity is dependent on this signalling.

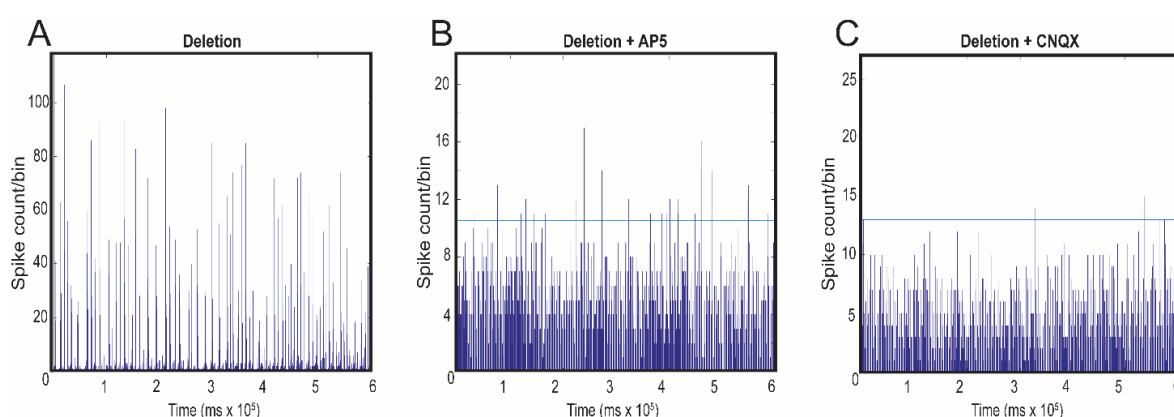


**Figure 3.21: Inhibition of AMPA or NMDA signaling in 1q21.1 deletion neuronal cultures.** **A** Example of an array-wide spike detection rate (ASDR) plot from 1q21.1 deletion cultures after 100 days of differentiation. **B** Example of an array-wide spike detection rate plot from 1q21.1 deletion cultures after 100 days of differentiation. The culture was incubated with AP5 immediately before recording. **C** Example of an array-wide spike detection rate (ASDR) plot from 1q21.1 deletion cultures after 100 days of differentiation. The culture was incubated with CNQX immediately before recording.

The use of MEAs allows not only the analysis of activity in terms of a temporal component but also in terms of a spatial component examining the network bursting of cultures. This type of activity is characterized in a similar fashion to simple bursting however rather than simply quantifying the number of spikes in a given period, network bursting also takes into account the number of electrodes which are active in the same period. Therefore, this metric examines the true network behaviour of the system rather than simply analysing temporally linked activity which may not be due to complex network behaviour and may be due to a small subset of or a single highly active electrode. It is clear after 100 days of differentiation network bursts become apparent in both control and 1q21.1 deletion cultures with each network burst featuring the majority of active electrodes followed by periods of very low activity (Figure 3.23). Examining the frequency of these network bursts shows no significant difference between control and 1q21.1

deletion cultures. Furthermore, examining the number of spikes which are present in these network bursts also showed no significant difference between control and 1q21.1 deletion cultures (Figure 3.23). These results indicate that while there is increased activity and an increased amount of bursting in 1q21.1 deletion cultures compared to controls there is no change in the frequency of network activity.

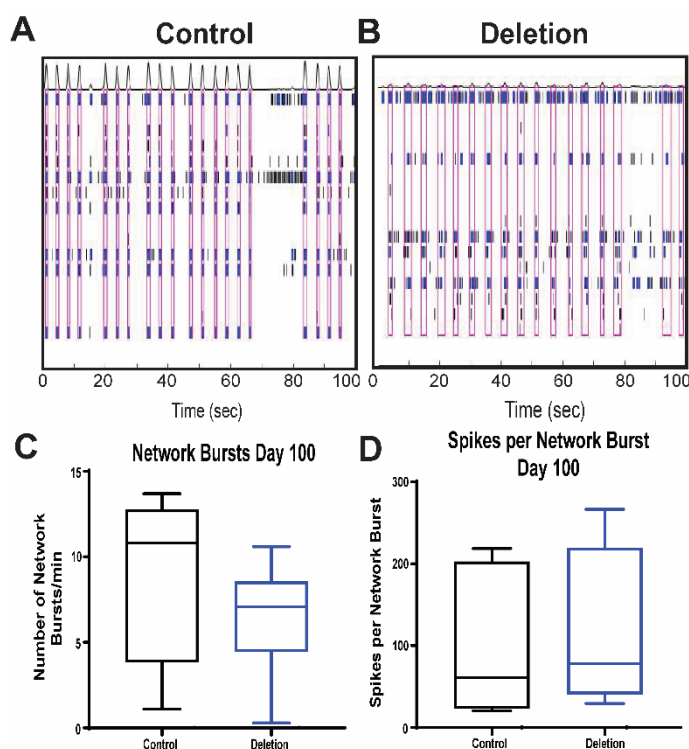


**Figure 3.22: The effect of 1q21.1 deletion on complex neuronal network behaviors.** **A,B** Representations of synchronicity within cultures, purple boxes denote synchronized network activity (when 3 or more electrode are active within the same time frame) and height of peaks in the above histogram represents this synchronized network activity as a function of total activity. **C** Quantification of the number of network bursts per minute in each culture measured after 100 days of differentiation (Control N=2, Deletion N=3 and n=3). **D** Quantification of the number of spikes within each network bursts across all cultures and all recordings. Measured after 100 days of differentiation (Control N=2, Deletion N=3 and n=3).

While the frequency of network bursting is unaffected by 1q21.1 deletions the duration of network bursts is significantly different between 1q21.1 deletion cultures and controls. Interestingly the increase in network bursts duration is seen at both day 80 when organised network activity begins and at day 100 suggesting that this change is not directly due to the large increase in activity seen at later time points in 1q21.1 deletion cultures (Figure 3.24). Furthermore, there is no significant difference between the interval between bursts after either 80 or 100 days of differentiation. Taken together these results show that 1q21.1 deletion cultures have longer network bursts however the interval between bursts and the number of spikes within the bursts are not significantly different. Meaning

therefore, 1q21.1 deletion cultures have longer periods of network activity with no corresponding increase in network activity.

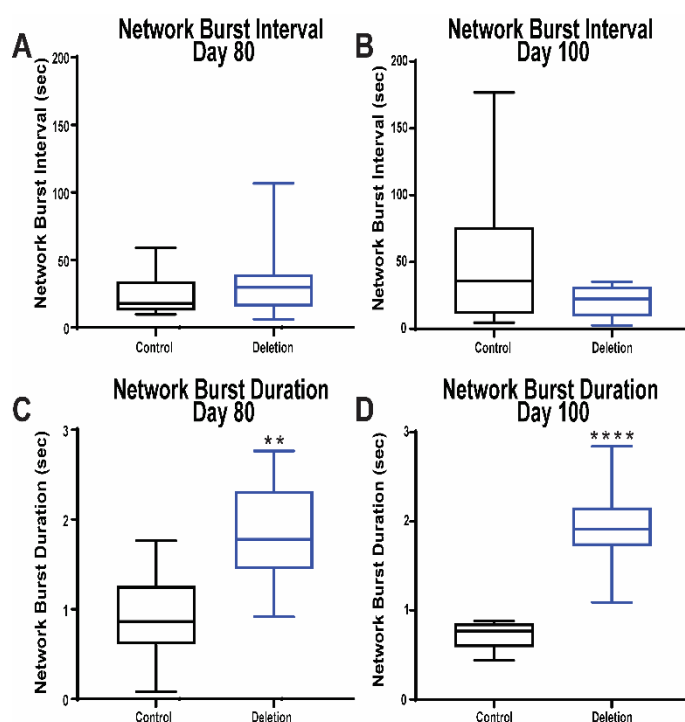


**Figure 3.23: The effect of 1q21.1 deletion on complex neuronal network bursting behaviour.** **A** Quantification of the time between network bursts measured after 80 days of differentiation (Control N=2, Deletion N=3 and n=3). **B** Quantification of the time between network bursts measured after 100 days of differentiation (Control N=2, Deletion N=3 and n=3). **C** The duration of network bursts in cultures after 80 days of differentiation (Control N=2, Deletion N=3 and n=3). **D** The duration of network bursts in cultures after 100 days of differentiation (Control N=2, Deletion N=3 and n=3). Data sets were analyzed by Students T-Test; \*\*P<0.01; \*\*\*\*P<0.0001 vs. control.

### 3.3.10 The use of drugs targeting calcium related pathways can modulate the physiological phenotypes associated with 1q21.1 mutations

Due to the changes in the expression of calcium channels associated with 1q21.1 CNVs, 4 drugs were selected to modulate the altered calcium exchange observe in 1q21.1 deletion or duplication neurons. The 4 drugs were selected based on their ability to modulate the function of neuronally expressed calcium channels with aim of rescuing the phenotypes observed in 1q21.1 mutant cultures. Clozapine (known to down regulate calcium transmission and effect T-type calcium channels<sup>248,249</sup>) and verapamil (an L-type calcium channel blocker<sup>250</sup>) were selected to decrease activity in 1q21.1 deletion neurons and calcitriol (which has neuroprotective effects<sup>251</sup>) and roscovitine (which slows the closing of P-type calcium channels<sup>252</sup>) were selected to induce activity in inactive 1q21.1 duplication cells. As these drugs were resuspended in either PBS or DMSO the latter was used as a vehicle control given it is far more likely to have an effect and was added in parallel to all drugs. The drugs were administered chronically for 10 days to allow for gene

expression changes to take hold. Similarly to previous results the 1q21.1 deletion and control cultures showed high levels of active cells with no significant differences between 1q21.1 deletion or control cultures in any condition tested (vehicle, clozapine or verapamil). However, the increased activity in 1q21.1 neurons was ameliorated by the addition of either drug (clozapine or verapamil) both decreasing the rate of calcium events by around half resulting in a lower level than that seen in control neurons (Figure 3.25). Both drugs also had a significant effect on the rate of calcium events in control neurons with clozapine reducing the rate to a similar level as that seen in 1q21.1 deletion neurons; however, this reduction is significantly smaller than that seen in 1q21.1 deletion neurons. Verapamil had an inverse effect on control neurons as 1q21.1 deletion neurons; increasing the rate of calcium events by around 1/3.

Neither calcitriol or roscovitine had a significant effect on the percentage of active neurons in either control or duplication cultures with duplication cultures having around ½ the percentage of active neurons seen in control cultures (Figure 3.25). In control neurons treatment with either calcitriol or roscovitine increased the rate of calcium events by around 50% resulting in a similar rate to that seen in 1q21.1 deletion neurons. However, in 1q21.1 duplication neurons only roscovitine had a significant effect; also increasing the rate of calcium events to a similar degree as that seen in controls. These results indicate that the duplication of 1q21.1 prevents the action of calcitriol but has no effect on the action of roscovitine. Furthermore, the cells which do not show any calcium activity in 1q21.1 duplication cultures remain inactive despite that addition of either calcitriol or roscovitine.

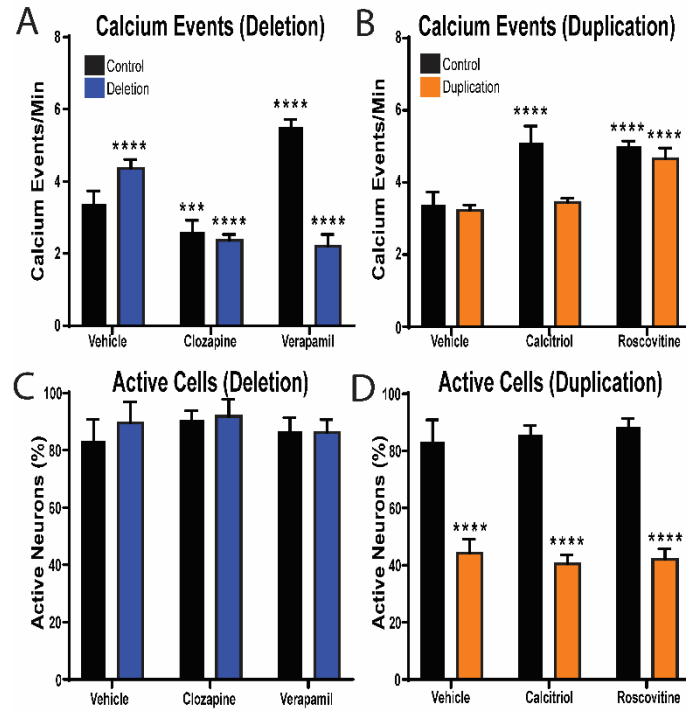


**Figure 3.24: Pharmacological modulation of calcium kinetics in neurons with 1q21.1 mutations.** **A** Number of characteristically neuronal calcium events recorded per minute in day 50 control and 1q21.1 deletion cultures treated for 10 days with vehicle (DMSO), clozapine or verapamil. Both genotype ( $F_{1,28}=71.64$ ;  $P<0.0001$ ; Control N=2, Deletion N=3, Duplication N=2 and n=3) and the addition of drugs ( $F_{2,28}=79.56$ ;  $P<0.0001$ ; Control N=2, Deletion N=3, Duplication N=2 and n=3) had significant effects on the average rate of calcium events. Furthermore, there was a significant interaction between the effect of genotype and drug ( $F_{2,28}=162.4$ ;  $P<0.0001$ ; Control N=2, Deletion N=3, Duplication N=2 and n=3) on the rate of calcium events. **B** Number of characteristically neuronal calcium events recorded per minute in day 50 control and 1q21.1 duplication cultures treated for 10 days with vehicle (DMSO), calcitriol or roscovitine. Both genotype ( $F_{1,22}=38.1$ ;  $P<0.0001$ ; Control N=2, Deletion N=3, Duplication N=2 and n=3) and the addition of drugs ( $F_{2,22}=63.87$ ;  $P<0.0001$ ; Control N=2, Deletion N=3, Duplication N=2 and n=3) had significant effects on the average rate of calcium events. Furthermore, there was a significant interaction between the effect of genotype and drug ( $F_{2,22}=16.06$ ;  $P<0.0001$ ; Control N=2, Deletion N=3, Duplication N=2 and n=3) on the rate of calcium events. **C** Quantification of soma which show at least 1 characteristically neuronal calcium event in day 50 control and 1q21.1 deletion cultures treated for 10 days with vehicle (DMSO), clozapine or verapamil (Control N=2, Deletion N=3, Duplication N=2 and n=3). **D** Quantification of soma which show at least 1 characteristically neuronal calcium event in day 50 control and 1q21.1 duplication cultures treated for 10 days with vehicle (DMSO), calcitriol or roscovitine. Only genotype had a significant effect on the percentage of active cells ( $F_{1,22}=463.9$ ;  $P<0.0001$ ; Control N=2, Deletion N=3, Duplication N=2 and n=3). Data sets were analyzed by two-way ANOVA with post hoc comparisons using Dunnett's multiple comparisons test comparing to control vehicle treated samples. Stars above points represent Dunnett-corrected post hoc tests. All data presented as means  $\pm$  SEM; \*\*\*\* $P<0.0001$  vs. vehicle treated control.

### 3.4 Discussion

#### 3.4.1 Mutations at the 1q21.1 locus differentially regulate neuronal differentiation

This study is the first examination of the effects of copy number variation at the 1q21.1 locus on human neuronal development and function. It is clear from this evidence that mutation of the distal 1q21.1 locus (either deletions or duplications) has no significant effect on the creation and pluripotent ability of iPSCs. However, both deletion and duplication of the 1q21.1 region result in aberrant neuronal differentiation. Specifically, the loss of neuronal production in 1q21.1 duplication cultures is consistent with other studies on syndromes linked to an increased risk of ASD. In a similar iPSC model, it has been shown that deletion of the 22q11.1 locus is associated with a decrease in the production of lower cortical layer neurons and an increase in upper cortical layer neurons<sup>136</sup>. Furthermore, this phenotype is also consistent with a study on Rett syndrome which found a decrease in the expression of neuronal markers<sup>253</sup>. In contrast a study by Mariani *et al.*<sup>254</sup> showed an increase in neuronal production associated with FOXP1 mutation (associated with Rett syndrome). However, this increase was suggested to be specific to GABAergic inhibitory neurons with similar production of glutamatergic neurons.

In this study 1q21.1 duplication cultures were shown to have decreased expression of *MAP2* after 50 days of differentiation and a similar decrease in the production of neurons after 30 days of differentiation. This phenotype is further compounded by the increase in *DCX* expression after 50 days of differentiation. Taken together these results suggest that the decrease of neurons seen in 1q21.1 duplication cultures may be due to a bottle neck in the transition of immature neurons into mature neurons (Figure 3.26). This results in particular is consistent with previous work on increased expression of *NOTCH2NL* which has been shown to prevent the differentiation of neurons from NPCs<sup>65,255</sup>. However due to the use of mitotic inhibitors in these differentiations the resulting phenotype is an increase of immature neurons rather than a maintenance of NPCs. This may be particularly relevant to the use of DAPT which is a  $\gamma$ -secretase inhibitor and therefore will decrease the overactivation of NOTCH signaling associated with duplication of the 1q21.1 region and has been shown to increase neuronal differentiation<sup>186</sup>. The lack of a decrease in the expression or number of TBR1 and CTIP2 positive cells in 1q21.1 duplication cultures may also be due to the use of mitotic inhibitors forcing cells which would otherwise remain as immature neurons to become lower layer cortical neurons.

While the duplication of the 1q21.1 locus is associated with an increased risk of ASD, deletion of this locus is primarily associated with an increased risk of schizophrenia. The association between neuronal differentiation and CNVs associated specifically with schizophrenia remains poorly understood. A study examining deletion of the 15q11.2 locus has shown an associated loss of NPC organization in iPSC models<sup>256</sup>. This study went on to use a mouse model of CYFIP1 hypofunction to show this phenotype was linked to abnormal cortical organization like that seen in the 1q21.1 microdeletion mouse model. The increase production of immature neurons in 1q21.1 deletion cultures is also somewhat consistent with findings from a study using iPSCs derived from idiopathic schizophrenic patients. This study showed that glutamatergic neurons from these patients failed to mature<sup>229</sup> therefore also suggesting a developmental phenotype.

The deletion of the distal 1q21.1 locus is associated with an increased production of all neuronal markers at day 50 of differentiation. There is also an increased production of CTIP2 neurons and increased expression of *TBR1*. After 30 days of differentiation there is clear evidence for the efficient conversion of immature neurons into maturing neurons as shown by the decreased *DCX* expression and the increased number of MAP2+ cells (Figure 3.26). Therefore, the subsequent increase in *DCX*, *NCAM* and *MAP2* seen at day 50 is likely due to the retention of proliferative cells in the intervening 20 days. The increase in both immature and maturing neurons in 1q21.1 deletion cultures at later time points could be due to an increase in proliferation at all stages of neuronal development or could be due to an increased proliferation of early immature neurons and then efficient conversion of these extra cells into later immature neurons and then mature neurons (Figure 3.26). Again these results somewhat recapitulate those seen in work on *NOTCH2NL* genes which has shown that loss of *NOTCH2NL* expression causes early transition of radial glial cells into neurons<sup>65,255</sup>. While consistent with the results at day 30 of differentiation this work does not fully explain the results seen after 50 days of differentiation.

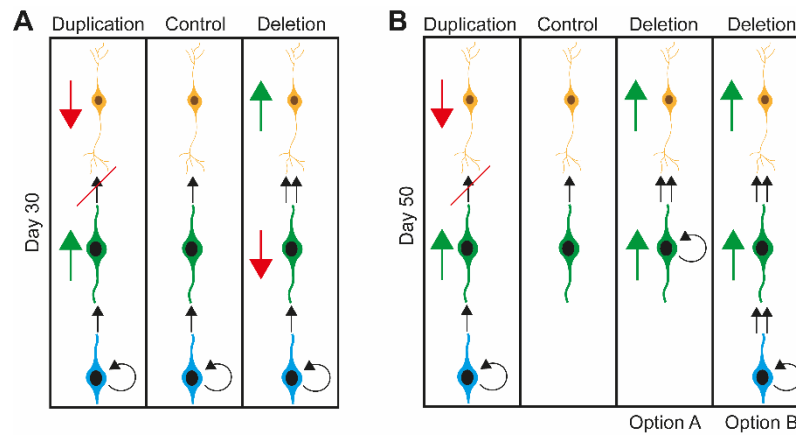


**Figure 3.25: Graphical explanations for the developmental phenotypes observed in 1q21.1 mutant cell lines.** **A** After 30 days of differentiation in control iPSC differentiations there are NPCs (blue) which are still proliferating and being converted into immature neurons (green) and maturing neurons (yellow). In 1q21.1 duplication differentiations the NPCs are also being converted to immature neurons however the lack of conversion to maturing neurons results in an increase in the proportion of immature neurons compared to controls. In 1q21.1 deletion differentiations there is highly efficient conversion of immature neurons into maturing neurons. This results in a decrease in the proportion of immature neurons and an increase in the proportion of maturing neurons. **B** After 50 days of differentiation in control iPSC differentiation there are very few NPCs with the remaining immature neurons being converted to maturing neurons. Similarly, to day 30 after 50 days of differentiation in 1q21.1 duplication differentiations there is a loss of maturing neurons due to a lack of conversion from immature neurons coupled with a retention of NPCs. In 1q21.1 deletion differentiations there are two possible explanations for the phenotype observed. Option A is there is increased proliferation of immature neurons with efficient conversion into maturing neurons. On the other hand, option B is a retention of NPCs with highly efficient conversion of NPCs into immature and then maturing neurons ultimately resulting in an increased proportion of both cell types compared to controls.

These results are also particularly relevant to the microcephaly and macrocephaly associated with the duplication and deletion of the distal 1q21.1 locus respectively<sup>45</sup>. The increase in neurons in 1q21.1 deletion cultures may be indicative of a premature maturation therefore resulting in smaller brain due to the premature loss of highly proliferative progenitors. In 1q21.1 duplication cultures the bottleneck in the conversion of immature neurons to maturing neurons would suggest an inability to produce neurons. However, if this results in the maintenance of a proliferative population past the point at which these cells should have been lost this would result in a longer period of proliferation and thereby result in a larger brain size. Work on 16p11.2 deletions and duplications which show similar macro and microcephaly suggested changes in neuronal morphology to be the cause of this phenotype<sup>224</sup>. In this study examination of neuronal morphology showed clear differences between controls and 1q21.1 mutants however it failed to recapitulate the clear reciprocal phenotypes associated with 16p11.2 mutations. Therefore, suggesting that this phenotype may not be related to the micro and macrocephaly. There is also evidence from studies into schizophrenia which do show decreased somal volume<sup>257-259</sup> like that found in 1q21.1 deletion neurons. However, studies have also reported a decrease in the length and number of dendrites<sup>260,261</sup>, and a decrease in the expression of SYN mRNA<sup>262,263</sup>

in contrast to the phenotypes observed in 1q21.1 deletion neurons. Therefore, while the developmental phenotypes provide strong evidence explaining the microcephaly and macrocephaly associated with these mutations the differences in neuronal morphology may be more related to psychiatric risk than changes in brain size.

#### 3.4.2 Abnormal calcium homeostasis and decreased neuronal activity associated with 1q21.1 duplication are phenotypes relevant to psychiatric disorders

As the primary association of 1q21.1 duplication is with ASD, it is critical to examine the relevance of the altered calcium homeostasis identified in this study to this disorder. There is a large body of evidence from GWAS studies<sup>264</sup> and targeted SNP analysis<sup>265</sup> for an association between mutations in the CACNA gene family (encoding voltage gated calcium channels) and ASD. Metanalysis of the signalling networks which underly the genetic component of ASD<sup>266</sup> also identifies calcium signalling particularly through the MAPK axis as a significant contributor to ASD. Specifically examining ASD related mutation in subunits of L-type calcium channels has shown that these mutation are linked with gain-of function specifically causing the channel to remain open due to a loss of inactivation or abnormal voltage gating<sup>267,268</sup>. This has been linked to increased cytosolic calcium concentration which may have detrimental effects on cellular health<sup>268</sup>. Furthermore, a study into timothy syndrome<sup>136</sup> caused by mutations in CACNA1C have shown that this mutation can cause developmental changes due to alterations in CREB signalling caused by increased calcium concentrations. There is strong evidence that mutations in voltage gated calcium channels are associated with ASD and these mutation may result in altered downstream signalling causing developmental phenotypes.

Examining other mutations known to be linked to ASD lends further evidence that altered calcium signalling is particularly relevant to this disorder. A study using patient fibroblasts showed that there is a decreased release of calcium through IP<sub>3</sub>Rs in three monogenic ASD syndromes therefore suggesting that deficits in calcium homeostasis are associated with multiple forms of syndromic ASD<sup>269</sup>. A loss of function mutation in ATP13A4 has also been linked to ASD and overexpression of this gene has been shown to cause an increase in intracellular calcium<sup>270</sup>. In animal models haploinsufficiency of PTEN (mutations in which have been linked to ASD) caused overexpression of a calcium activated potassium channel<sup>271</sup>. This overexpression was shown to increase the sensitivity to incoming signals and ultimately it was suggested to reduce the excitability of these cells. Finally, in human

patient post-mortem tissue a study showed that increased calcium concentrations resulted in the overactivation of the mitochondrial aspartate/glutamate carrier AGC1<sup>272</sup> which may result in increased oxidative stress. This evidence suggests that calcium homeostasis may be a hub for dysfunction in ASD having widespread effects on both neuronal health and function.

Given this body of evidence it is unsurprising to see changes in the expression of voltage gated calcium channels in association with duplication of the 1q21.1 locus. Furthermore, the loss of active cells in calcium imaging experiments suggests fundamental dysfunction in calcium homeostasis and signalling. However, this phenotype must also be viewed in a developmental context. Therefore, it is possible the fundamental phenotype may not be related to calcium transporters or signalling but may be one of altered development resulting in the abnormal calcium homeostasis seen in this study. To better understand the deficits associated with this mutation two drugs were applied to cultures chronically for 10 days to assess what effect they would have on calcium kinetics in an attempt to modulate the calcium kinetics in active cells or induce calcium activity in non-active cells. Both drugs were selected as they could modulate the function of key calcium channels. Calcitriol has been shown to have neuroprotective effects due to decreased expression of L-type calcium channels<sup>251</sup> and roscovitine causes p-type calcium channel to remain open for longer<sup>252</sup> therefore allowing more calcium movement.

In both cases the drugs had a significant effect on control cells causing an increase in the rate of calcium events (as measured by calcium imaging). However, in 1q21.1 duplication cultures only roscovitine had a positive effect on the rate of calcium events. But roscovitine had no effect on the proportion of active cells therefore suggesting that the inactive cells either do not express the P-type channel due to deficits in the neurons produced or because the inactive cells are too immature to express functionally linked proteins. However, the fact that this drug had an effect on the active cells suggests that functional 1q21.1 duplication neurons express P-type calcium channels and that by increasing the time these channels are open there is a corresponding increase in the number of calcium events. These channels remaining open longer may allow cells to return to base line faster therefore allowing further events to occur or may simply allow faster Ca<sup>2+</sup> movement due to the channel being open more. Roscovitine also has similar effects on potassium channels<sup>273</sup> which may also play a role in the increase of activity seen with the addition of this drug. Finally, roscovitine also functions as a cyclin-dependent kinase

(CDK) inhibitor (targeting cdk1, cdk2, cdk5, cdk7 and cdk9<sup>274</sup>) which may also play a role in effect of this drug.

In the case of calcitriol there was no effect on the rate of calcium events or the proportion of active cells in 1q21.1 duplication cultures. As calcitriol decreases the expression of L-type calcium channels the increase of calcium events in control neurons may be due to compensation from other calcium channels. Perhaps resulting in an increase in the proportion of other calcium channels with properties more likely to cause increased calcium movement. The increase of calcium events may also be linked to the neuroprotective role of calcitriol. The lack of any significant change in 1q21.1 duplication suggests the action of this drug is prevented by 1q21.1 duplication. This effect may be due to the time the drug was used for, as the translational changes which are the likely result of this drug may be delayed in 1q21.1 duplication cells; or this may be due to the already low expression of L-type calcium channels in 1q21.1 duplication cells. Therefore, suggesting these channels may not be critical to the calcium kinetics in these cells. These effects may be mediated by altered gene regulation caused by overexpression of CHD1L resulting in altered epigenetic regulation or other gene expression changes linked to 1q21.1 duplication with unknown intermediates. It is also conceivable that 1q21.1 duplication neurons are more functionally immature in general, resulting in a decreased production of synapses and preventing high levels of expression of L-type calcium channels. Finally, the lack of effect of either of these drugs on the proportion of active cells in these cultures lends further evidence toward an argument that these cells are unable to become active and therefore may either represent the population of DCX+ immature or a combination of this population and a population of MAP2 expressing immature neurons incapable of functioning.

While changes in calcium homeostasis may underly the functional deficits observed in 1q21.1 duplication cultures it is ultimately the neuronal activity as measured by MEAs which gives insight into the ability of these neurons to function as a neuronal network. Synchronised neuronal networks as seen in control cultures are believed to underly key functions of the cortex. Three ASD models have been specifically used to demonstrate the association between altered neuronal electrical activity and this disorder. Mutations in neuroligins have been linked to ASD and Gutierrez *et al*<sup>275</sup> showed that overexpression of neuroligin 3 increases synchronicity whereas a mutant form of this gene associated with ASD has no such effect. Similarly, in a CNTNAP2<sup>-/-</sup> mouse model it has been shown there is

a reduction in neuronal synchronisation and these animals also show behaviour deficits commonly associated with models of ASD<sup>276</sup>. Finally using cultures of primary mouse neurons with SHANK3 knocked out (mutations in which are associated with ASD) it has been shown that there is a decrease in neuronal activity and a modulation of synchronicity<sup>277</sup>.

Examining 1q21.1 duplication cultures on MEAs indicated a general lack of activity in comparison to controls and an inability to form neuronal networks. This result indicates an inability of 1q21.1 duplication neurons to function as a neuronal network however this may be due to flaws in the neurons themselves or may be due to changes in the population of cells. The fact that 1q21.1 duplication neurons which are active in calcium imaging experiments show similar levels of activity to controls suggests that those cells which have matured properly are able to function properly. Furthermore, examination of synapse production by 1q21.1 duplication neurons shows that these cells can produce the necessary machinery to form synapses, however this production is decreased compared to controls. Therefore, these results suggest some dysfunction in 1q21.1 duplication neurons but not a complete inability to function as neurons should. Therefore, the inability of these cells to produce functional neuronal networks may be due to the production of an inactive subpopulation of cells as seen in calcium imaging experiments which prevents the formation of large-scale functional networks.

Overall Evidence in this study shows that 1q21.1 duplication results in altered expression of CACNA genes and the development of a population of cells which show no significant movement or sequestration of calcium. This results in the loss of neuronal activity in 1q21.1 duplication cultures during successive MEA recordings. These results are consistent with other cellular models of ASD which also show reduced activity and/or reduced synchronicity. However, in the case of this study due to the developmental paradigm used the loss of activity may be compounded by the developmental phenotypes which are not present in other models or are overcome by the later stages of development when mouse cells are used. To better understand the role of 1q21.1 mutations on the activity of neurons further work could be done using a directed differentiation approach to generate neurons thereby bypassing the developmental phenotypes identified by this work. This would also allow a better understanding of the relationship between developmental insults and the resulting functional changes.

### 3.4.3 Increased neuronal activity and abnormalities in synchronicity associated with 1q21.1 deletion models the imbalance of excitation and inhibition common in psychiatric disorders

Deletion of the 1q21.1 region is most highly associated with an increased risk of developing schizophrenia and therefore it is essential that the phenotypes associated with this mutation be viewed in the context of this disorder. One of the most common cellular phenotypes which has been suggested as an underlying cause of schizophrenia and other psychiatric disorders is an altered balance between excitation and inhibition therefore causing aberrant network behavior. In this system there is a specific increase of excitatory neurons caused by loss of the 1q21.1 distal region. This mutation is also associated with an increase in neuronal activity therefore suggesting that the overall phenotype is an increase in the number and function of excitatory neurons. Dysfunction in excitatory neurons (specifically in glutamatergic neurotransmission) has long been established as a key driver of schizophrenia. Early work examining the effects of NMDA antagonists (e.g. PCP<sup>89</sup> and ketamine<sup>278</sup>) indicated that administration of these drugs can induce schizophrenia like symptoms. Furthermore, it is well established that NMDA receptor antagonists exacerbates the symptoms of schizophrenics<sup>92</sup>. As previously detailed, there is evidence from genetic studies that mutations in both genes coding for glutamate receptors and downstream signaling are associated with an increased risk for developing schizophrenia. Finally, a meta-analysis of magnetic resonance spectroscopy studies measuring glutamate indices showed an increase in the levels of glutamate in the medial prefrontal cortex of medication free or naïve patients<sup>279</sup>. This evidence suggests that the results of this study are consistent with cellular dysfunction commonly associated with schizophrenia.

This study shows that while 1q21.1 deletion cultures have a similar proportion of active cells; there are differences in the activity of these cells in both calcium and MEA analyses. Therefore, the increase in neuronal production and increase in the proportion of CTIP2 neurons does not have a significant effect on the proportion of active cells. On the other hand, the increase in activity seen in 1q21.1 deletion neurons is consistent with the increase in synapse related proteins indicating that these changes in protein expression may correlate with an increased connectivity in these cultures. In calcium imaging the increase in the number of neuronal events per minute is indicative of an increase in neuronal activity and the appearance of trains of events in which the fluorescence does not return to baseline further suggest a level of hyperexcitability only seen in 1q21.1 deletion neurons. This is also supported by the increased spike rate of 1q21.1 deletion cultures on

MEAs again indicating a level of hyperexcitability which also translates to an increase in synchronized activity. These results confirm that deletion of the 1q21.1 locus is associated with increased neuronal activity. However, while this work focused on glutamatergic neurons and therefore suggests that this increase in activity may be specific to this subtype further work is necessary to prove that this is the case and the impact this would have on more complex systems.

There is also dysfunction in the production of cortical neurons in the 1q21.1 microdeletion mouse model, however the core deficit previously identified in this model is dysregulation of dopamine. However, this model was also shown to be hypersensitive to PCP in pre-pulse inhibition (PPI) testing<sup>75</sup> therefore indicating a role for glutamate dysfunction in this model. While the dopamine and glutamate hypotheses are often presented as separate rationales for the cellular dysfunction underlying schizophrenia there are fundamental links between these two systems and dysfunction in one system is likely to have an effect on the other<sup>280</sup>. A recent study using RNA sequencing comparing mouse models of multiple CNVs associated with increased risk for psychiatric disorders<sup>281</sup> also suggests that the mouse model of 1q21.1 deletion shows changes in synapse related GO terms. While the original work on this model appears to identify phenotypes, which are separate from those identified in this work, more recent work begins to suggest that there may be similar dysfunction present in the 1q21.1 mouse model as that identified in the human iPSCs. Therefore, further investigations using this model are needed to ascertain if the primary cellular dysfunction is similar to that seen in the iPSC model.

While increases in excitatory activity, as presented in this work would likely affect the balance of excitation and inhibition in the cortex and wider brain, it is also important to consider that this protocol may produce a small population of inhibitory (GABAergic) neurons which may also effect the activity measured from these cultures. Work using the neonatal ventral hippocampal lesion mice model<sup>282</sup> which is widely used to model schizophrenia in a developmentally relevant paradigm indicates that deficits in interneuron formation or function are particularly salient. Similar results have also been shown in models based on perinatal insults including exposure to viral particles or bacterial endotoxins<sup>283</sup>. Models using prenatal stress to induce schizophrenia like behavior have also shown associated deficits in GABAergic neurons<sup>284</sup>. In cellular models of interneurons, it has been shown that cells generated from schizophrenia patients have intrinsic defects in signaling pathways<sup>285,286</sup> and functional systems<sup>287</sup>. Therefore, while there is only a small

population of inhibitory neurons in these cultures, dysfunction in these cells may have an impact on the network behavior of these systems. Further work is necessary to determine if 1q21.1 mutations are associated with dysfunction in inhibitory neurons and the effect this dysfunction may have on neuronal network behavior.

Irrespective of the cause, increased neuronal activity observed in 1q21.1 deletion neurons would suggest an increase in neuronal network activity which was not observed in this case. Therefore, suggesting that the increase in excitability is largely at the individual neuronal level as demonstrated by the calcium imaging and this increased activity does not translate to an increased network activity. This dichotomy between the increase in activity and lack of increase in network activity also suggests that there is an impairment of network activity in 1q21.1 deletion cultures, as if all else is equal an increase in activity and synchronized activity should result in an increase in network activity. While there is no increase in network activity in 1q21.1 deletion cultures the periods of network activity are longer with no commensurate increase in the number of spikes per period.

There is some evidence from previous studies on mouse cortical cultures using MEAs which shows as cultures mature the length of active periods increases however there is also a commensurate increase in the number of spikes within these periods<sup>277</sup> which is not seen in this case. Therefore, there may be an abnormal maturation of these neuronal networks associated with 1q21.1 deletion resulting in an increase period of network activity without the increase in neuronal activity. Equally, the increased length of these active periods may be due to the hyperexcitability of these neurons resulting in a failure to correctly regulate the period of high activity.

These results are of particular import given the large body of evidence suggesting a that impaired neuronal synchronicity is a key feature of schizophrenia. Studies using noninvasive imaging techniques have suggested schizophrenia as a syndrome of dysconnectivity<sup>288,289</sup>. However, as yet there is a lack of evidence linking these complex functional abnormalities with cellular dysfunction. The neuronal network dysfunction observed in this study, suggests that the phenomenon of dysconnectivity may have a cellular basis in increase activity. Furthermore, these results suggest that while simple metrics measuring the activity of single cells are critical to understand the cellular dysfunction in question these results may not translate into the expected dysfunction of neuronal networks. With a view towards understand the interplay between genetic risk for schizophrenia and the loss of synchronicity in neuronal networks associated with this

disorder further work using 1q21.1 and other CNVs must focus on high order functional phenotypes.

Finally, similarly to 1q21.1 duplication, both drugs used to modulate calcium homeostasis had a significant effect on 1q21.1 deletion neurons. The administration of either clozapine or verapamil decrease the rate of calcium events while have no effect on the percentage of active cells therefore suggesting that while the effect was significant it did not prevent the activity of any of the cells. While the precise method of clozapine action is unknown it has been shown to effect calcium homeostasis in the rat cerebral cortex<sup>248</sup> and has also been shown to target T-type calcium channels<sup>249</sup> which are highly expressed in these neurons. On the other hand, verapamil is an L-type calcium channel blocker with antiepileptic effects linked to its effects on calcium homeostasis<sup>250</sup>. Therefore, both drugs had the desired effect on calcium events in 1q21.1 deletion neurons causing a decrease in the rate of calcium events. However, while clozapine had a similar effect on control neurons application of verapamil caused an increase in the rate of calcium events in control neurons. Similarly, to results seen using roscovitine (which also targets L-type calcium channels) the reduction of the activity of these channels increased the rate of calcium events in control cells. This may be due to a compensatory mechanism caused by the prolonged use of these drugs coupled with the effect this may have on a continuously developing system. Furthermore, this would suggest that targeting L-type calcium channels to modulate the neuronal activity in these cultures may be confounded by unexpected results in control cultures. Therefore, increased activity in 1q21.1 deletion neurons can be modulated by manipulating the activity of calcium channels also suggesting a role for calcium channel dysfunction in 1q21.1 deletion neurons.

#### 3.4.4 Study limitations and future perspectives

While the use of a developmental paradigm for the generation of neurons in this study has many advantages it also results in limitations. Protocols based on dual SMAD inhibition are known to produce heterogenous cultures with some small-scale production of both GABAergic inhibitory neurons and astrocytes and while these populations are small, they may significantly contribute to the phenotypes presented in this study. Both the differential production of and any dysfunction in these two cell types associated with 1q21.1 mutations may compound, or mask phenotypes examined in this study. This is especially relevant in functional assays as both astrocytes and GABAergic inhibitory

neurons play critical roles in the development of neuronal networks. However, the overwhelming production of excitatory glutamatergic neurons using this protocol means that the phenotypes identified are likely significantly if not totally driven by this population of neurons. Furthermore, any consistent differential production of astrocytes, inhibitory neurons or altered function of these cell types would be due to the 1q21.1 mutations and therefore while not examined in this study would not discredit the relevance of the functional phenotypes identified. The specific phenotypes examining the production of lower cortical layer neurons are specifically examining the production of excitatory neurons and therefore, reconfirms that mutations of the distal 1q21.1 locus does affect the development of the cortex.

A second limitation is the use of gene expression as a marker for changes in the proportion of neuronal populations. While changes in gene expression are a critical methodology allowing the large-scale assessment of changes in complex systems induced by mutations these changes can often be much larger than those seen at protein level. As demonstrated in this study the changes in gene expression at the level of mRNA do not always translate into changes in protein level. However, the directionality of these changes remains consistent with the scale of these changes often reduced. These changes may be explained by post-transcriptional controls on mRNA which can regulate the half-life of these molecules or control the level of protein produced from mRNAs. The changes in gene expression are also at a population level and therefore may mask changes in small subpopulations of cells. Finally, large gene expression changes may be due to smaller changes in a large population of cells or large changes in a smaller population of cells. While some of these limitations were addressed by examining protein expression and cell staining there remains some ambiguity in gene expression changes which are not further investigated by these methodologies. While single cell RNA sequencing and large-scale proteomic analysis may address some of these concerns there will likely remain some ambiguity. However, an essential focus on patient relevant functional phenotypes means dissecting precise changes in gene expression is often secondary.

The use of large-scale omics analysis would also allow the investigation of the molecular systems driving the changes in differentiation and function observed in this study. While there is compelling evidence from previous studies that mutations in NOTCH2NL genes likely play a role in the developmental phenotypes identified in this work. The similar phenotype seen in the 1q21.1 microdeletion mouse model lacking NOTCH2NL

genes suggests that the phenotypes associated with 1q21.1 distal mutations are more complex than those caused by changes in NOTCH2NL gene dosage. Other genes such as BCL9, CHD1L and PRKAB2 were shown to be expressed in 1q21.1 neurons in a manner dependant on 1q21.1 mutations and therefore may play a role in the phenotypes seen in this study. However, without a systematic gene expression or proteomic data set it remains difficult to ascertain the precise molecular mechanism driving these phenotypes. An alternative approach to this is the use of CRISPR lines with mutations in these 3 genes individually or in combination which could be used to probe the effect of loss of each of these genes to the phenotypes identified in this study.

In an effort to reduce the contamination of resurgent NPCs in later stage cultures and to synchronize the transition of NPCs into neurons compounds which act as mitotic inhibitors were applied. As previously discussed, these compounds are likely to have significant effects on the phenotypes which have been identified in this study and therefore while their use is critical to produce functional neuronal networks removal of these compounds may alter the developmental phenotypes. Therefore, using a separate protocol to examine the effect of 1q21.1 mutations on development may be of particular interest. However, using a protocol with no cell sorting or purification step results in a heterogeneous population of cells at different stage of development which would be exacerbated by removal of the mitotic inhibitors from the process. Therefore, sorting cells at early stages using markers such as CD133 and CD184 would allow the purification of a more homogenous NPC population in which the rate of proliferation or conversion to neurons may be measured. Therefore, allowing the dissection of which stage of development is specifically affected by the 1q21.1 mutation without the confounds of the mitotic inhibitors. This approach would need to be combined with a directed differentiation approach to determine if the functional phenotypes are intrinsically linked to the changes in development as removal of the mitotic inhibitors will prevent the use of MEAs to analyse neuronal networks.

The final key limitation of this study is the lack of complex tools for the analysis of MEA results. The result of MEAs is a complex readout of neuronal activity linked to both time and space and therefore analysis can be carried out comparing the activity across both time (bursting) and space (network activity) however these metric are currently limited and do not examine the spatial component of this analysis fully. The use of MEAs for the analysis of neuronal network behaviour is an emerging field and therefore there remains a lack of

consensus on the critical metrics which properly define the features of these networks. Further analysis may be carried out using the data already obtained in this study to examine the community structures of the neuronal networks produced. Using MEA systems with a higher number of electrodes per culture would also allow the further dissection of how these networks form; the size and shape of them, and how these parameters are affected by 1q21.1 mutations. The functional phenotypes identified in this study are highly relevant to psychiatric disorders associated with these mutations and therefore further investigation into the link between these mutations and aberrant neuronal network behaviour remains critical.

In conclusion the evidence presented in this study demonstrates the power of using 1q21.1 mutations as models of developmental dysfunction associated with an increased risk of developing psychiatric disorders. However, having identified both developmental and functional deficits associated with these mutations further investigations are needed to understand both these deficits individually and therefore to understand the contribution of the former to the later. Consequently, alternative approaches for the generation of neurons need to be employed to directly assess these questions and the use of genetically altered iPSC lines is necessary to allow the investigation of the genetic drivers of these phenotypes.

## 4. Mutations of the Distal 1q21.1 Locus are Associated with Decreased Oligodendrocyte Specification and Altered Oligodendrocyte Differentiation

### 4.1 Introduction

#### 4.1.1 Evidence for white matter dysfunction associated with psychiatric disorders from human imaging studies

White matter is neuronal tissue primarily comprised of myelinated axons; the maturation of this tissue throughout childhood and early adolescence is important for cognitive<sup>290</sup>, behavioral<sup>291</sup>, emotional<sup>292</sup> and motor<sup>293</sup> development. The myelination of axons is critical for the saltatory conduction of electrical currents allowing the propagation of depolarization across nodes of Ranvier rather than entire axonal membranes. Importantly while neurogenesis and gliogenesis are largely complete before birth the process of myelination and thus the development of white matter continues after birth and into early adulthood<sup>294</sup> (Figure 4.1). The persistence of oligodendrocyte progenitor cells (OPCs) and the continued production of oligodendrocytes in adulthood<sup>295</sup> mark this cell type as critically important to long term central nervous system (CNS) function. The continued production of myelin throughout life is important for normal functioning, combating injuries and diseases but also in plasticity and learning<sup>296</sup>. Loss of myelin can have profound effects on health with multiple sclerosis as the prototypic example, caused by an autoimmune mediated loss of myelin leading to wide range of symptoms including pain, fatigue, muscle spasms and cognitive issues<sup>297</sup>. Therefore, the proper process of myelination mediated by oligodendrocytes and maintenance of this phenomenon is critical for the proper function of the central nervous system.

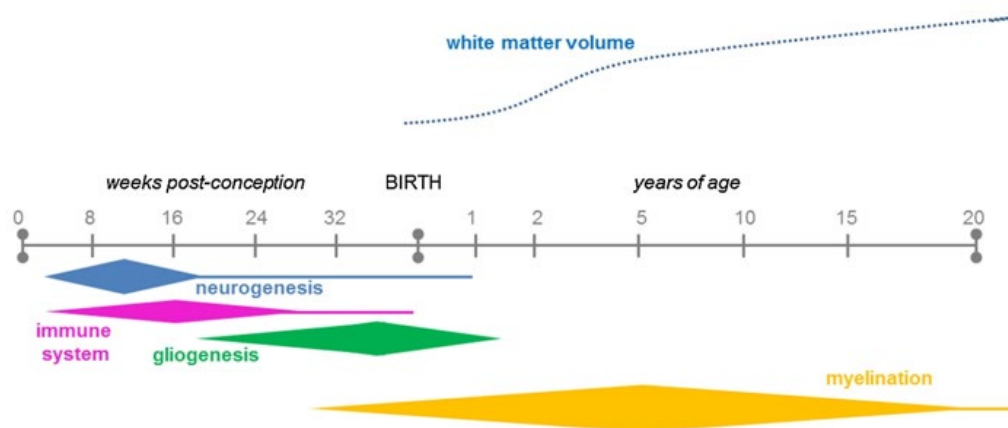


**Figure 4.1: Key processes in the course of neurodevelopment.** Neurogenesis, gliogenesis and infiltration of microglia into the CNS (immune system development) are largely complete before birth. However, the process of myelination and the development of white matter continues into adulthood resulting in an increasing white matter volume observed during early life. Image adapted from Semple et al.<sup>294</sup>

The generation of oligodendrocytes in the CNS is complex when compared to other cell types with the generation of multiple intermediary cells with some persisting until adulthood. Like most cells in the CNS oligodendrocytes originate from a pool of neuronal progenitor cells which are then specified to the glial lineage producing OPCs. OPCs are still multipotent retaining the ability to produce both oligodendrocytes and astrocytes. These cells also persist through adulthood and are thought to have functions beyond the repopulation of lost oligodendrocytes<sup>298</sup>. The conversion of OPCs into pre-myelinating oligodendrocytes is a critical stage in the development of this lineage involving the loss of motility (a critical function of OPCs). The conversion of pre-myelinating oligodendrocytes to mature myelinating oligodendrocytes is the final stage of development involving the large-scale production of myelin and the ensheathment of axons.

There are three waves of oligoneogenesis in the forebrain, the first is driven by ventral SHH signaling in the medial ganglionic eminence and is under the control of the transcription factor NKX2.1<sup>299</sup>. These oligodendrocyte progenitors move dorsally and tangentially throughout the developing forebrain<sup>300,301</sup>. The second wave of oligodendrocyte production originates in the lateral ganglionic eminence and are under the transcriptional control of GS Homeobox 2 (GSH2)<sup>302</sup>. This second wave migrates dorsally to invade the developing cortex<sup>300,301</sup>. The final wave of oligodendrocyte production occurs late in development and projects radially from the sub ventricular zone and are marked by Empty Spiracles Homeobox 1 (EMX1)<sup>300</sup>. This last wave of oligodendrocytes is mainly involved in the myelination of the corpus callosum with some involvement in the myelination of cortical neurons.

Unsurprisingly given the critical nature of glial cells and specifically the complex development of oligodendrocytes in the developing CNS, increasing evidence is emerging that glial and specifically oligodendrocyte dysfunction may play a role in the pathogenesis of neurodevelopmental and psychiatric disorders. Early evidence that white matter abnormalities were associated with psychiatric disorders came from magnetic resonance imaging (MRI) studies. These studies indicated a decrease in white matter volume in effected compared to healthy twins<sup>303,304</sup>. With more modern techniques like diffusion tensor imaging (DTI) it is now possible to look more closely at the changes indicated in these early studies<sup>305</sup>. DTI is a technique used in brain imaging which can give indications of abnormalities in the white matter by measuring fractional anisotropy (FA). FA is a measure of the diffusivity of water molecules in specific areas of the brain (Figure 4.2) with an

increased FA denoting a system with more constrained diffusivity suggesting a more organized system. Conversely a reduced FA is due to a less constrained system.

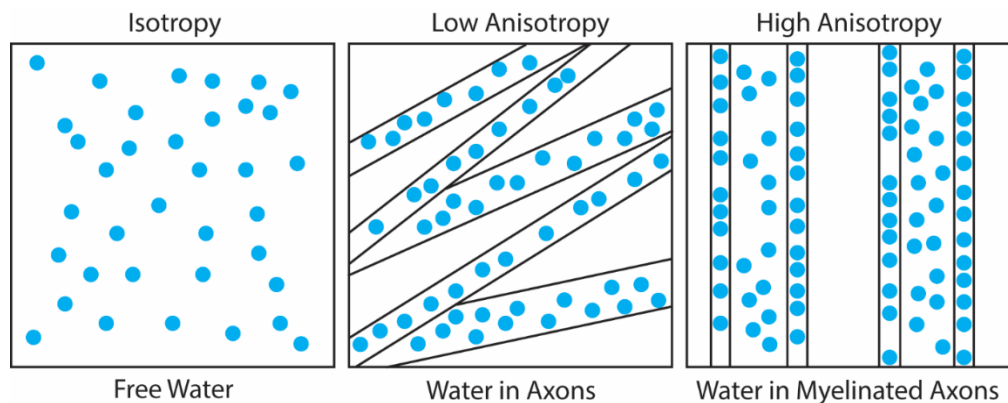


**Figure 4.2: Schematic representation of fractional anisotropy.** Moving from a system with no constraints (isotropy) to a system with some constraints on water movement caused by the introduction of axons resulting in low anisotropy and then finally a system with large constraints on water movement caused by the introduction of myelinated axons resulting in higher anisotropy.

The normal trajectory of FA in white matter tracts is increasing FA over time<sup>306</sup> this increase is thought to be largely due to the myelination of axons which increases the constraints put on water molecules. The first study using this technique to demonstrate white matter abnormalities in psychiatric disorders was published by Buchsbaum *et al.*<sup>307</sup> which showed a decreased FA in schizophrenic patients. Since then many studies have replicated this finding in other neuropsychiatric disorders (for a review see Whitford, Kubicki and Shenton<sup>308</sup>). Although there is no single explanation of reduced FA it is believed to indicate abnormalities in axon integrity or myelination.

Several studies have been carried out, to understand the biological basis of the reduced FA seen in the DTI studies. These studies have found that there is a significant loss of oligodendrocyte number or density in certain areas of the brains of patients with schizophrenia<sup>309,310</sup>. There is also more specific evidence that oligodendrocyte and myelin dysfunction are associated with neuropsychiatric disorders through gene expression studies. Tkachev *et al.*<sup>311</sup> showed a significant reduction in the expression of key genes (including SRY-Box Transcription Factor 10: SOX10, Myelin Basic Protein: MBP and Myelin Associated Glycoprotein: MAG) associated with oligodendrocytes and myelin in patient brain samples compared to controls. A number of groups have also now provided evidence from GWAS studies of genetic association between the genes identified by Tkachev *et al.*<sup>311</sup> and schizophrenia, including transcription factors (like Oligodendrocyte Transcription Factor 2, OLIG2 and SOX10) involved in oligodendrocyte differentiation<sup>312-314</sup>.

#### 4.1.2 Evidence for the pathogenic role of oligodendrocyte dysfunction in psychiatric disorders

While there is clear evidence from imaging, genetic and serological studies in humans that there is an association between the loss of myelin and the development of psychiatric disorders this link cannot be proven causative in these systems. Therefore, investigations in animal models have been carried out to determine if the oligodendrocyte and myelin pathology identified in humans plays a causative role in the development of psychiatric disorders. Firstly, there is evidence that abnormalities in myelination in mouse models such as the *shiverer* (*shi/shi*) mice (a model with severe hypomyelination) can cause a reduced FA similar to that seen in humans<sup>315,316</sup>. Recent work by Silva *et al*<sup>317</sup> on a rat haploinsufficiency model of CYFIP1 (a model of 15q11.2 microdeletion) has shown clear linkages between a reduction of FA similar to that seen in human studies and a loss of oligodendrocytes. Furthermore, this work also showed that the oligodendrocytes present have functional deficits associated with loss of CYFIP1 expression.

Demyelination/dysmyelination has also been shown to present with psychiatric symptoms in rodent models adding further evidence to the argument that oligodendrocyte dysfunction has a role in the pathogenesis of psychiatric disorders. A chemical lesion (cuprizone) model of demyelination has been used in schizophrenia related behavioral studies where it has shown a reduction in: anxiety-like behavior (using the open field maze and elevated plus maze tests) and social interaction<sup>318,319</sup>. Application of lysolecithin (another demyelinating agent) directly into the hippocampus appeared to have opposing phenotypes inducing anxiety-like behavior in the same tests<sup>320</sup>. However, as Edgar and Sibille<sup>321</sup> point out, widespread demyelination has “severe locomotor, social and cognitive consequences ... making it difficult to discern emotionality changes specific to myelin disruption”.

An alternative method of generating rodent models of demyelination which ameliorates some of these concerns are genetic models. An example of this are the  $CNP1^{KO}$  and  $CNP1^{+/-}$  mice which have been shown to have low fear expression during phases of the fear conditioning protocol<sup>322</sup> and after aging show depression like symptoms<sup>323</sup>. A similar result was also shown in schizophrenic patients, who were homozygous for a partial loss of function  $CNP1$  allele, indicating an elevated score in tests qualifying depression associated symptoms<sup>324</sup>. Further work carried out by Lindahl *et al.*<sup>325</sup> has shown, using *in utero* administration of phencyclidine (PCP) as a model of schizophrenia in rats, there is an

associated delay in oligodendrocyte differentiation. Finally, there have been studies which have demonstrated chronic stress (used to model depression in rodents) inhibits oligodendrocyte proliferation and that this can be alleviated with antidepressant (fluoxetine) treatment<sup>326,327</sup>. Therefore, providing evidence that events likely to occur during early neurodevelopment may play a role in complex cellular functions of oligodendrocytes occurring throughout early life.

Finally, the advent of methodologies for generating oligodendrocytes *in vitro* are very new and therefore there is minimal work successfully using iPSC derived oligodendrocytes to model dysfunction associated with psychiatric disorders. However, using iPSC derived OPCs, Vrij *et al*<sup>328</sup> were able to show that Chondroitin Sulfate Proteoglycan 4 (CSPG4) mutation linked to increased risk for schizophrenia has effects on OPC morphology, viability and function (measured by myelination potential). However, one of the most convincing studies using human iPSC derived oligodendrocytes used a mouse chimera model replacing native murine oligodendrocytes with human iPSC derived counterparts<sup>329</sup>. Comparing mice with oligodendrocytes from control iPSCs or schizophrenia patient iPSCs showed a clear loss of myelination ability in cells derived from schizophrenic patients. Furthermore, the gene expression and functional changes in the oligodendrocytes from schizophrenic patients caused behavioral changes in the mice. Mice with oligodendrocytes from schizophrenic patients showed increased anxiety (measured using elevated plus maze), decrease sociability (measured using the 3-chamber sociability test) and cognitive impairments (measured by novel object recognition). Finally, McPhie *et al*.<sup>330</sup> showed that there was a reduced production of OPCs from schizophrenic patient iPSC lines compared to controls. These studies clearly demonstrate that functional defects in oligodendrocytes can be linked to psychiatric disorders and these deficits may play a key role in the development of these disorders. As Nave and Ehrenreich<sup>331</sup> suggest there are a number of ways in which the loss of oligodendrocytes and resulting hypomyelination may result in phenotypes relevant to psychiatric disorders. However, it is first important to identify the precise nature of the oligodendrocyte dysfunction associated with these disorders before attempting to understand the result this dysfunction may have on other cell types and the wider system.

#### 4.1.3 Generation of oligodendrocytes from human induced pluripotent stem cells

While the generation of neurons from human iPSCs was relatively simple, given the relative ease with which neural epithelia can be generated, the induction of glial lineages and especially oligodendrocytes was significantly more challenging. Early protocols were again developed using embryonic stem cells (ESCs) and induced glial cells by the addition of BDNF, EGF, retinoic acid and triiodothyronine<sup>332</sup>. While these cells did go through a SOX10 positive and O4 positive oligodendrocyte progenitor stage and could myelinate neurons when transplanted into myelin deficient mice it was not shown that these cells could produce myelin in monoculture. Similarly, to the production of protocols to generate specific subtypes of neurons the protocols to generate oligodendrocytes needed to be informed by the genesis of these cells *in vivo* and the specific signaling involved.

With the aim of the developmental patterning approaches to recapitulate early human neural development the logic was to generate oligodendrocytes from neural precursors with a ventral forebrain identity mirroring the early waves of oligodendrocyte production. This was possible as the medial ganglionic eminence is a key source of GABAergic interneurons and therefore protocols have been developed for generating neuronal progenitors with this ventral forebrain lineage. These protocols use the same dual SMAD inhibition to induce a neuronal fate with the addition of a Wnt inhibitor and the activation of SHH signaling to ventralize the neuronal precursors<sup>333,334</sup>. A similar effect was achieved by Douvaras *et al*<sup>156</sup> using a low dose of retinoic acid and a smoothed agonist to induce the activation of SHH signaling. This approach produced large amounts of OLIG2 expressing cells which could then be induced to form O4+ OPCs using the addition of growth factors chiefly including PDGF, HGF, T3 and cAMP. While this protocol robustly generated oligodendrocytes from an array of iPSC lines similarly to original protocols for generating neurons, this protocol was very long requiring at least 95 days to produce myelinating oligodendrocyte. Subsequent work has made minor modifications to this protocol limiting the use of PDGF, HGF, IGF-1 and NT3 therefore reducing the time taken to generate MBP+ cells to 75 days<sup>159</sup>.

While developmental patterning approaches to generate cell types of interest have proved to be invaluable tools to investigate the role of cellular dysfunction in complex neurological disorders the draw backs of these techniques (namely long and complex protocols) have prompted investigations into alternative approaches. One such approach which has become increasingly popular are so called 'Direct Reprogramming' protocols.

These protocols rely on the ability of a small number of genes to control the fate choices and ultimately the differentiation of cells. These master regulators are genes (usually transcription factors) which like the ‘Yamanaka factors’ can control the expression of a large portfolio of cell type specific genes. The overexpression of these genes therefore allows the conversion of either somatic cells (often fibroblasts) or already established iPSCs into a cell type of interest.

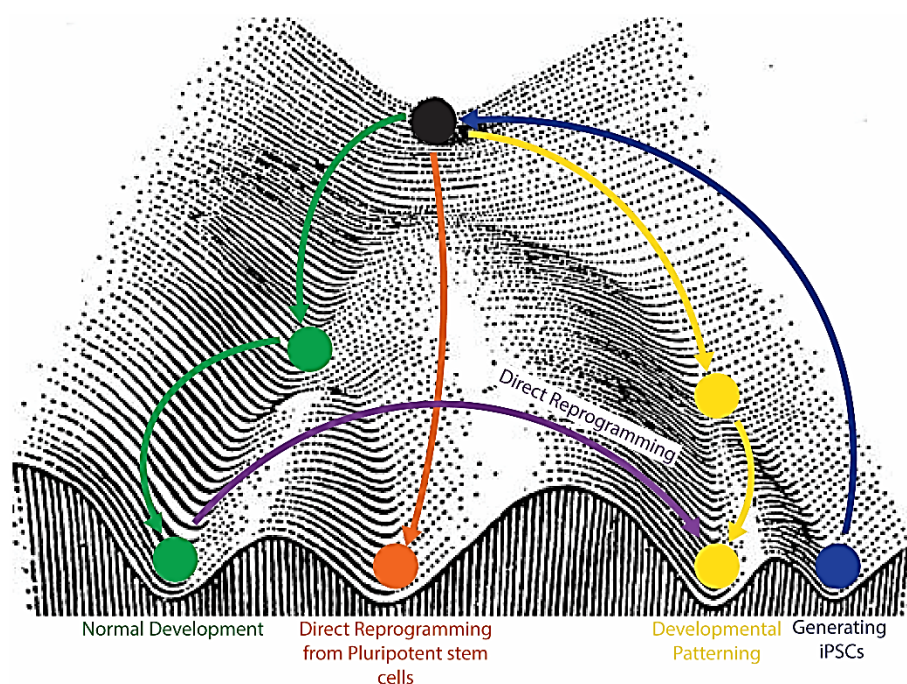


**Figure 4.3: Graphical representation of differentiation paradigms currently used to generate glial cells from human iPSC.** Normal development (green) involves success restrictive steps of development where a pluripotent stem cell (black) will go through multiple precursors before ending at a post mitotic somatic cell. Generating iPSCs (blue) is the opposite of this involving the regression of a somatic cell into a pluripotent stem cell. Once generate iPSCs or the natural equivalent (ESCs) can be differentiated using either a developmental patterning approach (yellow) which recapitulates normal development or a direct reprogramming approach (orange) which bypass intermediates. Finally, true direct reprogramming (purple) involves the generation of the cell type of interest directly from a somatic cell therefore bypassing any return to pluripotency (image adapted from Reik and Dean<sup>240</sup>).

However, using Waddington’s epigenetic landscape<sup>335</sup> as a model (Figure 4.3) one can see that conversion of one somatic cell type into another involves large scale lateral movement overcoming a large amount of already established features, while also establishing the features of the new cell type. One protocol has been published which allows this type of conversion, from fibroblasts to oligodendrocytes<sup>336</sup>, however the efficiency of OPC production as measured by O4 expression was relatively low (15-30%). Therefore, an alternative approach is to use iPSC derived NPCs as the basis for this direct reprogramming aiming to increase the speed at which the fate choice is made and to achieve higher proportion of the cell type of interest. This approach bypasses the difficulty

of replacing established gene expression patterns with alternatives by starting from a naive or regressed (in the case of iPSCs) starting point.

There have been two protocols published for the generation of human oligodendrocytes using a direct reprogramming approach from iPSCs. Both protocols<sup>337,338</sup> use a combination of developmental patterning and direct reprogramming to achieve this conversion. Human iPSCs are first differentiated into neuronal precursors using protocols developed under the banner of developmental patterning however when the cells would normally be enriched for oligodendrocyte precursors using complex media conditions the cells are instead induced to produce high levels of key transcription factors which convert the NPCs into functional oligodendrocytes. While this technique does produce the desired result significantly faster than the conventional developmental patterning approach the efficiency is quite low with only around 50%-60% of viral induced cells expressing the oligodendrocyte marker O4 and only 1/5 of these cells expressing MBP (the key functional marker for oligodendrocytes). Therefore, both direct reprogramming and developmental patterning protocols are available for the generation of oligodendrocytes from iPSCs. However developmental patterning approaches remain a more advantageous choice due to the high yield and recapitulation of key stages of development despite the long protocols.

#### 4.1.4 Limitation and challenges associated with *in vitro* generation of Oligodendrocytes

While both developmental patterning and direct differentiation protocols have been developed for the generation of functional oligodendrocytes from human iPSCs these protocols have key limitations. Developmental patterning approaches as previously stated require very long complex protocols which are highly labour intensive. On the other hand, the direct differentiation protocols are faster therefore significantly reducing associated labour costs. However, the direct differentiation protocols remain inefficient therefore ameliorating some of the benefit of a reduced cost. The critical distinction between these two approaches is in their ability to recapitulate key stages of development. While the direct differentiation protocol produces both O4+ and MBP+ cells by necessity it results in the loss of earlier progenitors therefore this approach may result in a loss of phenotypes specifically associated with the earlier developmental stages. Alternatively, developmental patterning approaches are able to recapitulate all key developmental stages of

oligodendrocytes and therefore despite the large time investment may be a more viable option for assessing developmentally associated oligodendrocyte dysfunction.

A further limitation of both approaches is the generation of non-oligodendrocytic cells. As OPCs are multipotent retaining the ability to differentiate into both astrocytes and oligodendrocytes the maintenance of OPC cultures without the production of astrocytes remains challenging. Furthermore, developmental patterning approaches for the generation of oligodendrocytes result in the generation of both neurons and astrocytes. The production of astrocytes may be due to the multipotency of OPCs or due to the maturation of persistent neuronal precursors which are also responsible for the creation of neurons. The generation of astrocytes in these conditions is a particular challenge as these cells remain proliferative whereas immature oligodendrocytes are post mitotic therefore even small-scale production of astrocytes can result in a proportional loss of immature and mature oligodendrocytes. While the isolation of OPCs from mixed cultures is common using both FACS and MACS approaches the multipotency of OPCs means that this approach does not prevent the reoccurrence of this phenomena.

Finally, while assessment of OPC morphology and gross oligodendrocyte function is possible in simple 2D monoculture systems the true functional capacity of oligodendrocytes cannot be measured in these systems. The critical function of oligodendrocytes is to myelinate axons and this process is driven by interactions between the oligodendrocytes and neurons therefore it is not possible to fully model dysfunction in this system in classic 2D cultures. Some studies have used more complex artificial axons which have been shown to induce myelination in oligodendrocytes. However, this system is reliant on oligodendrocytes recognising axon like structures and myelinating based on the morphological characteristics of these structures. Therefore, while these systems may offer insight into the process, they fail to recapitulate the complex interactions between oligodendrocytes and neurons which ultimately inform the myelination of axons. Ultimately it is only co-culture or transplantation studies which allow the complete analysis of this function. However, neuron and oligodendrocyte co-cultures remain highly challenging and to allow for myelination requires more complex scenarios than simple 2D culture-ware. Some progress has been made in developing a protocol for generating organoids which also produce oligodendrocytes however similarly to direct differentiation approach the number of oligodendrocytes produced is low<sup>339</sup>. Finally, while studies have shown that iPSC derived oligodendrocytes can be transplanted into rodent models these

experiments require large scale production of OPCs and costly generation and maintenance of mouse models. Therefore, while the assessment of oligodendrocyte function is possible using multiple paradigms with varying levels of physiological accuracy this remains a challenge to understanding the precise nature of any functional deficits associated with patient derived oligodendrocytes. Overall the generation of oligodendrocytes from human iPSC is possible however the methodology selected to do so must be assessed for its relevance to the hypothesis being tested. Furthermore, the maintenance and functional assessment of these cells present unique challenges which must be considered and addressed.

#### 4.2 Chapter 2: Hypothesis and aims

My hypothesis is that deletions and duplications of the 1q21.1 locus detrimentally effect the production and maturation of oligodendrocytes. Therefore, the aims of this chapter are to investigate the role of 1q21.1 deletion and duplication on the course of oligodendrocyte specification and function. Oligodendrocytes will be produced using a developmental patterning approach and cells will be screened for critical lineage markers and key functional readouts at developmentally important stages. Further investigations will be carried out using functionally mature oligodendrocytes to ascertain how these mutations may impact myelination. These results will then be combined with results from both an animal model and small-scale human data to elucidate a more complete picture of the effect of 1q21.1 mutation on oligodendrocytes and myelination.

## 4.3 Results

### 4.3.1 Human brain imaging of 1q21.1 carriers show changes in DTI metrics in the corpus callosum

Changes in DTI metrics have been widely associated with psychiatric disorders<sup>340</sup> which has formed the basis for the current interest in oligodendrocyte dysfunction associated with these disorders. However, assessing the effect of 1q21.1 mutations on changes in DTI metrics indicative of white matter dysfunction has yet to be carried out. To this end Dr. Ana Silva carried out a preliminary analysis using UK biobank data to confirm the key clinical finding of altered brain size and to examine the effect of 1q21.1 mutations on DTI metrics in the corpus callosum.

Firstly, the intracranial volume of 1q21.1 deletion and duplication carriers was assessed in this sample. The results show that 1q21.1 deletion carriers had a decreased intracranial volume compared to controls and 1q21.1 duplications carriers had an increased intracranial volume compared to controls (Figure 4.4). Recapitulating the association of microcephaly with 1q21.1 deletion and macrocephaly with 1q21.1 duplication.

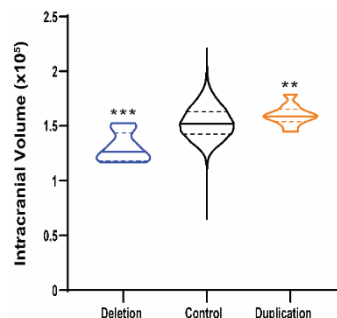


**Figure 4.4: Intracranial volumes of individuals carrying 1q21.1 mutations.** Intracranial volume as measure by MRI from individuals carrying no known pathogenic CNV and individuals with either 1q21.1 deletions or duplications. Data is presented as distributions with median (solid line) and quartiles (dotted lines) marked. Data was analyzed by unpaired t-tests with Welch's correction: \*\* $P < 0.01$ ; \*\*\* $P < 0.001$ ; Deletion  $n=8$ , Control  $n=15159$ , Duplication  $n=10$ .

Having demonstrated the trend towards smaller brain sizes in 1q21.1 deletion carriers and the inverse in 1q21.1 duplications carriers it was then important to assess if there were similar reciprocal changes in DTI metrics of the white matter taking into account the changes in brain volume. To assess the effect of 1q21.1 mutations on the organization of white matter four metrics were assessed; axial diffusivity (AD), fractional anisotropy (FA), mode of anisotropy (MA) and radial diffusivity (RD) in the corpus callosum. The corpus callosum was divided into three separate white matter tracts (body, genu and splenium) each of which was assessed individually for changes in each metric. This analysis showed

that 1q21.1 deletion was associated with a decrease in FA in the genu of the corpus callosum as compared to controls (Figure 4.5). However, this result did not survive corrections for multiple testing. There was also a decrease in the MA in 1q21.1 deletion carriers compared to controls in the splenium which did survive correction for multiple testing (Figure 4.5). To assess the magnitude of these effects Cohen's d effect sizes were calculated which showed that the effect size of the change in FA was medium to large however the effect size of the change in MA was very large. Taken together these results suggest that 1q21.1 mutations have effects on FA and MA in the corpus callosum pointing towards effects on oligodendrocyte formation or function.

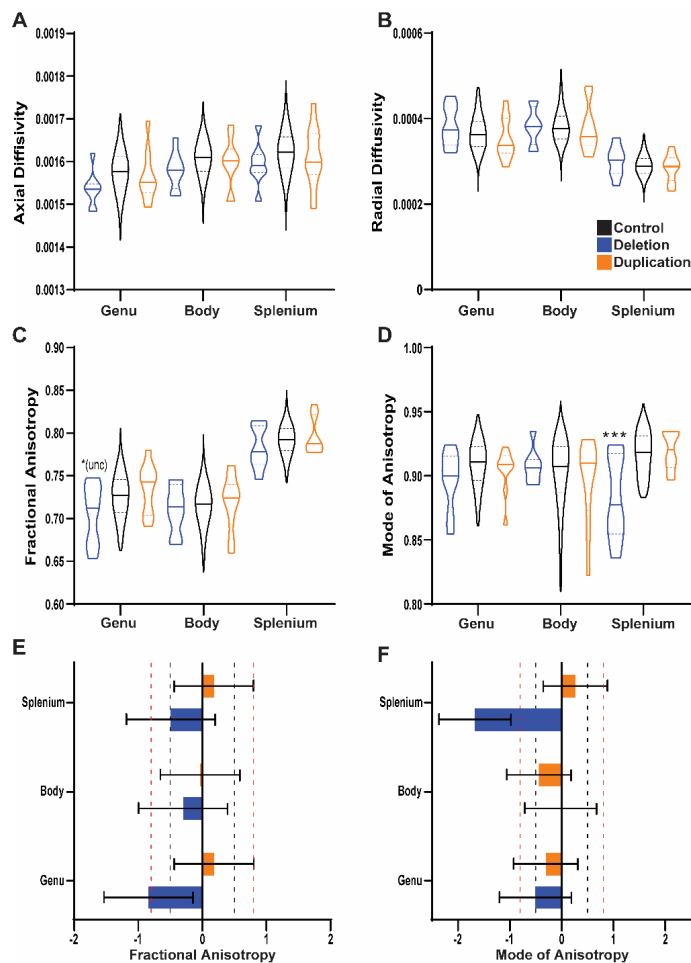


**Figure 4.5: DTI metrics in the corpus callosum of individuals with CNV at the 1q21.1 locus.** **A** Axial diffusivity of 3 white matter tracts (genu, body and splenium) in the corpus callosum. **B** Radial diffusivity of 3 white matter tracts (genu, body and splenium) in the corpus callosum. **C** Fractional anisotropy of 3 white matter tracts (genu, body and splenium) in the corpus callosum. **D** Mode of anisotropy of 3 white matter tracts (genu, body and splenium) in the corpus callosum. Data is presented as distributions with median (solid line) and quartiles (dotted lines) marked. Data sets were analyzed by linear regression comparing each white matter tract separately, regressing out age, sex and intracranial volume (ICV) as covariates of no interest. Following this, post hoc pairwise comparisons were performed comparing 1q21.1 mutations to controls. Stars represent either uncorrected P values (marked by unc) or FDR corrected P value. \*P<0.05; \*\*\*P<0.001; Deletion n=8, Control n=15159, Duplication n=10. **E** Cohen's d effect sizes comparing fractional anisotropy of 3 white matter tracts (genu, body and splenium) in the corpus callosum in 1q21.1 deletion vs controls and 1q21.1 duplication vs controls. **F** Cohen's d effect sizes comparing mode of anisotropy of 3 white matter tracts (genu, body and splenium) in the corpus callosum in 1q21.1 deletion vs controls and 1q21.1 duplication vs controls. Cohen's d effect sizes used adjusted means of each group based on residuals from the linear regression models  $\pm$  SEM. Medium effect size ( $d>0.5$ ) is marked by black dotted line and large effect size ( $d>0.8$ ) is marked by red dotted line.

#### 4.3.2 A mouse model of 1q21.1 microdeletion shows a loss of oligodendrocytes in the corpus callosum

Significant changes in DTI metrics point towards dysfunction in oligodendrocyte production or function. Therefore, to assess if 1q21.1 mutations influence the production of oligodendrocytes in the corpus callosum the number of oligodendrocytes (marked by co-localisation of Olig2 and anti-adenomatous polyposis coli: Cc1 staining) was quantified in the corpus callosum of the 1q21.1 microdeletion mouse model. This analysis showed that in the 1q21.1 microdeletion mouse model there was a significant decrease in the number of oligodendrocytes in the corpus callosum (Figure 4.6). This metric was normalised to both the total cell number and the area of the corpus callosum therefore suggesting that this difference is due to a loss of oligodendrocytes in this area rather than gross structural changes.

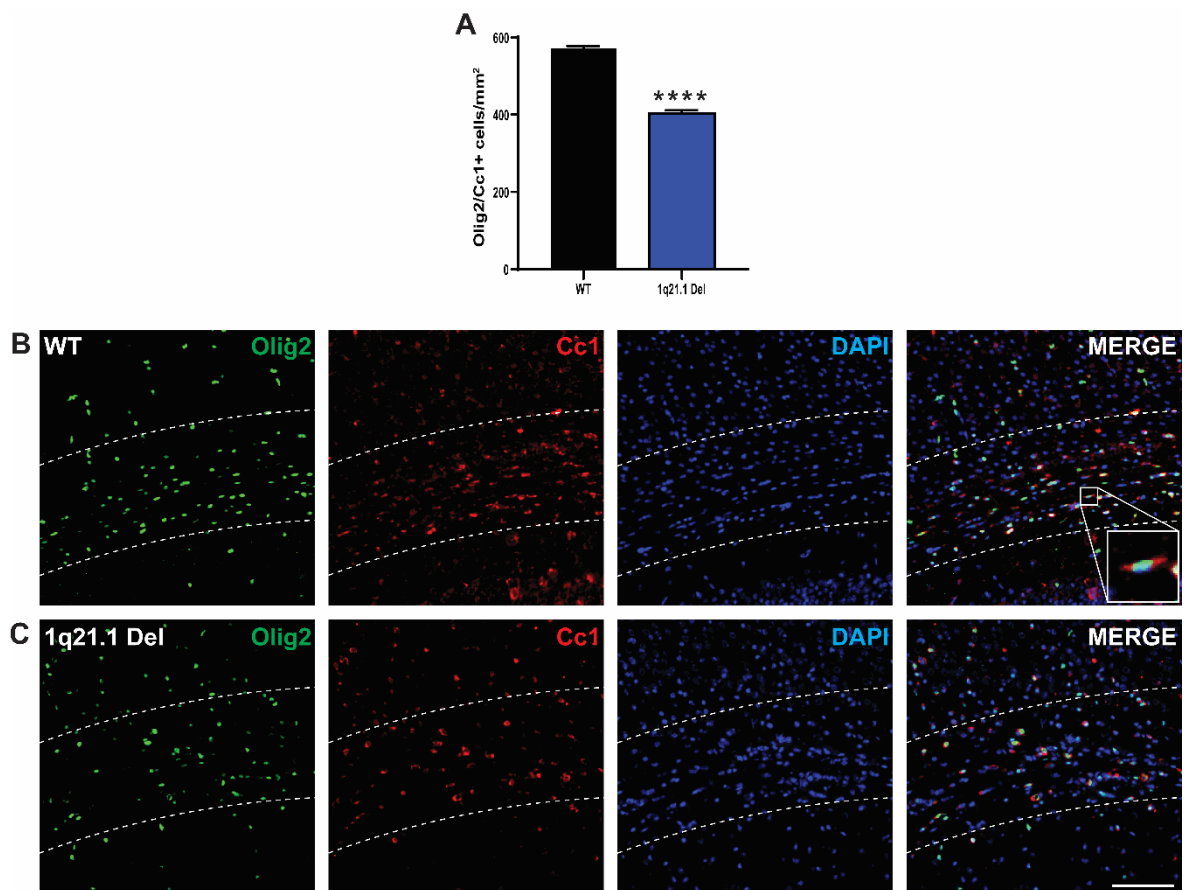


**Figure 4.6: Changes in the number of oligodendrocytes in the corpus callosum of the 1q21.1 microdeletion mouse model.** **A** Quantification of the number of oligodendrocytes (Olig2/Cc1+ cells) in a 0.045mm<sup>2</sup> area of the corpus callosum of the 1q21.1 microdeletion mouse model (1q21.1) and litter mate controls (WT). Data is presented as mean  $\pm$  SEM and data sets were analyzed by Students T-Test; \*\*P<0.01; vs. WT, 6 animals were used per group and n=3 per animal. **B** Example images of the corpus callosum of wild type mice stained with Olig2 and Cc1. **C** Example images of the corpus callosum of 1q21.1 microdeletion mice stained with Olig2 and Cc1. Scale bar = 50  $\mu$ m.

### 4.3.3 Differentiation of iPSCs into oligodendrocytes

Given the results from both human imaging and the 1q21.1 micro deletion mouse model, iPSC cells were differentiated into oligodendrocytes with a view towards assessing how this process is affected by 1q21.1 mutations in humans. The protocol used for generating oligodendrocytes is complex involving both adherent and non-adherent stages (Figure 4.7). At early stages iPSCs transition to NPCs in a similar fashion to during neuronal differentiations marked by the expression of PAX6 (Figure 4.7). After 12 days of patterning cell are dissociated and allowed to form spheres in non-adherent culture-ware. Spheres are further patterned to enrich for oligodendrocyte precursor cells resulting in increasing expression of *OLIG2* and NK2 Homeobox 2 (*NKX2.2*) (Figure 4.7).

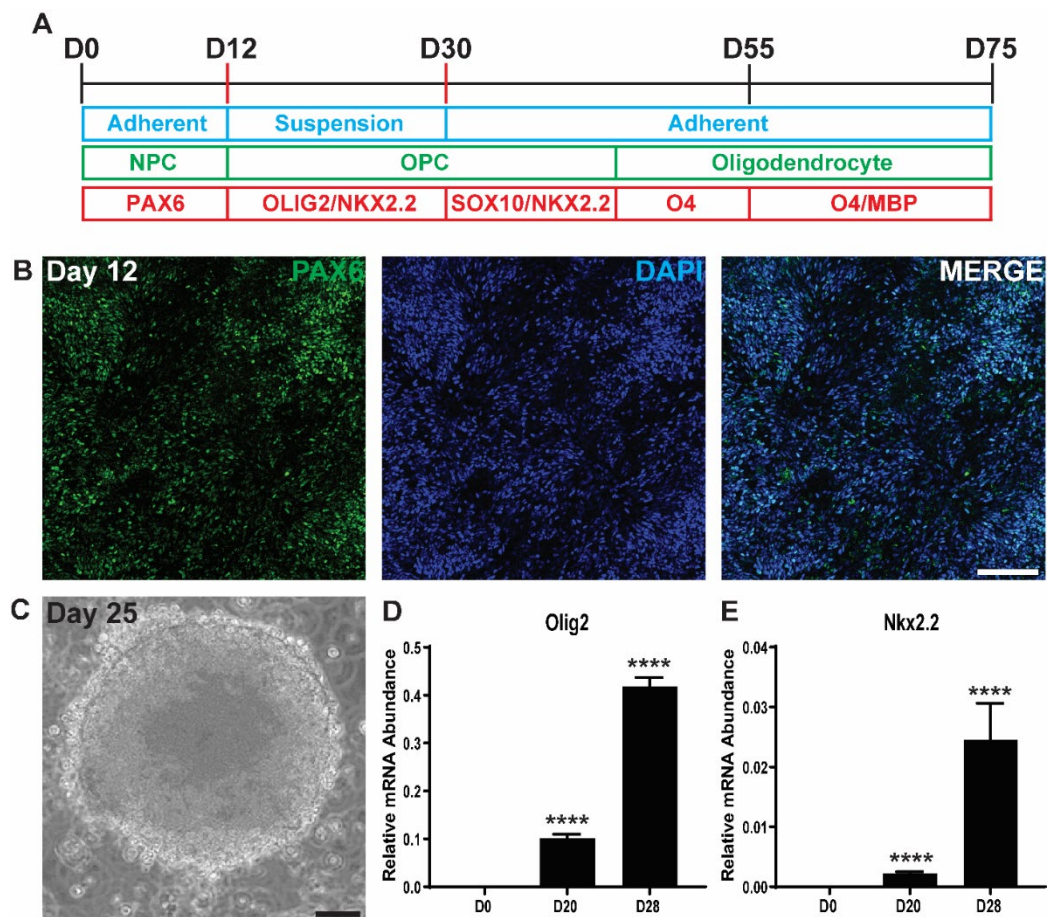


**Figure 4.7: Early oligodendrocyte differentiation from iPSC.** **A** Protocol for the generation for oligodendrocytes from iPSC. Key times are indicated and points at which passaging occurs are marked by red bars. Also indicated are types of culture (blue), predominant cell population (green) and key markers expressed by that population (red). Image adapted from Douvaras and Fossati<sup>65</sup> **B** Example staining for PAX6 in control iPSC differentiated for 12 days. **C** Example image of spheres produced in non-adherent cultures after 25 days of differentiation. Sale bar = 100  $\mu$ m. **D** Expression of *OLIG2* mRNA from D0 (iPSCs) to D20 (small spheres) and to D28 (large spheres). Relative mRNA abundance was calculated compared to *GAPDH* expression. **E** Expression of *NKX2.2* mRNA from D0 (iPSCs) to D20 (small spheres) and to D28 (large spheres). Relative mRNA abundance was calculated compared to *GAPDH* expression. Data is presented as mean  $\pm$  SEM and data sets were analyzed by Students T-Test; \*\*\*\*P<0.0001; vs. D0, Control N=1 and n=3.

Using this protocols the production of a large number of spheres was relatively easy but maintaining the spheres as distinct entities was difficult with many spheres sticking to each other and fusing into large conglomerations (Figure 4.8). These structures are not able to be used in further work and therefore represent a considerable loss of material at this stage in development. To address this issue after spheres were established (day 20 of differentiation) plates were placed onto an oscillating table within an incubator (oscillating at a rate of 50 rpm at an angle of 13°). Modifying the protocol in this way preventing the spheres from sticking together. To determine if this modification had a negative effect on the growth of the spheres the size of the spheres after 25 days of differentiation was measured. Comparing spheres grown under normal conditions and those grown on the oscillating table showed spheres grown on the oscillating table were significantly smaller by an average of  $\sim 0.25\text{mm}^2$  (Figure 4.8). This change may have been due to the loss of spheres joining and fusing together or because the change in methodology slowed the growth of the spheres. Critically the change in methodology had a beneficial effect on the variability of sphere sizes with spheres grown on the oscillating table having a significantly less variable size than those grown under the original protocol ( $F_{1,115}=8.813$ ,  $P<0.0001$ ,  $n=155$  original,  $n=338$  oscillating). Therefore, the adapted protocol was used for generating OPC spheres.

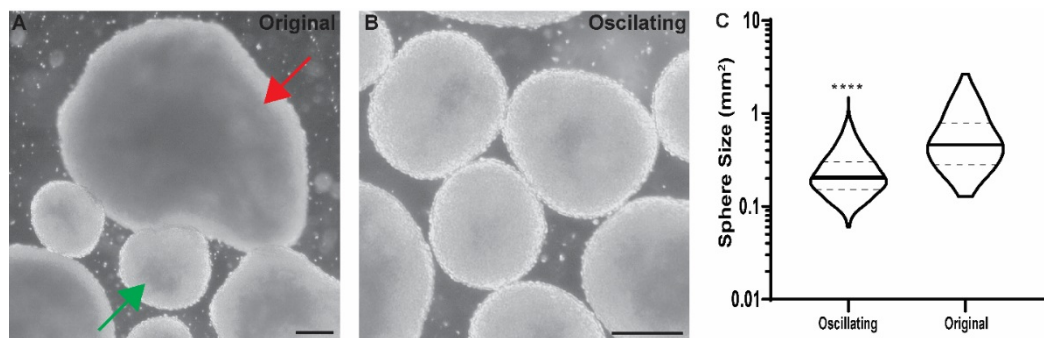


**Figure 4.8: Modification to the non-adherent growth stages of oligodendrocyte generation.** **A** Example image of spheres grown under the original protocol highlighting a large sphere (red arrow) generated by the fusion of a number of smaller spheres (green arrow). **B** Example image of spheres grown using the modified protocol with a oscillating table highlighting the lack of large fused spheres and the relative uniformity of sphere size. **C** Comparison of sphere sizes using the original and modified (oscillating) protocols. Data is presented as distributions with median (solid line) and quartiles (dotted lines) marked. Data sets were compared using unpaired t-test with Welch's correction: \*\*\*\* $P<0.0001$  vs original;  $n=115$  original;  $n=338$  oscillating.

Having selected for OPC using suspension cultures spheres were plated and cells were allowed to migrate out of these structures (Figure 4.9). First neuronal processes are produced and then OPCs can move along these structures and spread away from the spheres. After an extended period of time these OPCs can begin to produce myelin and given enough time it is possible for the oligodendrocytes produced in this manner to begin to interact with the surrounding neuronal processes (Figure 4.9). Therefore, using this protocol, it is possible to generate mature MBP+ oligodendrocytes from iPSCs.

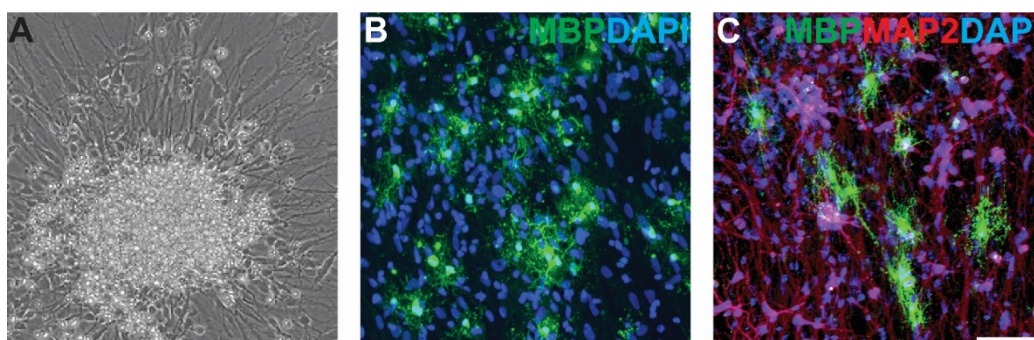


**Figure 4.9: Oligodendrocyte differentiation and maturation.** **A** Example image of OPC spheres plates and grown in adherent culture for 10 days. **B** Example staining for MBP of control iPSC derived oligodendrocytes after 75 days of differentiation. **C** Example staining for MAP2 and MBP of control iPSC derived oligodendrocytes after 110 days of differentiation. Scale bar = 50  $\mu$ m.

#### 4.3.4 Deletion and duplication of the 1q21.1 locus are associated with aberrant oligodendrocyte differentiation and function

The development of oligodendrocytes is complex involving the formation of NPCs, OPCs, pre-myelinating oligodendrocytes and finally myelinating oligodendrocytes. To assess the effect of 1q21.1 mutations on the differentiation of oligodendrocytes three stages of development were examined. This analysis was done with 1 control, 1 1q21.1 deletion and 1 1q21.1 duplication cell line to provide initial evidence for dysfunction in the generation or maturation of oligodendrocytes. Firstly, the development of a ventralized NPC population was examined by assessing the expression of *PAX6* (marking neuroectoderm specification) and *OLIG2* (marking a ventralized NPC population) after 12 days of differentiation. This analysis showed that deletion or duplication of the 1q21.1 locus was associated with decreased expression of *PAX6* but no significant changes in the expression of *OLIG2* (Figure 4.10).

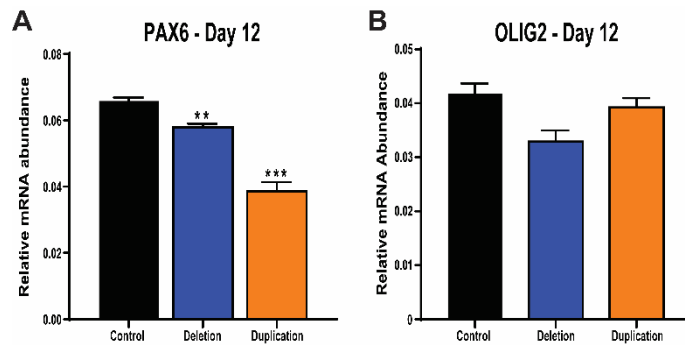


**Figure 4.10: Gene expression changes in 1q21.1 cell lines after 12 days of oligodendrocyte differentiation.** **A** Expression of *PAX6* in control 1q21.1 deletion and 1q21.1 duplication differentiations after 12 days of oligodendrocyte differentiation. **B** Expression of *OLIG2* in control 1q21.1 deletion and 1q21.1 duplication differentiation after 12 days of oligodendrocyte differentiation. Relative mRNA abundance was calculated compared to *GAPDH* expression. Data is represented as mean  $\pm$  SEM and data was analyzed by Students t-test: \*\* $P < 0.01$ ; \*\*\* $P < 0.001$  vs control; Control  $N = 1$ , Deletion  $N = 1$ , Duplication  $N = 1$  and  $n = 3$ .

To assess if the changes in the production of NPCs went on to affect the production of glial progenitors and OPCs the expression of 4 markers was assessed after 25 days of differentiation. To examine the production of NPCs the expression of *PAX6* was examined and to assess the production of ventralized glial precursors the expression of *OLIG2* and *NKX2.2* was examined. Finally, the expression of *SOX10* was examined as a marker of early oligodendrocyte specification. At this stage the expression of *OLIG2* had increased while the expression of *PAX6* had decreased in control cells compared to day 12 (Figure 4.11). Furthermore, markers of OPCs (*NKX2.2* and *SOX10*) were expressed although at lower levels (Figure 4.11). Examining the relative change in the expression of these markers in 1q21.1 deletion and duplication differentiations showed no significant changes in *PAX6* or *OLIG2* expression. However, duplication of the 1q21.1 locus was associated with a significant increase in *NKX2.2* expression and a significant decrease in *SOX10* expression (Figure 4.11). This period of oligodendrocyte differentiation is marked by a high rate of proliferation and therefore to assess if 1q21.1 mutations had any effect on proliferation the expression of Marker Of Proliferation Ki-67 (*KI67*) was also assessed. As expected, the expression of *KI67* was high in control differentiations. However, unlike changes in the expression of other markers the changes in the expression of *KI67* were reciprocal based on the deletion or duplication of the 1q21.1 locus. Specifically, deletion of 1q21.1 resulted in a decreased expression of *KI67* whereas duplication of this locus resulted in an increased expression. To further confirm this result and assess any gross effect this had on the growth of spheres the size of spheres was assessed. This analysis showed similar results to those

seen with *KI67* expression with 1q21.1 deletion associated with a decreased sphere size and 1q21.1 duplication associated with an increased sphere size (Figure 4.11).

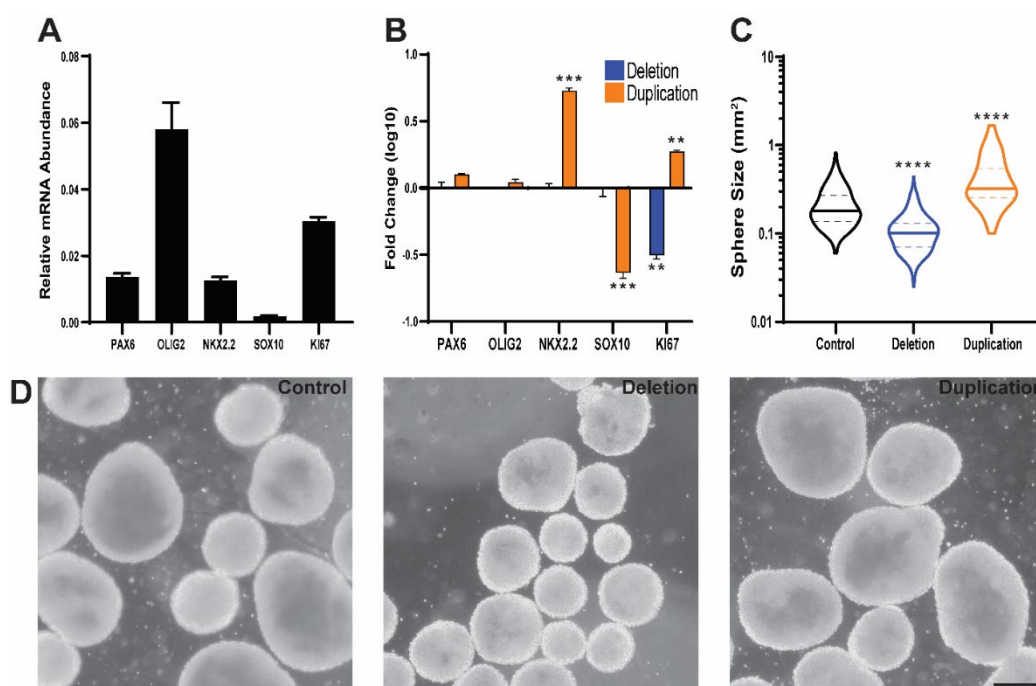


**Figure 4.11: Changes in proliferation during early stages of oligodendrocyte development.** **A** Expression of 4 oligodendrocyte lineage markers and the proliferation marker *KI67* in control differentiations after 25 days of oligodendrocyte differentiation (Control N=1 and n=3). Relative mRNA abundance was calculated compared to *GAPDH* expression. **B** Expression of 4 oligodendrocyte lineage markers and the proliferation marker *KI67* in 1q21.1 deletion and duplications after 25 days of oligodendrocyte differentiation. Fold change was normalized to control differentiations. Data is presented as mean  $\pm$  SEM and was analyzed by multiple t-test. Star represent Holm-Sidak corrected p-values: \*\*P<0.01; \*\*\*P<0.001 vs control; Control N=1, Deletion N=1, Duplication N=1 and n=3. **C** Sphere sizes measured after 25 days of oligodendrocyte differentiation. Data is presented as distributions with median (solid line) and quartiles (dotted lines) marked. Data sets were compared using unpaired t-test with Welch's correction: \*\*\*\*P<0.0001 vs control; n=193 control; n=153 deletion, n=109 duplication. **D** Example images of spheres produced from control, 1q21.1 deletion and 1q21.1 duplication cell lines. Scale bar = 100  $\mu$ m.

After plating spheres, it was observed that both 1q21.1 deletion and duplication spheres failed to produce the same number of cells migrating away from the spheres as controls. Therefore, to assess if the changes in proliferation and observations of migratory deficits were indicative of a loss of oligodendrocyte production the number of cells expressing MBP was assessed at two stages of development. After 75 days of differentiation control spheres had produced a large number of MBP+ oligodendrocytes. However, both 1q21.1 deletion and duplication were associated with a decreased number of MBP+ cells (Figure 4.12). Furthermore, while MBP+ cells had migrated away from the spheres producing them in control and 1q21.1 deletion differentiations MBP+ cells were only found in close proximity to spheres in 1q21.1 duplication differentiations (Figure 4.12). After 110 days of differentiation 1q21.1 deletion spheres were able to increase the production of MBP+ oligodendrocytes, however there remained significantly fewer of

these cells than in control differentiations (Figure 4.12). Furthermore, by this time point there were no MBP+ cells in 1q21.1 duplication differentiations. Due to the production of neuronal processes in these differentiations it is possible to observe MBP+ control oligodendrocytes interacting with neuronal processes. However, none of the MBP+ cells in 1q21.1 deletion differentiations could be observed interacting with neuronal process (Figure 4.12). Moreover, MBP+ cells in 1q21.1 deletion differentiations appeared smaller than those in control differentiations. Therefore, taken together these results suggest that mutations at the 1q21.1 locus are associated with dysfunction in the development and function of oligodendrocytes.

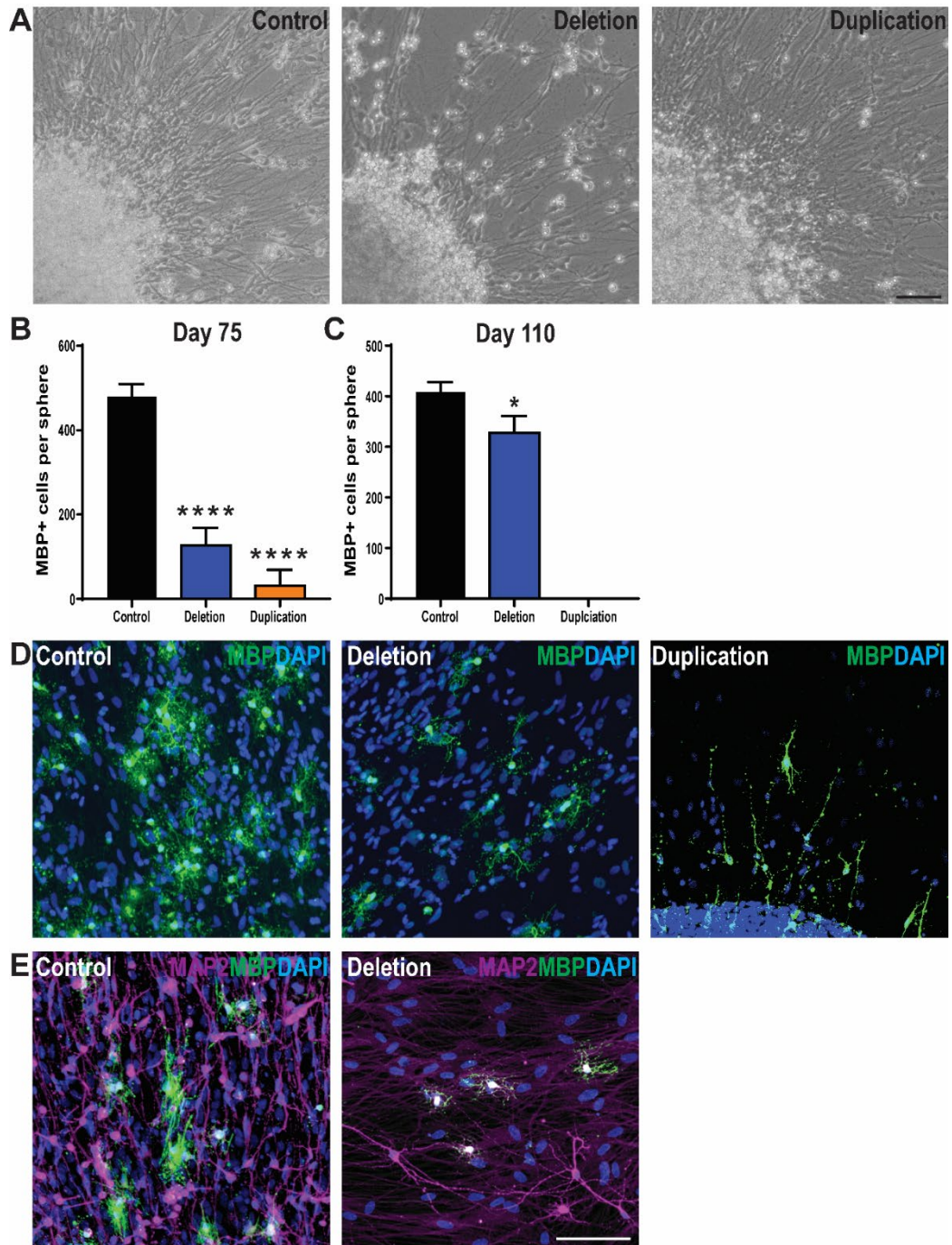


**Figure 4.12: Production of mature MBP+ oligodendrocytes in control and 1q.21.1 mutant oligodendrocyte differentiations.** **A** Example brightfield images of spheres 10 days after plating. **B** Number of MBP+ oligodendrocytes produced from control, 1q21.1 deletion and 1q21.1 duplication spheres after 75 days of differentiation. **C** Number of MBP+ oligodendrocytes produced from control, 1q21.1 deletion and 1q21.1 duplication spheres after 110 days of differentiation. All data is presented as mean  $\pm$  SEM and was analyzed by Students t-test: \* $P < 0.05$ ; \*\*\*\* $P < 0.0001$  vs control; Control  $N = 1$ , Deletion  $N = 1$ , Duplication  $N = 1$  and  $n = 48$ . **D** Example images of MBP+ cells in control, 1q21.1 deletion and 1q21.1 duplication differentiations after 75 days. **E** Example images of MBP+ cells in control and 1q21.1 deletion differentiations after 110 days.

#### 4.3.6 Deletion of the 1q21.1 locus is associated with decreased production of myelinating oligodendrocytes

To better understand the cellular dysfunction which underlies the loss of MBP+ oligodendrocytes in 1q21.1 deletions; oligodendrocyte differentiations were repeated using 2 control and 3 1q21.1 deletion iPSC lines. As results from the initial study showed clear evidence of decreased proliferation during the non-adherent stage of differentiation the same quantification was performed using the larger complement of cell lines. The result was replicated with 1q21.1 deletion cultures producing significantly smaller spheres than control cultures (Figure 4.13). To establish if this mutations also effected the ability to form spheres the number of spheres larger than 100  $\mu\text{m}$  in diameter was also assessed after 25 days of differentiation. The results indicated that 1q21.1 deletion was not associated with a change in the number of spheres produced (Figure 4.13) but was associated with a decrease in sphere size therefore suggesting that the proliferation deficit was occurring after sphere formation.

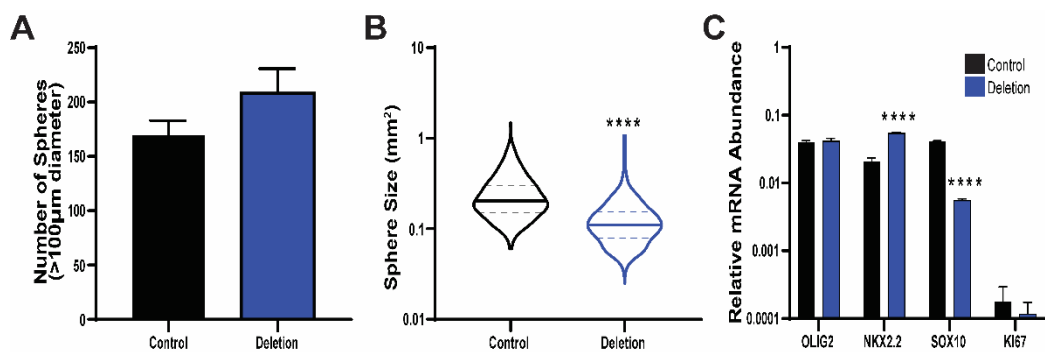


**Figure 4.13: Gene expression and proliferation changes associated with 1q21.1 deletion during early oligodendrocyte development.** **A** Number of spheres (produced from  $3 \times 10^6$  cells at day 12 of differentiation) with a diameter larger than 100  $\mu\text{m}$  after 25 days of oligodendrocyte differentiation (Control N=2, Deletion N=3 and n=3). Data is presented as mean  $\pm$  SEM and was analyzed by Students t-test. **B** Sphere sizes measured after 25 days of oligodendrocyte differentiation. Data is presented as distributions with median (solid line) and quartiles (dotted lines) marked. Data sets were compared using unpaired t-test with Welch's correction: \*\*\*\* $P < 0.0001$  vs control; n=339 control; n=625 deletion. **C** Expression of 3 key oligodendrocyte lineage markers and the proliferative marker KI67 after 30 days of oligodendrocyte differentiation (Control N=2, Deletion N=3 and n=3). Data is presented as mean  $\pm$  SEM and was analyzed by Students t-test: \*\*\*\* $P < 0.0001$  vs control.

There were no significant changes in the expression of key oligodendrocyte lineage markers after 25 days of differentiation in the initial study. Therefore, to establish if the changes in proliferation occurring at this stage influence gene expression at a later stage the expression of 3 key oligodendrocyte lineage markers was assessed after 30 days of differentiation. At this stage of development, the expression of both *NKX2.2* and *SOX10* was increased compared to day 25 of differentiation (Figure 4.13). Furthermore, deletion of the 1q21.1 locus resulted in a small but significant increase in *NKX2.2* expression and a

large decrease in the expression of *SOX10* (Figure 4.13). Finally, at this stage of development there was no significant changes in the expression of *KI67*. With the expression of *KI67* having dropped considerably from day 25 of differentiation. Therefore, the results further indicate that the changes in proliferation occur during large scale sphere expansion.

The next stage of oligodendrocyte development is the production of OPCs marked by the expression of the O4 antigen. However, the methodology used in the previous study (i.e. comparing the number of MBP+ cells per sphere) may introduce bias based on the formation and size of the spheres. Therefore, to begin to eliminate this confound the size of the area in which cells had migrated away from the spheres was measured relative to the sphere size. This metric showed that control spheres produced a larger area of cells even when accounting for the larger sphere size (Figure 4.14). However, to examine if this result was due to altered production of O4+ OPCs, spheres were dissociated and were sorted using MACS for A2B5 (which is expressed by glial progenitors and newly formed OPCs). Cells were maintained for 25 days and then the number of O4+ OPCs was quantified. In control cultures the majority of cells expressed O4 with a significant loss of O4+ cells in 1q21.1 deletion cultures (Figure 4.14). However, to prove that the selection process had enriched for O4+ cells or precursors of this cells type in both control and 1q21.1 deletion cultures, cells which were negative for A2B5 were also maintained for 25 days. Most cells which were negative for A2B5 expression stained positive for GFAP after 25 days of growth with no cells staining positive for O4 (Figure 4.14). There was also a smaller population of OLIG2+ cells in the A2B5- cultures suggesting some cells may have been A2B5- glial or neuronal precursors (Figure 4.14). There was also no significant differences in the number of GFAP+ or OLIG2+ cells in the A2B5 negative cultures (Figure 4.14) or in the proportion of A2B5+ cells from either control or 1q21.1 deletion differentiations. Taken together these results indicate that any differences in the A2B5+ cultures are due to the differentiation of these cells and not the process of selection.

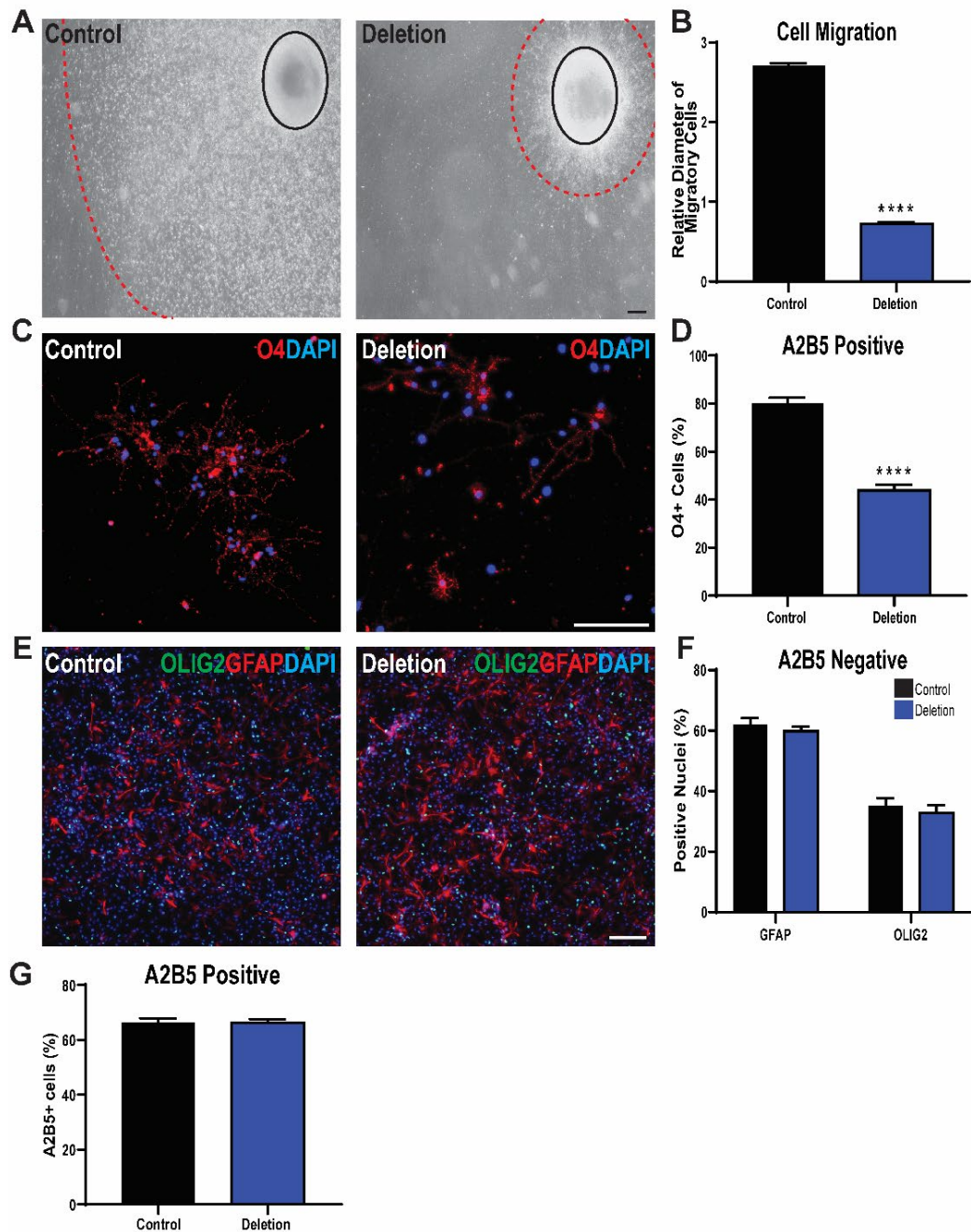


**Figure 4.14: The effect of 1q21.1 deletion on the production of OPCs.** **A** Example images of cells migrating away from spheres after 50 days of differentiation. Spheres are marked by black circles and the distance cells migrated from the spheres is marked by the dotted red lines. **B** Quantification of cell migration measured by the furthest distance cells migrated from the sphere relative to the size of the spheres (Control N=2, Deletion N=3 and n=24). **C** Example images of O4+ cells after 55 days of differentiation and sorting for A2B5 in control and 1q21.1 deletion cultures. **D** Number of O4+ cells after 55 days of differentiation and sorting for A2B5 relative to the total number of nuclei (Control N=2, Deletion N=3 and n=3). **E** Representative images of A2B5 negative cells stained for GFAP and OLIG2 after 55 days of differentiation. **F** Quantification of the percentage of nuclei which co-localized with GFAP or OLIG1 expression in A2B5 negative cultures after 55 days of differentiation (Control N=2, Deletion N=3 and n=3). **G** Percentage of cells which sorted positive for A2B5 using MACS (Control N=2, Deletion N=3 and n=3). All data is presented as mean  $\pm$  SEM and was analyzed using Student's t-test; \*\*\*\*P<0.0001 vs control. Scale bars = 100  $\mu$ m.

Finally, to assess the effect of 1q21.1 deletion on the production of functional oligodendrocytes the expression of key genes involved in the production of myelin and function of oligodendrocytes was assessed after 75 days of differentiation. The expression of both PLP1 and MBP was high in control differentiations (Figure 4.15). In 1q21.1 deletion differentiations there was a loss in the expression of both Proteolipid Protein 1 (*PLP1*) and *MBP* (Figure 4.15). To demonstrate if this loss of gene expression was associated with a loss of MBP+ oligodendrocytes; cultures were stained after 75 days of differentiation for MBP. In control cultures ~30% of cells were MBP+ whereas in 1q21.1 deletion cultures only ~5% of cells were MBP+ (Figure 4.15). These results confirm that 1q21.1 deletion is associated with a loss of functional oligodendrocytes.

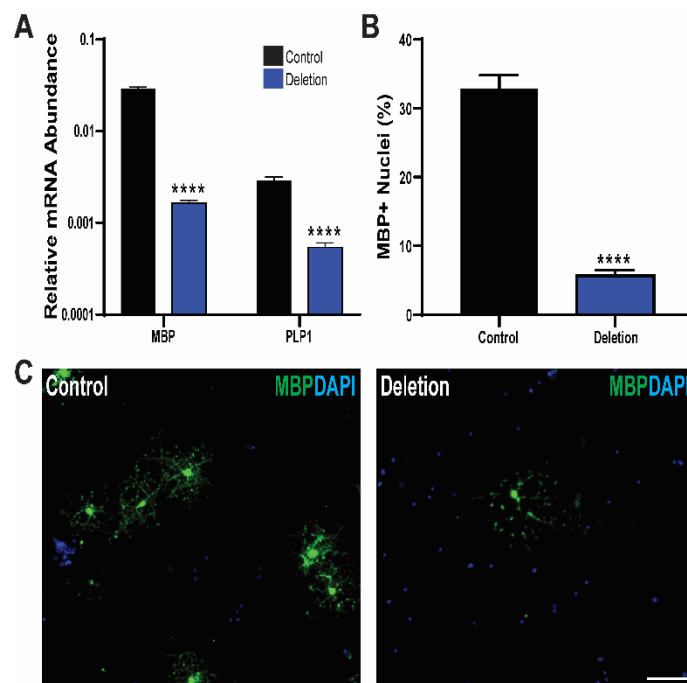


**Figure 4.15: The production of mature oligodendrocytes from control and 1q21.1 deletion iPSCs.** **A** Expression of two myelin related proteins (MBP and PLP1) in day 75 A2B5+ cultures. **B** Number of nuclei which co-localized with significant MBP staining after 75 days of differentiation. All data is represented as mean  $\pm$  SEM and data was analyzed by Students t-test: \*\*\* $P < 0.001$  vs control; Control  $N = 2$ , Deletion  $N = 3$  and  $n = 3$ . Relative mRNA abundance was calculated compared to *GAPDH* expression. **C** Representative images of MBP+ cells in control and deletion day 75 cultures. Scale bar = 100  $\mu\text{m}$ .

## 4.4 Discussion

### 4.4.1 Duplication of the 1q21.1 locus is associated with changes in early oligodendrocyte differentiation

This is the first study to examine the effect of 1q21.1 mutations on the differentiation and function of oligodendrocytes. Duplication of this locus was associated with changes in proliferation during early stages of development resulting in a loss of mature oligodendrocytes. However, the DTI metrics for 1q21.1 duplication patients show no significant association between changes in any measure and 1q21.1 duplication. However, the loss of mature oligodendrocytes seen in association with 1q21.1 duplication is consistent with some studies done on ASD and intellectual disability (both of which are associated with 1q21.1 duplication). Most similarly, work done on PAK3 (which is associated with non-syndromic intellectual disability) showed loss of this gene was associated with a loss of oligodendrocytes in a mouse model<sup>341</sup>. However, this loss was only found at early stages of development and the changes in cell number and myelin thickness recovered during adulthood. Therefore, it is conceivable that the divergence of evidence from *in vivo* (DTI) and *in vitro* (iPSC derived oligodendrocyte) studies is due to compensatory mechanism which occur during adolescence and adulthood as the human data in this study is from older individuals.

The loss of myelin reported in the PAK3 mouse model is also seen in the mouse model of down syndrome which also shows a loss of oligodendrocytes in white matter tracts<sup>342</sup>. Finally, in contrast to the results from animal studies a study of gene expression in the cerebellum of autistic patients showed an up regulation of oligodendrocyte lineage markers<sup>343</sup> including genes involved in both development and function of oligodendrocytes. However overall there are very few studies of oligodendrocyte dysfunction in ASD and intellectual disability and based on this study, and other studies using animal models it is clear that, while there may be dysfunction in this cell type associated with these disorders it may be temporally specific. Therefore, the study of this association must focus on early developmental time points.

The increased proliferation during early stages of development is also consistent with the reports of the effect of NOTCH2NL over expression. The over expression of NOTCH2NL was reported to prevent the maturation of NPCs into neurons<sup>65,255</sup>. Therefore, the increased proliferation reported in association with 1q21.1 duplication may be a result of a restriction of cells to an NPC or glial progenitor fate in which they are highly

proliferative. Furthermore, recent work by Nagarajan *et al*<sup>344</sup> suggests that NOTCH expression is linked to conversion of OPCs into oligodendrocytes and therefore decreased NOTCH signaling may have a similar effect on OPC to oligodendrocyte transition as seen with NPC to neuron transition. This would then result in the loss of functional oligodendrocytes seen in the 1q21.1 duplication differentiations. Ultimately, the lack of research on oligodendrocyte dysfunction associated with childhood and adolescent psychiatric disorders makes the study of the duplication of 1q21.1 particularly interesting and further examination of this association may provide further insight into these disorders.

#### 4.4.2 Loss of oligodendrocytes in 1q21.1 deletion is both physiologically relevant and indicative of psychiatric pathology

The use of three separate techniques and two model systems provides strong evidence that deletion of the 1q21.1 locus is associated with a decreased production and function of oligodendrocytes. Modelling oligodendrocyte development using iPSCs carrying 1q21.1 deletion has shown that this mutation is associated with a loss of mature oligodendrocytes similar to the 1q21.1 microdeletion mouse model which would also explain the changes in DTI metric reported in patients. These results are consistent with early work using post mortem samples<sup>345,346</sup> which clearly showed a loss of myelin associated with severe schizophrenia with similar results presented for bipolar disorder<sup>311</sup>. However the advent of DTI metrics used in this study to examine the white matter in live patients has further confirmed this associated with the most prevalent finding being a loss of FA<sup>340,347,348</sup> similar to that seen in this study. However, the use of a mouse and human iPSC model allows dissection of this finding at a cellular level.

Work by Windrem *et al*.<sup>329</sup> showed clear evidence that oligodendrocytes derived from schizophrenic patients were unable to produce the same level of myelination as healthy controls when transplanted into a myelin deficient mouse. In a similar fashion deletion of the 1q21.1 locus is associated with a loss of myelin production in the iPSC model and a loss of oligodendrocytes in the mouse model. However, isolating the development of this cells type using the iPSC model allows the determination that this phenotype is at least partially developmental. This result is similar to work done by McPhie *et al*.<sup>330</sup> who showed a loss of OPC production in iPSC differentiations from schizophrenic patients. Furthermore, two studies examining the effect of individual genes associated with risk for schizophrenia have also shown developmental deficits. Studying mutations in CSPG4 Vrij *et al*.<sup>328</sup> showed

that the mutant form of this gene, associated with schizophrenia, had negative effects on cellular morphology and viability resulting in a loss of myelination potential. Similarly examining loss of NEAT1 expression (another risk gene for schizophrenia) Katsel *et al.*<sup>349</sup> showed loss of NEAT1 expression was associated with a reduced expression of genes involved in oligodendrocyte differentiation in a mouse model.

In the present study 1q21.1 deletion was associated with a loss of O4+ cells; changes in proliferation, and gene expression at early (<30 days) developmental time points. The changes in proliferation at the earlier time points may suggest an influence from loss of NOTCH2NL expression. This phenotype is also particularly relevant given the association of 1q21.1 deletion with microcephaly<sup>42</sup>. As previously discussed, loss of NOTCH2NL expression has been shown to cause premature differentiation resulting in a loss of neuronal progenitors<sup>65</sup>. Therefore, while this system is driving the differentiation of oligodendrocytes rather than neurons it is conceivable that loss of NOTCH2NL expression results in premature exit from early proliferative stages in development. However, if this is the case the lack of an increase in O4+ or GFAP+ cells during the later stage of development would suggest that cells which have prematurely differentiated are not forming either astrocytes or OPCs. Therefore, these results may suggest a role for other 1q21.1 genes in the origin of this phenotype. The loss of cells which migrated away from the OPC spheres also suggests the deficits in differentiation and proliferation may be confounded by deficits in migration. In a similar fashion a cell migration deficit has been presented in association with CNTNAP2 deletion<sup>350</sup>. While this study did not focus solely on oligodendrocytes the migration of cells away from neurospheres was significantly hampered in the schizophrenic individual studied compared to control and a healthy carrier. Therefore, while the lack of migration may be at least partially due to the decreased production of O4+ migratory OPCs this phenotype may also be partially due to a loss of motility in these cells.

The gene expression changes associated with 1q21.1 deletion at early stage of oligodendrocyte development also point towards developmental deficits. Increased expression of *NKX2.2* without similar increase in *OLIG2* suggests a dysregulation in oligodendrocyte differentiation as both transcription factors are known to function in collaboration to drive the differentiation of oligodendrocytes<sup>351,352</sup>. The expression of *SOX10* is also of critical importance for oligodendrocyte development<sup>353,354</sup> and along with *SOX8* is important for the expression of myelin related genes such as *MOG*<sup>355</sup>. Therefore,

while the loss of *SOX10* expression observed in this study may be indicative of a loss of OPCs and or oligodendrocytes if there is a reduction of *SOX10* expression within the 1q21.1 deletion OPCs and oligodendrocytes at later stages of development this may impact the differentiation and function of these cells.

While deletion of the 1q21.1 locus is associated with a loss of both O4+ and MBP+ cells (after 55 and 75 days of differentiation respectively) the loss of MBP+ cells is more profound than the loss of O4+ cells. Therefore, this result suggests that beyond the deficits in differentiation there are key deficits in functional maturation associated with deletion of the 1q21.1 locus. Similarly, Chen *et al.*<sup>356</sup> examining the schizophrenia risk factor *FEZ1* showed that loss of *FEZ1* expression is associated with a loss of oligodendrocyte complexity in murine cells. Suggesting that specific deficits during the functional maturation of oligodendrocytes may be particularly relevant to risk for schizophrenia. Furthermore, reductions in *PLP1* and *SOX10* expression have been associated with bipolar disorder and schizophrenia<sup>311</sup> suggesting that the gene expression changes observed in this study may link to more fundamental changes associated with psychiatric pathology. Finally work done by Silva *et al.*<sup>317</sup> has shown that changes in DTI metrics (in a *CYFIP1* mouse model) similar to those seen in this study are associated with a loss of functional oligodendrocytes which is also linked with behavioral deficits. While further work is needed this study clearly demonstrates that deletion of the 1q.21 locus is associated with a loss of functional oligodendrocytes due to deficits in early development and functional maturation.

#### 4.4.3 Study limitations and future perspective

While the phenotypes identified in iPSC derived oligodendrocytes are supported by results from both human imaging and the 1q21.1 microdeletion mouse model; there is a lack of support for oligodendrocyte dysfunction associated with duplication of the 1q21.1 locus in the human imaging data. Furthermore, the initial study only used one 1q21.1 duplication cell line. However, given the consistency of control and 1q21.1 deletion cell lines across multiple differentiations and an increased number of cell lines it is reasonable to suggest these results constituent evidence that duplication of the 1q21.1 locus is associated with oligodendrocyte dysfunction. Further work using a large compliment of 1q21.1 duplication cell lines and closer examination of early developmental stages may further elucidate the precise deficits associated with this mutation in this cell type.

The limitations of a small sample size are also shared by the human imaging data which used only few 1q21.1 carriers and therefore this impacts the significance of the results. In particular the reduction in FA associated with 1q21.1 deletion is not significant after statistical correction using the Bonferroni method however due to the low sample size and high effect size observed in this case the result was included. However, increasing the number of participants in this study is critical to ascertain if this is a genuine effect. The low number of 1q21.1 participants in this study also means there is a risk of missing smaller changes in effect sizes. The data on DTI metrics of 1q21.1 carriers is also limited to the corpus callosum and therefore these results may not be indicative of changes across all white matter tracts. Many studies using DTI metrics similar to those presented in this study show different effects in different white matter tracts<sup>113</sup> therefore suggesting that the changes seen in the corpus callosum in this study may not be reflective of the entire brain. Further examination of this data for other white matter tracts and recruitment of a larger sample size of 1q21.1 carriers would allow further dissection of the effect of this mutation of white matter structure. However, recruitment of large cohorts of 1q21.1 carriers may introduce bias into future studies as healthy individuals carrying 1q21.1 mutations are unlikely to be screened for CNVs and therefore would be difficult to find and include. Ultimately given the clear associations between altered FA and schizophrenia<sup>113</sup> further work on larger cohorts must eliminate schizophrenia diagnosis as the only driver of the alterations seen in DTI metrics.

The use of the 1q21.1 microdeletion mouse model provides critical supporting evidence for a link between this mutation and dysfunction in oligodendrocyte production however this study was limited to examining the tissue after fixation and sectioning. Therefore, while the examination of oligodendrocyte number is possible the assessment of myelination was not possible in this study. Further work using this animal model may focus on imaging to determine the effect of this mutation on the structure of white matter and compare this to the human data or closer examination of myelin production using techniques such as electron microscopy. Examination of myelination in the 1q21.1 microdeletion mouse model in a similar fashion to that done by Silva *et al.*<sup>317</sup> would provide clear evidence that the loss of myelin seen in iPSC derived oligodendrocytes carrying 1q.21.1 deletions resulted in functional deficits.

The use of a developmental patterning approach to generate oligodendrocytes was selected for this study mainly due to the desire to examine the effect of 1q21.1 mutations

in a developmental context. However, to examine the effect of 1q21.1 mutations on the function of oligodendrocytes a direct differentiation approach may be more relevant. Using such an approach would negate the effects of 1q21.1 mutations on development and focus on the effects this mutation may have on oligodendrocyte function. However, while direct differentiation approaches for generating oligodendrocyte have been published<sup>337,338</sup>, the relatively low production of MBP+ cells remains concerning using this approach. Therefore, further development of a direction differentiation approach may be necessary before this can be successfully used to examine functional deficits of oligodendrocytes.

In a similar fashion to the development of protocols to generate neurons the inclusion of mitotic inhibitors may allow the synchronization of developmentally patterned differentiations resulting in a more homogenous and faster production of O4+ cells. While the use of cytarabine in this study would constitute mitotic inhibition<sup>357</sup>, this compound was applied during the later stages of differentiation after O4+ cells had exited the cell cycle to prevent any unwanted astrocyte growth. To this end further examination of the developmental patterning approach to oligodendrocyte differentiation may focus on reducing the production of astrocytes and other unwanted cell types produced by current methodologies.

Finally, while MBP+ oligodendrocytes were produced in this study the true function of these cells was not examined. There are two techniques which can be used to examine the myelination potential of oligodendrocytes. Oligodendrocytes can be plated only a substrate which mimics the diameter and organization of axons. Work has been done using electrospun fibres<sup>358</sup> however novel materials based on this concept have been and continue to be developed<sup>359-362</sup>. There is also limited evidence that 3D culture systems aid in the production of pre-myelinating oligodendrocytes<sup>363</sup>. Secondly human iPSC derived oligodendrocyte precursors can be transplanted in mouse models<sup>329</sup> which allows the closest approximation of human oligodendrocyte maturation. The use of either technique would allow further determination of the precise cellular deficits associated with 1q21.1 mutations. Overall this study provides clear evidence for an association between 1q.21.1 mutations and oligodendrocyte dysfunction however future work must focus on how these mutations effect the function of these cells and if it will impact the generation of myelin during development and disease.

## 5. Alginate Based Bio-inks modified with Key Extra-Cellular Matrix Proteins Provide a Substrate for Maintenance of Neuronal Cell Lineages in Defined 3D Cell Cultures

### 5.1 Introduction

#### 5.1.1 The lessons learnt from 2D cell culture and the emerging world of 3D cell culture

Simplistic 2D co-culture systems have already shown the importance of glia to the proper development of neurons for example simple experiments such as those done by Jones *et al*<sup>364</sup> clearly show the effect of astrocytes on neuronal complexity and further evidence has shown that astrocytes mediate the function of neuronal networks<sup>365</sup>. Furthermore, using a similar paradigm with microglia, Haenseler *et al*<sup>141</sup> have shown that the expression profile and functional response of microglia is altered in the presence of neurons. More advanced co-culture systems have been developed<sup>366</sup> which highlight the morphological differences observed between astrocytes cultured in 2D and those cultured in a 3D system. While these models are simplistic when compared to *in vivo* systems the profound effect that the combination of neurons and glia have on both cell types suggest that to understand the interplay between these two cell types more complex model systems are necessary.

One system which has been recently devised are organoids, this model offers a more complex view of neuronal development by allowing the system to develop in 3D. The development of cerebral organoids was first published in 2013<sup>367</sup> and highlighted the complex nature of the tissue which was developed. However, while the system produced structures similar to those seen *in vivo* due to the lack of patterning factors the products were highly heterogenous and could produce non-neuronal tissues<sup>368</sup>. Further protocols have been developed using some of the advances made in developmental patterning approaches for the generation of 2D neuronal systems resulting in the production of region specific brain organoids<sup>369,370</sup>. Recent advances in this field have shown that it is possible to generate both astrocytes and oligodendrocytes in these systems<sup>371</sup> however due to the non-neuronal origin of microglia, the introduction of patterning factors to drive more homogenous neuronal differentiation would preclude the induction of this cell type. While these approaches provide a critical insight into the development and maturation of neurons and glia, they are largely hampered by the heterogeneity introduced when systems can self-organize and pattern. Therefore, while these systems provide a much

more complex view of neuronal development, they remain highly heterogeneous and very costly therefore sharing some of the limitations of using animal models and remain unable to recapitulate the complete cellular environment of the developing brain.

An alternative approach to producing 3D models of neuronal systems which addresses the issues of heterogeneity and cost is to leverage 3D printing systems to allow greater control of the model produced. Bioprinting has been long established as a possible route for producing *in vivo* like tissue with a greater reproducibility than that seen in current iPSC-based cell models. This technique leverages advancements in technology, biochemical engineering and cell generation to generate complex models of specific tissues within the human body. The possible uses of these models are thought to be very broad including drug screening and cell replacement therapies. The major advantage of these systems over the organoid based paradigm is the control that can be exerted over the entire system. The ability to directly control the cell population in use and to control the relative proportions of these populations is a critical advantage of this technique. Furthermore, using a bioprinting system allows for the control of the acellular component of the model, allowing the introduction of complex neuronal specific compounds which aid in the recapitulation of *in vivo* like tissue. However, while these advantages are significant there is still a large amount of development needed before this technology can supersede other current approaches to complex 3D cell models.

#### 5.1.2 Current technology and techniques available for bioprinting

There are many methodologies used for bioprinting each with advantages and disadvantages. The use of technologies for bioprinting is largely limited by the negative effect the technique may have on cell viability and function. Therefore, bioprinting techniques must accommodate key aspects of cellular maintenance including; pH, temperature and pressure while also not introducing any inherently cytotoxic compounds. There are three main technologies used for bioprinting (Table 4.1) each of which has key advantages and disadvantages<sup>372</sup> which must be examined before a selection is made.

**Table 4.1: The three main techniques currently employed for 3D bioprinting.** Table adapted from Murphy and Atala<sup>405</sup>, and Mandrycky *et al.*<sup>372</sup>

	Bioprinting Technology		
	Inkjet	Extrusion	Laser assisted
Bioink Viscosity	3.5-12mPa/s	30->6x10 <sup>7</sup> mPa/s	1-300mPa/s
Crosslinking methods	Chemical or Light	Chemical, Light, Temperature or Sheer	Chemical or Light
Preparation time	Low	Low-Medium	Medium to High
Printing speed	Fast	Slow	Medium to Fast
Resolution	High	Moderate	High
Cell viability	>85%	40-80%	>95%
Cell Density	Low	High	Medium
Quality of Vertical Printing	Poor	Good	Fair
Printer Cost	Low	Medium	High

The original bioprinting technology was based on conventional inkjet printing<sup>373-375</sup> using either thermal or acoustic forces to eject drops of liquid from the printer head. Thermal inkjet printers use heat generated pressure to eject droplets<sup>376</sup> whereas acoustic inkjet printers use piezoelectric crystals to generate acoustic radiation forces<sup>374</sup> which have a similar effect. However, using thermal inkjet printing there is likely to be an effect on the cells based on the temperature and mechanical stress induced by the printing process. Similarly, using acoustic inkjet printing, the frequencies generated may damage or lyse cells. Therefore while the reported cell viability using these technologies is high (from 80-90%<sup>377,378</sup>) this technique may not be appropriate for all cell types.

While these bioprinters have been in use for many years they are limited by a number of factors the first being that they suffer from issues with clogging especially when trying to print high densities of cells<sup>379</sup> which are more physiologically relevant; also this can be effected by the settling effect caused by the low density of the bioinks<sup>380,381</sup>. Furthermore, the viscosity of the bioink is severely limited by this technology<sup>382</sup> limiting the compounds which can be used to generate these bioinks. To print using these systems the bioink must also be liquid which then requires the use of a crosslinker to solidify the bioink after bioprinting. Crosslinking can be done using chemicals, pH or ultraviolet light however many of these compounds or conditions are cytotoxic<sup>383</sup> and can be negatively affected by increasing cell density. Therefore, crosslinkers may have effects on cell viability beyond that of just the printing process and may limit the cell density which can be used.

This technology does however have several advantages perhaps chief among them the low cost and high printing speed achievable. These systems also allow a large amount of control over droplet size and ejection directionality allowing the printing of complex constructs with high resolution. Using open-pool nozzle-less ejection systems<sup>384</sup> can also reduce the amount of shear stress produced using these systems however the limitations on viscosity still remain<sup>385</sup>. This technology also allows the construction of more complex graduated structures by varying the densities and size of the drops used<sup>386</sup>. While advancements in this technique are still being made it has already been used to generate functional skin<sup>387</sup> and cartilage<sup>377</sup> *in situ* and layered cartilage using a combination of electrospinning and inkjet bioprinting<sup>388</sup>.

While inkjet bioprinting is a popular form of this technique perhaps the most popular and affordable method of bioprinting is extrusion based bioprinting. This technique uses robotically controlled extrusion most commonly through a standard needle which results in a continuous flow of bioink. This technique can be used to print small beads of material however due to the limitations in flow rate the resolution is significantly lower than alternative techniques. Due to the simplicity of this technique it is compatible with a large range of materials with a wide variety of mechanical properties<sup>389</sup>. Extrusion of the bioink can be driven by pressure exerted by either pneumatic or mechanical methods. Mechanical extrusion has thus far proved the most popular perhaps due to the relative simplicity of these mechanisms and the control that can be achieved over, flow rate. Using a screw based mechanical system also allows the printing of materials with significantly higher viscosities than other techniques and thus allows the deposition of much higher cell densities which are relevant to cell dense tissues.

In a similar fashion to inkjet bioprinting, extrusion based bioprinting also required the use of a crosslinker. Extrusion based bioprinting is often paired with thermally crosslinked bioinks which allow the layering of complex 3D constructs and this technique has been used in the development of scaffold less tissue spheroid bioprinting<sup>390</sup>. However, the major drawback with this technique is the effect on cell viability, most studies report a cell viability of 40-85% which is significantly lower than that reported using other bioprinting techniques<sup>391</sup>. Furthermore, the improvements in cell viability often come at the expense of printing speed and resolution therefore limiting the complexity of the construct which can be printed. While these limitations are significant this technique is still

widely used and has been successfully employed in the generation of aortic valves<sup>392</sup>, tumor models<sup>393</sup> and branched vasculature<sup>394</sup>.

Extrusion and inkjet bioprinting are based on simple techniques and are thus highly accessible whereas laser assisted bioprinting is significantly less common owing to the complex nature of these systems and the expense this incurs. These systems are based on laser-induced forward transfer<sup>395</sup> created by shining a laser onto an energy absorbing material which in turn creates a shockwave which can be used to transfer material from a donor material onto a second material. While the resolution of these systems is affected by many factors it is usually very high<sup>396</sup> and there are no issues with clogging as the system is nozzle free. While this system is not as versatile when it comes to bioink viscosity as extrusion-based systems it does allow a wider range than inkjet systems. However, similarly to inkjet systems, laser assisted systems have been shown to have a relatively small effect on cell viability<sup>397</sup>. Furthermore, laser assisted bioprinting can be done with high cell densities while maintaining high resolution printing<sup>398</sup> however the low overall flow rate does mean that printing using this technique is relatively slow<sup>399</sup>. While the high cell density is a powerful advantage of this system the fact that so-called aim and shoot systems can be used where each drop has a single cell in it make this system singularly powerful in terms of printing specific cell densities<sup>398</sup>.

Laser assisted bioprinting addresses many of the limitations of using extrusion or inkjet based bioprinting systems however it does introduce some limitations which are highly specific to this technique. The first is that the ribbon (which is the name given to the absorbing layer) is time consuming to create and may need to be specific to each cell type being printed therefore rendering the process less applicable to complex multi-cell tissues. Even though the resolution of constructs generated using this technique is high the ability to accurately position each individual drop/cell is limited. Additionally, the energy absorbing layer used to generate the force required for this type of bioprinting is transferred into the final construct, these materials are usually metallic and therefore may have significant effects on cell viability and cellular function. While avenues to eliminate this metallic transfer are being investigated, they further complicate the system and may introduce a further level of cost and specificity<sup>400,401</sup>. Despite key limitations, this technology has been used to print cellularized skin<sup>402</sup> however there remain concerns about the scalability of this approach for this application.

There are also several novel or alternative methods which can be used to bioprint or achieve a similar result. One of the more popular alternatives to the three classic approaches is the use of stereolithography. This technique is largely similar to laser assisted bioprinting however this technique uses light rather than a laser to solidify the bioink<sup>403,404</sup>. This has several advantages over the conventional bioprinting methodologies, as each layer of the construct is cured in one step by the projection of the construct onto the bioink therefore requiring movement in only one axis. Ultimately, this technique results in fast high-resolution printing with a high cell viability. However, this technique requires expensive equipment and compared to the majority of other techniques is procedurally complex and therefore is not as amenable to high throughput iterative techniques. In the end, choosing a bioprinting technology to use, is a balance between practical concerns and the capacities of the technology and while more complex technologies may have advantages for the majority of application the more readily available alternatives remain the obvious choices.

### 5.1.3 The role and importance of bioink

While the technique used for bioprinting may ultimately affect the ability to effectively print the desired construct, the bioink used will have an equally significant effect on the cell viability and ultimately the success of the bioprinting procedure. While the availability of bioinks is partially dictated by the bioprinting technique being used there remains vast array of compounds which can be used. There are 5 main features<sup>405</sup> of the bioinks which must be considered when selecting the appropriate compound to be used. These features are printability, biocompatibility, degradation, structure and biomimicry. The importance of each of these features also varies dependant on the desired final application and in the end different bioinks can be used to achieve the same result despite clearly different features.

Printability is simply the ability of the bioink to be printed effectively by the bioprinting technology being used and is largely dictated by the technique in use and the limitations associated with this. Biocompatibility is also a more complex feature referring to the effect the bioink has on the system and cells it is in contact with. This feature is particularly relevant when the construct is designed to be transplanted into a host. In this case the bioink must be able to facilitate the integration of the construct into the host system while not enlisting a large-scale immune response. While this feature is less relevant

to *in vitro* work it must not be discounted especially when using immune cells which may have a negative reaction to the bioink.

While biocompatibility is the effect of the bioink on systems beyond the bioprinted construct itself, biomimicry is the feature describing the effect of the bioink on the cells within the construct. For a large number of applications this is the most critical feature of the bioink selected, effective bioinks must allow the cells to interact within the matrix and with the matrix. Therefore, the bioink may have an effect on the properties of the cells including the differentiation, proliferation, size and shape. Furthermore, most cells are unable to grow free floating and therefore require some interaction with the bioink. Many currently available bioinks focus on this feature heavily, introducing specific ligands which cells can interact with allowing a more complex system to form and thus recapitulating part of the extra cellular matrix (ECM) which is naturally formed by cells *in vivo*. The interaction of the cells with the bioink may also effect the function of these cells as while the major constitutive components of the ECM are shared across many tissues, the ECM remains a highly tissue specific system and therefore the ability of cells to move and function within the bioink is likely to be intrinsically linked with the cells ability to interact with the ECM.

The final two features of bioinks, degradation and structure relate more to the physical properties of the bioink rather than the biology underlying its interaction with the cells. Degradation of the bioink is largely function dependant and is more critical if the construct is being used as an implant where the bioink may be designed to degrade into non-toxic components and be replaced by naturally secreted ECM. For most *in vitro* work bioinks are designed to be non-degradable over the relatively short periods of time needed for the work. The final feature is the structure of the bioink, which is particularly relevant in complex tissues where cells must communicate and migrate. The mechanical properties including stiffness and pore size are of particular relevance and many bioinks are developed which allow the modification of these factors while maintaining the biochemical properties of the bioink. Ultimately all these features must be considered to some extent when selecting an appropriate bioink.

Cell-laden hydrogels are currently the most popular family of bioinks, these compounds can be used in droplet, extrusion and laser based bioprinting systems. Hydrogels can be formed from a wide variety of natural compounds such as agarose, alginate, chitosan, collagen, gelatin, fibrin and hyaluronic acid. While more limited there are also hydrogels formed from synthetic compounds namely pluronic and polyethylene

glycol. Natural hydrogels (except agarose and alginate) have inherent bioreactivity with hydrogels formed using collagen and fibrin able to mimic the non-linear elasticity of human soft tissues<sup>406,407</sup>. While synthetic and some natural hydrogels do not have the inherent bioreactivity of their natural counterparts it is possible to functionalize these compounds by combining them with specific ligands which can interact with cells in the bioink<sup>408</sup>. Hydrogel based bioinks are printed as a polymer solution and then this solution is cross-linked to form a structurally stable construct. Cross-linking can be mechanical or chemical in nature, mechanical cross-linking may involve hydrophobic or ionic interactions and chemical cross-linking usually requires the formation of covalent bonds. Chemically cross-linked hydrogels are mechanically more stable than physically cross-linked hydrogels and evidence suggests<sup>409,410</sup> that this mechanical stability is particularly important to stem cells and their ability to differentiate. Current work is focussed on developing bioinks which are, more tissue specific and allow for fully functional long-term cell maintenance and growth which involves adapting complex ECM structures into bioprintable alternatives.

#### 5.1.4 Bioprinting as it relates to neuronal systems

While the technique and technology of bioprinting is not novel development of neuronal based bioinks has been limited when compared to bioinks for other tissues<sup>411</sup>. This may be due to the inherent complexity of the neuronal system, with a mix of motile and stationary cells both of which require complex interactions with the ECM. Early work on bioprinting neuronal systems used murine primary tissue as the cell source and a number of groups had success in bioprinting using this tissue. One of the first groups to report success in this field was Lee *et al*<sup>412</sup> who used a pH-sensitive collagen based bioink and then went on to develop a similar system which allowed growth factors (like VEGF) to be integrated into the bioink<sup>413</sup>. This work demonstrated the relevance of a more complex bioink and how this can affect cellular morphology and function. Other groups such as Lozano *et al*<sup>414</sup> have shown that high viability can be achieved using a functionalized form of a natural but non bio-reactive polymer. However again the cell type used for this work was primary murine cortical neurons which are significantly hardier than their human iPSC derived counterparts.

The development of hydrogels and bioprinting using neural stem cells and human derived cell types has largely focussed on the applications in cell replacement therapy. It has long been established that suitable hydrogels are of critical importance when

developing cell replacement therapies. As such groups have developed complex hydrogels which can be used in combination with NSCs as the basis for cell replacement therapies. Hsieh *et al*<sup>415</sup> used a biodegradable hydrogel in combination with murine NSCs to improve the recovery of zebrafish with CNS injuries. Whereas Chen *et al*<sup>416</sup> used a collagen based bioink crosslinked using heparin sulphate to improve recovery in a rat model of spinal cord injury. Work has also been carried out using similar 3D printed constructs as the basis to study nerve regeneration *in vitro* using human tissue. For example the system developed by Gu *et al*<sup>417</sup> used agarose and alginate based bioink functionalised by the addition of chitosan which allowed the differentiation of human cortical NSCs into both functional neurons and glia.

Despite the promise of this technology there has been limited advancement towards bioprinting systems which are capable of printing complex multi cell type neuronal constructs derived from human ESCs or iPSC. Proof of concept experiments carried out by Gu *et al*<sup>418</sup> demonstrated that human iPSC are capable of surviving bioprinting and maintaining their pluripotency however this work did not maintain the cells as bioprinted constructs but rather used this as a transient step to achieve the desired cell aggregate size. Similarly Lindborg *et al*<sup>419</sup> used a modified hydrogel to generate cerebral organoids, again demonstrating the viability of an aspect of the technique. Early work by Bouyer *et al*<sup>420</sup> using a highly complex bioprinting system has shown some success in bioprinting human ESC derived neurons and glia, however this technique is complex therefore negating many of the proposed advantages of 3D bioprinting. Furthermore, while cells are shown to survive and express some markers of neurons the morphology of these cells is questionable, and the functionality has not been assessed. In the end, when developing a bioprinting system for generating neuronal and glial 3D cultures it is critical to assess the success on multiple levels.

As this work is largely multidisciplinary most focus on one aspect of this process either developing a novel bioprinting system or use of the system with a focus on the cellular output. A large body of work has focused on developing complex bioink/bioprinting procedures which allow cells to survive with very little focus on the cellular health or function beyond simple live dead metrics. This has resulted in a large number of different bioinks and bioprinting technologies using simplified cell systems (like HEK cells) which are not the obvious goal of this technology. Therefore, to successfully demonstrate the viability of this approach and technology, development must be carried out using the desired final

cell types namely iPSC derived neurons and glia with a greater focus on the cellular component of this system.

#### 5.1.5 Current paradigms for the use of bioprinted 3D neuronal constructs

While it is obvious that 3D culture systems offer a more realistic view of neuronal development and neuronal systems, there are certain paradigms where current 3D models (i.e. organoids) are not appropriate. Perhaps the most obvious of these is as drug discovery platforms where 3D bioprinting is lauded as a paradigm shift in the process of drug development. Successful drug discovery platforms are highly scalable and must be highly replicable. Whereas organoids are highly variable and 2D culture systems do not have the complexity necessary 3D bioprinted constructs would allow for large scale drug screening. Bioprinting by design can print large numbers of identical constructs with known cell contributions, density and distribution therefore lending itself to this type of process. This would not only allow the assessment of multiple cell types responses to the drugs of interest but would also start to recapitulate some of the issues associated with drug delivery as the constructs would have a natural density and therefore some lack of permeability.

Bioprinting also allows the combination of multiple cell types which can be derived from separate lineages which is particularly important when developing models of the blood brain barrier and neuroinflammation. While all cells in the brain react and play a role in neuroinflammation it is microglia which are the largest mediators of this response<sup>421</sup>. While there has been some suggestion that microglia can be generated in un-patterned organoids<sup>368</sup> the fact that this cell type is naturally derived from outside the brain<sup>422</sup> necessitates the development of a more complex system. The ability of bioprinting to allow combination of disparate cell types while maintaining control over distribution and density is highly advantageous. Recent work from Park *et al.*<sup>423</sup> used a microfluidic platform to generate a human triculture system combining astrocytes, neurons and microglia. This system recapitulated the critical effect microglia have in the pathogenesis of Alzheimer's disease and critically allows the dissection of neuronal-gial interaction within this pathological setting. However, this system was limited as it relied on the recruitment of microglia from outside the construct and therefore was unable to regulate the density of these cells. Bioprinting offers an attractive paradigm for investigating the role of

neuroinflammation in complex pathologies and as this system can be highly controlled and regulated it may allow elucidation of more subtle interactions.

The second model where bioprinting is of particular interest is in modelling the blood brain barrier. Degradation of the BBB is known to be particularly relevant in injury and due to the complex nature of this structure most research in this field focusses on the more complex and costly animal models. As Potjewyd *et al.*<sup>424</sup> examine in their review development of a bioprinting platform used to generate neurovascular units would allow the examination of how cells interact within these complex structures and how these interactions are altered in conditions associated with neurovascular dysfunction. Unlike the neuroinflammation model this system would not only benefit from the ability of combining cells for disparate lineages but would also benefit from the ability to modify the mechanical properties of the construct. If successful, this paradigm would allow investigation of a complex neuronal structure which is not highly amenable to *in vitro* analysis. Whether it be modelling the BBB, recapitulating neuroinflammation or drug screening bioprinting offers new possibilities for understanding the complexities of neural systems while still maintaining the necessarily reductionist approach needed for biological research.

## 5.2 Chapter 3: Hypothesis and aims

My hypothesis is that alginate based bioink can be modified to allow the survival of neurons and astrocytes in co-culture. To this end the aims of this chapter are to demonstrate the feasibility of using bioprinting as an alternative for generating complex 3D neuronal cultures. Alginate based bioinks will be used as a basis for bioprinting and will be modified and combined with various extra cellular matrix components to develop a neuronal bioink which can be using with iPSC derived neurons and glia. Neurons generated by developmental patterning will be combined with human iPSC derived astrocytes to generated 3D co-cultures which provide a proof of principle for the use of 3D bioprinting neuronal systems.

### 5.3 Methods

Contained in this section are methods specific to the bioprinting of neurons and astrocytes using alginate based bioinks.

#### 5.3.1 Neuronal differentiation

The protocol for generation of cortical excitatory neurons is based on the dual SMAD inhibition protocol published by Chambers *et al.*<sup>145</sup> and is a minor modification of neuronal differentiation presented in section 2.2.

##### Media formations

**N2B27 media:** was comprised of 2/3 DMEM/F12 and 1/3 Neurobasal supplemented with N2 supplement (1:150) and B27 supplement (1:150) either with (denoted by +) or without vitamin A (denoted by -) depending on the stage of differentiation. This media was further supplemented with  $\beta$ -mercaptoethanol (50  $\mu$ M) and a cocktail of antibiotics and antimycotics (1:100).

##### Generation of immature neurons

The generation of immature neurons followed the same protocol as the generation of NPCs detailed in section 2.2.2. After 20 days of differentiation cells were incubated with Y-27632 at 10  $\mu$ M in N2B27- for 1 hour and the media was collected. Cells were then passaged using versene solution onto poly-D-lysine (10  $\mu$ g/mL) and laminin (20  $\mu$ g/mL) coated plates at a 1:3 ration in conditioned media. The media was replaced with N2B27+ after 2 days and then half the media was replaced every 2 days until day 30 of differentiation at which point cells were used for bioprinting

#### 5.3.2 Astrocyte differentiation

All astrocytes were generated by Tanya Singh. The protocol for generation of astrocytes is based on work by Tcw *et al.*<sup>425</sup> with minor modifications.

##### Media formations

**N2B27 media:** was comprised of 2/3 DMEM/F12 and 1/3 Neurobasal supplemented with N2 supplement (1:150) and B27 supplement without vitamin A (1:150). This media was further supplemented with  $\beta$ -mercaptoethanol (50  $\mu$ M) and a cocktail of antibiotics and antimycotics (1:100).

**Astrocyte Media:** was comprised of DMEM/F12 supplemented with N2 supplement (1:100) and B27 supplement without vitamin A (1:50), NEAA (1x), alanyl-glutamine (2 mM), FBS (2%) and Astrocyte Growth Supplement (1:100, Caltag Medsystems). This media was further supplemented with  $\beta$ -mercaptoethanol (50  $\mu$ M) and a cocktail of antibiotics and antimycotics (1x).

#### Generation of astrocytes

Neuronal precursors were generated as detailed in section 2.2.2. Cells were passaged using Accutase™ as detailed previously (see section 2.2.3) at a ratio of (1:4) onto fibronectin (10  $\mu$ g/mL). The media was then changed to Astrocyte differentiation media (ADM) and cells were left to adhere and recover for 48 hours. Half the media was replaced every 48 hours with fresh ADM until day 30 of differentiation. Cells were then maintained at between 30-90% confluency. To passage astrocytes were washed and then treated with TrypLE™ Express (Gibco™) for 5 minutes. TrypLE™ Express was inactivated by diluting 1:5 in DMEM/F12 and cells were collected by centrifugation (200r.c.f. for 5 minutes) cells were then re-plated on untreated TC culture ware at a ratio greater than 1:3.

#### 5.3.3 Glutamate Assay

The glutamate assay was performed by Tanya Singh using a kit from Abcam according to the manufacturer recommended protocol. Briefly  $2 \times 10^6$  astrocytes were dissociated using TrypLE™ Express for 5 minutes and then collected by centrifugation (200r.c.f. for 5 minutes). Cells were resuspended in 100  $\mu$ L assay buffer and then incubated on ice for 15-30 minutes. Debris was removed by centrifugation at top speed in a microcentrifuge for 2-5 minutes at 4°C. The assay was performed with 10  $\mu$ L of samples diluted in 50  $\mu$ L of assay buffer. Reaction mix comprised of assay buffer, developer and enzyme mix was added and then incubated at 37°C in the dark for 30 minutes. Colour change was measure at a wavelength of 450 nm on a microplate reader. Samples were compared to standards ranging from 0 to 10 nM Glutamate.

#### 5.3.4 Viral generation

##### Production of plasmids for viral production

Plasmids were all commercially available and were grown on LB agar plates supplemented with the required antibiotics and then small-scale cultures before being using to generate glycerol stocks by combining turbid cultures with 50% glycerol (Sigma-aldrich) at a 1:1 ratio.

To recover bacteria from glycerol stocks the stocks were removed from the -80°C freezers and maintained on dry ice. The surface of the stocks was scratched, and the resulting small volume of culture was used to streak onto a new LB agar plate containing the required antibiotic. The plates were incubated at 37°C overnight and a single colony was picked and used to seed a small-scale (5mL) culture which was incubated in a shaking incubator (shaking at >180rpm) at 37°C for a minimum of 4 hours.

This small culture was then used to seed a large (250mL) culture which was grown under identical conditions overnight. The large culture was then aliquoted into 50mL tubes and centrifuged (at 1,800r.c.f.) for 40 minutes. The supernatant was removed, and the plasmid was isolated from the pellets using a PureYield™ maxiprep kit (Promega) with minor modifications. The pellets were re-suspended in a total of 4mL resuspension solution and after washing the membrane was dried for a maximum of 2 minutes. Once purified plasmids were sized using gel electrophoresis to confirm against manufacturers information and were stored at -20°C.

##### Production of lentivirus

Lentivirus was produced using human embryonic kidney cells (HEK293) in accordance with genetically modified organism project number GM130/699. HEK293 cells were maintained in advanced DMEM/F12 (Gibco™) supplemented with 7% FBS and 2mM Alanyl-glutamine. For passaging cells were washed once with DPBS; then dissociated using TrypLE™ Express (incubated for 3-5 minutes) which was inactivated by diluting 1:5 in DMEM/12 and removed by centrifugation (at 200r.c.f.) for 5 minutes. Cells were plated at a density of 15,000 to 20,000 cells per cm<sup>2</sup> and were used to generate virus when the confluency reached between 80% and 90%.

Cells were transfected with the three plasmids necessary to make 2<sup>nd</sup> generation lentivirus (Pax2, VsVg and transfer plasmid) using TransIT Virusgen (Mirus); the mixture of plasmids was a 2:3:5 ratio of each plasmid respectively (Pax2, VsVg and transfer plasmid)

with 3  $\mu$ L of TransIT virusgen used per 1  $\mu$ g of plasmids. The transfection complexes were made in Opti-MEM media (Gibco™) and incubated for 10-20 minutes before adding directly onto the HEK293 cells distributing the mixture across multiple sites to prevent unwanted cell death. Cells were then left for 24 hours before the media was discarded and replaced with fresh media and then cells were left for a further 24 hours. Media was then collected from cells and filtered through a 0.22  $\mu$ m PES membrane (Star Lab) and was cooled to 4°C before it was combined with lenti-X concentrator (Takara) at a ratio of 1:3 (concentrator: viral supernatant).

The solution was mixed thoroughly by inversion and was incubated at 4°C for between 1 and 24 hours. The solution was centrifuged at 1,500r.c.f. at 4°C for 45 minutes and the supernatant was removed. The pellet was resuspended in 1/100<sup>th</sup> of the original media used to produce the virus using Opti-MEM media. Virus was then aliquot into PCR tubes with 20  $\mu$ L of virus added to each tube and then tubes were double bagged and stored at -80°C.

#### Testing virus

Viral supernatant was tested for the presence of lentiviral particles using the lenti-X GoStix system (Takara) which shows a positive result in the presence of large amounts of lentiviral p24. If the test appeared negative, then the viral supernatant was discarded and fresh HEK293 cells were transfected. Where appropriate HEK293 cells used to produce lentivirus were maintained after viral supernatant was removed and tested for the presence of the transfer plasmid using either presence of fluorescence or an antibiotic selection when transfer plasmid had such markers. Again, if the fluorescent marker was not observable or the cells were not resistant to the antibiotic then the supernatant was discarded, and the process repeated.

#### 5.3.5 Plasmids

**pCW57-GFP-2A-MCS** (Plasmid #71783) – 3<sup>rd</sup> generation lentiviral vector with a multi-clonal site combined with turbo GFP using a P2A self-cleaving linker and all under the control of a tetracycline responsive promotor. Also contains constitutively expressed puromycin resistance and tetracycline response element. pCW57-GFP-2A-MCS was a gift from Adam Karpf (Addgene plasmid # 71783; <http://n2t.net/addgene:71783>; RRID: Addgene\_71783)

**pCW57-RFP-P2A-MCS** (Plasmid #78933) – 3<sup>rd</sup> generation lentiviral vector with a multi-clonal site combined with turbo RFP using a P2A self-cleaving linker and all under the control of a tetracycline responsive promoter. Also contains constitutively expressed puromycin resistance and tetracycline response element. pCW57-RFP-P2A-MCS was a gift from Adam Karpf (Addgene plasmid # 78933; <http://n2t.net/addgene:78933>; RRID: Addgene\_78933)

**psPAX2** (Plasmid #12260) – 2<sup>nd</sup> generation lentiviral packaging plasmid for use with both 2<sup>nd</sup> and 3<sup>rd</sup> generation lentiviral vectors. psPAX2 was a gift from Didier Trono (Addgene plasmid # 12260; <http://n2t.net/addgene:12260>; RRID: Addgene\_12260)

**pMD2.g** (Plasmid #12259) – plasmid expressing the VSV-G envelope protein for production of 2<sup>nd</sup> or 3<sup>rd</sup> generation lentivirus. pMD2.G was a gift from Didier Trono (Addgene plasmid # 12259; <http://n2t.net/addgene:12259>; RRID: Addgene\_12259)

### 5.3.6 Bioprinting

#### Cell preparation and dissociation

Bioprinting was carried out using neurons at day 30 of differentiation and astrocytes which had been passaged as astrocytes a minimum of 3 times. Where appropriate these cells were generated from stable GFP or RFP expressing lines. Neurons were pre-incubated with RevitaCell™ supplement for 1 hour before dissociation with Accutase™ as previously described (see section 2.2.3). Astrocytes were dissociated using TrypLE™ Express in a similar fashion to Accutase™ dissociation using a 2-4-minute incubation. Cells were resuspended in the relevant media and the number of cells was quantified. Cells were again centrifuged and resuspended at a density of 10<sup>6</sup> immature neurons and 2.5x10<sup>5</sup> astrocytes per 1 mL of media.

#### Preparing bioink

A 26% w/w solution of pluronic® F-127 (Sigma-Aldrich) in PBS was prepared and then autoclaved. After autoclaving the pluronic solution was mixed in sterile conditions using a pipet tip until the solution appeared homogeneous. Once prepared the Pluronic® F-127 solution was maintained at 4°C before use. Sodium alginate (Sigma) was sterilised by

suspending in a large volume of 99.9% ethanol (VWR) and spreading on 15cm petri dishes and left for the ethanol to evaporate under UV light in sterile conditions. To make the final bioink sodium alginate (Sigma) was added to the Pluronic® F-127 solution under sterile conditions finishing with a 6% w/w alginate and a 13% w/w Pluronic® F-127 solution with the remaining liquid made up from DMEM/F12.

When available the bioink was then mixed in a dual asymmetric centrifuge to incorporate the alginate into the Pluronic® F-127 solution. When a dual asymmetric centrifuge was unavailable the solution was mixed by hand using a pipet tip. However due to the large amount of air this incorporates into the solution the bioink was decanted into a 50mL centrifuge tube and was centrifuged in a fixed angle rotor at top speed for 10 minutes. When testing the addition of extra cellular matrix components into the bioink powdered components (Chitosan, Collagen IV and Hyaluronic acid all from Sigma-Aldrich) and Matrigel (Corning) were added at the same point as alginate at a 2% w/w with functionalised alginate (GRGDSP-Alginate, Dupont™) the lone exception which was used at the same concentration but was used to replace the same amount of conventional alginate. Liquid ECM components were also added prior to mixing using 500 ng/mL laminin, 15 µg/mL fibronectin, 100 ng/mL Tenascin R (R&D Systems) and 20 ng/mL FGF.

### Bioprinting

Cells were added to the bioink (100 µL of cell suspension per 1mL bioink) and mixed in using a dual asymmetric centrifuge when available and if unavailable using a pipet tip. Bioink was loaded into a 1.5 mL syringe (VWR) using a small spatula and the bioink was printed by extrusion using a 1.5 mL syringe with a 16-gauge needle (VWR) on a MendelMax3 printing system (Maker's tool works) adapted for 3D bioprinting or by hand. Constructs were 1.5cm<sup>2</sup> squares with a thickness of around 5mm. The printing surface was heated to 37°C and the constructs were cross linked by the addition of either calcium or magnesium chloride. Once the calcium or magnesium chloride was removed the constructs were resuspended in N2B27+ and were maintained at 37°C and 5% CO<sub>2</sub>.

#### 5.3.7 Live/dead Imaging

To assess viability live constructs or cells were stained with Calcein-AM (Sigma-Aldrich) at a final concentration of 0.1 µM and dead cells were stained with propidium iodide (Sigma-Aldrich) at a final concentration of 1 µg/mL. Live and dead stains were

removed after a minimum of 20 minutes and constructs or cells were resuspended in appropriate media. Constructs or cells were then imaged on a Leica DMI600B inverted microscope using z-stacks with a maximum of 50 images per stack spanning a maximum of 2 mm. For each construct 3 random fields were imaged and for each condition a minimum of 3 and a maximum of 6 constructs were imaged. The z-stacks were then compressed using the maximum intensity method in ImageJ<sup>163</sup>. The quantification of live and dead cells was carried out using CellProfiler<sup>162</sup>.

#### 5.3.8 Statistical analysis

Statistical analysis was carried out using GraphPad prism version 7.00 and 8.00 for Windows (GraphPad Software; La Jolla, CA, USA, Available from [www.graphpad.com](http://www.graphpad.com)). All technical replicates were averaged before statistical analysis and specific statistical tests used for each data analysis are detailed in figure legends. In all cases analysis was carried out using only 1 control iPSC cell line from the same differentiation therefore n numbers listed in figure legends are the number of separate constructs or wells used for each analysis.

## 5.4 Results

### 5.4.1 Functional neurons and astrocytes can be generated from iPSC

As previously demonstrated (see section 3) neurons can be generated from iPSC using a developmental patterning protocol which produced neurons with characteristic morphology. These cultures transition from predominantly NPCs to predominantly neurons from day 20 to day 50 of differentiation and are capable of forming functional neuronal networks as measured using MEAs (Figure 5.1). For the purposes of this study neurons were bioprinted after 30 days of differentiation when the population expresses high levels of DCX and therefore most cells are committed to a neuronal fate but remain migratory and therefore, likely to survive the stress of bioprinting better than more mature neurons.

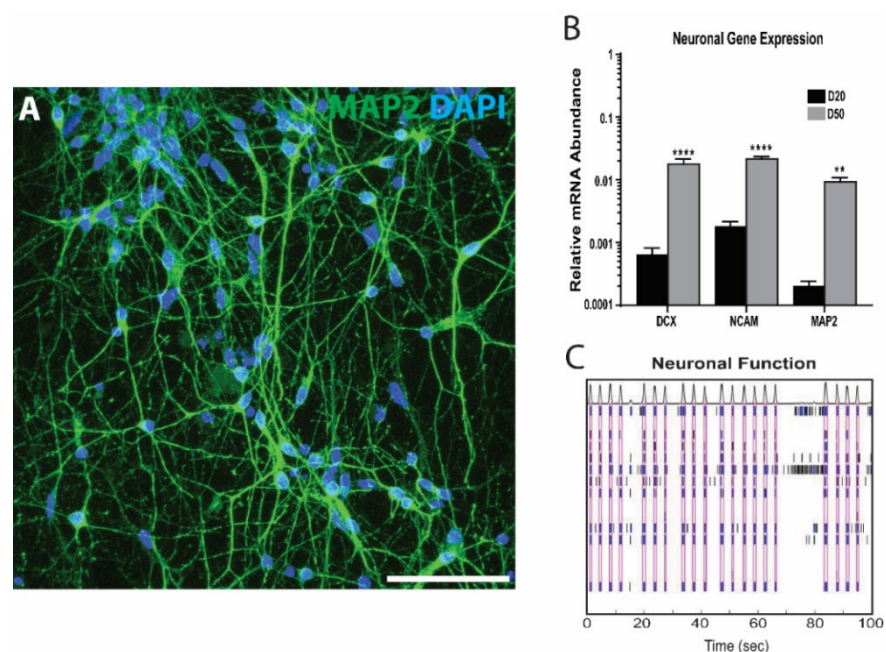


**Figure 5.1: Generation and assessment of neurons generated from control iPSCs.** **A** MAP2 staining of day 50 neuronal cultures, scale bar = 100  $\mu\text{m}$ . **B** The expression of *DCX*, *NCAM* and *MAP2* mRNA at day 20 and 50 of neuronal differentiation. The time point samples were taken had a significant effect on expression of the three markers ( $F_{1,30}=98.4$ ;  $P<0.0001$ ; Control  $N=2$  and  $n=3$ ) with all three markers showing an increase in expression from day 20 to day 50. Relative mRNA abundance was calculated compared to *GAPDH* expression. Data sets were analyzed by two-way ANOVA with post hoc comparisons comparing to day 20 samples. Stars above points represent Sidak-corrected post hoc tests. All data presented as means  $\pm$  SEM \*\* $P<0.01$ ; \*\*\*\* $P<0.0001$  vs. day 20. **C** Representations of synchronicity within day 100 neuronal cultures, purple boxes denote synchronized network activity (when 3 or more electrode are active within the same time frame) and high of peaks in the above histogram represents this synchronized network activity as a function of total activity.

Astrocytes were produced using a similar developmental patterning approach beginning with NPCs generated using dual SMAD inhibition and then were converted to astrocytes using a simplified media containing FBS. The astrocytes produced from this protocol show characteristic morphology with large flat cell bodies in 2D culture. Furthermore, these cells express astrocytic markers such as S100 $\beta$  and VIMENTIN (Figure 5.2). Finally, these cells are capable of performing key astrocytic functions such as removing glutamate from the media which is a critical function of astrocytes specifically relevant to the neurons produced under this protocol. Astrocytes were used for bioprinting after 40 days of differentiation to prevent any contamination from remaining NPCs and as astrocytes are a hardier cell type than neurons these cells are more likely to survive the stress of bioprinting.

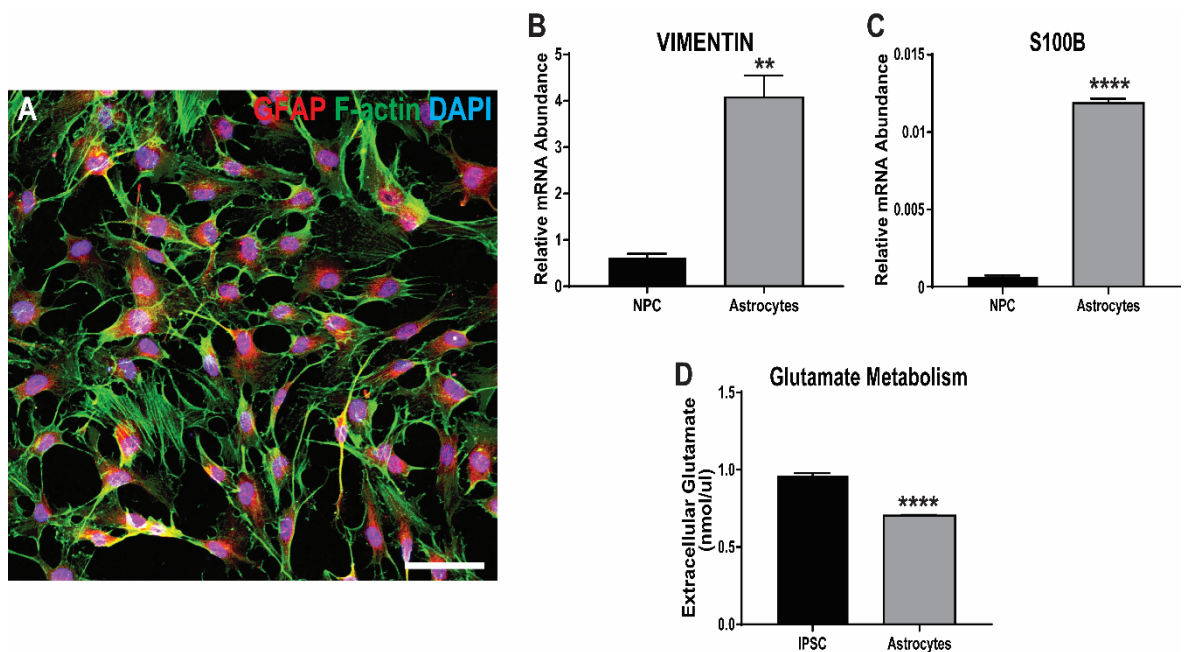


**Figure 5.2: Generation and assessment of astrocytes generated from control iPSCs.** **A** GFAP and F-actin staining of astrocytes after 30 days of differentiation. Scale bar = 100  $\mu$ m. **B, C** Gene expression of VIMENTIN and S100 $\beta$  in NPCs compared to astrocytes. Relative mRNA abundance was calculated compared to *GAPDH* expression. **D** Levels of extracellular glutamate after incubation with either iPSC or astrocytes. Data sets were analyzed by students T-Test, all data presented as means  $\pm$  SEM \*\* $P$ <0.01; \*\*\*\* $P$ <0.0001, Control  $N=2$  and  $n\geq 3$ .

#### 5.4.2 Key components of the bioprinting process show no inherent cytotoxicity

Alginate based bioink was selected for its simplicity and low-cost lending itself to high throughput systems. However, using this bioink also had the advantage of offering a stable and inert platform which could be adapted towards the cells which were being printed. The bioink used in this study was originally developed by Armstrong *et al.*<sup>426</sup> using Pluronic F-127 to stabilize the structure of alginate at 37°C therefore allowing efficient crosslinking. The bioink could be crosslinked using either CaCl<sub>2</sub> or MgCl<sub>2</sub> at 50mM or 25mM respectively. To assess the effect of bioink, day 30 neuronal differentiations were dissociated and re-plated on to fibronectin coated culture ware suspended in bioink. Media was added to the bioink after 10 minutes however the bioink was not crosslinked, and cells were allowed to settle and adhere to the plasticware. After 24 hours the media and bioink was removed and the cultures were washed before the cell viability was assessed. There was a significant increase in cell viability in cultures when cells were plated in bioink compared to those when cells were simple re-plated after passaging with no contact with bioink (Figure 5.3). This confirms that the presence of bioink is not cytotoxic and may protect cells from the stress of passaging.

Given that constructs must be crosslinked after bioprinting the effect of either CaCl<sub>2</sub> or MgCl<sub>2</sub> on 2D day 30 neuronal cultures was also assessed. In this case both salts were added at a low concentration and the desired concentration for crosslinking to assess if the effects on cell viability were concentration dependant. Salts were added in water for 10 minutes (the minimum time needed for crosslinking alginate based bioinks) and then removed, cultures were washed using DMEM/F12; fresh media was added, and cultures were allowed to recover for 24 hours. A low concentration of MgCl<sub>2</sub> had no significant effect on cell viability however the higher concentration necessary for crosslinking had a negative effect on cell viability reducing cell viability by around 30% (Figure 5.3). In the case of CaCl<sub>2</sub> a low concentration had a negative effect on cell viability, however the higher concentration of CaCl<sub>2</sub> necessary for cross linking had no significant effect on cell viability. Therefore, these results indicate that the bioink proposed for this work is not inherently cytotoxic and that crosslinking should be carried out using CaCl<sub>2</sub> as this had no significant effect on cell viability.

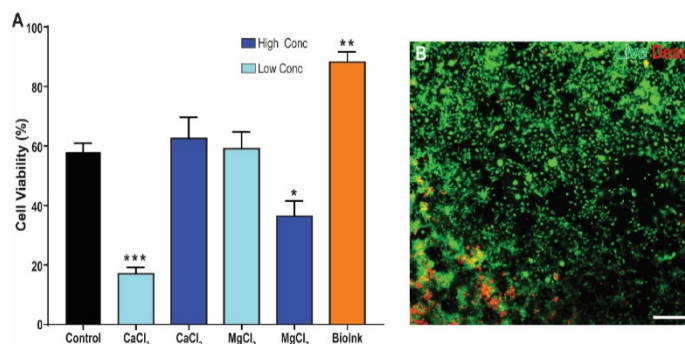


**Figure 5.3: Testing the cytotoxicity of alginate based bioink and crosslinking salts.** **A** Cell viability measured by exposing day 30 neuronal cultures to indicated compounds and then allowing 24 hours recovery. Crosslinking salts were applied at a low (light blue) and a high (dark blue) concentration in each case the high concentration is necessary for crosslinking which is 50nM or 25nM for CaCl<sub>2</sub> or MgCl<sub>2</sub> respectively. Lower concentrations are 1/10<sup>th</sup> the high concentrations. Data sets were analyzed by one way ANOVA, all data presented as means ± SEM stars represent significance compared to control (with Dunnett's multiple comparisons testing applied) \*P<0.05; \*\*P<0.01; \*\*\*P<0.001, n≥3. **B** Example image of day 30 neuronal cultures exposed to alginate based bioink during passaging after 24 hours recovery. Live cells are marked in green (by Calcein-AM) and dead cells are marked red (by propidium iodide). Scale bar = 100 μm.

#### 5.4.2 Bioprinting neurons using un-modified alginate based bioink results in low cell viability

Bioprinting was carried out using an extrusion based bioprinter; this methodology was selected due to its wide accessibility and low cost therefore lending itself to use as a high throughput methodology. To test the effect of bioprinting on day 30 neuronal cultures, unmodified cultures were dissociated and added to the bioink at a 1x10<sup>6</sup> cell/mL density. Constructs were then printed using a 16-gauge needle and crosslinking was performed using 50mM CaCl<sub>2</sub>. Constructs remained stable in neuronal media for 24 hours after which cell viability was assessed. Bioprinting in this manner resulting in a very low cell viability with an average viability of around 5.5% (Figure 5.4). Given the lack of effect of bioink on cell viability the first consideration for the cause of this loss of viability was the procedure involved in bioprinting.

There are four key areas of bioprinting procedure which are most likely to affect cell viability. The first is mixing the cells into the bioink, originally this was carried out using a dual asymmetric centrifuge as this results in a homogeneous mix of cells and bioink. However, this type of centrifugation results in complex forces being applied to the cells which may have negative effects on cell viability. Therefore, cells were manually mixed into the bioink avoiding any stress which may be conferred by the centrifugation; however, this may result in an uneven mixture of cells and does incorporate more air into the bioink.

The second consideration is the speed of transition from dissociation to bioprinting as both activities constitute significant stress on the cells. Therefore, to prevent a long

period of constant stress and to allow cells to recover from the stress of dissociation and introduction to the bioink a delay of 10 minutes was introduced between mixing cells into the bioink and bioprinting. As previous experiments showed an increase of cell viability when cells were incubated in bioink for 10 minutes this was unlikely to have negative effects on cell viability.

The third consideration of procedural effects from bioprinting on cell viability is the process of bioprinting itself. As previously discussed, extrusion based bioprinting methodology are likely to have a negative effect on cell viability however viabilities of >60% are regularly reported. The cause of this loss of cell viability is likely the sheer forces applied when cell pass through the needle. To ameliorate this effect bioink was distributed in cell culture ware using a spatula rather than bioprinting through a needle to remove any sheer force introduced by the needle.

Finally, the automation of the bioprinting process required bioink to be under constant pressure to allow for the smooth stream of bioink to be generated. However, this may also have negative effects on cell viability. To address this concern bioprinting was carried out manually simply by extruding ink through a needle using manual force allowing pressure to only be applied during printing and released when not actively printing. While this change may have a positive effect on cell viability it may have an inverse effect resulting in uneven or excess pressure on the bioink resulting in increased sheer force therefore the effect of this change was assessed separately from all other changes (which would likely have a positive effect if any).

The combination of manually mixing cells into the bioink, delaying bioprinting and not bioprinting through a needle was assessed for effects on cell viability after cross linking and a 24-hour recovery period. This combination resulted in a minor but not significant increase in cell viability (Figure 5.4) therefore suggesting that the low cell viability is not due to the stress of combining cells and bioink or the bioprinting procedure itself. Finally, manually bioprinting through a needle also had no significant effect on cell viability (Figure 5.4) therefore further confirming that the bioprinting procedure had minimal effect on cell viability.

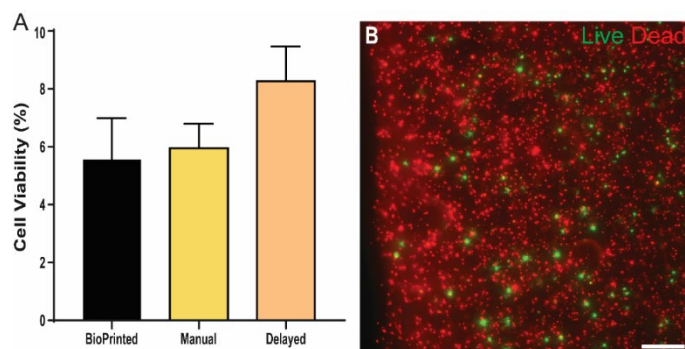


**Figure 5.4: Testing the effect of bioprinting and procedural modifications on cell viability.** **A** Quantification of cell viability after 24 hours. Manual refers to bioprinting manually and delayed refers to a combination of manually mixing cells into the bioink; delaying bioprinting and not printing through a needle. All bioprinting was performed using day 30 neuronal cultures. Data sets were analyzed by Students T-Test, all data presented as means  $\pm$  SEM,  $n \geq 3$ . **B** Representative image of cells after bioprinting with no procedural modifications. Live cells are marked in green (by Calcein-AM) and dead cells are marked red (by propidium iodide). Scale bar = 100  $\mu$ m.

#### 5.4.3 Addition of neuronal extra cellular matrix compounds significantly increases neuronal viability

The lack of positive effects from procedural modification to the bioprinting process suggested that the low cell viability may be related more to the interactions between cells and the bioink; as when cells were able to adhere to a basement membrane the cell viability was high. Under this paradigm the low cell viability was a likely result of the lack of interaction between the bioink and the cells due to the inert and unreactive nature of the alginate structure. On the other hand, the extra cellular matrix of neuronal tissues is highly complex with many compounds functioning as both mechanical and biochemical support systems. Both laminin and fibronectin are used as basement membranes to grow NPCs and early immature neurons and both compounds are known to support neuronal survival. Therefore, fibronectin and laminin were added individually and in combination to the cells before they were added to the bioink, this resulted in these compounds having effect like media supplements as neither compound is known to directly interact with the alginate bioink structure. Therefore, while these compounds are present in the bioink they provide no structural support to the cells. The addition of either laminin alone or a combination of laminin and fibronectin but not fibronectin alone had minor but significant positive effects on neuronal cell viability. These results indicate that addition of ECM components to the bioink may result in significantly improved cell viabilities.

While laminin and fibronectin are present and important in the ECM of neuronal nests these compounds do not form the majority of this ECM and therefore may not be the ideal compounds to recapitulate these interactions in culture. Therefore 5 other ECM

components were selected each of which is either found in high abundance in the ECM of neuronal nests or is known to have neurotrophic effects and therefore may offer both structural support and increase neuronal survival. These compounds were tested against the addition of Matrigel to the bioink over the course of 48 hours to allow for complete recovery from the bioprinting procedure. Matrigel is a complex mixture of proteins which is known to provide structural support to a large number of cell types in both 2D and 3D cultures systems. However due to the variation in Matrigel composition it is not ideal as a bioink component but provides a control for which the effect of addition of other compounds may be judged.

The addition of chitosan, collagen IV or tenascin R resulted in a significant increase in cell viability. Introduction of any of these compounds into the bioink resulted in a similar increase in cell viability to that seen with addition of Matrigel therefore suggesting that the addition of these compounds is providing some level of structural support. However, the addition of hyaluronic acid produced a much larger increase in cell viability resulting in a cell viability around 40%. Hyaluronic acid has been used in other bioprinting systems and is known to polymerise and therefore may form a larger structure within the bioink allowing greater interaction with and between cells. Furthermore, the addition of hyaluronic acid increased the viscosity of the bioink which may also have beneficial effects on cell viability.

These results strongly suggest that increasing the interaction between the cells and the bioink is likely to increase cell viability; as cells are unable to interact with the alginate bioink and therefore are in a facsimile of suspension culture rather than in a true 3D culture system. Therefore, replacing some of the alginate used in these bioinks with an alginate functionalised with an Arginylglycylaspartic acid (RGD) peptide was also tested for effects on cell viability along with the other ECM compounds. The functionalised alginate had a similar effect to the hyaluronic acid resulting in a large increase in cell viability. These results further confirm that adding a structural component to the bioink which allows for cell adhesion results in significant increases in cell viability.

Finally, the addition of the general growth factor FGF2 was tested for an effect on cell viability. This compound is widely used in 2D and 3D culture to promote cell survival and proliferation. Addition of FGF alone had significant but minor beneficial effects on cell viability. Therefore, as addition of FGF is unlikely to interfere with the action of either hyaluronic acid or RGD-alginate this compound was also added to both bioinks. Testing either alginate/hyaluronic acid or alginate/RGD-alginate bioinks combined with cells

suspended in laminin, fibronectin and FGF2 resulted in significantly higher cell viabilities than controls (alginate bioink alone), after both 24 and 72 hours. However, the hyaluronic acid bioink preserved a similar level of cell viability to that seen in similar experiments at 24 and 48 hours suggesting that this combination of ECM components and growth factors is the most beneficial for neuronal cell survival.

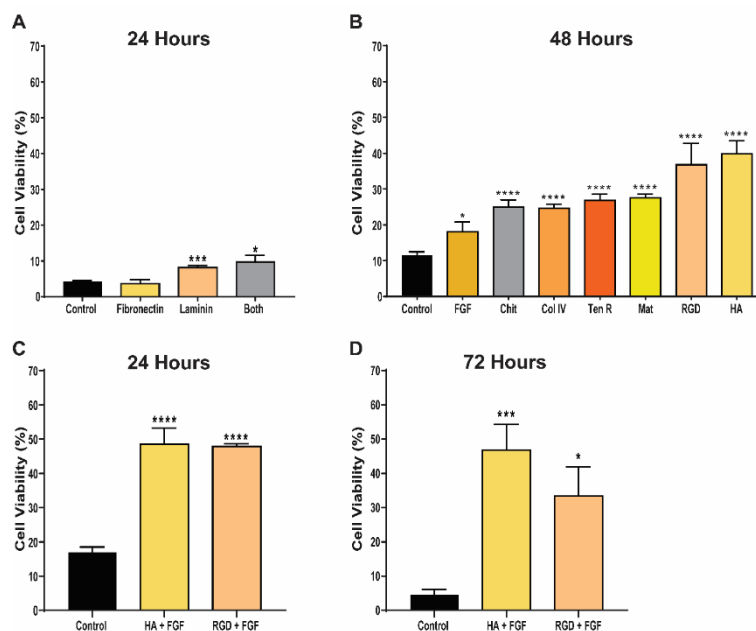


**Figure 5.5: The effect of adding neuronal ECM components into bioinks.** **A** Quantification of cell viability 24 hours after bioprinting with the addition of ECM components (laminin, fibronectin or a combination of both laminin and fibronectin). **B** Quantification of cell viability 48 hours after bioprinting with the addition of ECM components. All condition incorporated both fibronectin and laminin. **C** Quantification of cell viability 24 hours after bioprinting with the addition of ECM components. All condition incorporated fibronectin, FGF and laminin. **D** Quantification of cell viability 72 hours after bioprinting with the addition of ECM components. All condition incorporated fibronectin, FGF and laminin. All bioprinting was performed using day 30 neuronal cultures. Chit = Chitosan, Col IV = Collagen IV, Ten R = Tenascin R, Mat = Matrigel, RGD = Alginate functionalized with an RGD peptide and HA = Hyaluronic acid. Data sets were analyzed by students T-Test, all data presented as means  $\pm$  SEM \* $P < 0.05$ ; \*\* $P < 0.01$ ; \*\*\* $P < 0.001$ ; \*\*\*\* $P < 0.0001$  vs control,  $n \geq 3$ .

#### 5.4.5 Astrocytes show higher initial cell viability after bioprinting which is maintained by complex neuronal specific bioink

Having established a bioink which can support neuronal cell viability and survival the effect of this bioink on astrocytes was assessed. To begin astrocytes were bioprinted using a simple neuronal bioink containing only laminin and fibronectin to assess basal survival. This was done using day 40 astrocyte cultures which were dissociated and added to the bioink at a  $2 \times 10^5$  cell/mL density. Constructs were then printed using a 16-gauge needle and crosslinking was performed using 50mM  $\text{CaCl}_2$ . Whereas neurons in this type of bioink show a very low cell viability ( $\sim 10\%$ ), astrocytes showed a high cell viability ( $\sim 80\%$ ). However, when cultures were maintained for 72 hours in this system the cell viability significantly decreased indicating that while astrocytes are able to better survive the initial

transition from 2D culture into bioprinted 3D culture they eventually succumb in a similar manner to neurons. Therefore, astrocytes were printed using the more complex neuronal bioinks (containing fibronectin, laminin, FGF and either RGD and HA) which had shown beneficial effects on neuronal cell viability. This showed that while the initial astrocyte cell viability was lower in these more complex bioinks this viability was maintained after 72 hours in contrast to the simpler bioinks. These results suggest that astrocytes are more able to survive the transition from 2D culture to 3D culture however in a similar manner to neurons without the structural support and interaction with the matrix the long-term survival of the cells is negatively impacted.

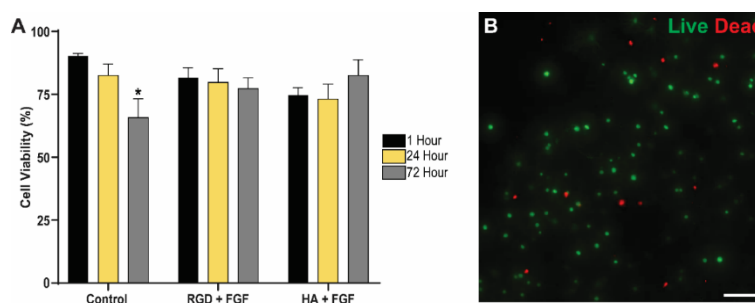


**Figure 5.6: Testing the effect of bioprinting using complex neuronal bioinks on astrocyte cell viability.** **A** Quantification of cell viability after 1 hour (black) 24 hours (yellow) and 72 hours (grey) using basic and complex neuronal bioinks. All bioprinting was performed using day 30 astrocyte cultures. The time point samples were taken or the type of bioink used had no significant effect on cell viability, however there was a significant interaction between the time point and bioink used ( $F_{4,66}=2.564$ ;  $P=0.0463$ ;  $n\geq 3/\text{group}$ ). Data sets were analyzed by two-way ANOVA with post hoc comparisons comparing to cell viability in control bioink after 1 hour. Stars above points represent Sidak-corrected post hoc tests. All data presented as means  $\pm$  SEM \* $P<0.05$ ; vs. Control 1 hour. **B** Representative image of cells 72 hours after bioprinting with no procedural modifications. Live cells are marked in green (by Calcein-AM) and dead cells are marked red (by propidium iodide). Scale bar = 100  $\mu\text{m}$ .

#### 5.4.6. Bioprinting co-cultures of neurons and astrocytes results in viable 3D constructs

Astrocytes and neurons can survive over the course of 72 hours in the modified neuronal bioink (containing hyaluronic acid). Therefore, to establish if the combination of these two cell types into a single construct has any effect on cell viability both cell types were combined in the same bioink and printed in a similar manner to the single cell suspensions. In this case the overall cell viability was ~60% however the cell viability assay is not cell specific and therefore this cell viability is a combination of the very high astrocyte cell viability and the lower neuronal cell viability resulting in a value in between the two. To assess the morphology of astrocytes in the bioprinted constructs; astrocytes were labelled with a doxycycline inducible GFP lentivirus which was induced by the addition of doxycycline 48 hours before bioprinting and induction was maintained throughout the process. Imaging astrocytes after 72 hours in the bioprinted constructs showed some star like morphology with short processes emerging from the body of the astrocytes. These

results indicate that the combination of astrocyte and neurons into a single bioink does not have a negative effect on overall cell survival and that astrocytes in this scenario begin to show some indications of astrocytic morphology.

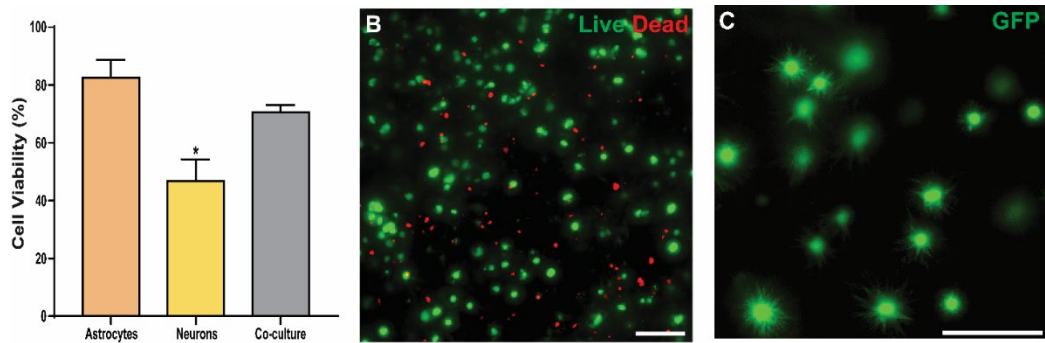


**Figure 5.7: The effect of neuron and astrocyte co-culture on cell viability and morphology.** **A** Quantification of cell viability 72 hours after bioprinting using day 30 cultures of neurons, astrocytes or a combination of both. All condition used neuronal bionk with hyaluronic acid and FGF. Data sets were analyzed by students T-Test, all data presented as means  $\pm$  SEM \* $P < 0.05$ ; vs Co-culture,  $n \geq 3$ . **B** Representative image of bioprinted co-culture after 72 hours. Live cells are marked in green (by Calcein,AM) and dead cells are marked red (by propidium iodide). **C** Representative image of astrocytes labelled with GFP 72 hours after bioprinting. Scale bars = 100  $\mu$ m.

## 5.5 Discussion

### 5.5.1 The inclusion of ECM compounds into 3D cell culture is critical for the survival of neuronal cells

The key finding of this study is the criticality of ECM proteins to the survival of both neurons and astrocytes. This finding suggests that both cell types are unable to survive without a surface to hold on to and while these cells may be capable of producing a complex ECM, they are unable to form this matrix in a suspension-like culture. While there has long been an understanding of the complexity of ECM across tissues this has largely been unimportant in the development of cellular models to date. Adherent monoculture required simple basement membranes and while in the extreme cases (i.e. Matrigel) these compounds can be complex mixtures of multiple proteins they are mostly simple single proteins which allow the adherence of cells to the culture ware in use. Indeed, astrocytes require no ECM for growth in 2D and therefore this may explain the increased initial survival when cultured in 3D. Ultimately, the transition from simple 2D cultures into more complex multicellular 3D cultures requires examination of the complex nature of the ECM and its role in the maintenance and function of cell types<sup>427</sup>.

This limitation has been identified by numerous groups and currently two overarching strategies have been employed to address this dilemma. Many groups have started to use decellularized extracellular matrices<sup>428-433</sup>. This system involves removing the cells from a tissue of interest but preserving the proteins within the extracellular space. These proteins can then be combined with an existing bioink or can be modified in such a way to create a bioink. This therefore allows bioprinting in a system which very closely mimics the *in vitro* tissue. This substrate has also been shown to improve the generation and maturation of iPSC derived oligodendrocytes<sup>434</sup> further confirming the necessity of ECM to the function of neuronal cells. Recent work by Sood *et al*<sup>435</sup> has also shown that foetal brain ECM has a greater effect than adult brain ECM. Further analysis showed changes in many ECM components from foetal to adult ECM among which chondroitin sulfates and hyaluronic acid were thought to be critical. Therefore, while limited work using this methodology points towards key components of the brain ECM being particularly important for 3D neuronal cultures.

However, this methodology is severely limited as the production of the bioink is directly tied to the availability of animal tissue which introduces the constraints associated with production and acquisition of this material, particularly in the case of foetal brain ECM.

Furthermore, this system will be heterogeneous based on the individual animal used to generate the decellularized tissue and as, yet it remains unclear how much the ECM changes between individuals. Therefore, while the use of decellularized tissue has shown promise it is critical that a simplified system can be developed which is not beholden to this material.

The second approach which many groups have adopted is to use functionalized bioinks like those used in this study. Inert bioinks can be functionalized by the addition of key amino acids and bioinks can also be modified by the addition of ECM protein which form a structural component in the bioink<sup>436</sup>. These approaches negate many of the limitations posed by the use of decellularized animal tissue however due to the complexity of ECMs it remains difficult to determine the exact composition of proteins or peptides needed to recapitulate the functions of the ECM. This is especially difficult in neuronal systems due to the high level of complexity in the neuronal ECM. As outlined by Lau *et al*<sup>437</sup> there are three main types of neuronal ECM each made up of largely similar constituents but with varying quantities. The basement membrane is mainly made of a combination of laminin and fibronectin whereas the ECM of perineuronal nests (ECM directly surrounding neurons) and the neuronal interstitial matrix (the ECM between cells) are both mainly made of hyaluronic acid and chondroitin sulphate proteoglycans (Neurocan being the most common). Therefore, it is unsurprising that laminin and fibronectin are effective basement membrane for 2D culture but have minimal effect on 3D culture as the ECM is transitioning from a basement membrane to a neuronal interstitial matrix or perineuronal nest ECM. This transition also explains the large benefit seen using hyaluronic acid as this forms a large part of these matrices and therefore the incorporation of this into the bioink creates an ECM more similar to that seen *in vitro*.

However, the similar benefit of the RGD coupled alginate suggests that this benefit is at least in part due to the stability of the hyaluronic acid within the bioink. The RGD peptide is most closely associated with fibronectin and therefore if the only benefit was from the addition of a compound which cells can bind to, we would expect the effect to be similar between RGD-alginate and fibronectin. Furthermore, some groups<sup>438</sup> have used hyaluronic acid as a major component in bioinks and have shown clear benefits from the inclusion of this compound. Therefore, this study clearly indicates that examination of the neuronal ECM is critical to the production of effective bioinks and that incorporation of compounds such as hyaluronic acid which are abundant in the tissue ECM being modelled

but also for a structural component of the bioink are critical to the success of this endeavour.

#### 5.5.2 Study limitations and future perspectives

This study clearly illustrates the viability of bioprinting as a technique for developing complex multicellular 3D neuronal models. However, the technology associated with bioprinting is still progressing very quickly and therefore with the advent of newer bioprinters it is now possible to have much greater control over the printing itself which may allow further optimizations resulting in higher cell viability. Furthermore, this approach is limited by the use of extrusion based bioprinting because as explained previously this technique is known to have significant negative effects on cell viability due to the stress cells are put under. While there are many studies using this technique a large number of them used hardier cells or cells which are able to proliferate therefore negating the issue of low initial cell viability. Other bioprinting techniques discussed previously do not share this limitation however they largely remain inaccessible due to cost or expertise. To gain a better understanding of the influence of this technique on initial cell viability a cell type which is able to survive in suspension culture may be employed which would then give a clearer picture as to the highest cell viability one would expect from this system.

A second key limitation is the lack of imaging modalities due to the relatively large thickness of the constructs. While imaging the live and dead dyes used in this study was relatively easy using a standard fluorescence microscope due to the brightness of these dyes. Imaging fine cellular processes remains very difficult, this is due to a combination of the lower fluorescent intensity seen in these areas and the 3D nature of the constructs. The inducible expression of GFP used to image astrocytes in this study is a powerful technique due to the lack of fine processes and the high expression of GFP. However, imaging neurons in a similar manner is difficult as the processes are much finer and the high expression of GFP necessary to attempt imaging has negative effects on cell health which may be compounded by the stress of bioprinting. Furthermore, due to the inherent 3D nature of these constructs the growth of cells should also be 3D and therefore imaging cells in their entirety requires very large Z-stacks which further compounds the difficulty in imaging these constructs. Finally, again due to the thickness of the constructs created, fixation and downstream imaging using classical antibody-based modalities remains difficult. Therefore, further examination is needed to determine the best system for imaging cells within these

constructs and methodological modification may be necessary to allow for alternative staining approaches.

While novel limitations associated with bioprinting as a cell culture system are critical there remain limitations which are shared between both 2D and 3D culture systems. These limitations largely center around the generation of the cell types needed for bioprinting. In the case of astrocytes, the generation of these cells using developmental patterning approaches is robust and can generate large numbers of functionally active cells. However, in the case of neurons while developmental patterning approaches can produce large number of functional neurons and as discussed previously this approach is particularly effective at modelling neuronal development this system may be limited when used for bioprinting. To prevent very low cell viability neuronal cells were bioprinted after 30 days of differentiation at which stage the cells are predominantly immature neurons. However, at this stage of differentiation cells will likely not become functional neurons for 10-20 days, furthermore developmental patterning neuronal differentiations produce astrocytes at a low level in 2D cultures. This phenomenon has been accepted in 2D developmentally patterned differentiations and therefore while confounding some results, is unlikely to critically change outcomes. However, due to the stress of bioprinting this may result in an enrichment for hardier cells (i.e. astrocytes), furthermore, as shown by this study astrocytes are more able to survive bioprinting therefore this phenomenon may result in a loss of neuronal cells in favor of astrocytes.

To address these concerns adopting a direct differentiation approach may be of interest for future work. As previously discussed, direct differentiation strategies have been developed for many cell types including neurons and while their use to examine neurodevelopment is compromised, they can be used in place of functionally mature cells. This strategy would allow large scale production of neurons which can be functional in under 15 days assuming bioprinting was carried out using iPSC. Given that bioprinting would be done on an intermediate cell type it is likely that cells would become functional neurons in under 10 days therefore negating the concern of protracted protocols associated with developmental patterning approaches. Moreover, this approach would prevent any production of astrocytes from the neuronal population used during bioprinting. In future studies it may be advantageous to use a direct differentiation approach for generating neurons to be used in bioprinting however this work must determine if cells generated in

this manner survive after bioprinting to a similar degree as their developmentally patterned counterparts.

This study also focused on the use of astrocytes and neurons and therefore in future the focus must be on developing this system further to include all cell types found in the CNS. This would introduce further concerns especially with the addition of oligodendrocytes which remain difficult to generate as discussed previously and are known to be less hardy than other neuronal cells. Therefore, the next step would be to introduce microglia into this system, as these cells are highly mobile and have been shown to infiltrate 3D cellular constructs in the past<sup>423</sup>. With this in mind it would also be critical to assess the movement of microglia through the constructs. With the addition of microglia, it is then critical to begin to examine the readouts which are possible using this system. Examining the morphology of cells may be possible using specialized imaging modalities however delving deeper into the interactions between these cell types and the role that mutations or other cellular insults may play requires re-examining the current paradigms used for assessing cell health and function. Finally, further work may consider the interaction between 3D bioprinting and development in an effort to understand how a 3D environment effects cellular development. Therefore, while this work clearly demonstrates the feasibility of 3D bioprinting as a system for modelling iPSC derived neuronal systems the focus must be on how to adapt current assays and techniques to this and other emerging 3D culture systems.

## 6. General Discussion

### 6.1 Duplication of the 1q21.1 distal locus is associated with altered early neuronal development

The main finding of this work are deficits in early neuronal and oligodendrocyte differentiation associated with 1q21.1 duplication which can be logically linked to the macrocephaly observed in patients. The convergence of phenotypes at early developmental time points, despite the differential precursor population points towards a fundamental deficit in early neuronal development. Specifically, in both the neuronal and oligodendrocyte differentiations there is a retention of a proliferative precursor population at the expense of producing a large functionally mature population.

In a similar fashion to work presented by Keeney *et al.*<sup>439</sup> the increased proliferation of neuronal stem cells can drive an increase in brain and specifically cortical volume. Furthermore, phenotypes such as macrocephaly are often observed late in gestation<sup>440</sup> after most neurons are produced; during stages when there is a large production of glia. Therefore, it is conceivable that the same deficit resulting in retention of proliferative precursors results in changes in both the neuronal and glial populations combining to produce the macrocephaly observed in 1q21.1 duplication patients. Many genetic disorders have been linked to macrocephaly including psychiatric disorders (specifically non-syndromic ASD<sup>441</sup>) and as Ernst<sup>442</sup> discusses there is a link between neurodevelopmental disorders and altered cell proliferation.

While the precise cause of the deficits in differentiation and proliferation associated with 1q21.1 duplication remain unclear as previously discussed recent work on NOTCH2NL suggests that this gene may at least partially underly this phenotype<sup>65,255</sup>. However, despite this link other genes within the 1q21.1 locus may also play a role in the developmental deficits associated with this mutation. Further work remains necessary to understand the individual contribution of genes within the 1q21.1 distal locus and their effects on the phenotypes seen in both neuronal and oligodendrocyte development.

Ultimately the consequences of the changes in proliferation at early stages of development appear to be a loss of functionally mature cells in both neuronal and oligodendrocyte differentiations. However, the DTI data from human 1q21.1 duplication carriers suggests that at least in the corpus callosum there are no changes in the function of oligodendrocytes. This discrepancy may be due to the small sample size of this study in respect to both the brain area examined and the number of individuals used. However,

since individuals examined using the DTI metric were adults this may suggest that compensatory mechanisms during early life and adolescence are able to recover functional deficits associated with loss of oligodendrocytes. This may also suggest that the loss of functional neurons seen in 1q21.1 duplication differentiations may not have such a profound effect on neuronal network behavior *in vivo* as that seen *in vitro*. Therefore, while the loss of neurons associated with 1q21.1 duplication in this study has profound effects on neuronal network formation and function the effect seen in patients is unlikely to be as profound as the effects seen in this study. Further examination of imaging data from individuals with 1q21.1 duplications may shed light on the link between the phenotypes identified in this study and the clinical phenotypes seen in patients. However, given the phenotypes identified in this study the examination of younger patients may be of interest.

6.2 Deletion of the 1q21.1 distal locus is associated with deficits in cellular function distinct from deficits in early differentiation

The main phenotypes associated with 1q21.1 deletion identified in this work are an increased neuronal activity resulting in aberrant network activity and a loss of functional oligodendrocytes. Both phenotypes can be linked to the clinical presentation of 1q21.1 deletion patients and present further evidence for associations between aberrant neuronal network activity and a loss of oligodendrocytes with schizophrenia. Compared to phenotypes associated with 1q21.1 duplication most phenotypes associated with deletion of the distal 1q21.1 locus occur later in development in both neuronal and oligodendrocyte differentiations. Specifically, in neuronal differentiations 1q21.1 deletion is associated with an increased production of neurons whereas in oligodendrocyte differentiations 1q21.1 deletion is associated with a loss of proliferation at early developmental stages. In a similar fashion to 1q21.1 duplication these changes may play a role in the functional changes seen in these differentiations. However, as discussed previously the results from functional characterization of the 1q21.1 deletion neurons and quantification of MBP+ cells in oligodendrocyte differentiations points towards a separate origin for these phenotypes. Therefore, while the development of neurons and oligodendrocytes may be altered in association with 1q21.1 deletion this CNV also influences cellular function beyond development.

The deficits in differentiation and proliferation associated with 1q21.1 deletion again point to a role for NOTCH2NL in the development of this phenotype<sup>65,255</sup>. However, while the increased expression of NOTCH2NL would explain the increased production of neurons and the decreased proliferation at early stages of oligodendrocyte development it does not explain the functional changes observed in these two cell types. In neurons the increase activity of individual cells and changes in neuronal network behavior speak to further cellular dysfunction. Furthermore, the loss of both O4+ and MBP+ cells in oligodendrocyte differentiations does not fit with the increased pace of maturation indicated by the work on loss of NOTCH2NL expression. Finally, the correlation of results from both the mouse and human studies indicate a conserved mechanism underlying these phenotypes which again points away from NOTCH2NL as this is a human specific paralog. Therefore, in the case of 1q21.1 deletion it is especially critical to examine the role of other genes in the 1q21.1 locus; to determine what is driving the functional deficits which may ultimately be particularly relevant to the association with psychiatric disorders.

The dichotomy between the phenotypes identified in neuronal and oligodendrocyte differentiations also points towards a divergent functional outcome from these two systems. Imagining these two phenotypes present in a single individual, the increased activity of neurons would be at odds with the decreased myelination resulting from the loss of oligodendrocytes. The loss of myelination would result in a slowing of the propagation of action potentials therefore likely resulting in a decrease in neuronal activity. It also must be pointed out that while oligodendrocytes originating in the medial ganglionic eminence (like those modelled in this study) are critical to the myelination of the cortex, cells originating from dorsal progenitors also play a critical role in cortical myelination<sup>443</sup>. As neuronal differentiations are based on the production of dorsal progenitors and are marked by increased production of maturing cells, this may suggest that the loss of oligodendrocytes seen when modelling ventrally produced precursors would not occur in their dorsally produced counterparts. Therefore, the loss of functional oligodendrocytes in association with 1q21.1 deletion presented in this study may be less likely to effect cortical grey matter due to compensation from dorsally produced oligodendrocytes. Instead the loss of oligodendrocytes is likely to effect white matter tracts producing similar effects to those seen in the DTI and mouse studies.

It is also important to consider that myelination is a dynamic process occurring throughout early life and is informed by many factors including the activity of neurons. It

has long been established that the myelination of neurons in the CNS can be driven by neuronal activity<sup>444,445</sup>. With studies suggesting the activity dependent release of growth factors such as neuregulin1 from neurons<sup>446</sup> can increase production of NMDA receptors in oligodendrocytes therefore inducing activity-dependent myelination<sup>447</sup>. This suggests there are complex interactions between neurons and oligodendrocytes ultimately resulting in myelination. Therefore, the altered neuronal behavior seen in 1q21.1 deletion neurons is likely to effect the function of oligodendrocytes. It is also possible the increased activity seen in 1q21.1 neurons may drive abnormal myelination, which coupled with the apparent loss of oligodendrocytes resulting from this mutation would result in a complex cellular phenotype. Ultimately while the identification of isolated cellular phenotypes associated with CNV at the 1q21.1 locus is critical to understand the impact of this mutation; viewing these phenotypes in isolation cannot give a complete picture of the complex cellular dysfunction resulting from the combination of these cells.

### 6.3 Mutations of the 1q21.1 locus model key aspects of cellular pathology associated with psychiatric disorders

As previously discussed, the individual phenotypes identified in neurons and oligodendrocytes separately are highly relevant to the development of psychiatric disorders. The integration of phenotypes from both neuronal and oligodendrocyte studies provides more evidence for an important role of these phenotypes in the development of psychiatric disorders. As discussed by Takahashi *et al.*<sup>448</sup> the loss of oligodendrocytes and resulting hypomyelination may lead to changes in synapse formation and function which may compound the dysfunction already seen in 1q21.1 deletion neurons. Furthermore, as Cassoli *et al.*<sup>449</sup> suggest neuronal dysconnectivity may result from hypomyelination in white matter tracts connecting key brain regions with small changes in myelination resulting in large effects on neuronal synchrony<sup>450</sup>. This concept has been further investigated with a recent study finding that there are fundamental links between white matter structure and neuronal synchronization<sup>290</sup>. Furthermore, alterations in white matter structure and neuronal synchronization were shown to significantly effect cognitive processing. Therefore, this study suggests that deletion of the 1q21.1 region results in altered neuronal

synchronicity at a micro-scale, which is compounded by deficits in oligodendrocyte production and function; resulting in alterations in neuronal synchrony at a macro-scale.

The deficits associated with 1q21.1 duplication occur earlier in development with little evidence of deficits in later development which are not connected to early developmental alterations. However, these deficits in early development are highly relevant to the development of ASD. There is a large body of evidence (see review by Courchesne *et al.*<sup>451</sup>) linking early brain overgrowth followed by a slow or arrested growth with the development of ASD. More recent work has also suggested that early overgrowth can also be predictive of ASD diagnosis<sup>452</sup> indicating the fundamental nature of this phenotype to ASD. This early brain overgrowth is also seen in both grey and white matter<sup>197,453</sup> further indicating the relevance of the retention of neuronal precursors seen in both neuronal and oligodendrocyte elements of this study. This is also in-line with the scheme presented by Priven *et al.*<sup>454</sup> proposing a cascade of developmental changes in ASD. There is also evidence from genetic studies which show an enrichment for genes related to neuronal induction and early maturation<sup>455</sup> in association with ASD diagnosis. Furthermore, analysis of two ASD risk genes (AUTS2<sup>456</sup> and MET<sup>457</sup>) show they are expressed in neuronal progenitors and in the case of MET is involved in key early developmental processes. Altering the developmental trajectories of cortical cells has also been shown to lead to behavioral changes in a mouse model consistent with clinical features of ASD<sup>458</sup>. Finally, similar to schizophrenia developmental deficits in ASD have been suggested to result in altered neuronal connectivity with increased local and decreased long-distance connectivity<sup>459</sup>. Therefore, cementing the need for further examination of functional phenotypes in the 1q21.1 models presented in this study.

Ultimately this study provides further evidence for the role of glia in the development of neurodevelopmental and psychiatric disorders. This phenomena is increasingly becoming clear with evidence from studies into astrocytes<sup>460</sup>, microglia<sup>461</sup> and oligodendrocytes<sup>154,462</sup> all suggesting dysfunction associated with psychiatric disorders. A recent publication from Dietz *et al.*<sup>463</sup> suggests that the interaction between neurons and glia throughout development play a critical role in the development of schizophrenia. This work also suggests that the individual deficits in each cell type additively produce the neuronal dysfunction which leads to the symptoms associated with schizophrenia.

Therefore, it is becoming increasingly critical to establish models which can be used to examine the combined effect of dysfunction in these separate cell types. While

organoids remain an important area of study the difficulty, time and expense of producing organoids limits the utility of this system to understanding complex functional multicellular phenotypes. Hence, systems such as bioprinting which can allow the investigation of how previously characterized cells types interact together and the phenotypes resulting from this interaction are particularly important. While advancements in this technology are constant<sup>464,465</sup> the lack of studies using iPSC derived neuronal cells presents a clear gap in the advancement of this technology which has begun to be filled by this study. This study demonstrates that bioprinting using alginate based bioinks can allow for astrocytic and neuronal survival. While further development of this technique is needed establishing a complete bioprinted 3D model using iPSC derived neurons and glia would provide an invaluable tool to investigate the effects glia on neuronal health and function.

#### 6.4 Conclusions and future perspectives

The studies presented in this work demonstrate that iPSC models of 1q21.1 deletions and duplications can be used to identify cellular dysfunction associated with these mutations. With the identification of phenotypes associated with 1q21.1 mutations in both neuronal and oligodendrocyte development speaking to the complexity of psychiatric risk. While some of the phenotypes are mirrored between 1q21.1 deletion and duplication there are also several shared phenotypes speaking to the convergence of cell-based risk for neurodevelopmental and psychiatric disorders. Functional deficits in 1q21.1 deletion neurons provide an interesting window into the interplay between neuronal dysfunction and abnormalities in neuronal network behavior. However, deficits in early neuronal differentiation in 1q21.1 duplication cultures present a challenge to understanding the effect of this mutation on neuronal function. Therefore, assessing the functional phenotypes in a direct differentiation model may allow differentiation between the developmental phenotypes and those that emerge purely in a mature neuronal population.

Modulating the calcium movement by targeting calcium channel activity begins to suggest that the phenotypes identified in this study can be pharmacologically targeted. However further examination of neuronal functionality after pharmacological intervention is necessary to establish if this manipulation can restore neuronal activity and neuronal

network behavior. Therefore, future work may focus on targeting the neuronal activity and network behavior phenotypes identified using the MEAs, as rescuing these phenotypes is likely to be more relevant to patients' clinical presentations.

Deficits in the production of oligodendrocytes associated with both 1q21.1 deletion and duplication point again to a level of commonality in phenotypes despite the opposing mutations. However, the core phenotype driving the loss of oligodendrocytes appears to be different depending on the type of 1q21.1 mutation. Again, duplication of the 1q21.1 locus is associated with early developmental deficits which result in a decreased production of oligodendrocytes. On the other hand, deletion of the 1q21.1 locus is associated with a loss of OPCs and reduced differentiation of OPCs into oligodendrocytes. Critically future work must focus on examining how these mutations effect the ability of oligodendrocytes to myelinate to establish if the deficits are specific to differentiation. Based on the effect of interventions during neuronal differentiation it would also be important to determine the effect of drugs on oligodendrocyte differentiation and function to establish if the same pharmacological intervention can rescue both cell types.

While these studies have provided insight into the cellular deficits associated with 1q21.1 deletion and duplication the precise underlying mechanisms are yet to be understood. The complexity of the genes within the 1q21.1 locus and the diversity of the phenotypes identified suggests that these effects may be driven by changes in multiple genes. Therefore, to elucidate the molecular underpinnings of these phenotypes large scale transcriptomics and a program of genetic manipulation targeting genes within the 1q21.1 locus is necessary.

Finally, further examination of the effect of 1q21.1 mutations on remaining glia may provide additional insight into the pathologies associated with 1q21.1 mutations. However further development of bioprinting technologies and other similar techniques which can encompass the complexity of the human CNS are likely to prove critical in providing a holistic understand of cellular dysfunction associated with psychiatric risk. Work presented in this study suggests that modifying simple bioinks using neuronal ECM components is a potentially strategy for developing complex multicellular bioprinted neuronal constructs which would provide a viable alternative to organoids. However, expanding this work using other neuronal cells and cell generated using other methods is critical to establishing this as a robust model for future study.

## 7. Bibliography

- 1 Steel, Z. *et al.* The global prevalence of common mental disorders: a systematic review and meta-analysis 1980-2013. *Int J Epidemiol* **43**, 476-493 (2014).
- 2 McMillen, J. C. *et al.* Prevalence of psychiatric disorders among older youths in the foster care system. *J Am Acad Child Psy* **44**, 88-95 (2005).
- 3 Charlson, F. *et al.* New WHO prevalence estimates of mental disorders in conflict settings: a systematic review and meta-analysis. *Lancet* **394**, 240-248 (2019).
- 4 Emerson, E. Deprivation, ethnicity and the prevalence of intellectual and developmental disabilities. *J Epidemiol Commun H* **66**, 218-224 (2012).
- 5 Jarbrink, K. & Knapp, M. The economic impact of autism in Britain. *Autism* **5**, 7-22 (2001).
- 6 Van Os, J., Kenis, G. & Rutten, B. P. The environment and schizophrenia. *Nature* **468**, 203-212 (2010).
- 7 Myint, A. M. Inflammation, neurotoxins and psychiatric disorders. *Mod Trends Pharmacopsychiatry* **28**, 61-74 (2013).
- 8 Estes, M. L. & McAllister, A. K. Maternal immune activation: Implications for neuropsychiatric disorders. *Science* **353**, 772-777 (2016).
- 9 Crow, T. J. 'The missing genes: what happened to the heritability of psychiatric disorders?'. *Molecular Psychiatry* **16**, 362-364 (2011).
- 10 Shih, R. A., Belmonte, P. L. & Zandi, P. P. A review of the evidence from family, twin and adoption studies for a genetic contribution to adult psychiatric disorders. *International Review of Psychiatry* **16**, 260-283 (2004).
- 11 Pardiñas, A. F. *et al.* Common schizophrenia alleles are enriched in mutation-intolerant genes and in regions under strong background selection. *Nature genetics* **50**, 381 (2018).
- 12 Ikeda, M. *et al.* A genome-wide association study identifies two novel susceptibility loci and trans population polygenicity associated with bipolar disorder. *Molecular psychiatry* **23**, 639 (2018).
- 13 Skene, N. G. *et al.* Genetic identification of brain cell types underlying schizophrenia. *Nature genetics* **50**, 825 (2018).
- 14 Thapar, A. & Cooper, M. Copy number variation: what is it and what has it told us about child psychiatric disorders? *J Am Acad Child Adolesc Psychiatry* **52**, 772-774 (2013).
- 15 Liskay, R. M., Letsou, A. & Stachelek, J. L. Homology Requirement for Efficient Gene Conversion between Duplicated Chromosomal Sequences in Mammalian-Cells. *Genetics* **115**, 161-167 (1987).
- 16 Hastings, P. J., Lupski, J. R., Rosenberg, S. M. & Ira, G. Mechanisms of change in gene copy number. *Nature Reviews Genetics* **10**, 551-564 (2009).
- 17 Redon, R. *et al.* Global variation in copy number in the human genome. *nature* **444**, 444 (2006).
- 18 Sebat, J. *et al.* Large-scale copy number polymorphism in the human genome. *Science* **305**, 525-528 (2004).
- 19 Perry, G. H. *et al.* Diet and the evolution of human amylase gene copy number variation. *Nat Genet* **39**, 1256-1260 (2007).
- 20 Emes, R. D. *et al.* Evolutionary expansion and anatomical specialization of synapse proteome complexity. *Nat Neurosci* **11**, 799-806 (2008).

- 21 Gonzalez, E. *et al.* The influence of CCL3L1 gene-containing segmental duplications on HIV-1/AIDS susceptibility. *Science* **307**, 1434-1440 (2005).
- 22 Aldred, P. M., Hollox, E. J. & Armour, J. A. Copy number polymorphism and expression level variation of the human alpha-defensin genes DEFA1 and DEFA3. *Hum Mol Genet* **14**, 2045-2052 (2005).
- 23 Breunis, W. B. *et al.* Copy number variation of the activating FCGR2C gene predisposes to idiopathic thrombocytopenic purpura. *Blood* **111**, 1029-1038 (2008).
- 24 Aitman, T. J. *et al.* Copy number polymorphism in Fcgr3 predisposes to glomerulonephritis in rats and humans. *Nature* **439**, 851-855 (2006).
- 25 Bayes, M., Magano, L. F., Rivera, N., Flores, R. & Perez Jurado, L. A. Mutational mechanisms of Williams-Beuren syndrome deletions. *Am J Hum Genet* **73**, 131-151 (2003).
- 26 Baldini, A. DiGeorge syndrome: an update. *Curr Opin Cardiol* **19**, 201-204 (2004).
- 27 Bi, W. *et al.* Genes in a refined Smith-Magenis syndrome critical deletion interval on chromosome 17p11.2 and the syntenic region of the mouse. *Genome Res* **12**, 713-728 (2002).
- 28 Murray, R. M. & Lewis, S. W. Is schizophrenia a neurodevelopmental disorder? *British medical journal (Clinical research ed.)* **295**, 681 (1987).
- 29 Fatemi, S. H. & Folsom, T. D. The neurodevelopmental hypothesis of schizophrenia, revisited. *Schizophrenia bulletin* **35**, 528-548 (2009).
- 30 Cotney, J. *et al.* The autism-associated chromatin modifier CHD8 regulates other autism risk genes during human neurodevelopment. *Nature communications* **6**, 6404 (2015).
- 31 O'Hearn, K., Asato, M., Ordaz, S. & Luna, B. Neurodevelopment and executive function in autism. *Development and psychopathology* **20**, 1103-1132 (2008).
- 32 Sanches, M., Keshavan, M. S., Brambilla, P. & Soares, J. C. Neurodevelopmental basis of bipolar disorder: a critical appraisal. *Progress in Neuro-Psychopharmacology and Biological Psychiatry* **32**, 1617-1627 (2008).
- 33 Ansorge, M. S., Hen, R. & Gingrich, J. A. Neurodevelopmental origins of depressive disorders. *Current opinion in pharmacology* **7**, 8-17 (2007).
- 34 Owen, M. J. Intellectual disability and major psychiatric disorders: a continuum of neurodevelopmental causality. *The British Journal of Psychiatry* **200**, 268-269 (2012).
- 35 Schork, A. J. *et al.* A genome-wide association study of shared risk across psychiatric disorders implicates gene regulation during fetal neurodevelopment. *Nature neuroscience* **22**, 353 (2019).
- 36 Clifton, N. E. *et al.* Dynamic expression of genes associated with schizophrenia and bipolar disorder across development. *Translational Psychiatry* **9** (2019).
- 37 Shprintzen, R. *et al.* A new syndrome involving cleft palate, cardiac anomalies, typical facies, and learning disabilities: velo-cardio-facial syndrome. *The Cleft palate journal* **15**, 56-62 (1978).
- 38 Scambler, P. *et al.* Velo-cardio-facial syndrome associated with chromosome 22 deletions encompassing the DiGeorge locus. *The Lancet* **339**, 1138-1139 (1992).
- 39 Bassett, A. S. *et al.* Clinical features of 78 adults with 22q11 deletion syndrome. *American journal of medical genetics Part A* **138**, 307-313 (2005).
- 40 Bassett, A. S. & Chow, E. W. Schizophrenia and 22q11. 2 deletion syndrome. *Current psychiatry reports* **10**, 148 (2008).

- 41 Malhotra, D. & Sebat, J. CNVs: harbingers of a rare variant revolution in psychiatric genetics. *Cell* **148**, 1223-1241 (2012).
- 42 Mefford, H. C. *et al.* Recurrent rearrangements of chromosome 1q21. 1 and variable pediatric phenotypes. *New England Journal of Medicine* **359**, 1685-1699 (2008).
- 43 Cooper, G. M. *et al.* A copy number variation morbidity map of developmental delay. *Nat Genet* **43**, 838-846 (2011).
- 44 Cooper, G. M. *et al.* A copy number variation morbidity map of developmental delay. *Nature genetics* **43**, 838 (2011).
- 45 Brunetti-Pierri, N. *et al.* Recurrent reciprocal 1q21. 1 deletions and duplications associated with microcephaly or macrocephaly and developmental and behavioral abnormalities. *Nature genetics* **40**, 1466-1471 (2008).
- 46 Ballif, B. C. *et al.* Expanding the clinical phenotype of the 3q29 microdeletion syndrome and characterization of the reciprocal microduplication. *Molecular Cytogenetics* **1**, 8 (2008).
- 47 Doornbos, M. *et al.* Nine patients with a microdeletion 15q11. 2 between breakpoints 1 and 2 of the Prader–Willi critical region, possibly associated with behavioural disturbances. *European Journal of Medical Genetics* **52**, 108-115 (2009).
- 48 Burnside, R. D. *et al.* Microdeletion/microduplication of proximal 15q11. 2 between BP1 and BP2: a susceptibility region for neurological dysfunction including developmental and language delay. *Human genetics* **130**, 517-528 (2011).
- 49 Van Bon, B. *et al.* Further delineation of the 15q13 microdeletion and duplication syndromes: a clinical spectrum varying from non-pathogenic to a severe outcome. *Journal of medical genetics* **46**, 511-523 (2009).
- 50 Sharp, A. J. *et al.* A recurrent 15q13. 3 microdeletion syndrome associated with mental retardation and seizures. *Nature genetics* **40**, 322 (2008).
- 51 Miller, D. T. *et al.* Microdeletion/duplication at 15q13. 2q13. 3 among individuals with features of autism and other neuropsychiatric disorders. *Journal of medical genetics* **46**, 242-248 (2009).
- 52 Ramalingam, A. *et al.* 16p13. 11 duplication is a risk factor for a wide spectrum of neuropsychiatric disorders. *Journal of human genetics* **56**, 541 (2011).
- 53 Nagamani, S. C. S. *et al.* Phenotypic manifestations of copy number variation in chromosome 16p13. 11. *European Journal of Human Genetics* **19**, 280 (2011).
- 54 Moreno-De-Luca, D. *et al.* Deletion 17q12 is a recurrent copy number variant that confers high risk of autism and schizophrenia. *The American Journal of Human Genetics* **87**, 618-630 (2010).
- 55 Malhotra, D. *et al.* High frequencies of de novo CNVs in bipolar disorder and schizophrenia. *Neuron* **72**, 951-963 (2011).
- 56 Grozeva, D. *et al.* Rare copy number variants: a point of rarity in genetic risk for bipolar disorder and schizophrenia. *Archives of general psychiatry* **67**, 318-327 (2010).
- 57 Priebe, L. *et al.* Genome-wide survey implicates the influence of copy number variants (CNVs) in the development of early-onset bipolar disorder. *Molecular psychiatry* **17**, 421 (2012).
- 58 Rucker, J. J. *et al.* Genome-wide association analysis of copy number variation in recurrent depressive disorder. *Molecular psychiatry* **18**, 183 (2013).

- 59 Brunetti-Pierri, N. *et al.* Recurrent reciprocal 1q21. 1 deletions and duplications associated with microcephaly or macrocephaly and developmental and behavioral abnormalities. *Nature genetics* **40**, 1466 (2008).
- 60 Hall, J. G. Thrombocytopenia and Absent Radius (Tar) Syndrome. *Journal of Medical Genetics* **24**, 79-83 (1987).
- 61 Soemedi, R. *et al.* Phenotype-specific effect of chromosome 1q21. 1 rearrangements and GJA5 duplications in 2436 congenital heart disease patients and 6760 controls. *Human molecular genetics* **21**, 1513-1520 (2011).
- 62 Christiansen, J. *et al.* Chromosome 1q21. 1 contiguous gene deletion is associated with congenital heart disease. *Circulation research* **94**, 1429-1435 (2004).
- 63 Crespi, B. J. & Crofts, H. J. Association testing of copy number variants in schizophrenia and autism spectrum disorders. *Journal of neurodevelopmental disorders* **4**, 15 (2012).
- 64 Stelzer, G. *et al.* The GeneCards Suite: From Gene Data Mining to Disease Genome Sequence Analyses. *Curr Protoc Bioinformatics* **54**, 1 30 31-31 30 33 (2016).
- 65 Fiddes, I. T. *et al.* Human-specific NOTCH2NL genes affect Notch signaling and cortical neurogenesis. *Cell* **173**, 1356-1369. e1322 (2018).
- 66 Kramps, T. *et al.* Wnt/wingless signaling requires BCL9/legless-mediated recruitment of pygopus to the nuclear beta-catenin-TCF complex. *Cell* **109**, 47-60 (2002).
- 67 Xu, C. *et al.* BCL9 and C9orf5 are associated with negative symptoms in schizophrenia: meta-analysis of two genome-wide association studies. *PLoS One* **8**, e51674 (2013).
- 68 Dawe, H. R., Shaw, M. K., Farr, H. & Gull, K. The hydrocephalus inducing gene product, Hydin, positions axonemal central pair microtubules. *BMC Biol* **5**, 33 (2007).
- 69 Zepeda-Mendoza, C., Goodenberger, M. L., Kuhl, A., Rice, G. M. & Hoppman, N. Familial segregation of a 5q15-q21.2 deletion associated with facial dysmorphism and speech delay. *Clin Case Rep* **7**, 1154-1160 (2019).
- 70 Koscielny, G. *et al.* The International Mouse Phenotyping Consortium Web Portal, a unified point of access for knockout mice and related phenotyping data. *Nucleic Acids Res* **42**, D802-809 (2014).
- 71 Mena, A. *et al.* Reduced prepulse inhibition as a biomarker of schizophrenia. *Frontiers in behavioral neuroscience* **10**, 202 (2016).
- 72 Swerdlow, N. R. *et al.* Deficient prepulse inhibition in schizophrenia detected by the multi-site COGS. *Schizophrenia research* **152**, 503-512 (2014).
- 73 Powell, S. B., Zhou, X. & Geyer, M. A. Prepulse inhibition and genetic mouse models of schizophrenia. *Behavioural brain research* **204**, 282-294 (2009).
- 74 Nagy, S. *et al.* AMPK signaling linked to the schizophrenia-associated 1q21.1 deletion is required for neuronal and sleep maintenance. *PLoS Genet* **14**, e1007623 (2018).
- 75 Nielsen, J. *et al.* A mouse model of the schizophrenia-associated 1q21.1 microdeletion syndrome exhibits altered mesolimbic dopamine transmission. *Transl Psychiatry* **7**, 1261 (2017).
- 76 Howes, O. D. & Kapur, S. The dopamine hypothesis of schizophrenia: version III—the final common pathway. *Schizophrenia bulletin* **35**, 549-562 (2009).
- 77 Lieberman, J., Kane, J. & Alvir, J. Provocative tests with psychostimulant drugs in schizophrenia. *Psychopharmacology* **91**, 415-433 (1987).

- 78 Meltzer, H. Y. & Stahl, S. M. The dopamine hypothesis of schizophrenia: a review. *Schizophrenia bulletin* **2**, 19 (1976).
- 79 Li, P., L Snyder, G. & E Vanover, K. Dopamine targeting drugs for the treatment of schizophrenia: past, present and future. *Current topics in medicinal chemistry* **16**, 3385-3403 (2016).
- 80 Featherstone, R., Kapur, S. & Fletcher, P. The amphetamine-induced sensitized state as a model of schizophrenia. *Progress in Neuro-Psychopharmacology and Biological Psychiatry* **31**, 1556-1571 (2007).
- 81 Inta, D., Meyer-Lindenberg, A. & Gass, P. Alterations in postnatal neurogenesis and dopamine dysregulation in schizophrenia: a hypothesis. *Schizophrenia bulletin* **37**, 674-680 (2011).
- 82 Ozawa, K. *et al.* Immune activation during pregnancy in mice leads to dopaminergic hyperfunction and cognitive impairment in the offspring: a neurodevelopmental animal model of schizophrenia. *Biological psychiatry* **59**, 546-554 (2006).
- 83 Zuckerman, L., Rehavi, M., Nachman, R. & Weiner, I. Immune activation during pregnancy in rats leads to a postpubertal emergence of disrupted latent inhibition, dopaminergic hyperfunction, and altered limbic morphology in the offspring: a novel neurodevelopmental model of schizophrenia. *Neuropsychopharmacology* **28**, 1778-1789 (2003).
- 84 Vuillermot, S., Weber, L., Feldon, J. & Meyer, U. A longitudinal examination of the neurodevelopmental impact of prenatal immune activation in mice reveals primary defects in dopaminergic development relevant to schizophrenia. *Journal of Neuroscience* **30**, 1270-1287 (2010).
- 85 Lipska, B. K. & Weinberger, D. R. A neurodevelopmental model of schizophrenia: neonatal disconnection of the hippocampus. *Neurotoxicity research* **4**, 469-475 (2002).
- 86 Tseng, K. Y., Chambers, R. A. & Lipska, B. K. The neonatal ventral hippocampal lesion as a heuristic neurodevelopmental model of schizophrenia. *Behavioural brain research* **204**, 295-305 (2009).
- 87 Kesby, J., Eyles, D., McGrath, J. & Scott, J. Dopamine, psychosis and schizophrenia: the widening gap between basic and clinical neuroscience. *Translational psychiatry* **8**, 1-12 (2018).
- 88 Luby, E. D., Gottlieb, J. S., Cohen, B. D., Rosenbaum, G. & Domino, E. F. Model psychoses and schizophrenia. *American Journal of Psychiatry* **119**, 61-67 (1962).
- 89 Javitt, D. C. Negative schizophrenic symptomatology and the PCP (phencyclidine) model of schizophrenia. *Hillside J Clin Psychiatry* **9**, 12-35 (1987).
- 90 Farber, N. B., Newcomer, J. W. & Olney, J. W. in *Progress in brain research* Vol. 116 421-437 (Elsevier, 1998).
- 91 Morris, B. J., Cochran, S. M. & Pratt, J. A. PCP: from pharmacology to modelling schizophrenia. *Current opinion in pharmacology* **5**, 101-106 (2005).
- 92 Malhotra, A. K. *et al.* Ketamine-induced exacerbation of psychotic symptoms and cognitive impairment in neuroleptic-free schizophrenics. *Neuropsychopharmacology* **17**, 141-150 (1997).
- 93 Carlsson, M. & Carlsson, A. The NMDA antagonist MK-801 causes marked locomotor stimulation in monoamine-depleted mice. *Journal of neural transmission* **75**, 221-226 (1989).

- 94 Adams, B. & Moghaddam, B. Corticolimbic dopamine neurotransmission is temporally dissociated from the cognitive and locomotor effects of phencyclidine. *Journal of Neuroscience* **18**, 5545-5554 (1998).
- 95 Krystal, J. *et al.* Modulating ketamine-induced thought disorder with lorazepam and haloperidol in humans. *Schizophrenia Research* **15**, 156-157 (1995).
- 96 Ripke, S. *et al.* Biological insights from 108 schizophrenia-associated genetic loci. *Nature* **511**, 421-427 (2014).
- 97 Fromer, M. *et al.* De novo mutations in schizophrenia implicate synaptic networks. *Nature* **506**, 179-184 (2014).
- 98 Purcell, S. M. *et al.* A polygenic burden of rare disruptive mutations in schizophrenia. *Nature* **506**, 185-190 (2014).
- 99 Moghaddam, B. & Javitt, D. From revolution to evolution: the glutamate hypothesis of schizophrenia and its implication for treatment. *Neuropsychopharmacology* **37**, 4-15 (2012).
- 100 Steiner, J. *et al.* Bridging the gap between the immune and glutamate hypotheses of schizophrenia and major depression: potential role of glial NMDA receptor modulators and impaired blood–brain barrier integrity. *The World Journal of Biological Psychiatry* **13**, 482-492 (2012).
- 101 Kondziella, D., Brenner, E., Eyjolfsson, E. M. & Sonnewald, U. How do glial–neuronal interactions fit into current neurotransmitter hypotheses of schizophrenia? *Neurochemistry international* **50**, 291-301 (2007).
- 102 Hashimoto, K., Shimizu, E. & Iyo, M. Dysfunction of glia–neuron communication in pathophysiology of schizophrenia. *Current Psychiatry Reviews* **1**, 151-163 (2005).
- 103 Hu, W., MacDonald, M. L., Elswick, D. E. & Sweet, R. A. The glutamate hypothesis of schizophrenia: evidence from human brain tissue studies. *Annals of the New York Academy of Sciences* **1338**, 38 (2015).
- 104 Gordon, J. A. Testing the glutamate hypothesis of schizophrenia. *Nature neuroscience* **13**, 2-4 (2010).
- 105 Nelson, S. B. & Valakh, V. Excitatory/inhibitory balance and circuit homeostasis in autism spectrum disorders. *Neuron* **87**, 684-698 (2015).
- 106 Rubenstein, J. & Merzenich, M. M. Model of autism: increased ratio of excitation/inhibition in key neural systems. *Genes, Brain and Behavior* **2**, 255-267 (2003).
- 107 Amaral, D. G., Schumann, C. M. & Nordahl, C. W. Neuroanatomy of autism. *Trends in neurosciences* **31**, 137-145 (2008).
- 108 Judson, M. C., Eagleson, K. L. & Levitt, P. A new synaptic player leading to autism risk: Met receptor tyrosine kinase. *Journal of neurodevelopmental disorders* **3**, 282 (2011).
- 109 Rudie, J. D. *et al.* Autism-associated promoter variant in MET impacts functional and structural brain networks. *Neuron* **75**, 904-915 (2012).
- 110 Haigh, S. M., Keller, T. A., Minshew, N. J. & Eack, S. M. Reduced White Matter Integrity and Deficits in Neuropsychological Functioning in Adults With Autism Spectrum Disorder. *Autism Research* (2020).
- 111 Sheffield, J. M. & Barch, D. M. Cognition and resting-state functional connectivity in schizophrenia. *Neuroscience & Biobehavioral Reviews* **61**, 108-120 (2016).
- 112 Li, T. *et al.* Brain-wide analysis of functional connectivity in first-episode and chronic stages of schizophrenia. *Schizophrenia bulletin* **43**, 436-448 (2017).

- 113 Kelly, S. *et al.* Widespread white matter microstructural differences in schizophrenia across 4322 individuals: results from the ENIGMA Schizophrenia DTI Working Group. *Mol Psychiatry* **23**, 1261-1269 (2018).
- 114 Jiang, Y. *et al.* White-matter functional networks changes in patients with schizophrenia. *NeuroImage* **190**, 172-181 (2019).
- 115 Klauser, P. *et al.* White matter disruptions in schizophrenia are spatially widespread and topologically converge on brain network hubs. *Schizophrenia bulletin* **43**, 425-435 (2017).
- 116 Osimo, E. F., Beck, K., Marques, T. R. & Howes, O. D. Synaptic loss in schizophrenia: a meta-analysis and systematic review of synaptic protein and mRNA measures. *Molecular psychiatry* **24**, 549-561 (2019).
- 117 Berdenis van Berlekom, A. *et al.* Synapse pathology in schizophrenia: a meta-analysis of postsynaptic elements in postmortem brain studies. *Schizophrenia Bulletin* **46**, 374-386 (2020).
- 118 Feinberg, I. Schizophrenia: caused by a fault in programmed synaptic elimination during adolescence? *Journal of psychiatric research* **17**, 319-334 (1982).
- 119 Wang, Q. *et al.* A Bayesian framework that integrates multi-omics data and gene networks predicts risk genes from schizophrenia GWAS data. *Nature neuroscience* **22**, 691-699 (2019).
- 120 Onwordi, E. C. *et al.* Synaptic density marker SV2A is reduced in schizophrenia patients and unaffected by antipsychotics in rats. *Nature Communications* **11**, 1-11 (2020).
- 121 Guang, S. *et al.* Synaptopathology involved in autism spectrum disorder. *Frontiers in cellular neuroscience* **12**, 470 (2018).
- 122 Auerbach, B. D., Osterweil, E. K. & Bear, M. F. Mutations causing syndromic autism define an axis of synaptic pathophysiology. *Nature* **480**, 63-68 (2011).
- 123 Tang, G. *et al.* Loss of mTOR-dependent macroautophagy causes autistic-like synaptic pruning deficits. *Neuron* **83**, 1131-1143 (2014).
- 124 Tsai, N.-P. *et al.* Multiple autism-linked genes mediate synapse elimination via proteasomal degradation of a synaptic scaffold PSD-95. *Cell* **151**, 1581-1594 (2012).
- 125 Isshiki, M. *et al.* Enhanced synapse remodelling as a common phenotype in mouse models of autism. *Nature communications* **5**, 1-15 (2014).
- 126 Vargas, D. L., Nascimbene, C., Krishnan, C., Zimmerman, A. W. & Pardo, C. A. Neuroglial activation and neuroinflammation in the brain of patients with autism. *Annals of Neurology: Official Journal of the American Neurological Association and the Child Neurology Society* **57**, 67-81 (2005).
- 127 Morgan, J. T. *et al.* Microglial activation and increased microglial density observed in the dorsolateral prefrontal cortex in autism. *Biological psychiatry* **68**, 368-376 (2010).
- 128 Suzuki, K. *et al.* Microglial activation in young adults with autism spectrum disorder. *JAMA psychiatry* **70**, 49-58 (2013).
- 129 Onore, C., Careaga, M. & Ashwood, P. The role of immune dysfunction in the pathophysiology of autism. *Brain, behavior, and immunity* **26**, 383-392 (2012).
- 130 Patterson, P. H. Immune involvement in schizophrenia and autism: etiology, pathology and animal models. *Behavioural brain research* **204**, 313-321 (2009).
- 131 Hsiao, E. Y. & Patterson, P. H. Activation of the maternal immune system induces endocrine changes in the placenta via IL-6. *Brain Behavior and Immunity* **25**, 604-615, doi:10.1016/j.bbi.2010.12.017 (2011).

- 132 Sellgren, C. M. *et al.* Increased synapse elimination by microglia in schizophrenia patient-derived models of synaptic pruning. *Nature Neuroscience* **22**, 374+ (2019).
- 133 Weinberger, D. R. Implications of normal brain development for the pathogenesis of schizophrenia. *Archives of general psychiatry* **44**, 660-669 (1987).
- 134 Cetin-Karayumak, S. *et al.* White matter abnormalities across the lifespan of schizophrenia: a harmonized multi-site diffusion MRI study. *Mol Psychiatry*, doi:10.1038/s41380-019-0509-y (2019).
- 135 Takahashi, K. *et al.* Induction of pluripotent stem cells from adult human fibroblasts by defined factors. *cell* **131**, 861-872 (2007).
- 136 Paşca, S. P. *et al.* Using iPSC-derived neurons to uncover cellular phenotypes associated with Timothy syndrome. *Nature medicine* **17**, 1657 (2011).
- 137 Nadadhur, A. G. *et al.* Neuron-Glia Interactions Increase Neuronal Phenotypes in Tuberous Sclerosis Complex Patient iPSC-Derived Models. *Stem Cell Reports* **12**, 42-56 (2019).
- 138 Nehme, R. *et al.* Combining NGN2 Programming with Developmental Patterning Generates Human Excitatory Neurons with NMDAR-Mediated Synaptic Transmission. *Cell Reports* **23**, 2509-2523 (2018).
- 139 Wang, S. *et al.* Human iPSC-derived oligodendrocyte progenitor cells can myelinate and rescue a mouse model of congenital hypomyelination. *Cell stem cell* **12**, 252-264 (2013).
- 140 Emdad, L., D'Souza, S. L., Kothari, H. P., Qadeer, Z. A. & Germano, I. M. Efficient Differentiation of Human Embryonic and Induced Pluripotent Stem Cells into Functional Astrocytes. *Stem Cells Dev* **21**, 404-410 (2012).
- 141 Haenseler, W. *et al.* A highly efficient human pluripotent stem cell microglia model displays a neuronal-co-culture-specific expression profile and inflammatory response. *Stem cell reports* **8**, 1727-1742 (2017).
- 142 García-León, J. A. *et al.* SOX10 single transcription factor-based fast and efficient generation of oligodendrocytes from human pluripotent stem cells. *Stem cell reports* **10**, 655-672 (2018).
- 143 Canitano, R. & Pallagrosi, M. Autism spectrum disorders and schizophrenia spectrum disorders: excitation/inhibition imbalance and developmental trajectories. *Frontiers in psychiatry* **8**, 69 (2017).
- 144 Nageshappa, S. *et al.* Altered neuronal network and rescue in a human MECP2 duplication model. *Molecular Psychiatry* **21**, 178-188 (2016).
- 145 Chambers, S. M. *et al.* Highly efficient neural conversion of human ES and iPS cells by dual inhibition of SMAD signaling. *Nature biotechnology* **27**, 275-280 (2009).
- 146 Telezhkin, V. *et al.* Forced cell cycle exit and modulation of GABAA, CREB, and GSK3 $\beta$  signaling promote functional maturation of induced pluripotent stem cell-derived neurons. *American Journal of Physiology-Cell Physiology* **310**, C520-C541 (2016).
- 147 Stamou, M., Streifel, K. M., Goines, P. E. & Lein, P. J. Neuronal connectivity as a convergent target of gene x environment interactions that confer risk for Autism Spectrum Disorders. *Neurotoxicology and teratology* **36**, 3-16 (2013).
- 148 van den Heuvel, M. P., Scholtens, L. H., de Reus, M. A. & Kahn, R. S. Associated microscale spine density and macroscale connectivity disruptions in schizophrenia. *Biological psychiatry* **80**, 293-301 (2016).

- 149 Schmitt, A., Simons, M., Cantuti-Castelvetri, L. & Falkai, P. A new role for oligodendrocytes and myelination in schizophrenia and affective disorders? *European Archives of Psychiatry and Clinical Neuroscience* **269**, 371-372 (2019).
- 150 Toker, L., Mancarci, B. O., Tripathy, S. & Pavlidis, P. Transcriptomic Evidence for Alterations in Astrocytes and Parvalbumin Interneurons in Subjects With Bipolar Disorder and Schizophrenia. *Biological Psychiatry* **84**, 787-796 (2018).
- 151 Fields, R. D. White matter in learning, cognition and psychiatric disorders. *Trends in neurosciences* **31**, 361-370 (2008).
- 152 Feng, Y. Convergence and divergence in the etiology of myelin impairment in psychiatric disorders and drug addiction. *Neurochemical research* **33**, 1940-1949 (2008).
- 153 Sokolov, B. P. Oligodendroglial abnormalities in schizophrenia, mood disorders and substance abuse. Comorbidity, shared traits, or molecular phenocopies? *International Journal of Neuropsychopharmacology* **10**, 547-555 (2007).
- 154 Tkachev, D. *et al.* Oligodendrocyte dysfunction in schizophrenia and bipolar disorder. *Lancet* **362**, 798-805 (2003).
- 155 Wang, S. *et al.* Human iPSC-Derived Oligodendrocyte Progenitor Cells Can Myelinate and Rescue a Mouse Model of Congenital Hypomyelination. *Cell Stem Cell* **12**, 252-264, doi:10.1016/j.stem.2012.12.002 (2013).
- 156 Douvaras, P. *et al.* Efficient generation of myelinating oligodendrocytes from primary progressive multiple sclerosis patients by induced pluripotent stem cells. *Stem Cell Reports* **3**, 250-259 (2014).
- 157 Trujillo, C. A. & Muotri, A. R. Brain Organoids and the Study of Neurodevelopment. *Trends Mol Med* **24**, 982-990 (2018).
- 158 Qi, Y. *et al.* Combined small-molecule inhibition accelerates the derivation of functional cortical neurons from human pluripotent stem cells. *Nature biotechnology* **35**, 154-163 (2017).
- 159 Douvaras, P. & Fossati, V. Generation and isolation of oligodendrocyte progenitor cells from human pluripotent stem cells. *Nat. Protocols* **10**, 1143-1154 (2015).
- 160 Jang, M. J. & Nam, Y. NeuroCa: integrated framework for systematic analysis of spatiotemporal neuronal activity patterns from large-scale optical recording data. *Neurophotonics* **2**, 035003 (2015).
- 161 Patel, T. P., Man, K., Firestein, B. L. & Meaney, D. F. Automated quantification of neuronal networks and single-cell calcium dynamics using calcium imaging. *J Neurosci Methods* **243**, 26-38 (2015).
- 162 McQuin, C. *et al.* CellProfiler 3.0: Next-generation image processing for biology. *Plos Biol* **16**, e2005970 (2018).
- 163 Schneider, C. A., Rasband, W. S. & Eliceiri, K. W. NIH Image to ImageJ: 25 years of image analysis. *Nat Methods* **9**, 671-675 (2012).
- 164 Fantuzzo, J. A. *et al.* Intellicount: High-Throughput Quantification of Fluorescent Synaptic Protein Puncta by Machine Learning. *eNeuro* **4** (2017).
- 165 Wang, X., Spandidos, A., Wang, H. & Seed, B. PrimerBank: a PCR primer database for quantitative gene expression analysis, 2012 update. *Nucleic Acids Res* **40**, 1144-1149 (2012).
- 166 Livak, K. J. & Schmittgen, T. D. Analysis of relative gene expression data using real-time quantitative PCR and the 2- $\Delta\Delta$ CT method. *methods* **25**, 402-408 (2001).
- 167 Kendall, K. M. *et al.* Cognitive Performance Among Carriers of Pathogenic Copy Number Variants: Analysis of 152,000 UK Biobank Subjects. *Biological Psychiatry* **82**, 103-110 (2017).

- 168 Miller, K. L. *et al.* Multimodal population brain imaging in the UK Biobank prospective epidemiological study. *Nature Neuroscience* **19**, 1523-1536 (2016).
- 169 Alfaro-Almagro, F. *et al.* Image processing and Quality Control for the first 10,000 brain imaging datasets from UK Biobank. *Neuroimage* **166**, 400-424 (2018).
- 170 Warland, A., Kendall, K. M., Rees, E., Kirov, G. & Caseras, X. Schizophrenia-associated genomic copy number variants and subcortical brain volumes in the UK Biobank. *Mol Psychiatry* (2019).
- 171 Benjamini, Y. & Hochberg, Y. Controlling the False Discovery Rate - a Practical and Powerful Approach to Multiple Testing. *Journal of the Royal Statistical Society Series B-Statistical Methodology* **57**, 289-300 (1995).
- 172 Knapp, T. R. Statistical Power Analysis for the Behavioral-Sciences, 2nd Edition - Cohen, J. *Educational and Psychological Measurement* **50**, 225-227 (1990).
- 173 Silva, A. I. *et al.* Reciprocal White Matter Changes Associated With Copy Number Variation at 15q11.2 BP1-BP2: A Diffusion Tensor Imaging Study. *Biological Psychiatry* **85**, 563-572 (2019).
- 174 Yuan, F. *et al.* Generation of a KCNJ11 homozygous knockout human embryonic stem cell line WAe001-A-12 using CRISPR/Cas9. *Stem Cell Res* **24**, 89-93 (2017).
- 175 Sese, M. *et al.* Hypoxia-mediated translational activation of ITGB3 in breast cancer cells enhances TGF-beta signaling and malignant features in vitro and in vivo. *Oncotarget* **8**, 114856-114876 (2017).
- 176 Prihantono, P. *et al.* Ki-67 Expression by Immunohistochemistry and Quantitative Real-Time Polymerase Chain Reaction as Predictor of Clinical Response to Neoadjuvant Chemotherapy in Locally Advanced Breast Cancer. *J Oncol* **2017**, 6209849 (2017).
- 177 Hu, B. Y., Du, Z. W., Li, X. J., Ayala, M. & Zhang, S. C. Human oligodendrocytes from embryonic stem cells: conserved SHH signaling networks and divergent FGF effects. *Development* **136**, 1443-1452 (2009).
- 178 Ren, J. J. & Meng, X. K. A relative quantitative method to detect OCT4A gene expression by exon-junction primer and locked nucleic acid-modified probe. *J Zhejiang Univ Sci B* **12**, 149-155 (2011).
- 179 Jiang, Z. *et al.* eIF2alpha Phosphorylation-dependent translation in CA1 pyramidal cells impairs hippocampal memory consolidation without affecting general translation. *J Neurosci* **30**, 2582-2594 (2010).
- 180 Zhang, H. *et al.* Reprogramming A375 cells to inducedresembled neuronal cells by structured overexpression of specific transcription genes. *Mol Med Rep* **14**, 3134-3144 (2016).
- 181 Varghese, D. S., Parween, S., Ardah, M. T., Emerald, B. S. & Ansari, S. A. Effects of Aminoglycoside Antibiotics on Human Embryonic Stem Cell Viability during Differentiation In Vitro. *Stem Cells Int* **2017**, 2451927 (2017).
- 182 Ehm, O. *et al.* RBPJkappa-dependent signaling is essential for long-term maintenance of neural stem cells in the adult hippocampus. *J Neurosci* **30**, 13794-13807 (2010).
- 183 Boros, E. *et al.* Elevated Expression of AXL May Contribute to the Epithelial-to-Mesenchymal Transition in Inflammatory Bowel Disease Patients. *Mediators Inflamm* **2018**, 3241406 (2018).
- 184 Zhang, S.-C., Wernig, M., Duncan, I. D., Brüstle, O. & Thomson, J. A. In vitro differentiation of transplantable neural precursors from human embryonic stem cells. *Nature biotechnology* **19**, 1129 (2001).

- 185 Hu, B.-Y. & Zhang, S.-C. Differentiation of spinal motor neurons from pluripotent  
human stem cells. *Nature protocols* **4**, 1295 (2009).
- 186 Crawford, T. Q. & Roelink, H. The notch response inhibitor DAPT enhances  
neuronal differentiation in embryonic stem cell-derived embryoid bodies  
independently of sonic hedgehog signaling. *Developmental dynamics: an official  
publication of the American Association of Anatomists* **236**, 886-892 (2007).
- 187 Kemp, P. J. *et al.* Improving and accelerating the differentiation and functional  
maturation of human stem cell-derived neurons: role of extracellular calcium and  
GABA. *The Journal of physiology* **594**, 6583-6594 (2016).
- 188 Gunhanlar, N. *et al.* A simplified protocol for differentiation of  
electrophysiologically mature neuronal networks from human induced pluripotent  
stem cells. *Mol Psychiatry* **23**, 1336-1344 (2018).
- 189 Tian, Y. *et al.* Alteration in basal and depolarization induced transcriptional  
network in iPSC derived neurons from Timothy syndrome. *Genome Med* **6** (2014).
- 190 Lin, M. Y. *et al.* Integrative transcriptome network analysis of iPSC-derived  
neurons from schizophrenia and schizoaffective disorder patients with 22q11.2  
deletion. *Bmc Syst Biol* **10** (2016).
- 191 Gorski, J. A. *et al.* Cortical Excitatory Neurons and Glia, But Not GABAergic  
Neurons, Are Produced in the Emx1-Expressing Lineage. *The Journal of  
Neuroscience* **22**, 6309-6314 (2002).
- 192 Hu, J. S., Vogt, D., Sandberg, M. & Rubenstein, J. L. Cortical interneuron  
development: a tale of time and space. *Development* **144**, 3867-3878 (2017).
- 193 Hutsler, J. J., Lee, D. G. & Porter, K. K. Comparative analysis of cortical layering and  
supragranular layer enlargement in rodent carnivore and primate species. *Brain  
Res* **1052**, 71-81 (2005).
- 194 Rimol, L. M. *et al.* Cortical Volume, Surface Area, and Thickness in Schizophrenia  
and Bipolar Disorder. *Biological Psychiatry* **71**, 552-560 (2012).
- 195 Hartberg, C. B. *et al.* Cortical thickness, cortical surface area and subcortical  
volumes in schizophrenia and bipolar disorder patients with cannabis use. *Eur  
Neuropsychopharm* **28**, 37-47 (2018).
- 196 Shaw, P., Gogtay, N. & Rapoport, J. Childhood Psychiatric Disorders as Anomalies  
in Neurodevelopmental Trajectories. *Hum Brain Mapp* **31**, 917-925 (2010).
- 197 Schumann, C. M. *et al.* Longitudinal Magnetic Resonance Imaging Study of Cortical  
Development through Early Childhood in Autism. *Journal of Neuroscience* **30**,  
4419-4427 (2010).
- 198 Wallace, G. L., Dankner, N., Kenworthy, L., Giedd, J. N. & Martin, A. Age-related  
temporal and parietal cortical thinning in autism spectrum disorders. *Brain* **133**,  
3745-3754 (2010).
- 199 Hodgkinson. Disrupted in schizophrenia 1 (DISC1): Association with schizophrenia,  
schizoaffective disorder, and bipolar disorder (vol 75, pg 862, 2004). *American  
Journal of Human Genetics* **76**, 196-196 (2005).
- 200 Kamiya, A. *et al.* A schizophrenia-associated mutation of DISC1 perturbs cerebral  
cortex development. *Nature Cell Biology* **7**, 1167-1178 (2005).
- 201 Sun, Z., Williams, D. J., Xu, B. & Gogos, J. A. Altered function and maturation of  
primary cortical neurons from a 22q11.2 deletion mouse model of schizophrenia.  
*Transl Psychiatry* **8**, 85 (2018).
- 202 Shu, Y. S., Hasenstaub, A. & McCormick, D. A. Turning on and off recurrent  
balanced cortical activity. *Nature* **423**, 288-293 (2003).

- 203 Chattopadhyaya, B. & Cristo, G. D. GABAergic circuit dysfunctions in neurodevelopmental disorders. *Front Psychiatry* **3**, 51 (2012).
- 204 Glausier, J. R. & Lewis, D. A. Dendritic spine pathology in schizophrenia. *Neuroscience* **251**, 90-107 (2013).
- 205 Hutsler, J. J. & Zhang, H. Increased dendritic spine densities on cortical projection neurons in autism spectrum disorders. *Brain Res* **1309**, 83-94 (2010).
- 206 Konopaske, G. T., Lange, N., Coyle, J. T. & Benes, F. M. Prefrontal cortical dendritic spine pathology in schizophrenia and bipolar disorder. *JAMA Psychiatry* **71**, 1323-1331 (2014).
- 207 de Bartolomeis, A., Latte, G., Tomasetti, C. & Iasevoli, F. Glutamatergic Postsynaptic Density Protein Dysfunctions in Synaptic Plasticity and Dendritic Spines Morphology: Relevance to Schizophrenia and Other Behavioral Disorders Pathophysiology, and Implications for Novel Therapeutic Approaches. *Molecular Neurobiology* **49**, 484-511 (2014).
- 208 Leblond, C. S. *et al.* Meta-analysis of SHANK Mutations in Autism Spectrum Disorders: a gradient of severity in cognitive impairments. *PLoS Genet* **10**, e1004580 (2014).
- 209 Mueller, H. T. & Meador-Woodruff, J. H. NR3A NMDA receptor subunit mRNA expression in schizophrenia, depression and bipolar disorder. *Schizophrenia Research* **71**, 361-370 (2004).
- 210 Demontis, D. *et al.* Association of GRIN1 and GRIN2A-D with schizophrenia and genetic interaction with maternal herpes simplex virus-2 infection affecting disease risk. *Am J Med Genet B Neuropsychiatr Genet* **156B**, 913-922 (2011).
- 211 Banerjee, A., Macdonald, M. L., Borgmann-Winter, K. E. & Hahn, C. G. Neuregulin 1-erbB4 pathway in schizophrenia: From genes to an interactome. *Brain Res Bull* **83**, 132-139 (2010).
- 212 Perez-Garcia, C. G. ErbB4 in Laminated Brain Structures: A Neurodevelopmental Approach to Schizophrenia. *Front Cell Neurosci* **9**, 472 (2015).
- 213 Guidotti, A. *et al.* Decrease in reelin and glutamic acid decarboxylase67 (GAD67) expression in schizophrenia and bipolar disorder: a postmortem brain study. *Arch Gen Psychiatry* **57**, 1061-1069 (2000).
- 214 Thompson Ray, M., Weickert, C. S., Wyatt, E. & Webster, M. J. Decreased BDNF, trkB-TK+ and GAD67 mRNA expression in the hippocampus of individuals with schizophrenia and mood disorders. *J Psychiatry Neurosci* **36**, 195-203 (2011).
- 215 Akbarian, S. & Huang, H. S. Molecular and cellular mechanisms of altered GAD1/GAD67 expression in schizophrenia and related disorders. *Brain Res Rev* **52**, 293-304 (2006).
- 216 Davenport, E. C. *et al.* Autism and Schizophrenia-Associated CYFIP1 Regulates the Balance of Synaptic Excitation and Inhibition. *Cell Rep* **26**, 2037-2051 e2036 (2019).
- 217 Grayton, H. M., Missler, M., Collier, D. A. & Fernandes, C. Altered Social Behaviours in Neurexin 1 alpha Knockout Mice Resemble Core Symptoms in Neurodevelopmental Disorders. *Plos One* **8** (2013).
- 218 De Rubeis, S. *et al.* CYFIP1 Coordinates mRNA Translation and Cytoskeleton Remodeling to Ensure Proper Dendritic Spine Formation. *Neuron* **79**, 1169-1182 (2013).
- 219 Bozdagi, O. *et al.* Haploinsufficiency of Cyfip1 Produces Fragile X-Like Phenotypes in Mice. *Plos One* **7** (2012).

- 220 Das, D. K. *et al.* Genetic and morphological features of human iPSC-derived neurons with chromosome 15q11.2 (BP1-BP2) deletions. *Mol Neuropsychiatry* **1**, 116-123 (2015).
- 221 Toyoshima, M. *et al.* Analysis of induced pluripotent stem cells carrying 22q11.2 deletion. *Transl Psychiatry* **6**, e934 (2016).
- 222 Zhao, D. J. *et al.* MicroRNA Profiling of Neurons Generated Using Induced Pluripotent Stem Cells Derived from Patients with Schizophrenia and Schizoaffective Disorder, and 22q11.2 Del. *Plos One* **10** (2015).
- 223 Shcheglovitov, A. *et al.* SHANK3 and IGF1 restore synaptic deficits in neurons from 22q13 deletion syndrome patients. *Nature* **503**, 267 (2013).
- 224 Deshpande, A. *et al.* Cellular Phenotypes in Human iPSC-Derived Neurons from a Genetic Model of Autism Spectrum Disorder. *Cell Reports* **21**, 2678-2687 (2017).
- 225 Hoffman, G. E. *et al.* Transcriptional signatures of schizophrenia in hiPSC-derived NPCs and neurons are concordant with post-mortem adult brains. *Nature Communications* **8** (2017).
- 226 Wen, Z. X. *et al.* Synaptic dysregulation in a human iPS cell model of mental disorders. *Nature* **515**, 414-+ (2014).
- 227 Yoon, K. J. *et al.* Modeling a Genetic Risk for Schizophrenia in iPSCs and Mice Reveals Neural Stem Cell Deficits Associated with Adherens Junctions and Polarity. *Cell Stem Cell* **15**, 79-91 (2014).
- 228 Topol, A. *et al.* Altered WNT Signaling in Human Induced Pluripotent Stem Cell Neural Progenitor Cells Derived from Four Schizophrenia Patients. *Biological Psychiatry* **78**, E29-E34 (2015).
- 229 Robicsek, O. *et al.* Abnormal neuronal differentiation and mitochondrial dysfunction in hair follicle-derived induced pluripotent stem cells of schizophrenia patients. *J Mol Neurosci* **51**, S100-S100 (2013).
- 230 Yoon, K. J. *et al.* Modeling a Genetic Risk for Schizophrenia in iPSCs and Mice Reveals Neural Stem Cell Deficits Associated with Adherens Junctions and Polarity (vol 15, pg 79, 2014). *Cell Stem Cell* **16**, 339-339 (2015).
- 231 Brennand, K. Modeling Schizophrenia Using Human Induced Pluripotent Stem Cells. *Biological Psychiatry* **71**, 24s-24s (2012).
- 232 Hartley, B. J., Tran, N., Ladrán, I., Reggio, K. & Brennand, K. J. Dopaminergic differentiation of schizophrenia hiPSCs. *Molecular Psychiatry* **20**, 549-550 (2015).
- 233 Hook, V. *et al.* Human iPSC Neurons Display Activity-Dependent Neurotransmitter Secretion: Aberrant Catecholamine Levels in Schizophrenia Neurons. *Stem Cell Reports* **3**, 531-538 (2014).
- 234 Roussos, P., Guennewig, B., Kaczorowski, D. C., Barry, G. & Brennand, K. J. Activity-Dependent Changes in Gene Expression in Schizophrenia Human-Induced Pluripotent Stem Cell Neurons. *Jama Psychiatry* **73**, 1180-1188 (2016).
- 235 Barry, G. *et al.* The long non-coding RNA Gomafu is acutely regulated in response to neuronal activation and involved in schizophrenia-associated alternative splicing. *Molecular Psychiatry* **19**, 486-494 (2014).
- 236 Marchetto, M. C. N. *et al.* A Model for Neural Development and Treatment of Rett Syndrome Using Human Induced Pluripotent Stem Cells. *Cell* **143**, 527-539 (2010).
- 237 Tropea, D. *et al.* Partial reversal of Rett Syndrome-like symptoms in MeCP2 mutant mice. *Proceedings of the National Academy of Sciences of the United States of America* **106**, 2029-2034 (2009).

- 238 Sheridan, S. Epigenetic characterization of the FMR1 gene and aberrant neurodevelopment in human induced pluripotent stem cell models of fragile X syndrome. *Abstr Pap Am Chem S* **243** (2012).
- 239 Doers, M. E. *et al.* iPSC-Derived Forebrain Neurons from FXS Individuals Show Defects in Initial Neurite Outgrowth. *Stem Cells Dev* **23**, 1777-1787 (2014).
- 240 Irwin, S. A. *et al.* Abnormal dendritic spine characteristics in the temporal and visual cortices of patients with fragile-X syndrome: A quantitative examination. *American Journal of Medical Genetics* **98**, 161-167 (2001).
- 241 Griesi-Oliveira, K. *et al.* Modeling non-syndromic autism and the impact of TRPC6 disruption in human neurons. *Mol Psychiatry* **20**, 1350-1365 (2015).
- 242 Zaslavsky, K. *et al.* SHANK2 mutations associated with autism spectrum disorder cause hyperconnectivity of human neurons. *Nat Neurosci* **22**, 556-564 (2019).
- 243 Deneault, E. *et al.* CNTN5(-)/(+) or EHMT2(-)/(+) human iPSC-derived neurons from individuals with autism develop hyperactive neuronal networks. *Elife* **8** (2019).
- 244 Schafer, S. T. *et al.* Pathological priming causes developmental gene network heterochronicity in autistic subject-derived neurons. *Nature neuroscience* **22**, 243 (2019).
- 245 Yuan, S. H. *et al.* Cell-surface marker signatures for the isolation of neural stem cells, glia and neurons derived from human pluripotent stem cells. *PLoS One* **6**, e17540 (2011).
- 246 Shi, Y., Kirwan, P., Smith, J., Robinson, H. P. & Livesey, F. J. Human cerebral cortex development from pluripotent stem cells to functional excitatory synapses. *Nat Neurosci* **15**, 477-486, S471 (2012).
- 247 Plumbly, W., Brandon, N., Deeb, T. Z., Hall, J. & Harwood, A. J. L-type voltage-gated calcium channel regulation of in vitro human cortical neuronal networks. *Sci Rep* **9**, 13810 (2019).
- 248 Kedracka-Krok, S. *et al.* Clozapine influences cytoskeleton structure and calcium homeostasis in rat cerebral cortex and has a different proteomic profile than risperidone. *Journal of Neurochemistry* **132**, 657-676 (2015).
- 249 Choi, K. H. & Rhim, H. Inhibition of recombinant Ca(v)3.1 (alpha(1G)) T-type calcium channels by the antipsychotic drug clozapine. *Eur J Pharmacol* **626**, 123-130, doi: (2010).
- 250 Wiemann, M., Jones, D., Straub, H., Altrup, U. & Speckmann, E. J. Simultaneous blockade of intracellular calcium increases and of neuronal epileptiform depolarizations by verapamil. *Brain Res* **734**, 49-54 (1996).
- 251 Brewer, L. D. *et al.* Vitamin D hormone confers neuroprotection in parallel with downregulation of L-type calcium channel expression in hippocampal neurons. *Journal of Neuroscience* **21**, 98-108 (2001).
- 252 Yan, Z., Chi, P., Bibb, J. A., Ryan, T. A. & Greengard, P. Roscovitine: a novel regulator of P/Q-type calcium channels and transmitter release in central neurons. *J Physiol* **540**, 761-770 (2002).
- 253 Kim, K. Y., Hysolli, E. & Park, I. H. Neuronal maturation defect in induced pluripotent stem cells from patients with Rett syndrome. *Proc Natl Acad Sci U S A* **108**, 14169-14174 (2011).
- 254 Mariani, J. *et al.* FOXG1-Dependent Dysregulation of GABA/Glutamate Neuron Differentiation in Autism Spectrum Disorders. *Cell* **162**, 375-390 (2015).
- 255 Suzuki, I. K. *et al.* Human-Specific NOTCH2NL Genes Expand Cortical Neurogenesis through Delta/Notch Regulation. *Cell* **173**, 1370-+ (2018).

- 256 Yoon, K. J. *et al.* Modeling a genetic risk for schizophrenia in iPSCs and mice reveals neural stem cell deficits associated with adherens junctions and polarity. *Cell Stem Cell* **15**, 79-91 (2014).
- 257 Pierri, J. N., Volk, C. L., Auh, S., Sampson, A. & Lewis, D. A. Somal size of prefrontal cortical pyramidal neurons in schizophrenia: differential effects across neuronal subpopulations. *Biol Psychiatry* **54**, 111-120 (2003).
- 258 Sweet, R. A., Pierri, J. N., Auh, S., Sampson, A. R. & Lewis, D. A. Reduced pyramidal cell somal volume in auditory association cortex of subjects with schizophrenia. *Neuropsychopharmacology* **28**, 599-609 (2003).
- 259 Pennington, K., Dicker, P., Hudson, L. & Cotter, D. R. Evidence for reduced neuronal somal size within the insular cortex in schizophrenia, but not in affective disorders. *Schizophrenia Research* **106**, 164-171 (2008).
- 260 Black, J. E. *et al.* Pathology of layer v pyramidal neurons in the prefrontal cortex of patients with schizophrenia. *American Journal of Psychiatry* **161**, 742-744 (2004).
- 261 Broadbelt, K., Byne, W. & Jones, L. B. Evidence for a decrease in basilar dendrites of pyramidal cells in schizophrenic medial prefrontal cortex. *Schizophr Res* **58**, 75-81 (2002).
- 262 Perrone-Bizzozero, N. I. *et al.* Levels of the growth-associated protein GAP-43 are selectively increased in association cortices in schizophrenia. *Proc Natl Acad Sci U S A* **93**, 14182-14187 (1996).
- 263 Glantz, L. A. & Lewis, D. A. Reduction of synaptophysin immunoreactivity in the prefrontal cortex of subjects with schizophrenia. Regional and diagnostic specificity. *Arch Gen Psychiatry* **54**, 943-952 (1997).
- 264 Glessner, J. T., Connolly, J. J. & Hakonarson, H. Genome-wide association studies of autism. *Current Behavioral Neuroscience Reports* **1**, 234-241 (2014).
- 265 Lu, A. T. H., Dai, X. X., Martinez-Agosto, J. A. & Cantor, R. M. Support for calcium channel gene defects in autism spectrum disorders. *Mol Autism* **3** (2012).
- 266 Wen, Y., Alshikho, M. J. & Herbert, M. R. Pathway Network Analyses for Autism Reveal Multisystem Involvement, Major Overlaps with Other Diseases and Convergence upon MAPK and Calcium Signaling. *Plos One* **11** (2016).
- 267 Pinggera, A. *et al.* CACNA1D De Novo Mutations in Autism Spectrum Disorders Activate Cav1.3 L-Type Calcium Channels. *Biological Psychiatry* **77**, 816-822 (2015).
- 268 Splawski, I. *et al.* Ca(V)1.2 calcium channel dysfunction causes a multisystem disorder including arrhythmia and autism. *Cell* **119**, 19-31 (2004).
- 269 Schmunk, G., Boubion, B. J., Smith, I. F., Parker, I. & Gargus, J. J. Shared functional defect in IP3R-mediated calcium signaling in diverse monogenic autism syndromes. *Translational Psychiatry* **5** (2015).
- 270 Vallipuram, J., Grenville, J. & Crawford, D. A. The E646D-ATP13A4 Mutation Associated with Autism Reveals a Defect in Calcium Regulation. *Cell Mol Neurobiol* **30**, 233-246 (2010).
- 271 Garcia-Junco-Clemente, P. *et al.* Overexpression of calcium-activated potassium channels underlies cortical dysfunction in a model of PTEN-associated autism. *Proceedings of the National Academy of Sciences of the United States of America* **110**, 18297-18302 (2013).
- 272 Palmieri, L. *et al.* Altered calcium homeostasis in autism-spectrum disorders: evidence from biochemical and genetic studies of the mitochondrial aspartate/glutamate carrier AGC1. *Molecular Psychiatry* **15**, 38-52 (2010).
- 273 Buraei, Z., Schofield, G. & Elmslie, K. S. Roscovitine differentially affects CaV2 and Kv channels by binding to the open state. *Neuropharmacology* **52**, 883-894 (2007).

- 274 Meijer, L. *et al.* Biochemical and cellular effects of roscovitine, a potent and selective inhibitor of the cyclin-dependent kinases cdc2, cdk2 and cdk5. *Eur J Biochem* **243**, 527-536 (1997).
- 275 Gutierrez, R. C. *et al.* Altered Synchrony and Connectivity in Neuronal Networks Expressing an Autism-Related Mutation of Neuroligin 3. *Neuroscience* **162**, 208-221 (2009).
- 276 Penagarikano, O. *et al.* Absence of CNTNAP2 Leads to Epilepsy, Neuronal Migration Abnormalities, and Core Autism-Related Deficits. *Cell* **147**, 235-246 (2011).
- 277 Lu, C. *et al.* Micro-electrode array recordings reveal reductions in both excitation and inhibition in cultured cortical neuron networks lacking Shank3. *Molecular Psychiatry* **21**, 159-168 (2016).
- 278 Krystal, J. H. *et al.* Subanesthetic effects of the noncompetitive NMDA antagonist, ketamine, in humans. Psychotomimetic, perceptual, cognitive, and neuroendocrine responses. *Arch Gen Psychiatry* **51**, 199-214 (1994).
- 279 Poels, E. M. *et al.* Glutamatergic abnormalities in schizophrenia: a review of proton MRS findings. *Schizophr Res* **152**, 325-332 (2014).
- 280 Howes, O., McCutcheon, R. & Stone, J. Glutamate and dopamine in schizophrenia: an update for the 21st century. *J Psychopharmacol* **29**, 97-115 (2015).
- 281 Gordon, A. *et al.* Transcriptomic networks implicate neuronal energetic abnormalities in three mouse models harboring autism and schizophrenia-associated mutations. *Mol Psychiatry* (2019).
- 282 Tseng, K. Y. *et al.* A neonatal ventral hippocampal lesion causes functional deficits in adult prefrontal cortical interneurons. *J Neurosci* **28**, 12691-12699 (2008).
- 283 Feleder, C., Tseng, K. Y., Calhoon, G. G. & O'Donnell, P. Neonatal intrahippocampal immune challenge alters dopamine modulation of prefrontal cortical interneurons in adult rats. *Biol Psychiatry* **67**, 386-392 (2010).
- 284 Matrisciano, F. *et al.* Epigenetic modifications of GABAergic interneurons are associated with the schizophrenia-like phenotype induced by prenatal stress in mice. *Neuropharmacology* **68**, 184-194 (2013).
- 285 Shao, Z. C. *et al.* Dysregulated protocadherin-pathway activity as an intrinsic defect in induced pluripotent stem cell-derived cortical interneurons from subjects with schizophrenia. *Nature Neuroscience* **22**, 229-+ (2019).
- 286 Chung, D. W., Chung, Y., Bazmi, H. H. & Lewis, D. A. Altered ErbB4 splicing and cortical parvalbumin interneuron dysfunction in schizophrenia and mood disorders. *Neuropsychopharmacology* **43**, 2478-2486 (2018).
- 287 Ni, P. *et al.* Correction: iPSC-derived homogeneous populations of developing schizophrenia cortical interneurons have compromised mitochondrial function. *Molecular psychiatry*, 1-2 (2019).
- 288 Yu, Q. B. *et al.* Brain Connectivity Networks in Schizophrenia Underlying Resting State Functional Magnetic Resonance Imaging. *Current Topics in Medicinal Chemistry* **12**, 2415-2425 (2012).
- 289 Fitzsimmons, J., Kubicki, M. & Shenton, M. E. Review of functional and anatomical brain connectivity findings in schizophrenia. *Current Opinion in Psychiatry* **26**, 172-187 (2013).
- 290 Bells, S. *et al.* White matter plasticity and maturation in human cognition. *Glia* **67**, 2020-2037 (2019).
- 291 Kanai, R. & Rees, G. OPINION The structural basis of inter-individual differences in human behaviour and cognition. *Nature Reviews Neuroscience* **12**, 231-242 (2011).

- 292 Crespi, C. *et al.* Microstructural white matter correlates of emotion recognition  
impairment in Amyotrophic Lateral Sclerosis. *Cortex* **53**, 1-8 (2014).
- 293 Hadders-Algra, M. Reduced variability in motor behaviour: An indicator of  
impaired cerebral connectivity? *Early Human Development* **84**, 787-789 (2008).
- 294 Semple, B. D., Blomgren, K., Gimlin, K., Ferriero, D. M. & Noble-Haeusslein, L. J.  
Brain development in rodents and humans: Identifying benchmarks of maturation  
and vulnerability to injury across species. *Prog Neurobiol* **106**, 1-16 (2013).
- 295 Young, K. M. *et al.* Oligodendrocyte dynamics in the healthy adult CNS: evidence  
for myelin remodeling. *Neuron* **77**, 873-885 (2013).
- 296 Bergles, D. E. & Richardson, W. D. Oligodendrocyte Development and Plasticity.  
*Cold Spring Harbor Perspectives in Biology* **8** (2016).
- 297 Kutzelnigg, A. *et al.* Cortical demyelination and diffuse white matter injury in  
multiple sclerosis. *Brain* **128**, 2705-2712 (2005).
- 298 de Castro, F., Bribian, A. & Ortega, M. C. Regulation of oligodendrocyte precursor  
migration during development, in adulthood and in pathology. *Cellular and  
Molecular Life Sciences* **70**, 4355-4368 (2013).
- 299 Tekki-Kessarar, N. *et al.* Hedgehog-dependent oligodendrocyte lineage  
specification in the telencephalon. *Development* **128**, 2545-2554 (2001).
- 300 Kessarar, N. *et al.* Competing waves of oligodendrocytes in the forebrain and  
postnatal elimination of an embryonic lineage. *Nature neuroscience* **9**, 173 (2006).
- 301 Klämbt, C. Modes and regulation of glial migration in vertebrates and  
invertebrates. *Nature Reviews Neuroscience* **10**, 769 (2009).
- 302 Chapman, H., Waclaw, R. R., Pei, Z., Nakafuku, M. & Campbell, K. The homeobox  
gene *Gsx2* controls the timing of oligodendroglial fate specification in mouse  
lateral ganglionic eminence progenitors. *Development* **140**, 2289-2298 (2013).
- 303 Kiesepä, T. *et al.* Reduced left hemispheric white matter volume in twins with  
bipolar I disorder. *Biological psychiatry* **54**, 896-905 (2003).
- 304 Pol, H. E. H. *et al.* Gray and white matter volume abnormalities in monozygotic  
and same-gender dizygotic twins discordant for schizophrenia. *Biological  
psychiatry* **55**, 126-130 (2004).
- 305 Lim, K. & Helpert, J. Neuropsychiatric applications of DTI—a review. *NMR in  
Biomedicine* **15**, 587-593 (2002).
- 306 Barnea-Goraly, N. *et al.* White matter development during childhood and  
adolescence: a cross-sectional diffusion tensor imaging study. *Cerebral cortex* **15**,  
1848-1854 (2005).
- 307 Buchsbaum, M. S. *et al.* MRI white matter diffusion anisotropy and PET metabolic  
rate in schizophrenia. *Neuroreport* **9**, 425-430 (1998).
- 308 Whitford, T. J., Kubicki, M. & Shenton, M. E. Diffusion tensor imaging, structural  
connectivity, and schizophrenia. *Schizophrenia research and treatment* **2011**  
(2011).
- 309 Hof, P. R. *et al.* Loss and altered spatial distribution of oligodendrocytes in the  
superior frontal gyrus in schizophrenia. *Biological psychiatry* **53**, 1075-1085 (2003).
- 310 Uranova, N. A., Vostrikov, V. M., Orlovskaya, D. D. & Rachmanova, V. I.  
Oligodendroglial density in the prefrontal cortex in schizophrenia and mood  
disorders: a study from the Stanley Neuropathology Consortium. *Schizophrenia  
research* **67**, 269-275 (2004).
- 311 Tkachev, D. *et al.* Oligodendrocyte dysfunction in schizophrenia and bipolar  
disorder. *The Lancet* **362**, 798-805 (2003).

- 312 Georgieva, L. *et al.* Convergent evidence that oligodendrocyte lineage transcription factor 2 (OLIG2) and interacting genes influence susceptibility to schizophrenia. *Proceedings of the National Academy of Sciences* **103**, 12469-12474 (2006).
- 313 Maeno, N. *et al.* Association of SOX10 with schizophrenia in the Japanese population. *Psychiatric genetics* **17**, 227-231 (2007).
- 314 Hakak, Y. *et al.* Genome-wide expression analysis reveals dysregulation of myelination-related genes in chronic schizophrenia. *Proceedings of the National Academy of Sciences* **98**, 4746-4751 (2001).
- 315 Song, S.-K. *et al.* Diffusion tensor imaging detects and differentiates axon and myelin degeneration in mouse optic nerve after retinal ischemia. *Neuroimage* **20**, 1714-1722 (2003).
- 316 Nair, G. *et al.* Myelination and long diffusion times alter diffusion-tensor-imaging contrast in myelin-deficient shiverer mice. *Neuroimage* **28**, 165-174 (2005).
- 317 Silva, A. I. *et al.* Cyfip1 haploinsufficient rats show white matter changes, myelin thinning, abnormal oligodendrocytes and behavioural inflexibility. *Nature Communications* **10** (2019).
- 318 Franco-Pons, N., Torrente, M., Colomina, M. T. & Vilella, E. Behavioral deficits in the cuprizone-induced murine model of demyelination/remyelination. *Toxicology letters* **169**, 205-213 (2007).
- 319 Xu, H. *et al.* Behavioral and neurobiological changes in C57BL/6 mice exposed to cuprizone. *Behavioral neuroscience* **123**, 418 (2009).
- 320 Makinodan, M. *et al.* Lysophosphatidylcholine induces delayed myelination in the juvenile ventral hippocampus and behavioral alterations in adulthood. *Neurochemistry international* **53**, 374-381 (2008).
- 321 Edgar, N. & Sibille, E. A putative functional role for oligodendrocytes in mood regulation. *Translational psychiatry* **2**, e109 (2012).
- 322 Edgar, N., Touma, C., Palme, R. & Sibille, E. Resilient emotionality and molecular compensation in mice lacking the oligodendrocyte-specific gene *Cnp1*. *Translational psychiatry* **1**, e42 (2011).
- 323 Hagemeyer, N. *et al.* A myelin gene causative of a catatonia-depression syndrome upon aging. *EMBO molecular medicine* **4**, 528-539 (2012).
- 324 Peirce, T. R. *et al.* Convergent evidence for 2', 3'-cyclic nucleotide 3'-phosphodiesterase as a possible susceptibility gene for schizophrenia. *Archives of general psychiatry* **63**, 18-24 (2006).
- 325 Lindahl, J. S., Kjellsen, B. R., Tigert, J. & Miskimins, R. In utero PCP exposure alters oligodendrocyte differentiation and myelination in developing rat frontal cortex. *Brain research* **1234**, 137-147 (2008).
- 326 Czéh, B. *et al.* Chronic social stress inhibits cell proliferation in the adult medial prefrontal cortex: hemispheric asymmetry and reversal by fluoxetine treatment. *Neuropsychopharmacology* **32**, 1490-1503 (2007).
- 327 Banasr, M. *et al.* Chronic unpredictable stress decreases cell proliferation in the cerebral cortex of the adult rat. *Biological psychiatry* **62**, 496-504 (2007).
- 328 de Vrij, F. M. *et al.* Candidate CSPG4 mutations and induced pluripotent stem cell modeling implicate oligodendrocyte progenitor cell dysfunction in familial schizophrenia. *Molecular Psychiatry* **24**, 757-771 (2019).
- 329 Windrem, M. S. *et al.* Human iPSC Glial Mouse Chimeras Reveal Glial Contributions to Schizophrenia. *Cell Stem Cell* **21**, 195-+ (2017).

- 330 McPhie, D. L. *et al.* Oligodendrocyte differentiation of induced pluripotent stem cells derived from subjects with schizophrenias implicate abnormalities in development. *Translational Psychiatry* **8** (2018).
- 331 Nave, K. A. & Ehrenreich, H. Myelination and oligodendrocyte functions in psychiatric diseases. *JAMA Psychiatry* **71**, 582-584 (2014).
- 332 Reubinoff, B. E. *et al.* Neural progenitors from human embryonic stem cells. *Nature biotechnology* **19**, 1134 (2001).
- 333 Maroof, A. M. *et al.* Directed differentiation and functional maturation of cortical interneurons from human embryonic stem cells. *Cell stem cell* **12**, 559-572 (2013).
- 334 Magnani, D., Chandran, S., Wyllie, D. J. A. & Livesey, M. R. In Vitro Generation and Electrophysiological Characterization of OPCs and Oligodendrocytes from Human Pluripotent Stem Cells. *Methods Mol Biol* **1936**, 65-77 (2019).
- 335 Reik, W. & Dean, W. Epigenetic reprogramming: back to the beginning. *Nature* **420**, 127 (2002).
- 336 Matjusaitis, M. *et al.* Reprogramming of Fibroblasts to Oligodendrocyte Progenitor-like Cells Using CRISPR/Cas9-Based Synthetic Transcription Factors. *Stem cell reports* (2019).
- 337 Garcia-Leon, J. A. *et al.* SOX10 Single Transcription Factor-Based Fast and Efficient Generation of Oligodendrocytes from Human Pluripotent Stem Cells. *Stem Cell Reports* **10**, 655-672 (2018).
- 338 Ehrlich, M. *et al.* Rapid and efficient generation of oligodendrocytes from human induced pluripotent stem cells using transcription factors. *Proceedings of the National Academy of Sciences of the United States of America* **114**, E2243-E2252 (2017).
- 339 Kim, H. *et al.* Pluripotent Stem Cell-Derived Cerebral Organoids Reveal Human Oligodendrogenesis with Dorsal and Ventral Origins. *Stem Cell Reports* **12**, 890-905 (2019).
- 340 Samartzis, L., Dima, D., Fusar-Poli, P. & Kyriakopoulos, M. White matter alterations in early stages of schizophrenia: a systematic review of diffusion tensor imaging studies. *J Neuroimaging* **24**, 101-110 (2014).
- 341 Renkilaraj, M. R. L. M. *et al.* The intellectual disability protein PAK3 regulates oligodendrocyte precursor cell differentiation. *Neurobiology of Disease* **98**, 137-148 (2017).
- 342 Olmos-Serrano, J. L. *et al.* Down Syndrome Developmental Brain Transcriptome Reveals Defective Oligodendrocyte Differentiation and Myelination. *Neuron* **89**, 1208-1222 (2016).
- 343 Zeidan-Chulia, F. *et al.* Up-Regulation of Oligodendrocyte Lineage Markers in the Cerebellum of Autistic Patients: Evidence from Network Analysis of Gene Expression. *Molecular Neurobiology* **53**, 4019-4025 (2016).
- 344 Nagarajan, B. *et al.* CNS myelin protein 36K regulates oligodendrocyte differentiation through Notch. *Glia* (2019).
- 345 Hof, P. R., Haroutunian, V., Copland, C., Davis, K. L. & Buxbaum, J. D. Molecular and cellular evidence for an oligodendrocyte abnormality in schizophrenia. *Neurochemical research* **27**, 1193-1200 (2002).
- 346 Katsel, P., Davis, K. L. & Haroutunian, V. Variations in myelin and oligodendrocyte-related gene expression across multiple brain regions in schizophrenia: a gene ontology study. *Schizophr Res* **79**, 157-173 (2005).
- 347 Kubicki, M. *et al.* A review of diffusion tensor imaging studies in schizophrenia. *J Psychiatr Res* **41**, 15-30 (2007).

- 348 Tamnes, C. K. & Agartz, I. White Matter Microstructure in Early-Onset Schizophrenia: A Systematic Review of Diffusion Tensor Imaging Studies. *J Am Acad Child Adolesc Psychiatry* **55**, 269-279 (2016).
- 349 Katsel, P. *et al.* The expression of long noncoding RNA NEAT1 is reduced in schizophrenia and modulates oligodendrocytes transcription. *NPJ Schizophr* **5**, 3 (2019).
- 350 Lee, I. S. *et al.* Characterization of molecular and cellular phenotypes associated with a heterozygous CNTNAP2 deletion using patient-derived hiPSC neural cells. *NPJ Schizophr* **1** (2015).
- 351 Zhou, Q., Choi, G. & Anderson, D. J. The bHLH transcription factor Olig2 promotes oligodendrocyte differentiation in collaboration with Nkx2. 2. *Neuron* **31**, 791-807 (2001).
- 352 Qi, Y. *et al.* Control of oligodendrocyte differentiation by the Nkx2. 2 homeodomain transcription factor. *Development* **128**, 2723-2733 (2001).
- 353 He, D. Y. *et al.* Chd7 cooperates with Sox10 and regulates the onset of CNS myelination and remyelination. *Nature Neuroscience* **19**, 678-+ (2016).
- 354 Klum, S. *et al.* Sequentially acting SOX proteins orchestrate astrocyte- and oligodendrocyte-specific gene expression. *Embo Rep* **19** (2018).
- 355 Turnescu, T. *et al.* Sox8 and Sox10 jointly maintain myelin gene expression in oligodendrocytes. *Glia* **66**, 279-294 (2018).
- 356 Chen, X. *et al.* Novel schizophrenia risk factor pathways regulate FEZ1 to advance oligodendroglia development. *Transl Psychiatry* **7**, 1293 (2017).
- 357 Baker, W. J., Royer, G. L., Jr. & Weiss, R. B. Cytarabine and neurologic toxicity. *J Clin Oncol* **9**, 679-693 (1991).
- 358 Xie, J., MacEwan, M. R., Schwartz, A. G. & Xia, Y. Electrospun nanofibers for neural tissue engineering. *Nanoscale* **2**, 35-44 (2010).
- 359 Shah, S. *et al.* Guiding Stem Cell Differentiation into Oligodendrocytes Using Graphene-Nanofiber Hybrid Scaffolds. *Advanced Materials* **26**, 3673-3680 (2014).
- 360 Lee, S., Chong, S. Y. C., Tuck, S. J., Corey, J. M. & Chan, J. R. A rapid and reproducible assay for modeling myelination by oligodendrocytes using engineered nanofibers. *Nature Protocols* **8**, 771-782 (2013).
- 361 Li, Y. C. *et al.* Nanofibers Support Oligodendrocyte Precursor Cell Growth and Function as a Neuron-Free Model for Myelination Study. *Biomacromolecules* **15**, 319-326 (2014).
- 362 Weightman, A., Jenkins, S., Pickard, M., Chari, D. & Yang, Y. Alignment of multiple glial cell populations in 3D nanofiber scaffolds: Toward the development of multicellular implantable scaffolds for repair of neural injury. *Nanomedicine-Nanotechnology Biology and Medicine* **10**, 291-295 (2014).
- 363 Nazari, B. *et al.* Fibrin hydrogel as a scaffold for differentiation of induced pluripotent stem cells into oligodendrocytes. *Journal of Biomedical Materials Research Part B: Applied Biomaterials* (2019).
- 364 Jones, E. V., Cook, D. & Murai, K. K. in *Astrocytes* 341-352 (Springer, 2012).
- 365 Kuijlaars, J. *et al.* Sustained synchronized neuronal network activity in a human astrocyte co-culture system. *Scientific reports* **6**, 36529 (2016).
- 366 Krencik, R. *et al.* Systematic three-dimensional coculture rapidly recapitulates interactions between human neurons and astrocytes. *Stem cell reports* **9**, 1745-1753 (2017).
- 367 Lancaster, M. A. *et al.* Cerebral organoids model human brain development and microcephaly. *Nature* **501**, 373 (2013).

- 368 Ormel, P. R. *et al.* Microglia innately develop within cerebral organoids. *Nature communications* **9**, 4167 (2018).
- 369 Iefremova, V. *et al.* An organoid-based model of cortical development identifies non-cell-autonomous defects in Wnt signaling contributing to Miller-Dieker syndrome. *Cell reports* **19**, 50-59 (2017).
- 370 Qian, X. *et al.* Brain-region-specific organoids using mini-bioreactors for modeling ZIKV exposure. *Cell* **165**, 1238-1254 (2016).
- 371 Madhavan, M. *et al.* Induction of myelinating oligodendrocytes in human cortical spheroids. *Nature methods* **15**, 700-706 (2018).
- 372 Mandrycky, C., Wang, Z., Kim, K. & Kim, D. H. 3D bioprinting for engineering complex tissues. *Biotechnol Adv* **34**, 422-434 (2016).
- 373 Tuan, R. S., Boland, G. & Tuli, R. Adult mesenchymal stem cells and cell-based tissue engineering. *Arthritis Res Ther* **5**, 32 (2002).
- 374 Xu, T., Kincaid, H., Atala, A. & Yoo, J. J. High-throughput production of single-cell microparticles using an inkjet printing technology. *Journal of Manufacturing Science and Engineering* **130**, 021017 (2008).
- 375 Xu, T. *et al.* Characterization of cell constructs generated with inkjet printing technology using in vivo magnetic resonance imaging. *Journal of Manufacturing Science and Engineering* **130**, 021013 (2008).
- 376 Cui, X., Boland, T., D' Lima, D. & Lotz, M. Thermal inkjet printing in tissue engineering and regenerative medicine. *Recent patents on drug delivery & formulation* **6**, 149-155 (2012).
- 377 Cui, X., Breitenkamp, K., Finn, M., Lotz, M. & D' Lima, D. D. Direct human cartilage repair using three-dimensional bioprinting technology. *Tissue Engineering Part A* **18**, 1304-1312 (2012).
- 378 Xu, T. *et al.* Viability and electrophysiology of neural cell structures generated by the inkjet printing method. *Biomaterials* **27**, 3580-3588 (2006).
- 379 Saunders, R. E., Gough, J. E. & Derby, B. Delivery of human fibroblast cells by piezoelectric drop-on-demand inkjet printing. *Biomaterials* **29**, 193-203 (2008).
- 380 Pepper, M. E. *et al.* in *2011 Annual International Conference of the IEEE Engineering in Medicine and Biology Society*. 3609-3612 (IEEE).
- 381 Pepper, M. E., Seshadri, V., Burg, T. C., Burg, K. J. & Groff, R. E. Characterizing the effects of cell settling on bioprinter output. *Biofabrication* **4**, 011001 (2012).
- 382 Chang, C. C., Boland, E. D., Williams, S. K. & Hoying, J. B. Direct-write bioprinting three-dimensional biohybrid systems for future regenerative therapies. *Journal of Biomedical Materials Research Part B: Applied Biomaterials* **98**, 160-170 (2011).
- 383 Hennink, W. E. & van Nostrum, C. F. Novel crosslinking methods to design hydrogels. *Advanced drug delivery reviews* **64**, 223-236 (2012).
- 384 Demirci, U. & Montesano, G. Single cell epitaxy by acoustic picolitre droplets. *Lab on a Chip* **7**, 1139-1145 (2007).
- 385 Kim, J. D., Choi, J. S., Kim, B. S., Choi, Y. C. & Cho, Y. W. Piezoelectric inkjet printing of polymers: Stem cell patterning on polymer substrates. *Polymer* **51**, 2147-2154 (2010).
- 386 Campbell, P. G., Miller, E. D., Fisher, G. W., Walker, L. M. & Weiss, L. E. Engineered spatial patterns of FGF-2 immobilized on fibrin direct cell organization. *Biomaterials* **26**, 6762-6770 (2005).
- 387 Skardal, A. *et al.* Bioprinted amniotic fluid-derived stem cells accelerate healing of large skin wounds. *Stem cells translational medicine* **1**, 792-802 (2012).

- 388 Xu, T. *et al.* Hybrid printing of mechanically and biologically improved constructs for cartilage tissue engineering applications. *Biofabrication* **5**, 015001 (2012).
- 389 Ozbolat, I. T. & Hospodiuk, M. Current advances and future perspectives in extrusion-based bioprinting. *Biomaterials* **76**, 321-343 (2016).
- 390 Moldovan, N. I. Progress in scaffold-free bioprinting for cardiovascular medicine. *J Cell Mol Med* **22**, 2964-2969 (2018).
- 391 Chang, R., Nam, J. & Sun, W. Effects of dispensing pressure and nozzle diameter on cell survival from solid freeform fabrication-based direct cell writing. *Tissue Eng Part A* **14**, 41-48 (2008).
- 392 Duan, B., Hockaday, L. A., Kang, K. H. & Butcher, J. T. 3D bioprinting of heterogeneous aortic valve conduits with alginate/gelatin hydrogels. *J Biomed Mater Res A* **101**, 1255-1264 (2013).
- 393 Xu, F. *et al.* A three-dimensional in vitro ovarian cancer coculture model using a high-throughput cell patterning platform. *Biotechnology Journal* **6**, 204-212 (2011).
- 394 Norotte, C., Marga, F. S., Niklason, L. E. & Forgacs, G. Scaffold-free vascular tissue engineering using bioprinting. *Biomaterials* **30**, 5910-5917 (2009).
- 395 Barron, J. A., Ringeisen, B. R., Kim, H. S., Spargo, B. J. & Chrisey, D. B. Application of laser printing to mammalian cells. *Thin Solid Films* **453**, 383-387 (2004).
- 396 Guillemot, F., Souquet, A., Catros, S. & Guillotin, B. Laser-assisted cell printing: principle, physical parameters versus cell fate and perspectives in tissue engineering. *Nanomedicine* **5**, 507-515 (2010).
- 397 Gruene, M. *et al.* Laser Printing of Stem Cells for Biofabrication of Scaffold-Free Autologous Grafts. *Tissue Engineering Part C-Methods* **17**, 79-87 (2011).
- 398 Guillotin, B. *et al.* Laser assisted bioprinting of engineered tissue with high cell density and microscale organization. *Biomaterials* **31**, 7250-7256 (2010).
- 399 Guillotin, B. & Guillemot, F. Cell patterning technologies for organotypic tissue fabrication. *Trends Biotechnol* **29**, 183-190 (2011).
- 400 Kattamis, N. T., Purnick, P. E., Weiss, R. & Arnold, C. B. Thick film laser induced forward transfer for deposition of thermally and mechanically sensitive materials. *Applied Physics Letters* **91** (2007).
- 401 Duocastella, M., Fernandez-Pradas, J. M., Morenza, J. L., Zafra, D. & Serra, P. Novel laser printing technique for miniaturized biosensors preparation. *Sensors and Actuators B-Chemical* **145**, 596-600 (2010).
- 402 Michael, S. *et al.* Tissue Engineered Skin Substitutes Created by Laser-Assisted Bioprinting Form Skin-Like Structures in the Dorsal Skin Fold Chamber in Mice. *Plos One* **8** (2013).
- 403 Gauvin, R. *et al.* Microfabrication of complex porous tissue engineering scaffolds using 3D projection stereolithography. *Biomaterials* **33**, 3824-3834 (2012).
- 404 Gou, M. *et al.* Bio-inspired detoxification using 3D-printed hydrogel nanocomposites. *Nature communications* **5**, 3774 (2014).
- 405 Murphy, S. V. & Atala, A. 3D bioprinting of tissues and organs. *Nat Biotechnol* **32**, 773-785 (2014).
- 406 Gardel, M. L. *et al.* Elastic behavior of cross-linked and bundled actin networks. *Science* **304**, 1301-1305 (2004).
- 407 Storm, C., Pastore, J. J., MacKintosh, F. C., Lubensky, T. C. & Janmey, P. A. Nonlinear elasticity in biological gels. *Nature* **435**, 191-194 (2005).

- 408 Guvendiren, M. & Burdick, J. A. Engineering synthetic hydrogel microenvironments to instruct stem cells. *Curr Opin Biotechnol* **24**, 841-846 (2013).
- 409 Huebsch, N. *et al.* Harnessing traction-mediated manipulation of the cell/matrix interface to control stem-cell fate. *Nat Mater* **9**, 518-526 (2010).
- 410 Khetan, S. *et al.* Degradation-mediated cellular traction directs stem cell fate in covalently crosslinked three-dimensional hydrogels. *Nat Mater* **12**, 458-465 (2013).
- 411 Arslan-Yildiz, A. *et al.* Towards artificial tissue models: past, present, and future of 3D bioprinting. *Biofabrication* **8**, 014103 (2016).
- 412 Lee, W. G., Demirci, U. & Khademhosseini, A. Microscale electroporation: challenges and perspectives for clinical applications. *Integr Biol (Camb)* **1**, 242-251 (2009).
- 413 Lee, Y. B. *et al.* Bio-printing of collagen and VEGF-releasing fibrin gel scaffolds for neural stem cell culture. *Exp Neurol* **223**, 645-652 (2010).
- 414 Lozano, R. *et al.* 3D printing of layered brain-like structures using peptide modified gellan gum substrates. *Biomaterials* **67**, 264-273 (2015).
- 415 Hsieh, F. Y., Lin, H. H. & Hsu, S. H. 3D bioprinting of neural stem cell-laden thermoresponsive biodegradable polyurethane hydrogel and potential in central nervous system repair. *Biomaterials* **71**, 48-57 (2015).
- 416 Chen, C. *et al.* Collagen/heparin sulfate scaffolds fabricated by a 3D bioprinter improved mechanical properties and neurological function after spinal cord injury in rats. *J Biomed Mater Res A* **105**, 1324-1332 (2017).
- 417 Gu, Q. *et al.* Functional 3D Neural Mini-Tissues from Printed Gel-Based Bioink and Human Neural Stem Cells. *Adv Healthc Mater* **5**, 1429-1438 (2016).
- 418 Gu, Q., Tomaskovic-Crook, E., Wallace, G. G. & Crook, J. M. 3D Bioprinting Human Induced Pluripotent Stem Cell Constructs for In Situ Cell Proliferation and Successive Multilineage Differentiation. *Adv Healthc Mater* **6** (2017).
- 419 Lindborg, B. A. *et al.* Rapid Induction of Cerebral Organoids From Human Induced Pluripotent Stem Cells Using a Chemically Defined Hydrogel and Defined Cell Culture Medium. *Stem Cells Translational Medicine* **5**, 970-979 (2016).
- 420 Bouyer, C. *et al.* A bio-acoustic levitational (BAL) assembly method for engineering of multilayered, 3D brain-like constructs, using human embryonic stem cell derived neuro-progenitors. *Advanced Materials* **28**, 161-167 (2016).
- 421 Streit, W. J., Mrak, R. E. & Griffin, W. S. Microglia and neuroinflammation: a pathological perspective. *J Neuroinflammation* **1**, 14 (2004).
- 422 Ginhoux, F., Lim, S., Hoeffel, G., Low, D. & Huber, T. Origin and differentiation of microglia. *Front Cell Neurosci* **7**, 45 (2013).
- 423 Park, J. *et al.* A 3D human triculture system modeling neurodegeneration and neuroinflammation in Alzheimer's disease. *Nature neuroscience* **21**, 941 (2018).
- 424 Potjewyd, G., Moxon, S., Wang, T., Domingos, M. & Hooper, N. M. Tissue Engineering 3D Neurovascular Units: A Biomaterials and Bioprinting Perspective. *Trends Biotechnol* **36**, 457-472 (2018).
- 425 Tcw, J. *et al.* An Efficient Platform for Astrocyte Differentiation from Human Induced Pluripotent Stem Cells. *Stem Cell Reports* **9**, 600-614 (2017).
- 426 Armstrong, J. P., Burke, M., Carter, B. M., Davis, S. A. & Perriman, A. W. 3D bioprinting using a templated porous bioink. *Advanced healthcare materials* **5**, 1724-1730 (2016).

- 427 Krishnaswamy, V. R., Benbenishty, A., Blinder, P. & Sagi, I. Demystifying the extracellular matrix and its proteolytic remodeling in the brain: structural and functional insights. *Cell Mol Life Sci* **76**, 3229-3248 (2019).
- 428 Pati, F. & Cho, D. W. Bioprinting of 3D Tissue Models Using Decellularized Extracellular Matrix Bioink. *Methods Mol Biol* **1612**, 381-390 (2017).
- 429 Kim, B. S., Kim, H., Gao, G., Jang, J. & Cho, D. W. Decellularized extracellular matrix: a step towards the next generation source for bioink manufacturing. *Biofabrication* **9**, 034104 (2017).
- 430 Toprakhisar, B. *et al.* Development of Bioink from Decellularized Tendon Extracellular Matrix for 3D Bioprinting. *Macromol Biosci* **18**, e1800024 (2018).
- 431 Lee, H. *et al.* Development of Liver Decellularized Extracellular Matrix Bioink for Three-Dimensional Cell Printing-Based Liver Tissue Engineering. *Biomacromolecules* **18**, 1229-1237 (2017).
- 432 Choudhury, D., Tun, H. W., Wang, T. & Naing, M. W. Organ-Derived Decellularized Extracellular Matrix: A Game Changer for Bioink Manufacturing? *Trends Biotechnol* **36**, 787-805 (2018).
- 433 Pati, F. *et al.* Printing three-dimensional tissue analogues with decellularized extracellular matrix bioink. *Nat Commun* **5**, 3935 (2014).
- 434 Cho, A. N. *et al.* Aligned Brain Extracellular Matrix Promotes Differentiation and Myelination of Human-Induced Pluripotent Stem Cell-Derived Oligodendrocytes. *ACS Appl Mater Interfaces* **11**, 15344-15353 (2019).
- 435 Sood, D. *et al.* Functional maturation of human neural stem cells in a 3D bioengineered brain model enriched with fetal brain-derived matrix. *Sci Rep* **9**, 17874 (2019).
- 436 Parak, A. *et al.* Functionalizing bioinks for 3D bioprinting applications. *Drug Discov Today* **24**, 198-205 (2019).
- 437 Lau, L. W., Cua, R., Keough, M. B., Haylock-Jacobs, S. & Yong, V. W. Pathophysiology of the brain extracellular matrix: a new target for remyelination. *Nat Rev Neurosci* **14**, 722-729 (2013).
- 438 Law, N. *et al.* Characterisation of hyaluronic acid methylcellulose hydrogels for 3D bioprinting. *Journal of the mechanical behavior of biomedical materials* **77**, 389-399 (2018).
- 439 Keeney, J. G. *et al.* DUF1220 protein domains drive proliferation in human neural stem cells and are associated with increased cortical volume in anthropoid primates. *Brain Structure & Function* **220**, 3053-3060 (2015).
- 440 Malinger, G., Lev, D. & Lerman-Sagie, T. Assessment of fetal intracranial pathologies first demonstrated late in pregnancy: cell proliferation disorders. *Reprod Biol Endocrinol* **1**, 110 (2003).
- 441 Williams, C. A., Dagli, A. & Battaglia, A. Genetic disorders associated with macrocephaly. *Am J Med Genet A* **146A**, 2023-2037 (2008).
- 442 Ernst, C. Proliferation and Differentiation Deficits are a Major Convergence Point for Neurodevelopmental Disorders. *Trends Neurosci* **39**, 290-299 (2016).
- 443 Yue, T. *et al.* A critical role for dorsal progenitors in cortical myelination. *J Neurosci* **26**, 1275-1280 (2006).
- 444 Stevens, B., Porta, S., Haak, L. L., Gallo, V. & Fields, R. D. Adenosine: a neuron-glia transmitter promoting myelination in the CNS in response to action potentials. *Neuron* **36**, 855-868 (2002).
- 445 Demerens, C. *et al.* Induction of myelination in the central nervous system by electrical activity. *Proc Natl Acad Sci U S A* **93**, 9887-9892 (1996).

- 446 Ozaki, M., Itoh, K., Miyakawa, Y., Kishida, H. & Hashikawa, T. Protein processing and releases of neuregulin-1 are regulated in an activity-dependent manner. *J Neurochem* **91**, 176-188 (2004).
- 447 Lundgaard, I. *et al.* Neuregulin and BDNF induce a switch to NMDA receptor-dependent myelination by oligodendrocytes. *Plos Biol* **11**, e1001743 (2013).
- 448 Takahashi, N., Sakurai, T., Davis, K. L. & Buxbaum, J. D. Linking oligodendrocyte and myelin dysfunction to neurocircuitry abnormalities in schizophrenia. *Prog Neurobiol* **93**, 13-24 (2011).
- 449 Cassoli, J. S. *et al.* Disturbed macro-connectivity in schizophrenia linked to oligodendrocyte dysfunction: from structural findings to molecules. *NPJ Schizophr* **1**, 15034 (2015).
- 450 Pajevic, S., Basser, P. J. & Fields, R. D. Role of myelin plasticity in oscillations and synchrony of neuronal activity. *Neuroscience* **276**, 135-147 (2014).
- 451 Courchesne, E. *et al.* Mapping early brain development in autism. *Neuron* **56**, 399-413 (2007).
- 452 Hazlett, H. C. *et al.* Early brain development in infants at high risk for autism spectrum disorder. *Nature* **542**, 348+ (2017).
- 453 Hazlett, H. C. *et al.* Early Brain Overgrowth in Autism Associated With an Increase in Cortical Surface Area Before Age 2 Years. *Archives of General Psychiatry* **68**, 467-476 (2011).
- 454 Piven, J., Elison, J. T. & Zylka, M. J. Toward a conceptual framework for early brain and behavior development in autism (vol 25, pg 165, 2017). *Molecular Psychiatry* **23**, 165-165 (2018).
- 455 Casanova, E. L. & Casanova, M. F. Genetics studies indicate that neural induction and early neuronal maturation are disturbed in autism. *Frontiers in Cellular Neuroscience* **8** (2014).
- 456 Bedogni, F. *et al.* Autism susceptibility candidate 2 (Aut2) encodes a nuclear protein expressed in developing brain regions implicated in autism neuropathology. *Gene Expression Patterns* **10**, 9-15 (2010).
- 457 Peng, Y. *et al.* The autism-associated MET receptor tyrosine kinase engages early neuronal growth mechanism and controls glutamatergic circuits development in the forebrain. *Molecular Psychiatry* **21**, 925-935 (2016).
- 458 Chomiak, T., Karnik, V., Block, E. & Hu, B. Altering the trajectory of early postnatal cortical development can lead to structural and behavioural features of autism. *Bmc Neuroscience* **11** (2010).
- 459 Courchesne, E. & Pierce, K. Why the frontal cortex in autism might be talking only to itself: local over-connectivity but long-distance disconnection. *Current Opinion in Neurobiology* **15**, 225-230 (2005).
- 460 Moraga-Amaro, R., Jerez-Baraona, J. M., Simon, F. & Stehberg, J. Role of astrocytes in memory and psychiatric disorders. *Journal of Physiology-Paris* **108**, 240-251 (2014).
- 461 Reus, G. Z. *et al.* The Role of Inflammation and Microglial Activation in the Pathophysiology of Psychiatric Disorders. *Neuroscience* **300**, 141-154 (2015).
- 462 Davis, K. L. & Haroutunian, V. Global expression-profiling studies and oligodendrocyte dysfunction in schizophrenia and bipolar disorder. *The Lancet* **362**, 758 (2003).
- 463 Dietz, A. G., Goldman, S. A. & Nedergaard, M. Glial cells in schizophrenia: a unified hypothesis. *Lancet Psychiat* (2019).

- 464 Bailey, K. E. *et al.* Development of Hydrogel Bioinks and 3D Bioprinting Techniques to Support Extended 3D Lung Tissue Culture In Vitro. *American Journal of Respiratory and Critical Care Medicine* **199** (2019).
- 465 Heinrich, M. A. *et al.* 3D-Bioprinted Mini-Brain: A Glioblastoma Model to Study Cellular Interactions and Therapeutics. *Adv Mater* **31**, e1806590 (2019).